

UNIVERSITAT DE BARCELONA  
DEPARTAMENT D'ASTRONOMIA I METEOROLOGIA



EXPLORING THE EVOLUTION OF DARK ENERGY  
AND ITS EQUATION OF STATE



UNIVERSITAT DE BARCELONA



Memòria presentada per  
**Cristina España i Bonet**  
per optar al grau de  
Doctora en Ciències Físiques

Barcelona, octubre de 2007



*Per a l'Abril*



Aquesta tesi ha estat elaborada en el Departament d'Astronomia i Meteorologia de la Universitat de Barcelona, i ha estat possible gràcies al finançament en els inicis de la *European Research Training Network: The Physics of Type Ia Supernova Explosions* i en els darrers temps del *Ministerio de Educación y Ciencia* a través d'una beca Predoctoral de Formació de Personal Investigador. Però més que a les institucions en si, voldria agrair a les persones que en formen part. Agrair des de la secretaria del departament a la seva direcció. Des de tota l'ajuda i facilitats d'en J.R. fins a la gestió primer del Dr. Eduard Salvador i actualment del Dr. Jerónimo Lorente.

Des del punt de vista estrictament científic hi ha moltes persones culpables de la realització d'aquesta tesi. Per començar l'investigador principal del grup, el Dr. Ramon Canal, qui em va motivar i introduir en la cosmologia ja com a professor durant la carrera. Fins i tot més responsable n'és la directora de tesi, la Dra. Pilar Ruiz-Lapuente, amb qui he pogut treballar durant tot aquest temps. Un agraïment també al Dr. Joan Solà amb qui em vaig endinsar en la part més teòrica. Tot i que en aquest cas des de la distància, aquesta part és fruit també de la col·laboració amb el Dr. Ilya Shapiro. I am also very grateful to Prof. Robert Nichol and all the people of the Institute of Cosmology and Gravitation of Portsmouth, where I spent a couple of months.

Finalment agrair el suport, consells i comentaris de familiars i amics, tot i que potser no n'he fet molt de cas o no he seguit els consells adequats... Agrair a aquells que m'han de suportar en el dia a dia, i als que m'han hagut d'aguantar algun divendres inspirat. A aquells que ho han viscut des de dins, amb qui he compartit cafès, dinars, converses de física i pelis rares... Andreu, Rubén, Giuseppe i Sinue. I als que també ho han viscut molt de prop amb més cafès, converses, sopars... Glòria, Roser, Gerard, Montse, Alba, Roser i Laura. Gràcies a tots!



PROGRAMA DE DOCTORAT D'ASTRONOMIA I METEOROLOGIA

BIENNI 2002–2004

Memòria presentada per **Cristina España i Bonet**  
per optar al grau de Doctora en Ciències Físiques

DIRECTORA DE LA TESI

Cristina España i Bonet

Dra. Pilar Ruiz-Lapuente



---

# Contents

---

<b>Energia fosca variable a l'Univers</b>	<b>vii</b>
<b>1 Introduction</b>	<b>1</b>
1.1 The Big Bang theory . . . . .	1
1.1.1 A perfect complement: inflation . . . . .	3
1.2 The dark side supremacy . . . . .	4
1.3 Cosmological constant and dark energy . . . . .	6
1.4 Thesis framework and outline . . . . .	9
<b>I Evolving dark energy</b>	
<b>2 Dynamics of the Universe</b>	<b>15</b>
2.1 Einstein's field equations . . . . .	15
2.2 Dark energy in Einstein's equations . . . . .	18
2.2.1 Vacuum quantum energy and the cosmological constant . . . . .	18
2.2.2 Quintessence and other alternatives . . . . .	20
2.3 Solving Einstein's equations . . . . .	22
2.3.1 Cosmological principle and Robertson-Walker metric . . . . .	22
2.3.2 Distances in cosmology . . . . .	25
2.3.2.1 Proper distance . . . . .	25
2.3.2.2 Redshift . . . . .	26
2.3.2.3 Luminosity distance . . . . .	27
2.3.2.4 Angular distance . . . . .	29
2.3.3 Friedmann equations . . . . .	29
2.4 Parameterizing the dynamics . . . . .	32

2.4.1	Hubble constant and critical density . . . . .	33
2.4.2	Cosmological parameters . . . . .	34
2.4.3	Dark energy equation of state . . . . .	36
<b>3</b>	<b>Running of the cosmological constant</b>	<b>37</b>
3.1	Quantum field theory concepts . . . . .	37
3.1.1	Action . . . . .	37
3.1.2	Regularization and renormalization . . . . .	39
3.1.3	Renormalization Group Equations . . . . .	40
3.2	Renormalization Group Equations for the cosmological constant . . .	42
3.3	Cosmological scenarios . . . . .	45
3.3.1	Perturbative solution to the Renormalization Group Equations	45
3.3.1.1	Scenario 1: $m_i < \mu$ , $\mu \sim \rho_c^{1/4}(t)$ . . . . .	46
3.3.1.2	Scenario 2: $M_i > \mu$ , $\mu \sim \rho_c^{1/4}(t)$ . . . . .	47
3.3.1.3	Scenario 3: $M_i > \mu$ , $\mu \sim R^{1/2} \sim H(t)$ . . . . .	48
3.3.1.4	Comparisons . . . . .	49
3.3.2	Non-perturbative solution to the Renormalization Group Equations . . . . .	51
3.3.2.1	Scenario 4: $\mu \sim 1/t \sim H(t)$ . . . . .	51
3.3.3	Renormalization scale . . . . .	52
3.4	Cosmology in Scenario 3 . . . . .	53
3.4.1	Cosmological equations . . . . .	53
3.4.2	Cosmological index $\nu$ . . . . .	55
3.4.2.1	Case $\nu < 0$ . . . . .	55
3.4.2.2	Case $\nu = 0$ . . . . .	56
3.4.2.3	Case $0 < \nu < 1$ . . . . .	56
3.4.2.4	Case $\nu = 1$ . . . . .	57
3.4.2.5	Case $\nu > 1$ . . . . .	58
3.4.3	Primordial nucleosynthesis restrictions . . . . .	58
3.4.4	Behaviour in the physical range $ \nu  \ll 1$ . . . . .	60
3.4.5	Other characteristics . . . . .	63
3.4.5.1	Hubble parameter . . . . .	63
3.4.5.2	Cosmological sum rule . . . . .	66
3.4.5.3	Deceleration parameter . . . . .	68

<b>4</b>	<b>Dark energy equation of state</b>	<b>71</b>
4.1	Basics . . . . .	71
4.1.1	Classical energy conditions . . . . .	72
4.1.2	Quintessence . . . . .	73
4.2	Mimicking the equation of state $p = w\rho$ . . . . .	78
4.2.1	Evolving cosmological constant . . . . .	79
4.2.2	Chaplygin gas . . . . .	80
4.2.3	Cardassian models . . . . .	82
4.2.4	Modified Gravity . . . . .	83
4.2.4.1	Braneworld cosmologies . . . . .	84
4.2.4.2	Loop quantum cosmology . . . . .	87
4.3	Parameterizing the equation of state . . . . .	89
4.3.1	Common developments . . . . .	90
4.4	Degeneracy . . . . .	92
4.4.1	Degeneracy in the luminosity distance . . . . .	93

## II Observational constraints

<b>5</b>	<b>Cosmic distances and standard candles</b>	<b>101</b>
5.1	The cosmic distance ladder . . . . .	101
5.1.1	Standard candles . . . . .	102
5.2	Extragalactic sources as distance indicators . . . . .	103
5.3	Key distances for cosmology . . . . .	104
5.3.1	Low redshift, 2dFGRS . . . . .	104
5.3.2	Intermediate redshift, BAO . . . . .	105
5.3.3	Very high redshift, CMB . . . . .	106
5.4	Supernovae as standard candles . . . . .	107
5.4.1	Supernovae . . . . .	107
5.4.2	Physics of Type Ia supernovae . . . . .	110
5.4.3	Observational features . . . . .	113
5.4.3.1	Spectra . . . . .	114
5.4.3.2	Light curves . . . . .	115
5.5	Standardizing Type Ia supernovae . . . . .	116
5.5.1	$\Delta m_{15}$ template fitting . . . . .	117

5.5.2	Stretch factor . . . . .	118
5.5.2.1	Adding the extinction correction . . . . .	120
5.5.3	Multicolour Light Curve Shape (MCLS) . . . . .	120
5.5.4	Bayesian Adapted Template Match (BATM) . . . . .	121
5.5.5	Colour-Magnitude Intercept Calibration (CMAGIC) . . . . .	122
5.6	Uncertainties and systematics . . . . .	122
5.6.1	Time dilation and K-correction . . . . .	122
5.6.2	Galaxy and host extinction . . . . .	123
5.6.3	Gravitational lensing . . . . .	125
5.6.4	Sample contamination and selection effects . . . . .	125
5.6.5	Redshift uncertainty . . . . .	126
5.7	Data samples . . . . .	127
5.7.1	Bootstrap resampling . . . . .	130
<b>6</b>	<b>Looking for the underlying cosmology</b>	<b>133</b>
6.1	Parameter estimate: the maximum likelihood method . . . . .	133
6.1.1	$\chi^2$ as a maximum likelihood method . . . . .	134
6.1.2	Goodness-of-fit . . . . .	135
6.1.3	Confidence regions . . . . .	136
6.1.3.1	Monte Carlo errors . . . . .	137
6.1.4	Priors and marginalization . . . . .	137
6.1.5	Implementation and numerical issues . . . . .	139
6.2	Cosmological constant . . . . .	139
6.3	Running cosmological constant . . . . .	143
6.3.1	Scenario 1 . . . . .	145
6.3.2	Scenario 2 . . . . .	146
6.3.3	Scenario 3 . . . . .	147
6.4	Constant dark energy source . . . . .	149
6.5	Evolving equation of state . . . . .	152
6.6	Near future results . . . . .	154
<b>7</b>	<b>Reconstructing dark energy with an inverse method</b>	<b>157</b>
7.1	The problem . . . . .	157
7.2	Inverse problems . . . . .	158
7.2.1	A non-parametric non-linear inversion . . . . .	159

---

7.2.1.1	Control of the results . . . . .	165
7.2.2	Discrete parameters: the parametric non-linear inversion . . .	167
7.2.3	Implementation and numerical issues . . . . .	168
7.3	Determination of a continuous $w(z)$ . . . . .	168
7.3.1	Current data . . . . .	170
7.3.2	Near future results . . . . .	175
7.4	Determination of a parameterized $w(z)$ . . . . .	176
7.5	A running cosmological constant as an inverse problem . . . . .	178
<b>8</b>	<b>Future perspectives</b>	<b>183</b>
8.1	Oncoming surveys . . . . .	183
8.1.1	Generating data distributions . . . . .	185
8.2	The best perspectives from Earth . . . . .	187
8.2.1	LSST wide survey . . . . .	188
8.2.2	LSST deep survey . . . . .	194
8.3	Standard cosmology with space surveys, SNAP/JDEM . . . . .	197
8.4	The continuous determination of the equation of state . . . . .	198
8.5	The running of the cosmological constant . . . . .	203
<b>9</b>	<b>Conclusions</b>	<b>209</b>
<b>A</b>	<b>Notation</b>	<b>221</b>
A.1	Part I . . . . .	221
A.2	Part II . . . . .	226
	<b>List of figures</b>	<b>230</b>
	<b>List of tables</b>	<b>237</b>
	<b>Bibliography</b>	<b>239</b>



## Resum

---

# Energia fosca variable a l'Univers

---

*En algun lloc, alguna cosa increïble espera ser coneguda.*

Carl Sagan

## Introducció i motivació de la tesi

Un dels descobriments científics més sorprenents dels últims temps és el fet que l'Univers estigui en expansió accelerada. Avui en dia, hi ha un acord gairebé unànimement en la validesa del model de Big Bang: l'expansió de l'Univers es va originar a partir d'un estat inicial de densitat i temperatura molt elevades i, des d'aquell moment, ha estat creixent i refredant-se. Però, què passa amb l'efecte de la gravetat? No s'hauria d'estar frenant l'expansió? Per què està accelerant-se?

Aquesta tesi pretén contribuir a la resposta abordant el tema de l'*energia fosca*. El mateix nom ja ens indica la naturalesa del problema: desconeixement complet. L'adjectiu fosc s'utilitza per descriure alguna cosa que ajusta i reproduïx les observacions però que no coneixem. Habitualment es tracta com una nova forma d'energia. Per què no? Tot sembla ser finalment energia i la nostra ment està preparada i predisposada a conèixer-ne noves formes. Però aquesta no és l'única explicació possible. Altres aproximacions al problema proposen modificacions a la relativitat general. I fins i tot altres punts de vista més exòtics, o més senzills o revolucionaris s'haurien de tenir en compte i contrastar-los amb les observacions. Actualment, sembla que hi ha molts camins per tractar de respondre la pregunta,

però en tots ells s'està lluny d'arribar al final. Potser ni tan sols hem trobat el camí correcte encara. En aquesta tesi s'ha intentat avançar per un d'ells.

## El model de Big Bang o Gran Explosió

La descripció més acurada i propera al naixement de l'Univers que podem donar és que la seva expansió es va originar en una explosió que va fer que el teixit espaciotemporal amb tot el seu contingut comencés a estirar-se enormement. Aquesta teoria va ser presa seriosament per primera vegada als anys 30 com a conseqüència de les equacions d'Albert Einstein, la solució obtinguda per Georges Lemaître, i els resultats experimentals de Vesto Slipher i Edwin Hubble que demostraven que les galàxies s'estan allunyant de nosaltres. Al principi, en una societat que creia en un univers estàtic, la idea va generar molts detractors. A més, el fet que un univers en expansió impliqués un origen i, per a alguns, necessàriament un creador, causava problemes tant físics com filosòfics.

La interpretació del model ha anat canviant amb el temps i, actualment, s'entén per Big Bang la descripció de l'Univers fins a l'instant de Planck, sense suposicions sobre l'origen o instant inicial. Fins ara, aquest model està superant amb èxit els tests que se li plantegen i són diversos els resultats observacionals que li donen suport. El Big Bang està recolzat sobre quatre pilars ben sòlids, quatre prediccions que s'han pogut contrastar de manera acurada.

El primer, òbviament, la confirmació experimental que l'Univers està en expansió. Edwin Hubble i Milton L. Humason treballaven en la mesura de distàncies i *redshifts* a Mount Wilson. Les seves mesures juntament amb les de Slipher els van permetre veure que els espectres estaven més correguts cap al vermell com més llunyanes eren les galàxies. Les galàxies havien d'estar allunyant-se de nosaltres. Aquest resultat els va portar el 1929 a establir una relació entre la distància i la velocitat de recessió, la llei de Hubble [105].

Més tard, el 1948, George Gamow justificava les abundàncies químiques de l'Univers com a resultat de les reaccions que es van produir durant el Big Bang [8]. Aquesta nucleosíntesi primordial és la responsable de la formació dels elements més lleugers que el beril·li [135, 185].

El mateix Gamow va deduir en els seus càlculs que una explosió d'aquestes característiques on es produïa una gran quantitat de reaccions termonuclears havia de generar radiació. Des del moment en què els fotons es desacoblen de la matèria, comencen la seva evolució independent que els fa refredar paulatinament. Actualment s'haurien d'observar com un fons de microones: la radiació còsmica de fons (CMB). Per aquells temps, la tecnologia no era suficient per detectar una radiació d'energia tan baixa, però alguns anys més tard, el 1964, Arno Penzias i Robert Wilson van descobrir la radiació còsmica de fons gairebé per casualitat [143]. Curiosament, un grup dirigit per Robert Dicke estava treballant en la detecció del bany de fotons [62] i els dos grups van poder explicar les observacions conjuntament.

La detecció de la radiació predita va afermar el model de Big Bang com a model cosmològic estàndard, però encara quedava un quart test. Un cop l'Univers s'havia refredat suficientment com per estar dominat pels nuclis atòmics, la gravetat hauria fet col·lapsar qualsevol petita inhomogeneïtat, disposant les llavors per a la formació d'estructura. A banda de la prova palpable que estem envoltats d'agrupacions de matèria com ara galàxies i cúmuls, la radiació de fons ens proporciona una altra vegada un indicatiu de les llavors de la formació d'estructura donat per petites anisotropies de temperatura d'ordre  $10^{-5}$ . Aquestes anisotropies les va observar per primer cop el satèl·lit COBE (COsmic Background Explorer) el 1992 [178].

Tot i el gran èxit del model de Big Bang, hi ha resultats que no es poden explicar directament dels seus principis o que necessiten filar massa prim en els paràmetres lliures. Algun d'ells són els que podem anomenar problemes clàssics: Com pot ser l'univers observable homogeni si no podia estar causalment connectat poc després del Big Bang? Com podem observar un univers pla si això implicaria una precisió en el valor de la curvatura original de  $10^{-60}$ ? Què va produir l'evident asimetria entre matèria i antimatèria? I altres problemes estan més relacionats amb el coneixement dels que semblen els components majoritaris de l'Univers: Què és la matèria fosca? Com pot ser que l'Univers estigui en expansió accelerada? O, què és l'energia fosca?

## **Un complement perfecte: la inflació**

Per tal de solucionar principalment els dos primers problemes, els que hem anomenat clàssics, Alan Guth [96] i Andrei Linde [123, 4] van desenvolupar les primeres teories inflacionàries. Hi ha diverses variacions d'inflació, però en totes elles l'espai-temps

experimenta un període d'expansió exponencial. En la teoria original de Guth, l'Univers es troba encallat en un fals buit fins que decau a un estat d'energia més baixa. Les bombolles de buit real que es van creant en l'estat metastable s'expandeixen ràpidament. En la teoria de Linde, un camp escalar, l'inflató, descèn pel seu potencial creant una expansió accelerada fins que arriba al mínim i l'inflató decau a radiació.

La inflació en aquesta forma simple ja resol quatre problemes que el model de Big Bang sol no pot explicar. Primerament, una expansió exponencial diluiria la densitat de monopols de manera que fos prou baixa com perquè en el volum d'univers observable no se'n veiés cap. Segon, les fluctuacions quàntiques primordials quedarien *congelades* convertint-se en les llavors per a la formació d'estructura. A més, la ràpida expansió també suavitzaria qualsevol curvatura inicial de l'Univers apropant-lo a una geometria plana. Finalment, les petites regions causalment connectades abans de la inflació creixerien molt més ràpid que la transmissió d'informació durant el mateix període, i l'actual univers observable podria pertànyer completament a una d'aquestes regions, cosa impossible amb una expansió lineal. Això explicaria per què l'Univers és tan homogeni.

Algunes de les prediccions dels models inflacionaris es poden verificar amb observacions. Tres anys de dades de l'equip de WMAP [183] han confirmat la homogeneïtat i isotropia en una part entre  $10^5$  i la planor a la centèsima. Els models inflacionaris prediuen un espectre de fluctuacions de densitat gaussià i gairebé invariànt amb l'escala. Els resultats dels sondejos de galàxies i del CMB són compatibles amb aquestes assumpcions. A més, la polarització del CMB hauria de permetre detectar un fons d'ones gravitacionals generades a la inflació, una altra predicció de la teoria.

Com es pot veure, els models inflacionaris són adequats perquè a banda de descriure les observacions fan un gran número de prediccions contrastables. Això fa que la manca d'un mecanisme que generi la inflació i del coneixement del mateix inflató no hagi evitat que el model sigui àmpliament acceptat. Evidentment, és un camp de recerca molt actiu tant en el vessant teòric com en l'experimental, i propers models de la física de partícules conjuntament amb futures observacions haurien de completar en breu el nostre enteniment de la inflació.

---

## El costat fosc

A la vegada, hi ha una necessitat creixent d'incloure nous components *fosc* al model de Big Bang. Per una banda la *matèria fosca* es va convertir en un requeriment per tal de justificar les corbes de rotació de les galàxies mesurades [214, 163]. Per altra banda, l'*energia fosca* és l'ingredient clau per explicar l'acceleració de l'Univers [158, 145].

La matèria fosca és, per definició, un tipus de matèria que no interacciona amb els fotons. No és, doncs, visible i només es pot detectar per efectes gravitacionals. Pot ser tant bariònica com no bariònica i, probablement, n'hi ha de les dues classes. Nans marrons, planetes i forats negres són matèria fosca però no n'hi ha la quantitat suficient per cobrir tota la massa que falta. La matèria fosca no bariònica pot ser de dos tipus: relativista com els neutrins (matèria fosca calenta) i no relativista com els hipotètics WIMP (matèria fosca freda). Simulacions sobre la formació de l'estructura a gran escala mostren que la matèria fosca freda (CDM) és necessària per permetre que les agrupacions de matèria petites col·lapsin i es vagin fusionant fins formar les estructures observades. De l'ús dels resultats de corbes rotacionals, lents gravitatòries, distribucions de temperatura de gas calent o les anisotropies del CMB, es desprèn que la matèria fosca ha de ser uns set cops més abundant que la visible. La major part ha de ser, a més, desconeguda i no un component del model estàndard de partícules.

Quan les teories inflacionàries es van començar a imposar, la matèria fosca es va agafar com a solució per reconciliar la predicció d'un univers pla amb la quantitat insuficient de matèria visible. Als 90, el resultat de COBE van reforçar per la banda observacional la creença que l'Univers era pla, però ja en aquesta dècada les mesures de la densitat de matèria fosca eren prou precises per veure que la seva densitat tampoc era suficient per fer l'Univers pla. La constant cosmològica va sortir al rescat, tal com va passar quan Einstein volia descriure un Univers estàtic. S'apel·lava, doncs, a un tipus d'energia fosca.

L'energia fosca és una font d'energia amb pressió negativa que actua com a força repulsiva. Com a densitat, és una component addicional que s'afegeix a les conegudes per determinar la curvatura de l'Univers. Dinàmicament, però, la pressió negativa contraresta la gravetat i causa l'acceleració de l'expansió.

Les distàncies extragalàctiques són molt més sensibles a la dinàmica de l'Univers del que ho podria ser la radiació de fons de microones que només descriu un punt del passat. Així, doncs, la distància a supernoves llunyanes hauria de proporcionar una mesura més adequada de l'acceleració de l'Univers i, per tant, de l'energia fosca del que ho feia el CMB. Però va caler esperar fins al 1998 perquè un univers sense energia fosca fos descartat amb més d'un 99% de probabilitat.

El compendi de resultats establerts a final de segle ha configurat el que s'anomena model de concordança o model  $\Lambda$ -CDM. Un model coherent amb el Big Bang, la inflació, amb matèria fosca freda i constant cosmològica amb les densitats adients per obtenir un univers pla. Però aquest model ens deixa en una situació d'ignorància: només el 4% de l'Univers està fet de matèria ordinària, el 96% restant està en forma de matèria i energia fosca per als quals només som capaços d'aventurar algunes conjeitures teòriques. Resulta molt difícil construir una teoria que ens descrigui un univers del qual tot just un 4% del seu contingut ens resulta familiar.

Filosòficament, un univers d'aquest estil torna a canviar la concepció que tenim de nosaltres mateixos. Per als grecs, la Terra era el centre de tot i nosaltres ocupàvem una posició privilegiada a l'Univers. Després, el principi cosmològic ens va col·locar en una situació ben comuna. Estem orbitant una estrella típica que està a les afores d'una galàxia típica en un cúmul típic. A més, estem constituïts pel mateix material que la resta d'elements de l'Univers. Ara sembla que ens tornem a diferenciar, com a mínim sota el punt de vista que la nostra biologia està restringida als barions, que estan resultant ser un component rar de l'Univers.

## Constant cosmològica i energia fosca

El candidat més natural per accelerar l'Univers és la constant cosmològica. Primer, perquè és solució de les equacions d'Einstein. Segon, perquè segons la mecànica quàntica, el buit té una energia. Desafortunadament, una comparació directa entre la constant cosmològica de les equacions d'Einstein amb l'energia quàntica del buit discrepa de les observacions en  $10^{55}$  ordres de magnitud. I el desacord no és només amb les observacions sinó també amb qualsevol curvatura coherent amb l'experiència. Aquesta discordància o l'afinament necessari per compensar les dues constants i fer la seva suma compatible amb les observacions és el que es coneix com el problema de la constant cosmològica. Per què la densitat d'energia fosca és

tan petita avui? O en altres paraules, el problema de la coincidència temporal: Per què és tan propera a la densitat de matèria? (Per ampliar la informació veure per exemple [44, 167, 132].)

Una resposta al problema, la pot donar una constant cosmològica dependent del temps. Una funció d'aquest estil segueix sent solució de les equacions d'Einstein. Sota el punt de vista físic, la constant cosmològica ha d'experimentar un *running* si es considera dintre d'una teoria quàntica de camps. A l'espera d'una teoria quàntica de camps de la gravitació, l'aproximació semiclàssica hauria de ser suficient per permetre'ns contrastar la idea amb observacions. Aquesta possibilitat s'explorà en detall al llarg de la tesi.

El concepte d'energia fosca dependent del temps s'acostuma a tractar, però, a través d'un camp escalar dinàmic, el camp de quinta essència. La idea és una reminiscència de la inflació. Si la constant cosmològica interpretada com a energia quàntica del buit té similituds amb la teoria inflacionària de Guth, la quinta essència recorda el model de Linde. Un camp escalar va disminuint el seu potencial amb el temps [142, 57, 162]. Actualment, es troba prop del seu mínim amb velocitat gairebé nul·la, i això crea una energia constant i una pressió negativa amb efecte similar al de la constant cosmològica. També s'han considerat camps amb una energia cinètica no canònica, *k*-essència [12, 128]. De fet, hi ha moltes versions de la quinta essència original, però en tots els casos es fa necessari donar una interpretació física al camp escalar i afinar enormement els valors dels seus paràmetres.

Una branca diferent de models pretén explicar l'acceleració mitjançant modificacions de la relativitat general [150, 164, 138]. En alguns casos es considera l'existència de dimensions addicionals a les 4 espaciotemporals [64, 58, 71], en altres, s'inclouen termes extra dependents de la curvatura a les equacions d'Einstein [23, 120, 133, 130], o bé s'apel·la a teories tensorials de la gravitació [173, 61, 28, 72].

Dintre de l'àmplia bibliografia dedicada a l'energia fosca també es troben justificacions al valor de la constant cosmològica basats en principis antròpics [205, 86], i extensions per a camps de quinta essència per exemple [85]. Per acabar aquesta breu compilació que de cap manera pretén ser exhaustiva, comentarem que la formulació actual de la Teoria M necessita que la constant cosmològica sigui nul·la o tendeixi a zero en el futur; tot i això, s'està treballant en variacions que accepten valors com l'observat [33].

Amb aquest ventall de models resulta molt difícil destacar-ne un per davant dels altres. Tots es poden ajustar de manera que acabin descrivint les observacions, però aquests ajustos no tenen al darrera una teoria completa i consistent que els avalii. Per obtenir aquesta teoria, caldrà esperar a modificacions del model estàndard de partícules o a una combinació exitosa de la relativitat general i la mecànica quàntica de què se'n dedueixi la seva forma.

Per la banda observacional, *veure* l'energia fosca és tot un repte. És una component de densitat baixa, està distribuïda homogèniament i no interacciona amb la gravetat. A més, el seu domini ha de ser recent; d'altra manera les pertorbacions a la matèria no haurien pogut créixer per poder formar l'estructura a gran escala actual. Tanmateix, l'energia fosca afecta dos fenòmens que es poden quantificar: l'expansió de l'Univers i el creixement de l'estructura.

Les millors eines de què es disposa per estudiar l'expansió de l'Univers són les supernoves Ia (SNe Ia). La variació de la magnitud aparent d'aquests objectes amb la distància va proporcionar la primera indicació clara de l'acceleració de l'expansió [158, 145]. Avui en dia, encara són el mètode més precís de mesurar la quantitat d'energia fosca i la seva equació d'estat [160, 211].

De la mateixa manera, les oscil·lacions acústiques dels barions (BAO) es poden tractar com un regle estàndard que es pot mesurar com a funció del *redshift* [70, 144]. Encara que aquestes oscil·lacions són molt més sensibles a la densitat de matèria que d'energia fosca, la línia de degeneració entre els paràmetres és gairebé perpendicular a la degeneració de les supernoves, i la combinació d'ambdues mesures resulta tremendament útil.

Un altre fenomen físic que es veu influenciat per la presència d'energia fosca és la deflexió de la llum en travessar zones properes a grans acumulacions de massa. Les lents gravitacional dèbils ofereixen una gran quantitat de tests possibles. La mesura estadística de la distorsió induïda per l'estructura a gran escala [210, 104] o la cosmografia de correlació creuada que utilitza les distorsions a diversos *redshifts* [112, 27] són dues maneres d'obtenir resultats acurats i complementarietat amb les proves anteriors.

A més del seu paper com a lents gravitacionals, el cúmuls de galàxies es poden utilitzar directament per a aquesta tasca donat que la seva abundància i distribució espacial depèn de la quantitat d'energia fosca present. L'efecte en el número de

comptes de cúmuls com a funció del *redshift* ja s'està utilitzant per discriminar entre models [182, 129]. El mateix passa amb mesures del canvi de la fracció de gas que emet en raigs X en els cúmuls [6].

Finalment, la cosmologia no pot oblidar tota la informació amagada a la radiació còsmica de fons. Les mostres del CMB a favor d'un Univers pla [183] són i han estat una forta indicació de l'existència d'energia fosca. La seva naturalesa, però, s'explica millor amb altres experiments, mentre que el CMB és de màxima importància en l'estudi de l'Univers primordial i en la determinació de la densitat de matèria. De totes maneres, efectes relacionats com ara l'efecte Sachs Wolfe integrat (ISW) utilitzen aquesta radiació ben coneguda per tal de confirmar la detecció de l'energia fosca a través de mètodes complementaris [51, 88, 37].

## Models d'evolució de la constant cosmològica

La primera tasca d'aquesta tesi ha estat motivar un marc on la constant cosmològica experimenta de manera natural una evolució amb el temps. En aquest cas, l'evolució dependrà de les partícules de manera que el seu valor pot quedar justificat per aquestes i solucionar el problema de la constant cosmològica.

En el context d'una teoria quàntica de camps amb els camps situats en un espai-temps corbat (aproximació semiclàssica), l'acció de la teoria inclou un terme d'interacció amb el camp gravitatori. Per tal que la teoria sigui renormalitzable, cal afegir la constant cosmològica a l'acció de Hilbert-Einstein i nous termes amb derivades d'ordre superior de la mètrica a l'acció total. Després del procés de regularització, es trenca la invariança d'escala i els paràmetres de la teoria passen a dependre de l'energia. Aquesta dependència es veu reflectida en les equacions del grup de renormalització. Concretament la funció  $\beta$  és la que descriu l'evolució de la constant cosmològica (i la constant de Newton) amb l'escala de renormalització  $\mu$ .

El càlcul de la funció  $\beta$  resulta complicat en un espai-temps corbat i s'acostuma a fer pertorbativament sobre un espai-temps pla. Així, s'ha calculat  $\beta_\Lambda$  en l'esquema  $\overline{\text{MS}}$ :

$$\begin{aligned} \frac{d\Lambda}{d \ln \mu} &= \frac{1}{(4\pi)^2} \left( \sum_i A_i m_i^4 + \mu^2 \sum_j B_j M_j^2 + \mu^4 \sum_j C_j + \mu^6 \sum_j \frac{D_j}{M_j^2} + \dots \right) \\ &\equiv \sum_{n=0}^{\infty} \sum_i \alpha_{in} \mathcal{M}_i^4 \left( \frac{\mu}{\mathcal{M}_i} \right)^{2n} \equiv \beta_{\Lambda}(\mathcal{M}_i, \mu/\mathcal{M}_i), \end{aligned}$$

on  $m_i$  són els graus de llibertat lleugers amb  $\mu > m_i$ ,  $M_j$  són els pesants amb  $\mu < M_j$ , i  $i$  i  $j$  representen els camps massius.  $A, B, C$  i  $D$  són constants, i  $n$  l'ordre del desenvolupament.

Per solucionar els problemes d'interpretació d'aquest esquema cal plantejar diverses hipòtesis sobre el significat de l'escala de renormalització i sobre el desacoblament dels graus de llibertat massius. Això ens ha fet considerar tres escenaris cosmològics diferents:

Escenari	$\mathcal{M}$ actius	Partícules	$\mu$
1	$m_i < \mu$	neutrins	$\rho_c^{1/4}(t)$
2	$M_i > \mu$	SM	$\rho_c^{1/4}(t)$
3	$M_i > \mu$	Plank	$H(t)$

El domini dels graus de llibertat massius  $M_i$  és possible en el cas de la constant cosmològica perquè gràcies a la seva dimensionalitat experimenta el que s'anomena un desacoblament suau.

Amb les especificacions de la taula superior, l'evolució de la constant cosmològica per a l'Escenari 1 és:

$$\Lambda(\rho) = \Lambda_0 + \frac{1}{(4\pi)^2} \left( \frac{1}{2} m_S^4 - 4 \sum_{\nu} m_{\nu}^4 \right) \ln \frac{\rho}{\rho_0},$$

i per a l'Escenari 2:

$$\Lambda(\rho) = \Lambda_0 + \frac{1}{(4\pi)^2} \left[ \frac{1}{4} \left( m_H^2 + 3m_Z^2 + 6m_W^2 - 4 \sum_i N_i m_i^2 \right) \rho^{1/2} + \left( \frac{1}{2} \sum_i N_i - \frac{5}{4} \right) \rho \right].$$

Les conseqüències de l'Escenari 3 han estat desenvolupades especialment. Les equacions de la cosmologia depenen en aquest cas d'un únic paràmetre funció de les masses  $M$  properes a l'escala de Planck  $M_P$ :  $\nu = \sigma M^2 / 12 \pi M_P^2$ . La resolució de les equacions del grup de renormalització conjuntament amb l'equació de Friedmann i la de continuïtat mostren l'evolució de la constant cosmològica com a funció del *redshift*, la variable més convenient observacionalment:

$$\Lambda(z; \nu) = \Lambda_0 + \rho_M^0 \frac{\nu}{1-\nu} \left[ (1+z)^{3(1-\nu)} - 1 \right] + \rho_M^0 \frac{2\nu\Omega_K^0}{1-3\nu} \left\{ \frac{z(z+2)}{2} + \frac{\nu}{1-\nu} \left[ (1+z)^{3(1-\nu)} - 1 \right] \right\}.$$

Es produeix una transferència d'energia entre la matèria i la constant cosmològica, ja que el fet que aquesta evolucioni afegeix el terme d'intercanvi en l'equació de continuïtat. D'aquesta manera, la matèria també es veu afectada pel *running*. Això evidentment afecta l'expansió de l'Univers i té repercussió en observables com la distància-lluminositat. Per fer que l'evolució sigui compatible amb el model de Big Bang cal que l'índex cosmològic  $\nu$  estigui restringit al rang  $|\nu| \ll 1$ . Aquest límit no resta potència al model perquè el valor més natural obtingut per a  $M \sim M_P$  correspon a aquest interval:  $\nu_0 = 1/12\pi \approx 0,026$ .

Dintre d'aquest rang i comparant amb el model cosmològic estàndard amb  $\nu = 0$ , es pot veure (Fig. 1) que per un índex cosmològic negatiu la densitat de matèria creix més ràpid cap al passat, mentre que per  $\nu$  positiu el creixement és més lent que l'habitual  $(1+z)^3$ . Mirant cap al futur la distinció no és apreciable perquè per qualsevol valor de  $\nu$  la densitat de matèria tendeix a zero. El contrari passa per la constant cosmològica. És per  $\nu$  positiu (negatiu) que la constant cosmològica augmenta (disminueix) cap al passat, mentre que en el futur tendeix a un valor positiu i constant. Òbviament, el canvi en  $\rho(z; \nu)$  i  $\Lambda(z; \nu)$  respecte el cas estàndard causa variacions en altres paràmetres relacionats com ara el paràmetre de Hubble, el de desacceleració, o el *redshift* de transició en què es produeix el pas d'un univers dominat per matèria a un dominat per la constant cosmològica. Tots ells paràmetres que haurien d'ajudar a detectar l'evolució mitjançant observacions a distàncies properes.

Per altra banda, els tests sobre aquests models no s'haurien de restringir només a distàncies properes. Els efectes del *running* han estat comparats amb resultats del CMB o el creixement de les pertorbacions de densitat [136, 77] confirmant la necessi-

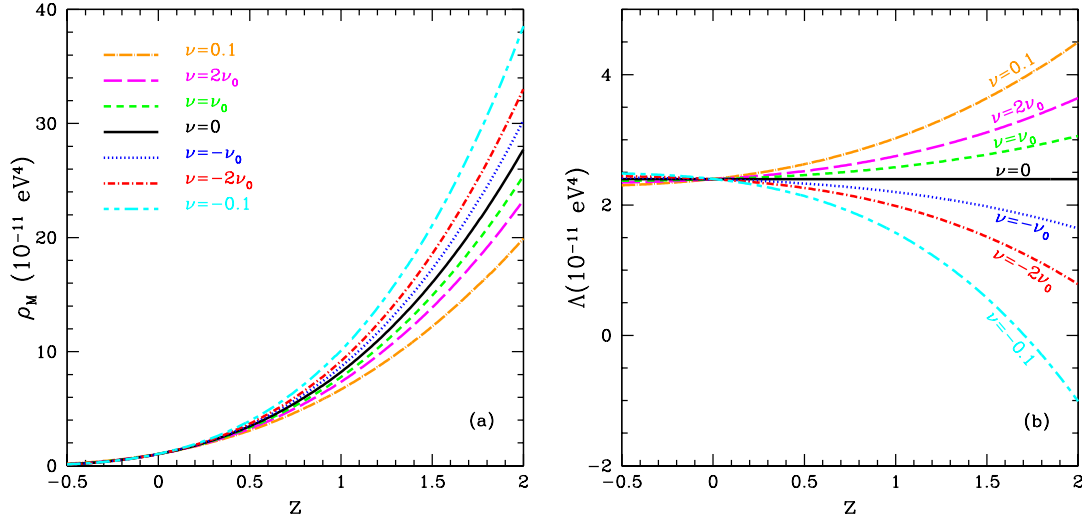


Figura 1: (a) Densitat de matèria i (b) constant cosmològica en un univers pla amb  $\Omega_M^0 = 0,3$  i  $\Omega_\Lambda^0 = 0,7$  segons el *running* a l'Escenari 3.

tat de  $|\nu| \ll 1$ . Dintre d'aquest treball tampoc s'han explorat les conseqüències que poden tenir els termes d'ordre més gran afegits a l'acció per motius de renormalitzabilitat, com ara la causa d'un període inflacionari. Si això fos així, es completaria una manera elegant de generar la inflació i, a la vegada, explicar l'acceleració actual. En aquesta tesi, però, ens hem centrat principalment en utilitzar les observacions de SNeIa que s'obtenen de l'Univers més proper,  $0 < z < 2$ , i comparar aquesta família de models amb altres tipus de fonts d'energia fosca.

Per poder fer la comparació pot ser útil caracteritzar tots els models d'una mateixa manera. Normalment aquesta manera és determinar la seva equació d'estat:  $p(t) = w(t)\rho(t)$ . Aquesta és la descripció per a un camp de quinta essència i aquí el considerarem com a arquetip. Matemàticament, però, la major part de les fonts d'energia fosca es poden reescriure com un fluid perfecte amb una pseudo-equació d'estat de la forma  $p = \tilde{w}(z)\rho$ . Això permet tractar qualsevol model en una mateixa equació de Friedmann amb la densitat d'energia fosca definida per  $\tilde{w}$  (Eq. 4.10). Hem deduït o compilat la quantitat  $\tilde{w}(z)$  per a alguns dels candidats d'energia fosca més prometedors: un gas Chaplygin, models Cardassian, modificacions a la relativitat general, models de loop quantum cosmology, i, evidentment, models d'evolució de la constant cosmològica per efectes de renormalització. És d'esperar que d'aquesta manera resulti més fàcil identificar el model real a partir d'observacions. Però en el fons, ens trobem davant una primera indicació del problema de degeneració que

afrontem amb l'energia fosca: si cada model es pot expressar com un fluid perfecte amb  $\tilde{w}$ , haurà d'estar degenerat amb el corresponent model de quinta essència amb  $w$  i amb les altres alternatives caracteritzades amb la mateixa  $\tilde{w}$ .

La degeneració en  $w(z)$  rep també altres contribucions. La forma matemàtica que relaciona l'equació d'estat amb l'observable distància-lluminositat, una integral doble, suavitza qualsevol evolució possible. Per altra banda, quan es determina conjuntament amb altres paràmetres, les correlacions entre ells augmenten la degeneració de l'equació d'estat amb petits canvis dels paràmetres cosmològics. La solució a aquest últim problema ve donada per incloure *priors* i combinar resultats d'altres mètodes. El primer problema és característic de l'ús de distàncies extragalàctiques i afectarà els nostres resultats amb SNe Ia. A més, la dispersió intrínseca de les supernoves actualment o el nivell de sistemàtics en experiments futurs limitarà també la discernibilitat que es podrà detectar, que acabarà sent el que defineixi el significat pràctic de degeneració.

## A la recerca de la cosmologia subjacent

Tot i les limitacions que acabem de nomenar en l'ús de les SNe Ia, aquesta candela estàndard calibrable segueix sent una de les millors eines de què es disposa, i les seves determinacions del model cosmològic de les més precises. A continuació, s'utilitzaran les dues compilacions de supernoves més recents: les 182 SNe Ia de Riess et al. (2006) [160] (R06) i les 162 SNe Ia de Wood-Vasey et al. (2007) [211] (VW07).

Cal dir que ambdós conjunts difereixen tant en el *redshift* mitjà com en els mètodes de calibració de les supernoves. És per això que mentre R06 afavoreix un univers de densitat elevada, VW07 es decanta per un univers de densitat més baixa. De fet, alguns dels resultats que es mostren a continuació són incompatibles entre ells a un nivell d' $1\sigma$  abans d'utilitzar informació *a priori* complementària (Fig. 2). Quan imposem que la cerca es restringeixi a un univers pla com indica l'estudi del CMB, aquesta discrepància entre la densitat de l'Univers és trasllada al comportament de l'energia fosca. Les dades de R06 tendeixen a universos on l'energia fosca s'està fent important ara, mentre que amb VW07 la seva densitat augmenta en el passat. Hem mostrat que la diferència en el *redshift* mitjà ( $\langle z_{R06} \rangle = 0,54 \pm 0,35$  vs.  $\langle z_{VW07} \rangle = 0,38 \pm 0,27$ ) no és exclusivament responsable d'aquest desacord obtenint resultats per al subconjunt de *redshift* més baix de R06 de manera que fos comparable

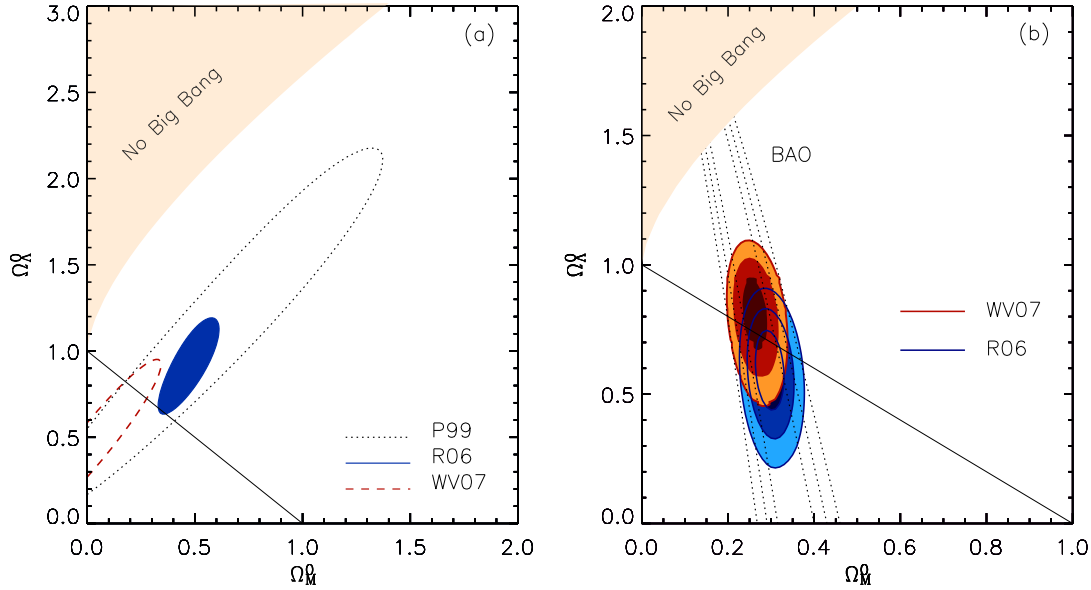


Figura 2: Regions de confiança per als paràmetres cosmològics utilitzant dos conjunts de dades: R06 [160] i VW07 [211]. (a) Regions  $1\sigma$  on es comparen els resultats actuals amb els que es tenien a finals dels 90 (Perlmutter et al. (1999) [145]). (b) Regions  $1\sigma$ ,  $2\sigma$  i  $3\sigma$  obtingudes en afegir la informació de les BAO. La inclusió dels *priors* afecta considerablement les conclusions obtingudes amb les SNe la soles.

amb VW07. Així, les diferències s'han d'atribuir majoritàriament a les tècniques de calibració, no només entre els dos conjunts de dades sinó també entre subconjunts com passa en la compilació de R06.

Per completitud utilitzem els dos conjunts de dades. Els paràmetres d'una cosmologia estàndard amb constant cosmològica o una font d'energia fosca que evoluciona amb el temps segons  $w(z) = w_0 + w_a z/(1+z)$  s'han determinat per diversos mètodes amb ambdós conjunts de dades. També han estat ajustades algunes teories alternatives per tal de comparar-les amb aquesta parametrització estàndard. En aquesta tesi, es presta una atenció especial als models de *running* de la constant cosmològica. Per cada un dels tres escenaris que hem descrit definim un paràmetre que engloba tots els efectes de l'evolució (en general els anomenem  $\theta$ ):

$$\tau \equiv \frac{1}{2}m_S^4 - 4 \sum_{\nu} m_{\nu}^4 \quad \text{per a l'Escenari 1,}$$

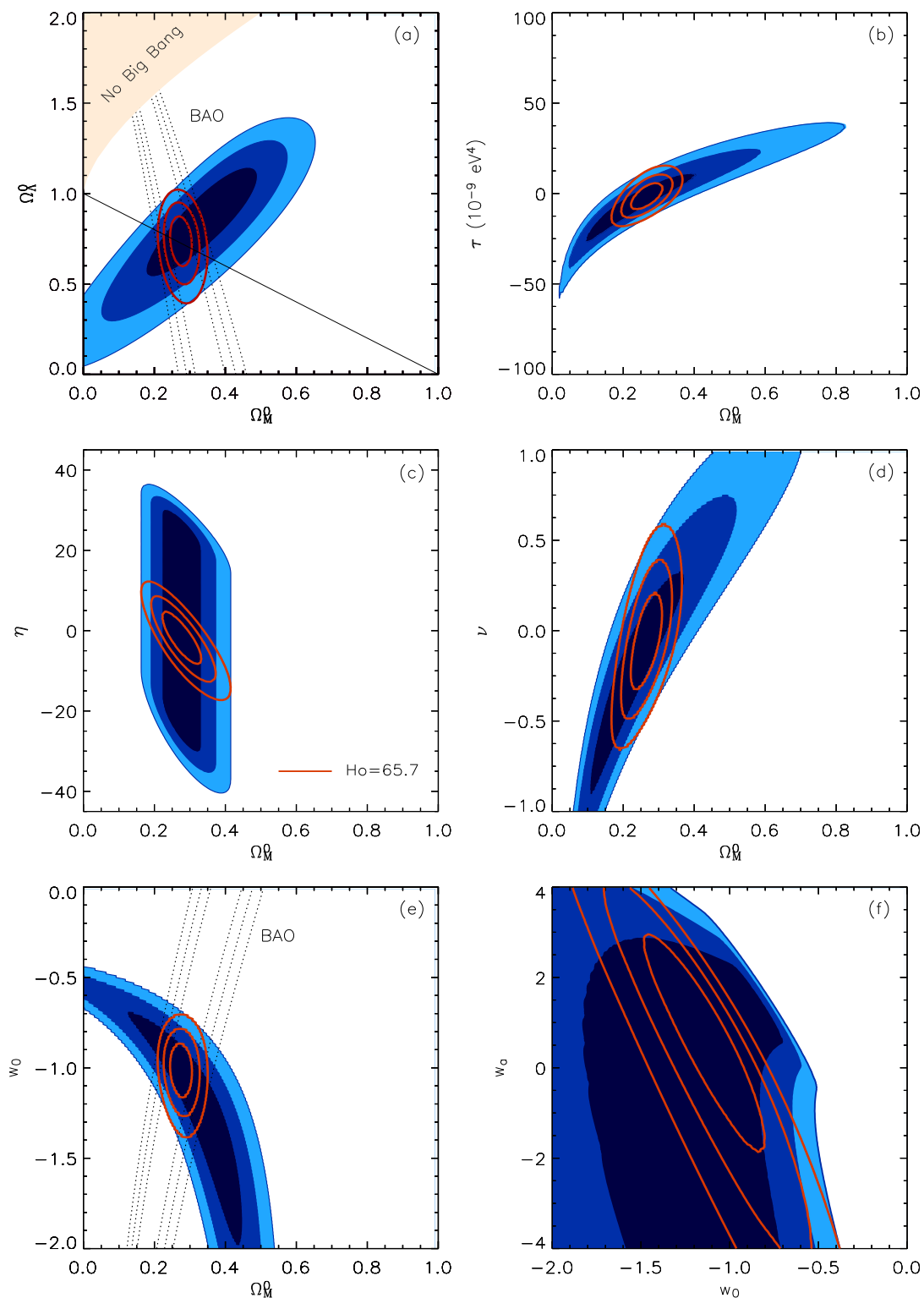


Figura 3: Regions de confiança per als paràmetres relacionats amb la forma de l'energia fosca obtinguts amb les dades de la Ref. [56]. Les corbes vermelles afegeixen un *prior* en les determinacions (veure Capítol 6 per als detalls).

$$\eta \equiv \frac{1}{2} \sum_i N_i - \frac{5}{4} \quad \text{per a l'Escenari 2,}$$

$$\nu \equiv \frac{\sigma}{12\pi} \frac{M^2}{M_P^2} \quad \text{per a l'Escenari 3.}$$

El paràmetre  $\tau$  de l'Escenari 1, és compatible marginalment a  $1\sigma$  amb l'absència observable de *running*. Els resultats amb les dades de VW07 estan més a prop de la constant cosmològica; els de R06 afavoreixen una evolució negativa amb el *redshift*. Aquesta evolució negativa permet de donar un límit superior a la massa dels neutrins més lleugers de  $m_\nu = 0,007 \pm 0,006 \text{ eV}$ . Per l'evolució positiva, la massa dominant ha de ser la d'un camp escalar que contraresta l'efecte dels neutrins de manera que l'evolució es comporta com si fos produïda per una massa efectiva de l'ordre de  $m_{eff} = 0,01 \pm 0,01 \text{ eV}$ . La degeneració de  $\tau$  amb  $\Omega_M^0$  és important, i afegir el *prior*  $\Omega_M^0 = 0,27 \pm 0,03$  disminueix la incertesa en la determinació a la meitat. Malgrat que d'aquesta manera el valor de  $\tau$  està més a prop de la manca d'evolució, la constant cosmològica o l'absència d'una evolució efectiva segueix estant a més d' $1\sigma$  del millor ajust.

A l'Escenari 2, el paràmetre que té en compte el *running*,  $\eta$ , està altament degenerat amb la constant de Hubble (de fet, en general amb qualsevol forma del punt zero de la magnitud). Això fa imprescindible la informació de  $H_0$  per poder trencar la degeneració. Un cop fixem el seu valor a aquell determinat per cada conjunt de dades, la constant cosmològica està dintre dels intervals de probabilitat d' $1\sigma$ , però el valor predit pel model estàndard de partícules,  $\eta = 10,75$ , s'aparta del millor ajust en més de  $2\sigma$  per les dades de R06 i just en el límit per VW07. Encara que sembla clar que el model estàndard es veurà modificat amb la inclusió de noves partícules a mesura que ens apropem a l'època de Planck, de moment això fa aquest escenari menys atractiu observacionalment que els altres dos.

Per a l'Escenari 3, les coses són molt similars a l'Escenari 1. El comportament de  $\nu$  i  $\tau$  és exactament el mateix, però  $\tau$  porta implícita la informació com una quarta potència,  $\tau \propto m^4$ , i el seu coneixement permet restringir el valor de la massa. En el cas de  $\nu$ , els models teòrics es decanten per valors molt propers a zero, i les dades actuals no poden obtenir la precisió adequada per diferenciar aquests valors de del cas d'una veritable constant cosmològica. Les dades de R06 descarten  $\nu_0 = 0,026$  a més d' $1\sigma$  i privilegien les evolucions negatives. Per VW07, en canvi,  $\nu_0$  és perfectament compatible, però les incerteses de més de 10 vegades el seu valor fan difícil de restringir-lo. Tot i així, s'afavoreix una evolució positiva i pronunciada

amb aquest conjunt. Cal notar que, en aquest cas, encara que s'arribés a determinar  $\nu = 0$  amb gran precisió això podria ser signe de l'absència de partícules properes a l'escala de Planck, i no implicarà necessàriament la invalidesa de la teoria.

En resum, veiem que les dades actuals de SNe Ia no són suficients per restringir significativament els paràmetres de la física de partícules, i els models de la física de partícules amb els paràmetres estàndard no acaben de descriure les observacions satisfactòriament, cosa que obre la porta a una nova física. No obstant això, hem vist que fins i tot el signe de l'evolució acaba depenent de les dades utilitzades, i caldrà esperar missions futures per tal d'obtenir valors acurats. De moment, els dos conjunts han estat combinats igualant els seus punt zero (Davis et al. (2007), D07, [56]). Aquesta combinació s'ha d'acabar fent amb la calibració de totes les dades amb un mateix mètode, però ara, serveix per obtenir una visió més general dels resultats. Com era d'esperar, els resultats estan a mig camí entre R06 i VW07 (Fig. 3). D'ells, no se'n desprèn cap necessitat de *running*, evolució o partença de  $w_0 = -1$ : si l'energia fosca no és la constant cosmològica almenys s'ha de comportar com si ho fos. De fet, el *running* ha d'existir si la constant cosmològica es considera dintre d'una teoria quàntica de camps, però els seu efecte actual seria inapreciable. Tanmateix, les regions de confiança encara estan lluny de poder restringir els models de *running* de la constant cosmològica, i, com acabem de dir, noves dades es fan necessàries.

En comparar aquests resultats amb els d'una equació d'estat constant, es pot veure que les dades actuals posen cotes molt més restringents per  $w_0$  que per  $\theta$ . R06 o VW07 acoten  $w_0$  amb una precisió del 10% si es considera el *prior* gaussià de les BAO. A més, la constant cosmològica sempre es manté dintre dels intervals d' $1\sigma$ . En els escenaris 1, 2 i 3, la constant cosmològica s'allunya de vegades fins a  $2\sigma$  del millor ajust i les incerteses en  $\tau$ ,  $\eta$  i  $\nu$  mai s'acosten a aquest 10%, i, el que és pitjor, en molts casos arriben a ser del 100%. La justificació està basada en el comportament de l'energia fosca. Per a les dues famílies de models, l'evolució s'engloba en un únic paràmetre, però la física és diferent perquè una  $\theta$  constant implica una  $\tilde{w}(z)$  amb evolució. Això fa que les diferències degudes al *running* siguin importants respecte a una veritable constant cosmològica a *redshifts* alts, mentre que a *redshift* zero ja es poden observar les diferències entre models d'equació d'estat constant. És degut a això que es necessiten dades a més alt *redshift* per detectar els escenaris amb *running* que no pas diferents equacions d'estat constants.

## Reconstruccions amb un mètode invers

Abans de veure com les missions futures per obtenir SNe Ia poden millorar el coneixement dels paràmetres anteriors, sembla profitós comprovar si determinacions de les funcions contínues  $\Lambda(z)$  i  $w(z)$  ens aporten més informació ja en l'actualitat. Per fer-ho, es necessita un mètode matemàtic que permeti recuperar funcions a partir d'un conjunt discret de dades. Els mètodes inversos acostumen a afrontar aquest problema. En aquest treball, n'adaptem una aproximació bayesiana no lineal i no paramètrica per a les reconstruccions.

Aquest mètode invers tracta les dades i les incògnites de la mateixa manera. Les dades són mesurables directament i es caracteritzen pel valor mesurat i la seva incertesa; les incògnites no són mesurables directament i s'han de descriure per informació *a priori*. Si s'assumeix que les dues quantitats estan distribuïdes de forma gaussiana, la funció objectiu a minimitzar es compon de dos termes que representen densitats de probabilitat gaussianes:

$$S \equiv \frac{1}{2} (\mathbf{y} - \mathbf{y}^{th}(\mathbf{M}))^* \mathbf{C}_y^{-1} (\mathbf{y} - \mathbf{y}^{th}(\mathbf{M})) + \frac{1}{2} (\mathbf{M} - \mathbf{M}_0)^* \mathbf{C}_0^{-1} (\mathbf{M} - \mathbf{M}_0).$$

La primera es correspon amb la informació donada per les dades i és la mateixa que en una minimització  $\chi^2$ . La segona afegeix la informació *a priori* en les incògnites, com havíem fet amb anterioritat en les parametritzacions discretes amb el teorema de Bayes. Aquesta és la raó per què diem que és una aproximació bayesiana, i és necessària per tal de regularitzar la inversió. La minimització de la funció objectiu s'ha fet mitjançant un mètode de Newton aproximant el hessià de manera que els termes de segon ordre no s'han tingut en compte. Això porta a una funció iterativa per a cada paràmetre (o funció) que es vol determinar, i, un cop s'ha arribat al mínim, a una expressió per a la incertesa. Per exemple, per a l'equació d'estat:

$$w_{[k+1]}(z) = w_0(z) + \sum_{i=1}^N W_{i[k]} \int_0^{z_i} C_w(z, z') g_{w[k]}(z') dz',$$

$$\tilde{\sigma}_{w(z)}(z) = \sqrt{\sigma_{w(z)}^2 - \sum_{i,j} C_w \cdot \frac{\partial y_i^{th}}{\partial w(z)} (S^{-1})_{i,j} \frac{\partial y_j^{th}}{\partial w(z)} \cdot C_w}.$$

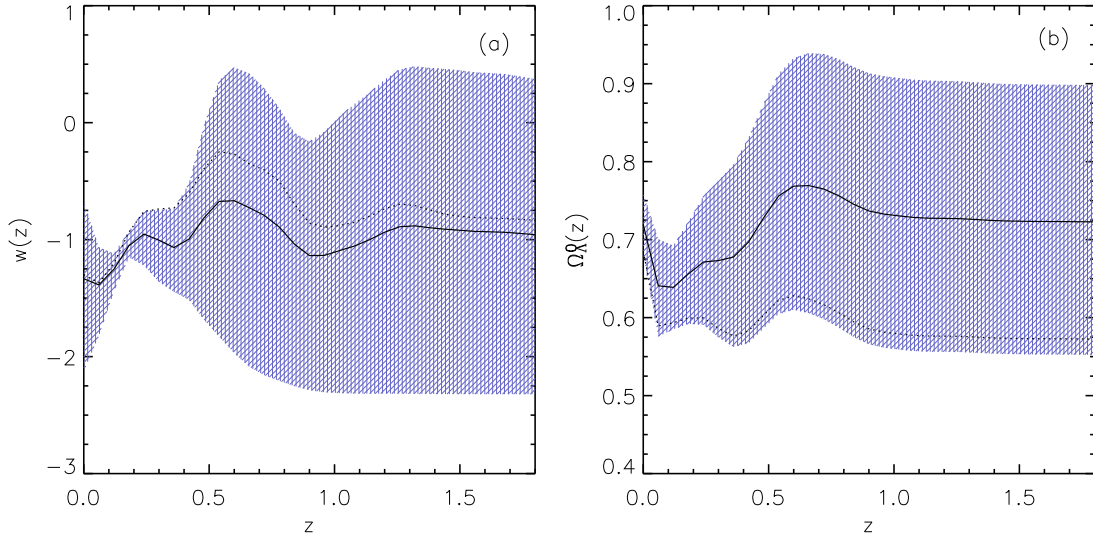


Figura 4: (a) Reconstrucció de  $w(z)$  i (b)  $\Omega_{\Lambda}^0(z)$  a partir de 1000 inversions de les dades de R06 amb *priors* aleatoris entre  $-3 < w(z)^0 < 1$ . La línia contínua mostra la mitjana de les inversions i la de punts la inversió amb  $S$  mínima.

Els *priors* sempre juguen un paper en aquest mètode. Tant la solució com la incertesa depenen del *prior*, però si aquests són prou amplis la dependència es debilita. El problema és que els *priors* amplis no sempre permeten la convergència de l'algoritme. Aquest contratemps se supera amb una exploració Monte Carlo de l'espai de solucions. Per a l'equació d'estat s'ha utilitzat  $-1,5 \leq w(z) \leq -0,5$  ampliant-lo a  $-3 \leq w(z) \leq 1$  en l'exploració Monte Carlo. En la reconstrucció de  $\Lambda(z)$ , s'ha deixat variar la densitat en el rang  $-0,1 < \Delta\Omega_{\Lambda}^0(z) < 0,1$ ,  $-0,2 < \Delta\Omega_{\Lambda}^0(z) < 0,2$  en l'exploració Monte Carlo.

En aquest enquadrament i les supernoves de R06,  $w(z)$  creix des de  $w < -1$  cap a  $w(z = 0,6) \gtrsim -0,5$  (Fig. 4 (a)). A *redshifts* més alts, es recupera el *prior* o la mitjana de l'interval de l'exploració Monte Carlo dependent del cas. Una funció anomenada *resolving kernel* ens indica la regió on les dades contenen prou informació com per millorar el coneixement *a priori*. Per al conjunt R06, els kernels són gairebé plans a  $z \gtrsim 0,6 - 0,7$ , cosa que indica l'absència d'informació. El mateix passa a  $z = 0$ . En el rang d'interès, el mètode recupera una evolució positiva, tal com havíem obtingut en la parametrització discreta. No obstant això, els errors Monte Carlo demostren que el resultat és compatible amb la constant cosmològica al nivell de probabilitat d' $1\sigma$  gairebé en tot el rang de *redshift*. Aquest tret és més fort per les dades de VW07, on la reconstrucció mostra oscil·lacions entorn un valor constant

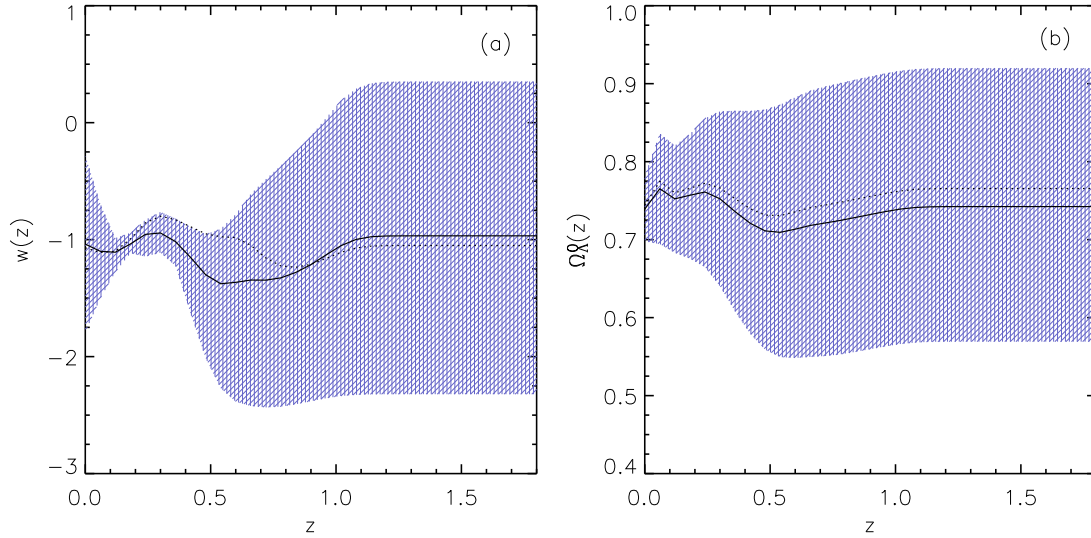


Figura 5: Com la Figura 4 per les dades de VW07.

de  $w(z) = -1$  (Fig. 5 (a)).

Sota el punt de vista de la densitat de constant cosmològica (o densitat d'energia fosca) evidentment es reproduïen els mateixos resultats. Per VW07 no es pot descartar una densitat constant, tot i que a *redshifts* intermedis hi ha una tendència suau amb pendent negativa, que queda amagada dintre les incerteses i la degeneració respecte  $\Omega_M^0$  (Fig. 5 (b)). Al igual de la resta de resultats, la Figura 4 (b) mostra que les dades de R06 afavoreixen una evolució positiva de  $\Omega_\Lambda^0(z)$ . Per a aquesta funció, els resultats s'aparten del *prior* també només a  $z \lesssim 0,6 - 0,7$ . El canvi en el pendent a *redshifts* més alts només apareix perquè la funció ha d'acabar tendint al *prior*. Per consegüent, resulta molt difícil detectar qualsevol dels escenaris de *running* de la constant cosmològica a partir d'aquestes reconstruccions, ja que el seu efecte només és important a alt *redshift* on hem recuperat la informació d'entrada.

La precisió donada per les dades actuals no permet identificar clarament el comportament d'un model d'energia fosca en concret. Amb les parametritzacions discretes, estem limitats a conèixer les funcions a partir dels seus valors actuals i, com a molt, de la primera derivada a *redshift* zero. Una part de la millora aconseguida amb el mètode invers ha estat calcular el valor de les funcions a altres *redshifts* on les dades poden ser més sensibles i obtenir precisions diferents a cada punt segons la quantitat d'informació en aquell lloc. Cada supernova s'utilitza en els càlculs de cada *redshift*, amb un pes superior aquelles que en són més properes. Aquesta és la

raó per la qual no hi ha cap guany en informació a  $z \gtrsim 0,7$ . La falta de conjunts de dades grans a *redshifts* alts no afecta només les determinacions d'aquests *redshifts*, sinó també les dels inferiors, ja que la contribució de les dades properes és escassa. Aquesta també és la raó per què les funcions estan molt millor determinades a  $z = 0,2$  que a  $z = 1,2$ , encara que els dos punts són valls en la densitat de supernoves. I, evidentment, és també la raó del mal ajust de  $z = 0$  en comparació amb els *redshifts* intermedis.

Per tal d'ampliar l'interval de *redshift* en què les SNe Ia contribueixen al guany en informació, el número de dades hauria d'augmentar significativament a alt *redshift*. Fins i tot així, les determinacions no podran ser tan bones com a *redshifts* intermedis perquè la mateixa energia fosca és menys rellevant al contingut i la dinàmica de l'Univers. De totes maneres, la incertesa disminuirà en conjunt a mesura que anem ampliant en número de SNe Ia proporcionalment al llarg del *redshift*. Per tal de quantificar aquesta millora, hem simulat dos conjunts de dades futures, les que obtindrà LSST com a representant dels projectes des de terra i SNAP com a prototip de les missions espacials.

## Perspectives futures

Avui en dia, s'estan dissenyant i planificant una gran quantitat de missions destinades a la detecció de SNe Ia i a l'estudi de l'energia fosca tant des de terra com des de l'espai. Tot i que LSST observarà unes 250000 SNe per any (al voltant de 10000 en l'exploració més profunda), es tracta d'un sondeig fotomètric i, per tant, la majoria de dades només tindran *redshifts* fotomètrics (photo- $z$ ). Aquest és un inconvenient habitual per a la majoria de missions massives des de terra, i la incertesa que es pugui aconseguir en els photo- $z$  repercuteix en la determinació dels paràmetres cosmològics i l'energia fosca. La incertesa en el *redshift* es trasllada a la magnitud de manera decreixent cap a *redshifts* alts. A baix  $z$ , la incertesa en la magnitud pot arribar a ser més gran que  $1\ mag$ , i el *redshift* a partir del qual s'estanca i es fa negligible depèn de la dispersió en els photo- $z$ . Per tant, si es vol minimitzar l'efecte dels photo- $z$  cal reduir la seva dispersió respecte els *redshifts* espectroscòpics, i el que és més important, eliminar completament els photo- $z$  de més baix  $z$  en favor de mesures espectroscòpiques.

Si s'aconsegueix fer aquests esforços en el tractament dels photo- $z$ , les dades

del LSST *deep survey* podrien millorar les determinacions de l'evolució de l'equació d'estat de l'energia fosca,  $w_a$ , dos (R06) o tres (VW07) vegades respecte els valors actuals, i aconseguir  $\sigma_{w_a} = 0,7$ . Aquest resultat és del mateix ordre del que es pot arribar amb SNAP, que, tot i arribar a *redshifts* més alts, té menys dades. Per contra, si no es té cap garantia de poder mesurar espectres per al conjunt de supernoves més properes, SNAP aconsegueix millors resultats, no únicament per aquest *redshift* límit més elevat, sinó pel seu millor control dels sistemàtics. Una equació d'estat constant es mesuraria en aquest cas amb una precisió de  $\sigma_{w_0} = 0,07$ , i l'evolució  $\sigma_{w_0} = 0,08$  i  $\sigma_{w_a} = 0,7$ . Aquestes incerteses s'haurien de comparar a les que es podran obtenir amb LSST *wide B*  $\sigma_{w_0} = 0,14$  i  $\sigma_{w_a} = 0,94$ , molt similars a les de LSST *deep*. En tots els casos, la inclusió del *prior* que aporten les BAO per una equació d'estat constant permet reduir apreciablement els errors.

Pel que fa als models on la constant cosmològica experimenta un *running* degut als efectes del grup de renormalització, els millors resultats s'obtenen amb les dades de SNAP, que divideix per la meitat les incerteses obtingudes amb LSST *deep* (Fig 6). Per SNAP, les incerteses en els paràmetres  $\theta$  per als tres escenaris són:  $\sigma_\tau = 2,1 \cdot 10^{-9} eV^4$  per a l'Escenari 1,  $\sigma_\eta = 1,1$  per a l'Escenari 2 i  $\sigma_\nu = 0,06$  per a l'Escenari 3. Això millora les incerteses actuals entre 5 i 10 cops depenent de l'escenari i el conjunt de dades. De totes maneres, tal com s'ha dit, aquesta família de models es diferencia d'una constant cosmològica a alt *redshift* perquè les evolucions són suaus i petites. Distribucions de dades que tinguin això en compte i amb la majoria de les dades a  $z > 1$  millorarien les determinacions significativament. Per donar un exemple, l'Escenari 3 amb un *running* moderat de  $\nu_0 = 0,026$  no es pot detectar ni tan sols amb SNAP ( $\sigma_\nu = 0,06$ ). Però una distribució alternativa d'aquest estil reduiria la incertesa a  $\sigma_\nu = 0,02$ , permetent així la distinció observacional entre el model amb *running* i una constant cosmològica real a més d' $1\sigma$ . D'altra manera, només es poden detectar els *runnings* més pronunciats. S'ha comprovat també si la mida de les regions de confiança depèn de la posició en el pla del millor ajust. De fet, els punts d'incertesa mínima són aquells amb  $\theta = 0$ , és a dir, sense *running*, però els canvis no són prou importants com per què evolucions molt suaus es puguin detectar únicament amb SNAP.

Finalment, la determinació de  $w(z)$  com a funció contínua també es veu afavorida pel major nombre de dades d'aquestes missions futures i pel *redshift* límit més alt que s'aconsegueix. La reconstrucció queda ben determinada fins a  $z = 0,7$  per LSST i  $z = 0,9$  per SNAP. A partir d'aquí, la incertesa en  $w(z)$  és molt asimètrica. Mentre

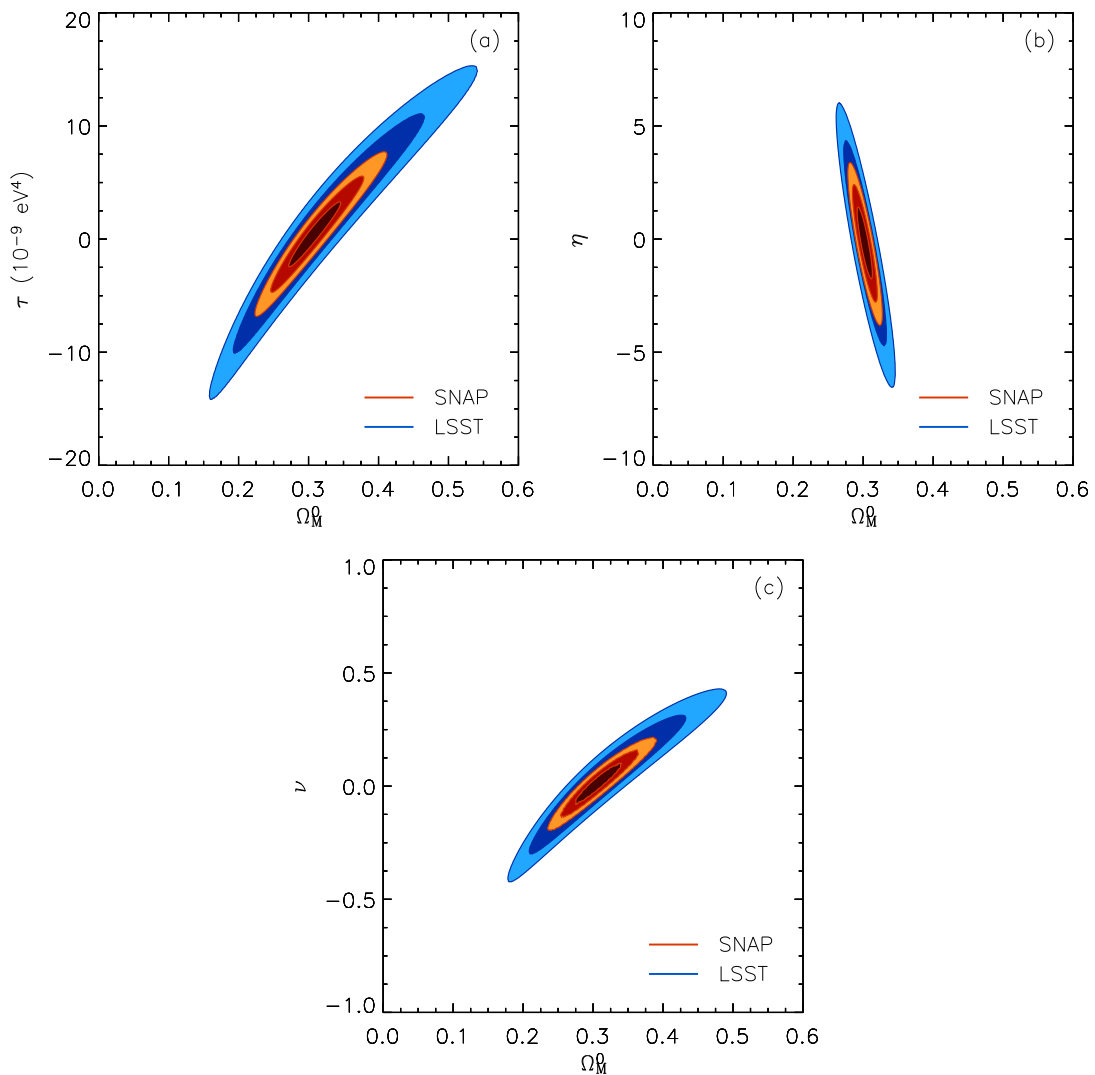


Figura 6: Regions de confiança  $1\sigma$ ,  $2\sigma$  i  $3\sigma$  per als paràmetres  $\theta$  del tres escenaris amb *running* de la constant cosmològica a l'espai  $(\Omega_M^0, \theta)$ . Els contorns blaus mostren les regions de probabilitat obtingudes amb LSST *wide survey* i les taronja amb SNAP.

que es manté moderada pel costat positiu fins a  $z = 1,2$  (LSST) o  $z = 1,5$  (SNAP), pel negatiu creix substancialment. Això és degut a la gran degeneració entre els models amb  $w < -1$  a alt *redshift*. Passat aquest punt, ni tan sols aquestes grans compilacions de dades són capaces de millorar el nostre coneixement *a priori*.

Amb aquestes simulacions de LSST i SNAP, s'han obtingut les millors perspectives que tenim per a l'estudi de l'energia fosca amb les SNeIa pel cap baix durant els propers 10 anys. A l'espera de nous mètodes matemàtics i físics, el guany en

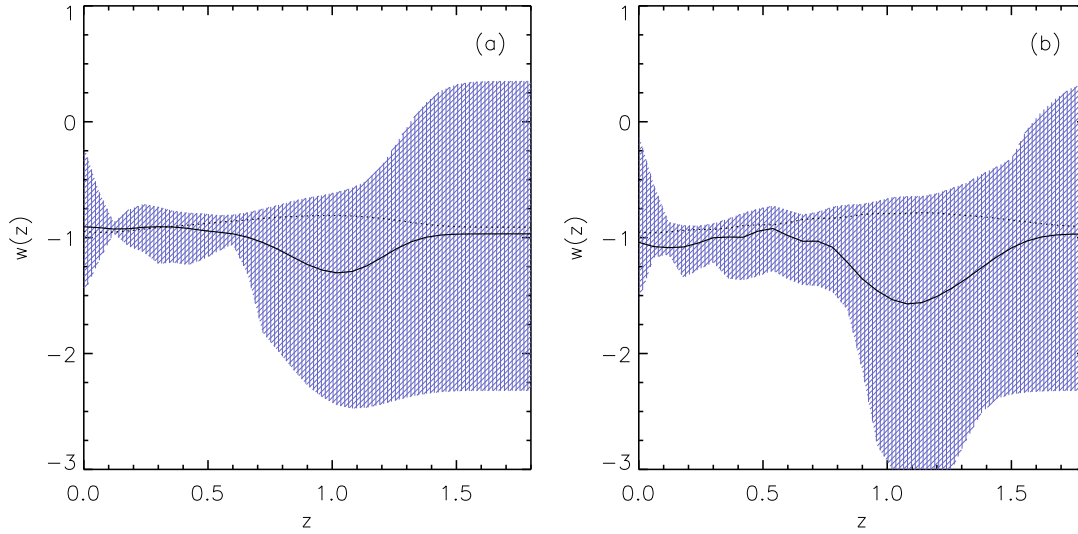


Figura 7: (a) Reconstrucció de  $w(z)$  i errors Monte Carlo obtinguts després de 1000 inversions de les dades de LSST *deep survey* amb  $\delta z = 0,01$  i  $\sigma_{sys} = 0,02$  i (b) SNAP amb  $\sigma_{sys} = 0,02 z/1,7$ .

precisió ens permetrà acotar el valor de  $w$  i  $\Lambda$ , però això no respondrà la pregunta de què és l'energia fosca, sobretot si els resultats són tan propers a una constant cosmològica com sembla. Estem força lluny de conèixer la funció de manera similar a com es coneix l'espectre de radiació del CMB, que de manera unívoca pot determinar que es tracta d'una emissió de cos negre a una temperatura de  $2,725 K$ . Per a l'energia fosca, ni les mesures arriben a aquest grau de precisió ni trobem al darrera una teoria física que les recolzi amb convicció. Si els resultats futurs descartessin la constant cosmològica, serien més fàcils d'interpretar o, com a mínim, més informatius, i potser concordarien amb prediccions d'alguna de les teories proposades. Si els resultats acaben confirmant un comportament com el de la constant cosmològica estem en un problema: no sabem que és la constant cosmològica físicament, almenys si no canvia en  $10^{55}$  ordres de magnitud.

Això obre tres possibles línies de treball. (i) Continuar treballant en teories que permetin acabar d'entendre el significat de la constant cosmològica ja que sembla la resposta més plausible donades les observacions. (ii) Justificar variacions d'un model de constant cosmològica amb models teòrics alternatius i validar-los amb el contrast amb observacions. (iii) Explicar l'acceleració de l'expansió a partir de noves idees i mirar d'atacar el problema per un altre costat.

Evidentment, s'haurien de seguir tots els camins ja que només el temps ens dirà quin és el correcte. Potser ja estem a punt d'interpretar correctament el significat de la constant cosmològica. O potser només estem fent com Ptolomeu ajustant epicles quan un canvi d'aproximació descriu clarament les observacions. Esperem no necessitar 15 segles per adonar-nos que estem equivocats... en cas que ho estiguem!



## Chapter 1

---

# Introduction

---

*The most exciting phrase to hear in science, the one that heralds new discoveries, is not 'Eureka!' but 'That's funny...'*

Isaac Asimov

One of the funniest and most counter-intuitive scientific discoveries of the last times is that the Universe is experiencing an accelerated expansion. Nowadays, there is almost full agreement about the Big Bang model: the Universe's expansion originated from an initial state of enormous density and temperature and, since then, it has always been growing and cooling. But, what about the effect of gravity? Shouldn't matter make the expansion slow-down? Why is it accelerating now?

### 1.1 The Big Bang theory

The closest thing we can say about the birth of the Universe is that its expansion began in an explosion which made its content and the fabric of the cosmos itself blow away. That was first taken seriously during the 30s as a consequence of Albert Einstein's equations, the solution reached by Georges Lemaître in the cosmological case, and the experimental results of Vesto Slipher and Edwin Hubble which proved that galaxies were receding from us. At first, the idea had lots of detractors, because it was against the common belief of a static universe. Besides, looking back in an expanding universe, one should find an initial point where everything was joined together. That implied an origin, and, for some people, a creator. The interpretation

has changed through time, and nowadays one understands the Big Bang model as a description of the Universe up to the Planck time, without any assumption of the origin point. Up to now, the Big Bang model has overcome all tests, and some crucial results clearly support it. There are four pillars on which the Big Bang theory is sustained, four main predictions accurately tested.

First of all, of course, the observational confirmation that the Universe was expanding. Edwin Hubble and Milton L. Humason were working on the measure of distances and redshifts at Mount Wilson. That together with Slipher's measures made the astronomers realise that the further the galaxy the more redshifted were the lines in the spectra. Therefore, galaxies had to be receding from us. As a consequence, they established a relation between distances and radial velocities of galaxies in 1929, the Hubble law [105].

Later, in 1948, George Gamow justified the chemical abundances in the Universe as a result of the reactions that took place during the Big Bang [8]. This primordial nucleosynthesis is responsible for the formation of all the observed elements lighter than beryllium [135, 185].

Gamow himself realised in its calculations that, as a remnant of such a big explosion and all the produced reactions, there should be a background of radiation cooling down since the explosion. At that time, technology was not prepared to measure such a low energy radiation, but some years later in 1964, Arno Penzias and Robert Wilson, almost by chance, discovered the Cosmic Microwave Background radiation (CMB) [143]. A group led by Robert Dicke was working then on the detection of the bath of photons [62] and they could jointly explain the observations.

The detection of the predicted radiation firmly settled the Big Bang model as the standard cosmological model. Even most of cosmologists supporters of a steady state universe could not find solid arguments against the Big Bang. Still, there is a fourth strong prediction. Once the Universe cooled enough in order to be dominated by matter, the force of gravity should make any overdense inhomogeneity collapse and be the seed for future clusters of matter: the observed large scale structure of the Universe. Besides the evident proof that we are surrounded by associations of matter such as galaxies or clusters, again the CMB radiation shows the seeds for the structure formation as small temperature anisotropies of order  $10^{-5}$ . These anisotropies were first observed by the COBE satellite (COsmic Background Explorer) in 1992 [178].



Figure 1.1: The four pillars of the standard hot Big Bang model.

Despite the great success of the Big Bang theory, there are some results that cannot be explained from its principles alone or that would need a very fine tuning. Some of them are what we could call the classical problems: How can all the observed universe be homogeneous at large scale if all of it could not be causally connected in the Big Bang? How can our Universe be so close to be flat if that implies an accuracy on the initial curvature of  $10^{-60}$ ? How did the asymmetry between matter and antimatter occur? Some others are linked to the knowledge of the new contents of the Universe being necessary to account for the observations: What is dark matter? Why is the Universe accelerating now? (Or what is dark energy?)

### 1.1.1 A perfect complement: inflation

As an idea for solving mainly the two first problems, the classical ones, Alan Guth [96] and Andrei Linde [123, 4] introduced the inflationary theories. There are several variations of inflation but in all of them the space-time experiments a period of exponential expansion. In Guth's original theory, a universe settled in a false vacuum decays to a lower vacuum state. The bubbles of the true vacuum in the metastable state rapidly expand. In Linde's theory, a scalar field, the inflaton, rolls down its potential causing an accelerated expansion until it reaches the minimum and the inflaton decays into radiation.

Inflation in this simple form already solves four of the problems that the standard Big Bang model alone cannot explain. First of all, such a rapid and enormous expansion would dilute the density of monopoles to such extent to make it small enough so that we do not see any of them in the observable universe. Secondly, it would allow the primordial quantum fluctuations to frozen and be the seeds for large scale structure formation. More related to this thesis is the fact that the exponential growth of the space would smooth any initial curvature and justify the measured flatness. Finally, the tiny spatial regions causally connected before inflation would grow much faster than the transmission of information in that epoch, and our observable universe could all belong to one of those regions, a thing otherwise impossible with a linear expansion. This can explain why it is so homogeneous.

Some of the predictions of an inflationary model can be checked against observations. After three years of WMAP data [183], the homogeneity and isotropy were confirmed to a ten thousandth part. Flatness to a few hundred per cent. Inflationary theories predict a nearly scale-invariant spectrum of Gaussian adiabatic density perturbations too, which is compatible with galaxy surveys results and anisotropies in the cosmic microwave background. Future results should further constrain these forecasts and even give some hints about the nature of the inflaton or the form of its potential energy. Polarization in the CMB should provide a measure of the amount of gravitational wave background generated by inflation, another prediction.

The good thing of inflation is that it makes a large number of testable predictions, as we see. Furthermore, it is so good at explaining the observations when combined with the Big Bang model that the lack of a concrete mechanism that generates inflation, such as the nature of the inflaton field itself, does not prevent the model from being widely accepted. Of course, it is an active field of research both theoretically and experimentally, and particle physics models together with future observations should lead to an eventual understanding of its insights.

## 1.2 The dark side supremacy

At the same time, there is an increasing necessity of including new *dark* ingredients into the Big Bang model. On the one hand, *dark matter* became a requirement in order to fit the rotation curves of galaxies [214, 163]. On the other hand, *dark energy* is the key to explain the accelerated expansion showed by supernovae [158, 145].

Dark matter is by definition a kind of matter that does not interact with photons. Therefore, it is not visible and can only be detected by gravitational means. It can be both baryonic and non-baryonic, and it is probably both of them. Brown dwarfs, planets, and black holes are dark matter, but their amount is not enough to justify all the missing mass. Non-baryonic matter can be relativistic particles such as neutrinos (hot dark matter) or non-relativistic as the hypothetical WIMPs (cold dark matter). Simulations of large scale structure show that CDM (cold dark matter) is needed in order to allow small objects to collapse and merge until the observed structure is formed. Using results on rotation curves, gravitational lensing, temperature distributions of hot gas or CMB anisotropies, dark matter is found to be around seven times more abundant than visible matter. Paying attention to simulations, most of it must be unknown and not a component of the Standard Model of particle physics.

In the 90s, COBE results reinforced the belief of the Universe being flat, but at that time, measurements of the density of dark matter started to point out that its density would not be enough to make the Universe flat either. Dark energy could account for the difference.

Dark energy is a source of energy with negative pressure that acts as a repulsive force. As a density, it is an additional component that sums up to determine the curvature of the Universe. But dynamically, the negative pressure counteracts gravity and makes the expansion accelerate.

Extragalactic distances are much more sensitive to the dynamics of the universe than the cosmic microwave radiation at a fixed point. Therefore, distances to supernovae should be more adequate to *see* the acceleration than COBE results were. However, supernovae results were compatible with no dark energy until 1998, when the precision was already high enough to discard a universe without dark energy with more than a 99% probability.

The combination of results established at the end of the century what was called a concordance model or the  $\Lambda$ -CDM model. A model that is consistent with the Big Bang theory, inflation, and that contains cold dark matter and a cosmological constant with the necessary densities to make the Universe flat. However, such a model put us in a situation of ignorance: just a 4% of the Universe is made of ordinary matter, the remaining 96% is in the form of dark matter or dark energy for which we can only pose some hypotheses. It is very hard to construct a theory

giving the full description of a universe for which only a 4% of its content is familiar to us. Imagine, as an analogy, how we could describe the visible universe if we only knew the existence of the elements heavier than beryllium, and we did not know what are and which are the constituents hydrogen and helium.

Philosophically, such a universe changes again the conception of ourselves. For the Greeks, the Earth was the centre of the cosmos and we occupied a privileged position in the Universe. Later, the cosmological principle, which stated the homogeneity and isotropy of the cosmos, put us in an ordinary situation. We are orbiting a common star, laying in the outskirts of a common galaxy situated in a common cluster. Besides, we are made up of the same material forming all the constituents of the Universe. Now, we seem to be singled out again, at least under the point of view that our biology is restricted to combinations of baryons, which turn out to be a rare component of the Universe.

### 1.3 Cosmological constant and dark energy

According to quantum mechanics the vacuum has a zero point energy. Unfortunately, a direct interpretation of Einstein's cosmological constant as the energy of the vacuum gives, at best, a discrepancy of  $10^{55}$  orders of magnitude with observations. In fact, not only with observations but with a geometry of space-time consistent with experience. This needed fine-tuning to make the cosmological constant small enough to agree with observations is known as the (old) cosmological constant problem. Why the energy density of dark energy is so small today? Or in other words, the time coincidence problem: Why is it so close to the matter density? (See more information in Refs. [44, 167, 132] for example.)

An answer to the problem is given by considering the cosmological constant as a dynamical term. Such a function is still solution of Einstein's equations. And, from the physical point of view, the cosmological constant must experiment a running when considered within a quantum field theory. Waiting for a quantum field theory of gravity, a semiclassical approach could provide us with the first tools to check the idea. We explore this possibility in detail in this thesis.

The most worked idea is not that of an evolving cosmological constant but of a dynamical scalar field, the quintessence field. If the cosmological constant as a

vacuum energy has similarities with Guth's first inflationary theory, quintessence shares the idea of Linde's formulation. The scalar field generates a potential and slowly rolls down with time [142, 57, 162]. At present, the field would be close to the minimum of its potential with almost null velocity, creating a constant energy and negative pressure similar to a cosmological constant. Generalizations with non-canonical kinetic terms, k-essence, have been considered too [12, 128]. In fact, the quintessence idea has given rise to multiple models, but all of them need fine tuning and an interpretation for the field.

A different branch of models opts for modifications to relativity to explain the observed acceleration [150, 164, 138]. Some of them consider the existence of extra dimensions [64, 58, 71], others include terms with an extra dependence on the curvature into Einstein's equations [23, 120, 133, 130], and tensorial theories of gravitation have been studied as well [173, 61, 28, 72].

On the other hand, we mention the possibility of maintaining the cosmological constant resorting to anthropic principles [205, 22, 86], arguments that can be adapted to other dark energy sources such as quintessence fields for example [85]. Lastly for this brief summary, notice that the current formulation of M-theory needs of a vanishing cosmological constant, although refinements to include a value as the observed one are being studied [33].

Within this zoo of alternative models it is very difficult to prefer one in front of the others. All of them can be tuned so that they describe present-day observations, but there is not a complete theoretical background that generates a source of dark energy yet. Modifications to the Standard Model of particle physics, or a successful union of general relativity and quantum mechanics could predict such a component or behaviour. On the observational side, current research tries to delimit the set of compatible models by determining the relation between the pressure and the density, the equation of state, of dark energy.

Observationally, *seeing* the dark energy is a challenge. It has a low density, is distributed smoothly and does only very weakly interact with gravity, that making it hard to detect. Besides, it must only dominate recently since matter perturbations could not have grown within its domination. However, dark energy affects two aspects of the Universe which can be quantified. First, it alters the expansion history, and second, the growth of large scale structure.

In order to trace the expansion history of the Universe, the best tool at our disposal are Type Ia supernovae (SNe Ia). The evolution of their observed magnitude along redshift gave us the first clear indication of the acceleration [158, 145]. Nowadays, they still provide us with the most precise measure of dark energy and its equation of state [160, 211].

Likewise, Baryonic Acoustic Oscillations (BAO) are a standard ruler that one can measure as a function of redshift [70, 144]. Although the oscillations are much more sensitive to the density of matter than to the density of dark energy, the line of degeneracy between the parameters is almost perpendicular to that obtained with SNe Ia, making the usage of both probes a perfect combination.

Another physical phenomenon which could be influenced because of dark energy is the deflection of light when traveling close to massive objects. Weak lensing for instance offers a variety of tests. Weak lensing tomography measuring the statistical signal induced by large-scale structure [210, 104] or cross correlation cosmography using the ratio of induced shears at different redshifts [112, 27] can give both accurate results and complementarity to the previous probes.

Besides their role in weak lensing, clusters of galaxies can be directly used to this task due to the fact that their abundance and spatial distribution is modified according to the amount of dark energy. The effect on the cluster number of counts along redshift is already used to contrast different theories [182, 129]. Measures of the evolution of the clusters X-ray gas mass fraction are tracing the evolution of dark energy as well [6].

And, of course, one cannot forget the great amount of information encoded in the cosmic microwave background. The tilt of CMB results towards a flat Universe [183] is and has been an important indication of the necessity of dark energy. However, detailed information of its nature is better addressed with other probes, and CMB is mostly used to study the youth of the Universe and to determine the density of matter. These are vital to understand dark energy too. Related tests such as the Integrated Sachs Wolfe effect (ISW) take advantage of this well known radiation to confirm the dark energy hypothesis via complementary methods. The measure of the change of a CMB photon energy that goes through the large scale structure (ISW) is an active field improving with recent results which correlate WMAP with SDSS [51, 88, 37].

## 1.4 Thesis framework and outline

After this brief description of the current state of the cosmological model, it can be noted that there are a lot of open fronts to work on and a lot of open questions to be answered.

This thesis has been carried out after the discovery of the acceleration of the space-time expansion and at the very peak of dark energy research. Figure 1.2 shows how the field has been growing through the last years as indicated by the number of published papers. The time axis spans from the first CMB results measured by COBE in 1992 to today. The amount of research is characterised here by papers in the arXiv database [13] where the key words *Dark Energy* or *Cosmological Constant* appear in the title or the abstract. Note that the arXiv is running from 1991, biasing the first years numbers and that the term dark energy was not coined until the end of 1998. Before Riess et al. (1998) [158] and Perlmutter et al. (1999) [145] papers where SNeIa ruled out a universe without dark energy at  $3\sigma$  level, the study of general dark energy models was scarce. Still, the cosmological constant was attracting the attention of some physicists working on particle physics and of cosmologists worried about the large ages of globular clusters and the flatness implied by COBE data.

This work starts a bit later, in the usually called age of precision cosmology. Now, the quality of measurements has improved remarkably and that allows a much finer analysis of the models. This new possibility motivated a research focused on three aspects. First, we attack the cosmological constant problem by exploring a context within which an evolving cosmological constant would naturally arise. That takes us to analyse the running experienced due to the renormalization group equations and to compare it with a constant term and with other sources of dark energy evolution. Second, the need to distinguish among the several alternative theoretical models with close predictions stimulated the development of a mathematical method to reconstruct continuous functions from a discrete data set. By solving the inverse problem we are able to recover the form of the cosmological constant and the dark energy equation of state along redshift from SNeIa magnitudes. And third, as a complement of the theoretical aspects it has also been analysed the use of SNeIa as cosmological tools and studied their contribution to our future knowledge of the cosmological model.

According to this workplan, the thesis has been divided in two parts. The first

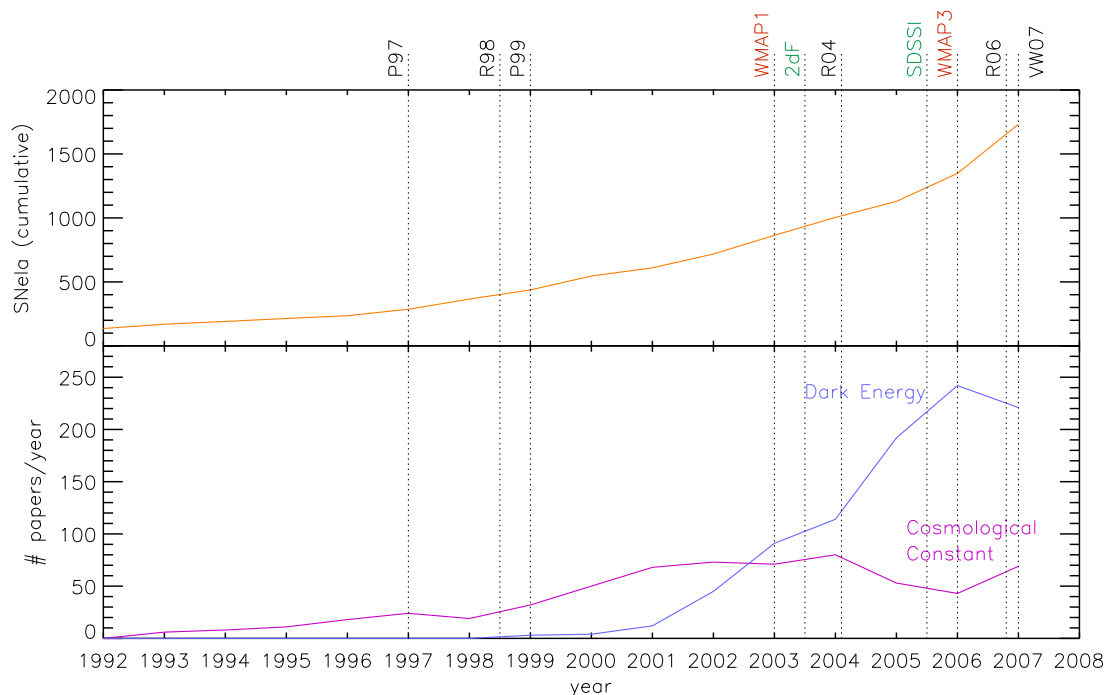


Figure 1.2: Increment of observed SNeIa in the recent years (data from the Padova-Asiago supernova catalogue [139]) and the corresponding increment in the number of papers where the key words *Dark Energy* or *Cosmological Constant* appear in the title or the abstract (arXiv database [13]).

part, the theoretical one, starts by introducing Einstein's equations and their solution in the cosmological case and for an evolving cosmological constant. Next, the running cosmological constant scenarios are developed and their cosmological consequences scrutinized. Finally, the general representation of dark energy via its equation of state is introduced. That served to express some popular dark energy models in this general parameterization and evaluating the degeneracy of the problem.

The aim of the second part is to give some observational constraints to dark energy. Chapter 5 introduces the use of extragalactic distances in cosmology with a special interest in SNeIa. Chapter 6 already uses this tool to determine the cosmological parameters, the parameters of the running cosmological constant scenarios and those of a general development of the equation of state. The analysis of the continuous functions is left to the next chapter where the reconstruction methodology is introduced as well. In Chapter 8, we make use of simulations of the oncoming

SNeIa surveys to see the future perspectives and to quantify the differences between photometric and spectroscopic surveys and between ground-based and space surveys. Finally, the last chapter is devoted to summarize the work and to draw the conclusions.



# Part I

## Evolving dark energy



## Chapter 2

---

# Dynamics of the Universe

---

After a very general introduction to the cosmological model, this chapter develops the main equations which dictate the evolution of the Universe, so Einstein's field equations are solved in the cosmological case and in the presence of some dark energy component. All the parameters that are used to parameterize the dynamics and which are determined along the rest of the thesis are also presented at the end of the chapter.

### 2.1 Einstein's field equations

The road towards the gravitational field equations was a really long one, and it took Albert Einstein more than seven years to eventually reach the end. However, despite the present name of "Einstein's field equations", Einstein was not the only responsible for the achievement. He did most of his work together with the mathematician Marcel Grossmann. In 1913, they already had a preliminary theory based on the invariant line element,

$$ds^2 = g_{\mu\nu} dx^\mu dx^\nu, \quad (2.1)$$

but although they thought that the covariant field equations should relate the Ricci tensor to the energy-momentum tensor, they gave up the idea when concluding that such equations would not yield, in the weak field approximation, the Poisson equation in Newton's theory of gravitation [69]. It was later, in 1915, when Einstein took up again these equations and obtained the *final* version of the gravitational field equations [66]. However, this paper was submitted at the same time as one

[14] Das Gleichungssystem (14) erlaubt jedoch eine naheliegende, mit dem Relativitätspostulat vereinbare Erweiterung, welche der durch Gleichung (2) gegebenen Erweiterung der Poissonschen Gleichung vollkommen analog ist. Wir können nämlich auf der linken Seite der Feldgleichung (13) den mit einer vorläufig unbekannten universellen Konstante  $-\lambda$  multiplizierten Fundamentaltensor  $g_{\mu\nu}$  hinzufügen, ohne daß dadurch die allgemeine Kovarianz zerstört wird; wir setzen an die Stelle der Feldgleichung (13)

$$G_{\mu\nu} - \lambda g_{\mu\nu} = -\kappa \left( T_{\mu\nu} - \frac{1}{2} g_{\mu\nu} T \right). \quad (13a)$$

Figure 2.1: First mention to the cosmological constant by Albert Einstein in his paper of 1917 [68].

from David Hilbert [102], which also formulated the field equations (in fact it was submitted five days later). Nevertheless, Hilbert's paper was accepted more than three months after Einstein's one, and it seems that during this period Hilbert made some changes to his proofs in order to make the theory generally covariant [52].

These *final* field equations were generalised in 1917 by Einstein himself [68], who added a cosmological term compatible with general covariance in order to obtain a closed static model of the Universe. Although this term is currently one of the most promising candidates to play the role of dark energy, in that moment Einstein only introduced it as a mathematical tool which allowed him to describe the Universe he was expecting. That can be seen in Figure 2.1, which shows the paragraph in the original text where the cosmological constant was introduced for the first time. The complete form of the gravitational field equations was given as well.

Next, some of the arguments to obtain the Einstein's field equations are reproduced, even though not the same steps followed by Einstein are developed here. An easier way to obtain the equations is through a generalisation of Newton's gravity law [204, 171]:

$$\nabla^2 \phi = 4\pi G_N \rho \quad \implies \quad G_{\mu\nu} = \alpha T_{\mu\nu}. \quad (2.2)$$

One must start by making the Newton's law consistent with a relativistic description of the Universe. Then, the sources of the gravitational field are not energy

densities  $\rho$  any more, but the energy-momentum tensor  $T_{\mu\nu}$ . In this way, no reference system where  $\rho$  is at rest is privileged. On the other hand, the fact that this is a second rank symmetrical tensor forces the left hand side of the equations, i.e., the space-time geometry, to be also a symmetrical tensor of rank  $\binom{0}{2}$ . The simpler tensor which fulfils these demands and is at most of order two in the derivatives of the metric is

$$R_{\mu\nu} + Cg_{\mu\nu}R + \lambda g_{\mu\nu}, \quad (2.3)$$

where  $C$  and  $\lambda$  are two constants,  $R_{\mu\nu}$  is the Ricci tensor and  $R$  is the curvature scalar. The constant  $C$  is determined by imposing the energy-momentum conservation  $\nabla_\nu T_{\mu\nu} = 0$ , and so, the conservation of the *Einstein's tensor*  $G_{\mu\nu}$ . Then, it is obtained  $C = -1/2$  and a redefinition of the cosmological constant as  $\Lambda \equiv \lambda/8\pi G_N$  is made. Finally, it must be determined the proportionality constant between energy and geometry,  $\alpha$ , which can be made in the weak field approximation of the Einstein's equations and in comparison to the Newton's law. Finally, the 16 field equations read:

$$G_{\mu\nu} + \lambda g_{\mu\nu} \equiv R_{\mu\nu} - \frac{1}{2}g_{\mu\nu}R + \lambda g_{\mu\nu} = -8\pi G_N T_{\mu\nu}. \quad (2.4)$$

It must be noticed that none of the arguments introduced here forbids a time dependent cosmological constant. Thus, a perfectly acceptable general form of the Einstein's equations can be written as:

$$G_{\mu\nu} + \lambda(t)g_{\mu\nu} = -8\pi G_N T_{\mu\nu}. \quad (2.5)$$

The compatibility of this time dependence with current observations is one of the main parts of this thesis, and so, most of its consequences are widely treated in Chapter 3.

## 2.2 Dark energy in Einstein's equations

The energy-momentum tensor  $T_{\mu\nu}$  appearing in Einstein's equations comprises any energy component, including those fields not related to matter and radiation. These various elements are joined under the *dark energy* denomination. It will be seen that the cosmological constant is not exactly in this situation, but it can also be included since its energy-momentum tensor can be defined. Modifications to the Einstein's equations are also possible and conform a family of *dark gravity* models. The latter are not specifically treated here, although the phenomenology can be similar in both cases and that is exploited in Chapter 4. This section has been restricted to interpret the most general and promising dark energy models.

### 2.2.1 Vacuum quantum energy and the cosmological constant

The cosmological constant, besides of being a mathematically sound term in Einstein's equations, has a first possible interpretation within the quantum field theory. The Standard Model of particle physics in which a spontaneous symmetry breaking is produced, works extremely well in order to give mass to the elementary particles, but it is the cause of one of the main problems in cosmology. The reason is that considering that there was a symmetry breaking at the early times of the Universe, let us say at the GUT's scale, produces a huge amount of vacuum energy.

Let us assume that the Higgs field  $\phi$  is the cause of the spontaneous symmetry breaking. As it generates a Higgs potential of the form

$$V_H = -\frac{1}{2}m_\phi^2\phi^2 + \frac{\lambda}{8}\phi^4, \quad (2.6)$$

the vacuum expected value is different from zero,

$$\langle \phi \rangle = \sqrt{\frac{2}{\lambda}} m_\phi \quad \Longrightarrow \quad \langle V_H \rangle = -\frac{m_\phi^4}{2\lambda} \sim 10^8 \text{ GeV}^4, \quad (2.7)$$

where the value is taken from the current particle physics experiments by the LEP

Higgs working group [1].

On the other hand, the expected value in the vacuum of the energy-momentum tensor of a scalar field is given in terms of its vacuum expected value  $\langle V_\phi \rangle$ :

$$\langle T_{\mu\nu} \rangle = g_{\mu\nu} \langle V_\phi \rangle . \quad (2.8)$$

Thus, when the Einstein's field equations are calculated in the vacuum, the only field in the standard model which contributes to  $T_{\mu\nu}$  is the Higgs field, since all the others have a null expected value. So, the geometry of the Universe is only affected by the Higgs and, in case of being considered as an independent source, by the original Einstein's cosmological constant:

$$R_{\mu\nu} - \frac{1}{2}g_{\mu\nu}R = -8\pi G_N (g_{\mu\nu} \langle V_H \rangle + g_{\mu\nu} \Lambda_{vac}) . \quad (2.9)$$

From this equation, one can define an effective cosmological constant,  $\Lambda_{eff}$ , which is the sum of that induced by the Higgs and the original one:

$$\Lambda_{eff} \equiv \langle V_H \rangle + \Lambda_{vac} = \Lambda_{ind} + \Lambda_{vac} . \quad (2.10)$$

Out of the vacuum, the Einstein's field equations can be rewritten in terms of this effective cosmological constant which is the only one that can be detected with observations.

$$R_{\mu\nu} - \frac{1}{2}g_{\mu\nu}R = -8\pi G_N (T_{\mu\nu} + g_{\mu\nu} \Lambda_{eff}) . \quad (2.11)$$

It is when joining theory and observations that one of the main problems in modern cosmology appears: the observed value of the cosmological constant is of order  $\Lambda_{eff} \sim 10^{-47} GeV^4$ , whereas we have just seen (Eq. 2.7) that according to the Standard model of particles the value induced by the Higgs is  $\Lambda_{ind} \sim 10^8 GeV^4$ . It would be necessary then a non null  $\Lambda_{vac}$ , but even more annoying, it would be necessary a precision of  $10^{55}$  orders of magnitude in order to reconcile theory and observations.

A last thing to notice is the fact that the cosmological constant was introduced as a constant related to the geometry of space-time in the previous section (Eqs. 2.3 and 2.4), but now it appears in Equation 2.11 as an energy. The only formal difference is the side in which it appears inside the field equations, but its interpretation differs. The treatment of the cosmological constant as an energy density allows to solve the flatness problem, that is, how we can live in a flat universe as CMB fluctuations show if we only measure a 30% of the necessary matter, but it has introduced another main problem in cosmology: the difference between its observed value and the theoretical one. An evolving cosmological constant can face this problem, and an evolution due to the renormalization group effects are analysed in Chapter 3. Other options for dark energy sources are mentioned in the following.

### 2.2.2 Quintessence and other alternatives

Many alternatives to the cosmological constant have been proposed in order to reconcile theory and observations. The most explored and successful is up to now the so-called *quintessence*. Thus dubbed by Steinhardt in 1998 [39] because of being the fifth contribution to the cosmic energy density (after the baryonic, dark matter, radiation and neutrinos ones), it had already been analysed, for instance, in [142] years before. The phenomenology is similar to the one observed for a time-variable cosmological constant, but the theoretical ground differs.

The basic idea is that, in a similar way as it happens with inflation and the inflaton field, an evolving scalar field could account for the present acceleration. By a quintessence field  $Q$ , it is actually understood a dynamical, evolving and spatially slightly inhomogeneous field with a negative pressure and a positive energy density greater than the modulus of the pressure. The field evolves in a potential  $V(Q)$  and has a positive kinetic energy  $1/2 \dot{Q}^2$ . The energy-momentum tensor of this component reads then as

$$T_{\mu\nu}^Q = \partial_\mu Q \partial_\nu Q - g_{\mu\nu} \left( \frac{1}{2} \partial^\alpha Q \partial_\alpha Q - V(Q) \right). \quad (2.12)$$

So, a quintessence energy density is taken into account by just inserting the energy-momentum tensor 2.12 into the Einstein's equations as a new source of energy.

Although the concept of quintessence is very general, there exists a particular kind of potentials which have very interesting behaviours for cosmology: the tracker potentials [212, 186]. A tracker field has the same solution to its equation of motion irrespective of the initial conditions for  $Q$  and  $\dot{Q}$ , at least in a very wide range. Besides, this attractor solution is such that the quintessence field is only dominant at late times. Since the field rolls down the potential, the kinetic energy diminishes as it reaches the minimum. There, the kinetic energy is very small compared to the potential, and so, at late times, the energy-momentum tensor can be written as

$$T_{\mu\nu}^Q = g_{\mu\nu} V(Q), \quad (2.13)$$

which acts exactly as a cosmological constant. The fact that for a wide range of initial conditions a cosmological constant-like behaviour is recovered, as it seems to be determined by observations, makes quintessence an appealing idea to solve the coincidence problem.

In the previous paragraphs, only scalar fields have been considered, but also vector or tensor fields, or topological defects could be characterized as  $Q$  components. Which of all these possibilities is the correct one, if any, should be determined by a final particle physics theory.

When supergravity or string theory are considered, the massless scalar degrees of freedom appear in the effective action not as a quintessence field but as a field with non-standard (non-linear) kinetic terms. These fields, which also show an attractor behaviour, are an example of what is called *k-essence* [12, 128] in analogy to quintessence. Now, the tensor to be introduced in the Einstein's equations for a field  $K$  is:

$$T_{\mu\nu}^K = V(K) \left( 2 \frac{\partial F(X)}{\partial X} \partial_\mu K \partial_\nu K - g_{\mu\nu} F(X) \right), \quad (2.14)$$

where  $F(X)$  is a kinetic function with  $X = \partial^\alpha K \partial_\alpha K$  and  $V(K)$  is the potential.

Other kinds of fields with a negative kinetic energy, the *phantom* fields, also drive to a late time acceleration [38, 40, 91]. However, these fields violate the null dominant energy condition (see Section 4.1), and some of them predict a universe which ends with a Big Rip. Nevertheless, phantom fields cannot be put aside since

data have seemed to favour a supernegative ( $w < -1$ ) equation of state, taken at their face values, although new observations give more conservative results.

$$T_{\mu\nu}^{Ph} = -\partial_\mu P \partial_\nu P + g_{\mu\nu} \left( \frac{1}{2} \partial^\alpha P \partial_\alpha P + V(P) \right). \quad (2.15)$$

To finish with this brief description of the most promising dark energy components, it is worth mentioning a quite different dark energy model, the *Cardassian* one [82, 81]. These models do not introduce a new and unknown field but they change the usual interpretation of matter as a pressureless fluid and allow it to interact, adding new terms to the usual matter density and pressure [90]. The energy-momentum tensor is for these models that of a perfect fluid (see Section 2.3.3) with a density of matter  $\rho = \rho_M + \rho_{Ca}$  and a pressure  $p = p_{Ca}$ , where the subindex *Ca* indicates the Cardassian contribution. It must be noted, however, that this is not the only interpretation for Cardassian models, since they can also be seen as a dark gravity source: the same parameterizations are obtained when it is considered that our 3-dimensional Universe is a brane embedded in extra dimensions [46].

## 2.3 Solving Einstein's equations

Einstein's field equations are a system of ten independent differential equations, which are, in general, difficult to solve. They must be solved simultaneously for a given geometry and matter distribution, but only some of these configurations can be solved analytically as for example spherical stars and black holes. In the cosmological case, some symmetries are applied to the metric to obtain the Robertson-Walker form, whereas the matter-energy content is modeled as a perfect fluid. With these assumptions the dynamics of the Universe is unravelled.

### 2.3.1 Cosmological principle and Robertson-Walker metric

The symmetries to apply in the cosmological framework are those given empirically by the cosmological principle. From the ancient times, the Earth was thought to be the centre of the Universe. This belief, already accepted by the Greeks, endured for more than twenty centuries. In the 4th century B.C., the Macedonian philosopher

Aristotle considered a sky of order and perfection formed by perfect spheres where stars lie around the Earth. Few important changes such as the introduction of epicycles to justify the observations, were made to the geocentric conception of the Universe until the Renaissance. It was in the late 15th century when Nicolas Copernicus started a revolution in astronomy: the Earth would not be the centre of the Universe any more and that position would be occupied by the Sun. However, this heliocentric view of the Universe was not fully accepted till the 17th century.

From then on astronomy, and cosmology, would advance faster, mainly due to the invention of the telescope. New objects in addition to the Solar System ones are observed, and Immanuel Kant suggests the existence of the *Island Universes* as extragalactic objects. The Universe did not seem to be homogeneous, groups of stars and nebulae were observed in the sky, and there was a privileged direction (the Galactic plane) where most of these objects were found. The idea of extragalactic objects, not taken very seriously yet, was recovered when Edwin Hubble determined the distances to some “nebulae” in 1929, and so, the thought of the Sun being the centre of everything lost meaning.

Nowadays, the everyday more powerful instruments and the possibility to see in various bands of the electromagnetic spectrum seem to indicate that the angular distribution of galaxies at large scale is *isotropic*. If we see that the Universe is isotropic, and there is no reason to think that we are in a privileged position, it must be isotropic with respect to any point, and thus, *homogeneous* too. This combination is the base of modern cosmology, and it is known as the cosmological principle:

*The Universe at large scale is homogeneous and isotropic  
with respect to any observer comoving with the cosmic fluid.*

These symmetries established by the cosmological principle can be now translated into conditions to apply to the generic form of the metric, Equation 2.1. That means that in the metric:

- There cannot be mixed terms of space and time ( $g_{i0} = 0$ ), otherwise the Universe would not be isotropic. This allows to define a cosmic time  $t$ , the same for all comoving observers.

- The space and time parts can be separated if, besides, the Universe is homogeneous. This defines the scale factor  $a(t)$ , where all the evolution in time is included.
- The curvature of the Universe must be constant ( $k$ ), and so, the Universe is spherically symmetric.

In this way, it has been defined a system of coordinates which describes the symmetries of the Universe and remain constant for any observer comoving with the cosmic fluid: the comoving coordinates  $(r, \theta, \varphi)$ . The mathematical expression of the cosmological principle is then the Robertson-Walker metric, which in its canonic form reads:

$$\begin{aligned} ds^2 &= c^2 dt^2 - a^2(t) \left[ \frac{dr^2}{1 - kr^2} + r^2 (d\theta^2 + \sin^2 \theta d\varphi^2) \right] \\ &= c^2 dt^2 - a^2(t) \left[ \frac{dr^2}{1 - kr^2} + r^2 d\Omega \right], \end{aligned} \quad (2.16)$$

where as it has been said,  $(r, \theta, \varphi)$  are the comoving coordinates,  $k$  is the spatial curvature and can only take three values:

$$\begin{aligned} k = +1 & \quad \text{closed space} & \quad (S^3 \text{ sphere}) \\ k = 0 & \quad \text{flat space} & \quad (R^3 \text{ euclidean space}) \\ k = -1 & \quad \text{open space} & \quad (H^3 \text{ hyperboloid}), \end{aligned} \quad (2.17)$$

and  $a(t)$  is the scale factor which depends on the cosmic time  $t$ . This unknown function is sometimes expressed as a Taylor expansion:

$$a(t) = a(t_0) \left[ 1 + H_0(t - t_0) - \frac{1}{2}q_0 H_0^2 (t - t_0)^2 + \dots \right], \quad (2.18)$$

where  $H_0 \equiv \dot{a}(t_0)/a(t_0)$  is the Hubble constant (see Section 2.4.1 for a widest comment) and  $q_0 \equiv -\ddot{a}(t_0)a(t_0)/\dot{a}^2(t_0)$  is the deceleration parameter.

Nevertheless, the radial coordinate  $r$  is not the most adequate in order to describe physical distances. It is the mathematical distance from the centre to the

3-dimensional surface of the universe, and so, it is a distance in a dimension outside the real universe. The distance in 3-dimensional space is given by the arc over the hypersurface. It is then useful to define the angle  $\chi$  as:

$$\chi(r) = \arcsinn r \equiv \begin{cases} \arcsin r & \text{for } k = +1 \\ r & \text{for } k = 0 \\ \operatorname{arcsinh} r & \text{for } k = -1 \end{cases} . \quad (2.19)$$

With this definition the metric can be rewritten in a more physical way, where  $r(\chi)$  is just the inverse of Equation 2.19:

$$ds^2 = c^2 dt^2 - a^2(t) [d\chi^2 + r^2(\chi) (d\theta^2 + \sin^2 \theta d\varphi^2)] . \quad (2.20)$$

## 2.3.2 Distances in cosmology

Such an intuitive concept as “distance” has a difficult formulation in cosmology, but it is indispensable in order to understand our Universe. In the previous section it has been seen that the coordinate distance  $r$  has not a real distance meaning in our three-dimensional spatial Universe, and instead of it, it has been defined the comoving coordinate  $\chi$ . However, this is not measurable and other distances between objects have to be defined, although all of them differ at large separations.

### 2.3.2.1 Proper distance

The most direct distance which can be obtained just from the spatial part of the metric is the proper distance. Let us consider an object situated at some fixed comoving coordinates  $(r_1, \theta_1, \varphi_1)$  – or  $(\chi_1, \theta_1, \varphi_1)$  –, and let us consider our position the origin of coordinates. At a given cosmic time  $t$ , the distance between us and that far object is the sum of differential distances which could be measured with light signals.

$$d_{prop}(t) = \int_0^{r_1} \sqrt{g_{rr}} dr = a(t) \int_0^{r_1} \sqrt{\frac{dr^2}{1 - kr^2}} = a(t) \chi_1 . \quad (2.21)$$

In the above expression, the meaning of the comoving coordinate  $\chi$  is seen. However, this definition is still not useful in practice, and it cannot be replaced by a more useful one like “measuring the time from a single light signal travelling between the emitter and the receptor at a given time”, as these two objects do not have to exist at the same time and so, it would be in general not measurable. But, although it is not then a good definition for a *physical* distance, it is worth mentioning since the rest of distances reduce to it at small separations.

### 2.3.2.2 Redshift

Before entering in the real physical distances, let us first define the cosmological redshift as a measure of the distance between two events connected by light.

Let us consider a light pulse that follows a null geodesic at constant  $\theta$  and  $\varphi$ . The comoving distance between the emission ( $e$ ) and the observation ( $o$ ) is given by

$$ds^2 = 0 = c^2 dt^2 - a^2(t) \frac{dr^2}{1 - kr^2} \quad \Longrightarrow \quad \chi = \int_{t_e}^{t_o} \frac{c dt}{a(t)}. \quad (2.22)$$

The next wave crest leaving from  $r_1$  at  $t_e + \delta t_e$  will arrive to the observer at  $t_o + \delta t_o$  and will have the same comoving coordinate  $\chi$  because  $a(t)$  is almost constant during a light period:

$$\chi = \int_{t_e + \delta t_e}^{t_o + \delta t_o} \frac{c dt}{a(t)}. \quad (2.23)$$

Comparing Equation 2.22 to 2.23 it is established a relation between the time between pulses for the observer and the emitter with the scale factor for both of them. This relation is the cosmic time dilation

$$\frac{\delta t_o}{a(t_o)} = \frac{\delta t_e}{a(t_e)}. \quad (2.24)$$

Since the frequency of the photons is the inverse of the time interval between pulses, the time dilation translates into a wavelength dilation, i.e., there is a shift in the emitted wavelength when it is received:

$$\frac{\lambda_e}{\lambda_o} = \frac{\nu_o}{\nu_e} = \frac{\delta t_e}{\delta t_o} = \frac{a(t_e)}{a(t_o)}, \quad (2.25)$$

$$z \equiv \frac{\lambda_o - \lambda_e}{\lambda_e} = \frac{a(t_o)}{a(t_e)} - 1. \quad (2.26)$$

For an expanding universe,  $a(t_o) > a(t_e)$  and a *redshift* is produced. The opposite would happen for a contracting universe. The *cosmological redshift* is then only produced because of the Universe expansion, and it has nothing to do with the motion of the objects. However, the measurable quantity is the sum of both this cosmological redshift and the one due to the proper motions. For distant objects far from intense gravitational fields, the observed redshift corresponds to the cosmological one, and allows to study the scale factor  $a(t)$ . A useful relation between the scale factor and the redshift actually ( $z = 0$  corresponding to  $a(t_o) = 1$ ) is:

$$a = \frac{1}{z + 1}. \quad (2.27)$$

### 2.3.2.3 Luminosity distance

The most practical way for obtaining extragalactical distances is from observables. The distance to an object from which the absolute luminosity is known can be obtained by measuring the apparent luminosity, whereas the distance to an object from which the diameter is known is obtained by observing its angular diameter. That defines two different measures of distance: the luminosity distance and the angular distance.

The main example of the importance of luminosity distances for cosmology is Type Ia supernovae (see Chapter 5). Let us consider a supernova exploding in a galaxy situated at a fixed comoving distance  $\chi_1$  (or  $r_1$ ). This object is emitting a luminosity  $\mathcal{L}_e$ , which is measured by us as a flux  $\mathcal{F}_o$  (see Figure 2.2). The observed flux is related to the luminosity in an euclidean universe by  $\mathcal{F}_o = \mathcal{L}_e/S = \mathcal{L}_e/(4\pi d_L^2)$ , and this can be used to define by analogy the luminosity distance  $d_L$  in any FLRW universe. Since the luminosity is nothing else but the rate of emitted energy ( $dE/dt$ ), the received luminosity is affected by a  $(1 + z)$  factor due to the time dilation and

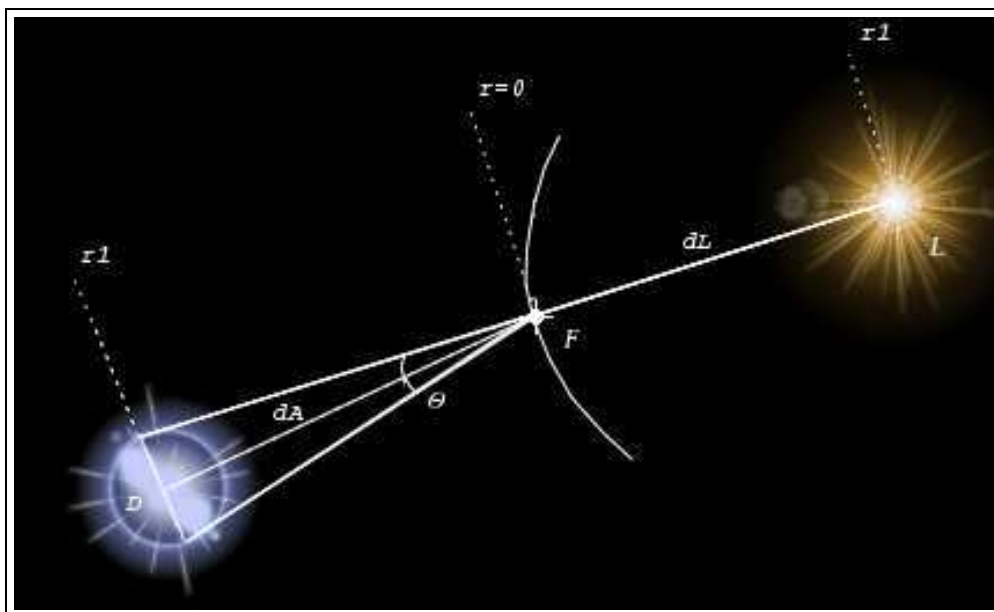


Figure 2.2: Quantities used in the calculations of the angular ( $d_A$ ) and luminosity ( $d_L$ ) distances by analogy to an euclidean universe. In a curved universe both measures are different for a same location.

another one due to the wavelength dilation (Equations 2.25 and 2.27). On the other hand, the proper surface  $S$  in a Robertson-Walker metric is given by

$$dS = g_{\theta\theta} g_{\varphi\varphi} \implies S = 4\pi a^2(t) r^2(\chi). \quad (2.28)$$

The combination of both facts allows to express the observed flux as a function of the source coordinates

$$\mathcal{F}_o = \frac{\mathcal{L}_o}{S} = \frac{\mathcal{L}_e}{4\pi a_0^2 r_1^2 (1+z)^2} \equiv \frac{\mathcal{L}_e}{4\pi d_L^2}, \quad (2.29)$$

and with the definition of luminosity distance, it can be obtained its general form as a function of the scale factor and the universe's curvature, the only two functions to be determined in the Robertson-Walker metric:

$$d_L = a_0 r_1 (1+z) = c(1+z) a_0 \text{sinn} \int_{t_e}^{t_o} \frac{dt}{a(t)}. \quad (2.30)$$

### 2.3.2.4 Angular distance

In a similar way as done for luminosity distances, angular distances can be obtained for objects from which the diameter is known such as radio galaxies or compact radio sources (some more comments on Section 5.2).

Let us consider a radio galaxy at a comoving distance  $r_1$  as shown in the left side of Figure 2.2. Its diameter is  $D$ , and its proper size is given in the Robertson-Walker metric by

$$dD^2 = g_{\theta\theta}^2 + g_{\varphi\varphi}^2 \implies D = a(t)r(\chi)d\Omega. \quad (2.31)$$

The angular distance  $d_A$  is defined also generalising the expression for an euclidean universe as:

$$d_A = \frac{D}{d\Omega} = a(t_e)r(\chi) = \frac{c a_0}{(1+z)} \text{sinn} \int_{t_e}^{t_o} \frac{dt}{a(t)}. \quad (2.32)$$

As it is seen from the comparison between Equation 2.30 and 2.32, both definitions of distance differ at high redshift. However, there is an easy relation between them, and both can be translated into proper and coordinate distances. This fact is very useful to join different sources of data as done in subsequent chapters.

$$d_{prop}(t_0) = \frac{d_L}{1+z} = (1+z) d_A. \quad (2.33)$$

## 2.3.3 Friedmann equations

Once it has been obtained the Robertson-Walker metric for describing the Universe at large scale, the independent Einstein's equations reduce to six, and can be solved for a given energy distribution. We will see that specifying the form of the energy-momentum tensor for all the sources of energy allows to determine the curvature  $k$  and the scale factor  $a(t)$  appearing in the metric, together with the energy content of the Universe.

Let us first introduce the cosmological constant term in the right hand side of the Einstein's field equations and define a new energy-momentum tensor,  $\tilde{T}_{\mu\nu}$ . As it is shown later on, this determines the form of the density and the pressure for the cosmological constant when considered as an energy source. For the sake of generality, we consider a time-dependent cosmological constant from now on, being the real cosmological constant just a particular case.

$$\tilde{T}_{\mu\nu} = T_{\mu\nu} + \Lambda(t) g_{\mu\nu}. \quad (2.34)$$

The energy-momentum tensor for a perfect fluid, that is, a fluid without heat conduction and viscosity, reads

$$T_{\mu\nu} = -p g_{\mu\nu} + (\rho + p) U_\mu U_\nu. \quad (2.35)$$

So, it can be defined the corresponding total density  $\tilde{\rho}$  and pressure  $\tilde{p}$  including all the energy sources and the cosmological constant. This way, the cosmological constant (in the general sense) can be interpreted as a perfect fluid with energy density  $\rho_\Lambda = \Lambda$  and pressure  $p_\Lambda = -\Lambda$ :

$$\tilde{\rho} = \rho + \Lambda, \quad \tilde{p} = p - \Lambda. \quad (2.36)$$

The energy-momentum tensor of the cosmic fluid is then the sum of the various energy components of the Universe: non-relativistic matter (baryonic and cold dark matter), radiation, cosmological constant and any other dark energy source which can be interpreted as a perfect fluid:

$$\tilde{T}_{\mu\nu} = T_{\mu\nu}^{matter} + T_{\mu\nu}^{radiation} + T_{\mu\nu}^{CC} + T_{\mu\nu}^{quintessence} + \dots \quad (2.37)$$

The relation between the pressure and the density for each of the perfect fluids is given by its equation of state. It is assumed that both quantities are proportional, and defined the barotropic index  $w(t)$  which is characteristic of each component

$$p(t) = w(t) \rho(t). \quad (2.38)$$

This simple relation is fulfilled by the most important components of the Universe. Only some kinds of dark energy models (as the Cardassian ones, for instance) depart from this Ansatz as it is widely described in Chapter 4. It must be noted that this is a known relation for matter and radiation, being only an Ansatz for dark energy since its nature is unknown. Below, some of the barotropic indexes for the different components are listed.

$w_R = 1/3$	radiation
$w_M = 0$	non-relativistic matter
$w_S = -1/3$	cosmic strings
$w_W = -2/3$	domain walls
$w_T = -1/3$	textures
$w_Q(t) > -1 \quad (dw_Q/dz > 0)$	quintessence
$w_K(t) > -1 \quad (dw_K/dz < 0)$	k-essence
$w_\Lambda = -1$	(evolving) cosmological constant
$w_{Ph}(t) < -1$	phantoms

All the ingredients to solve the Einstein's equations have already been presented. So, we can start with the conservation of the energy-momentum tensor we have just introduced. Only three components are considered: matter and radiation, an evolving cosmological constant and a quintessence field. The other dark energy components can take the role of quintessence.

By hypothesis, the quintessence field does not interact with ordinary matter or radiation, therefore it is separately conserved.

$$\nabla^\mu \tilde{T}_{\mu\nu} = 0 \quad \Longrightarrow \quad \dot{\Lambda} + \dot{\rho} + 3H(\rho + p) = 0 \quad (2.39)$$

$$\dot{\rho}_Q + 3H(\rho_Q + p_Q) = 0. \quad (2.40)$$

In the above equations  $H$  is the Hubble parameter defined as  $H \equiv \dot{a}/a$ , all derivatives are calculated respect the cosmic time  $t$ , the subindices  $Q$  indicate the quintessence field, and the pressure  $p$  and the density  $\rho$  correspond to both matter and radiation. For a truly constant cosmological constant, Equation 2.39 reduces to the usual conservation law. However, when the cosmological constant evolves with time, it appears an energy transfer between matter and cosmological constant.

The evolution of the cosmological constant is given, in this work, by its renormalization group equation (Section 3.2), whereas the quintessence field evolves following the Klein-Gordon equation:

$$\ddot{Q} + 3H\dot{Q} + V'(Q) = 0, \quad (2.41)$$

where the prime derivative is respect to the field  $Q$ .

The different components of the Einstein's equations provide the other independent equation describing the dynamics of the Universe. The temporal components,  $(\mu, \nu) = (0, 0)$ , drive to the Friedmann equation:

$$H^2(z) = \left(\frac{\dot{a}}{a}\right) = \frac{8\pi G}{3} [\rho(z) + \Lambda(z)] - k(1+z)^2. \quad (2.42)$$

On the other hand, the spatial components generate a new equation which is not independent from 2.39, 2.40 and 2.42:

$$\left(\frac{\ddot{a}}{a}\right) + \frac{1}{2} \left(\frac{\dot{a}}{a}\right)^2 = -4\pi G \sum_i p_i - \frac{k}{2}(1+z)^2. \quad (2.43)$$

To fully characterize the dynamics of the Universe, it is now only necessary to specify the form of the potential  $V(Q)$  in order to determine its equation of state. Finally, the system of equations 2.39, 2.40, 2.41, 2.42 and 3.12 can be solved. All the kinds of universes which are obtained from this set of equations are called Friedmann-Lemaître-Robertson-Walker universes (*FLRW*) in recognition to the first authors to solve the Einstein's equations in cosmology and to give a form for the metric of space-time.

## 2.4 Parameterizing the dynamics

All the interesting physical aspects of the dynamics of the Universe are already in the equations deduced in the previous sections. However, it is useful to define some parameters to ease the form of the equations and its dependencies. The concrete values in the present-day also deserve a special attention.

### 2.4.1 Hubble constant and critical density

The Hubble constant,  $H_0$ , has been defined in Section 2.3.1 as a parameter appearing in the expansion of the scale factor, and it is a measure of the speed at which the Universe is expanding per unit of distance.

Edwin Hubble measured its value in 1929. In fact, he established a linear relation between the velocity of some observed galaxies and the distance to us, from which the proportionality constant was  $H_0$ . This was the first observational evidence for an expanding Universe, and a support for Einstein's equations which had already predicted a non-static Universe. Hubble had very few data and with a large dispersion, however, he could find a first result for it:  $H_0 = 550 \text{ km/s/Mpc}$ . Although the Hubble law has been confirmed at first order, the value of the Hubble constant has diminished enormously. Freedman et al. for the Hubble Space Telescope Key Project have obtained  $H_0 = 72 \pm 8 \text{ km/s/Mpc}$  [79]. The inverse of the Hubble constant gives an estimation of the age of the Universe. For an accelerated universe this estimation is a lower limit, i.e., a Hubble constant of  $H_0 = 72 \text{ km/s/Mpc}$  implies that the Universe is, at least, 13.9 *Gyr* old.

The Hubble constant is of great importance in all cosmological determinations, and so, it is sometimes useful to define the dimensionless Hubble constant, which only introduces variations of order one in the expressions where it appears:

$$h_0 \equiv \frac{H_0}{100 \text{ Km/s/Mpc}}. \quad (2.44)$$

Another important definition is the critical density of the Universe. It is the density that a flat Universe would have now, and it can be calculated from the Friedmann equation taken without curvature at the present time,  $k = 0$  at  $z = 0$ .

$$\rho_c^0 \equiv \frac{3 H_0^2}{8 \pi G_N} \approx \left( 3 \sqrt{h_0} \times 10^{-3} \text{ eV} \right)^4 \sim 10^{-27} \text{ kg/m}^3 \quad (2.45)$$

Measured energies higher than the critical one indicate that we are living in a closed universe, whereas smaller energies reveal that our universe has an open geometry. Although usually one refers to the present-day critical density, it can also be defined as a function of redshift,  $\rho_c(z)$ , and that is of particular interest when dealing with

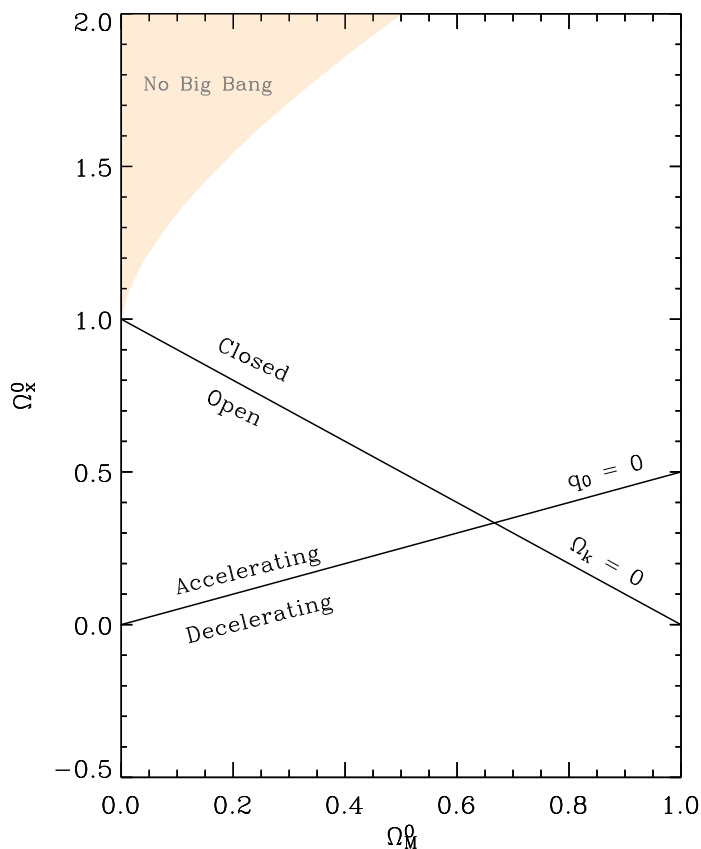


Figure 2.3:  $(\Omega_M^0, \Omega_\Lambda^0)$  plane. Combinations of the cosmological parameters divide the plane according to the geometry and the dynamics of the Universe.

an evolving cosmological constant.

## 2.4.2 Cosmological parameters

Once it has been defined a characteristic energy of the Universe, the current energy density for each component can be normalized to it. These dimensionless values, the cosmological parameters, show the percentage of energy of the component with respect to the total energy in a flat universe. It can be defined, for instance:

$$\Omega_M^0 \equiv \frac{\rho_M^0}{\rho_c^0}, \quad \Omega_\Lambda^0 \equiv \frac{\Lambda}{\rho_c^0}, \quad \Omega_Q^0 \equiv \frac{\rho_Q^0}{\rho_c^0}, \quad \Omega_{Ph}^0 \equiv \frac{\rho_{Ph}^0}{\rho_c^0}, \quad \Omega_{Ca}^0 \equiv \frac{\rho_{Ca}^0}{\rho_c^0}, \quad \text{etc.} \quad (2.46)$$

And, by analogy, also a curvature energy density as:

$$\Omega_K^0 \equiv \frac{-k}{a_0^2 H_0^2}. \quad (2.47)$$

However, it is habitual to use only one dark energy component. In case a single one is used to represent any of the options, the corresponding cosmological parameter is denoted by  $\Omega_X^0$ , and used together with  $\Omega_M^0$  and  $\Omega_K^0$  to depict the dynamics of the Universe.

Again, all these parameters can be defined as functions, and the utility of one or the other definition depends on the feature to be studied. In this thesis, it has been used the following notation:

$$\Omega_X^0 \equiv \frac{\rho_X^0}{\rho_c^0}, \quad \Omega_X^0(z) \equiv \frac{\rho_X(z)}{\rho_c^0}, \quad \Omega_X(z) \equiv \frac{\rho_X(z)}{\rho_c(z)}. \quad (2.48)$$

With these definitions, the Friedmann equation is rewritten as:

$$H^2(z) = H_0^2 [\Omega_M^0(1+z)^3 + \Omega_X^0(z) + \Omega_K^0(1+z)^2], \quad (2.49)$$

and particularizing at  $z = 0$  it is obtained the cosmological sum rule, which relates the cosmological parameters among them:

$$1 = \Omega_M^0 + \Omega_X^0 + \Omega_K^0. \quad (2.50)$$

These current values completely characterize the geometry and the dynamics of the Universe. In Figure 2.3, it is shown the  $(\Omega_M^0, \Omega_X^0)$  plane. Each point of the diagram represents a curvature given by Equation 2.50 and also a value for the present-day deceleration parameter, expressed as  $q_0 = \Omega_M^0/2 - \Omega_X^0$  (see its definition in Equation 2.18). The lines that separate the different behaviours have been overplotted, and the shadowed region marks the zone where the backward evolution of the Universe would not lead to a Big Bang.

All the observables that have been introduced in Section 2.3.2 to measure cosmological distances can be written as a function of the cosmological parameters, and

so, measuring extragalactical distances is a very good method to determine them. It is also the main method used in this thesis in order to determine both the cosmological parameters and the parameters of the theoretical models (also the dark energy equation of state). The general equations which will be used in the following for the luminosity and angular distances read:

$$\begin{aligned} d_L(z, \Omega_M^0, \Omega_X^0) &= c(1+z) a_0 \text{sinn} \int_{t_e}^{t_o} \frac{dt}{a(t)} = \\ &= \frac{c(1+z)}{H_0 \sqrt{|\Omega_K^0|}} \text{sinn} \left( \sqrt{|\Omega_K^0|} \int_0^z \frac{H_0 dz'}{H(z', \Omega_M^0, \Omega_X^0)} \right), \quad (2.51) \end{aligned}$$

$$\begin{aligned} d_A(z, \Omega_M^0, \Omega_X^0) &= \frac{c a_0}{(1+z)} \text{sinn} \int_{t_e}^{t_o} \frac{dt}{a(t)} = \\ &= \frac{c}{H_0(1+z) \sqrt{|\Omega_K^0|}} \text{sinn} \left( \sqrt{|\Omega_K^0|} \int_0^z \frac{H_0 dz'}{H(z', \Omega_M^0, \Omega_X^0)} \right). \quad (2.52) \end{aligned}$$

### 2.4.3 Dark energy equation of state

In absence of any hint of what the nature of dark energy is, the equation of state of dark energy is the best parameter to characterize it. For matter or radiation, the only unknown quantity is the current energy density, or equivalently, the corresponding cosmological parameter. Its equation of state is already assumed. On the contrary, for dark energy one needs to determine it too (an exception is the cosmological constant which has a fixed value of  $w(z) = -1$ ). A very important part of the thesis has been devoted to determine the function  $w(z)$  without any restriction (Chapter 7), although sometimes one restricts the space where its values can be found due to some physical arguments.

Several parameterizations are also tried for  $w(z)$ , mostly corresponding to Taylor developments of the equation of state (Chapter 4). So, we could be in the case to have an arbitrarily large set of parameters. The adequacy of each development is discussed later in the thesis.

## Chapter 3

---

# Running of the cosmological constant

---

This chapter continues with the theoretical part of the thesis by introducing a model based on the Renormalization Group Equations from Quantum Field Theory. In the first part, some concepts are defined, and straight afterwards some cosmological models with a running of the cosmological constant are sketched. The major part of the chapter is devoted to one of these models, which motivated two papers [176, 75].

### 3.1 Quantum field theory concepts

#### 3.1.1 Action

Any field theory, and in particular a Quantum Field Theory (from now on *QFT*), is characterized by the Lagrangian of the theory (see a general introduction in [111] for instance).

For the cosmological case, it is interesting a QFT which also incorporates gravity. Nowadays, there is not a complete quantum gravity theory, but one can start from a semiclassical approximation that locates the fields in a curved space-time. The gravitational field is treated then as a perturbation on a flat background ( $g_{\mu\nu} = \eta_{\mu\nu} + h_{\mu\nu}$ ), but it is not quantized.

The Lagrangian of the theory has the contributions of both the fields and the vacuum. The former include all the Standard Model fields in a flat space-time plus a non-minimal term of interaction with the gravitational field in order to guarantee renormalizability (Section 3.1.2). The latter, the vacuum, which is the most interesting in our case, introduces a first term corresponding to the Hilbert-Einstein ( $HE$ ) action with cosmological constant:

$$S_{HE} = - \int d^4x \sqrt{-g} \left( \frac{1}{16\pi G_{vac}} R + \Lambda_{vac} \right), \quad (3.1)$$

and, also for renormalizability reasons, one has to add some local terms depending on the curvature through higher orders of the metric derivatives [36]:

$$S_{vac} = \int d^4x \sqrt{-g} \left( a_1 R_{\mu\nu\alpha\beta}^2 + a_2 R_{\mu\nu}^2 + a_3 R^2 + a_4 \square R - \frac{1}{16\pi G_{vac}} R - \Lambda_{vac} \right). \quad (3.2)$$

It is important to notice that  $\Lambda_{vac}$  itself is necessary for renormalizability, and therefore, theories without cosmological constant are non-renormalizable. The remaining terms in Equation 3.2, the higher order terms, are only meaningful at high energies and they could be the cause of inflation. But, when dealing with the cosmological constant nowadays, at low energy, the Hilbert-Einstein action is a sufficient approximation.

For fields other than the ones in the Standard Model of particle physics, the action must include new terms. For instance, one of the most sound alternatives to the cosmological constant, the quintessence field, adds the following term:

$$S_Q = \int d^4x \sqrt{-g} \left( \frac{1}{2} \partial^\alpha Q \partial_\alpha Q - V(Q) \right). \quad (3.3)$$

The form of the Lagrangian for quintessence is explicitly given in Chapter 4 (Eq. 4.2). Other kinds of fields such as k-essence or phantom fields have a similar structure. In the previous chapter, it has been shown the form of the energy-momentum tensors for these fields, and from them, one can obtain the Lagrangian to construct their action.

### 3.1.2 Regularization and renormalization

Quantum field theories often present divergences in the integrals when considering high moments (ultraviolet divergences), and a good example of this is the theory described by the action in Equation 3.2. To deal with these theories, one might use regularization and renormalization techniques (see for instance [148]). The main idea is to absorb the divergences into the terms that represent non-observable magnitudes in the Lagrangian, so that all the observables remain finite.

The first step is to modify the original integrals by introducing a regularization parameter which makes the integrals finite. This can be done by

- cutting the integral at a certain momentum (cut-off),
- changing the dimension of the space and introducing the corresponding dimensional constant to maintain the original dimensionality, or
- discretizing the space-time and considering only a finite volume.

Despite the diversity of regularization methods, always the regularization parameter eventually tends to a constant and the integral takes a finite value. In this way, in renormalizable theories, all the techniques are equivalent.

Once regularized, the parameters of the Lagrangian (the masses  $m$  and the coupling constants  $\lambda$ ) must be written as a function of the regularization parameter  $\Lambda$ <sup>1</sup>. If, whether by this method or by also adding new terms to absorb the new divergences (counterterms), all the Green functions are finite, one says that the theory is renormalizable.

It can be shown that regularization breaks the scale invariance. However, if the theory had global or local gauge invariances, they should be conserved. That is achieved by adding new local terms to the Lagrangian which make the symmetry to be conserved in the Lagrangian as a whole.

---

<sup>1</sup>Although  $\lambda$  and  $\Lambda$  are not the best symbols to name these parameters in a thesis based on the study of the cosmological constant  $\Lambda$ , we do use them to maintain the habitual notation in the references.

The same as with regularization, there are several renormalization schemes. All of them have the function to absorb the divergences by replacing the masses and coupling constants originals in the Lagrangian (the naked values  $m_0$  and  $\lambda_0$ ) by the physical values obtained as a function of the regularization parameter. It is necessary, then, to specify the renormalization conditions that define the Green functions in an arbitrary point, the renormalization scale  $\mu$ . These conditions relate the naked parameters to the renormalized ones:

$$\begin{aligned} m &= m(m_0, \lambda_0, \Lambda, \mu), \\ \lambda &= \lambda(m_0, \lambda_0, \Lambda, \mu). \end{aligned} \tag{3.4}$$

In order to see the effects of QFT on the cosmological constant, we use two of the different renormalization schemes:

- Modified minimal subtraction scheme ( $\overline{\text{MS}}$ ). It eliminates the pole at  $1/(4-d)$  which has appeared in the regularization together with the other constant terms, by adding an arbitrary mass  $M$  to maintain the dimensions in the equation.
- Moment subtraction scheme. It considers the renormalization scale as the euclidean momentum and gives more physical results which depend on the mass.

### 3.1.3 Renormalization Group Equations

It has just been seen that a renormalized QFT is not, in general, scale invariant. This dependence of the QFT with the scale is described by the *Renormalization Group Equations* (from now on *RGE*).

Once the theory has been renormalized, the masses and the coupling constants become functions of the renormalization scale  $\mu$ , since although its naked values are fixed, a change in the renormalization scale varies their renormalized values:

$$\begin{aligned} \mu \longrightarrow \mu + \delta\mu &\implies m \longrightarrow m + \delta m \\ &\lambda \longrightarrow \lambda + \delta\lambda. \end{aligned} \tag{3.5}$$

The naked Green functions are, however, scale independent. Since renormalization rescales the fields following  $\phi = Z^{-1/2}\phi_0$  (where  $Z$  is a renormalization constant), going from the naked Green function ( $G_0$ ) to the renormalized one ( $G_R$ ) is achieved just by this scaling. Therefore, the conservation equation for  $G_0$  is simply converted into another differential equation for  $G_R$  at order  $n$ :

$$\mu \frac{d}{d\mu} G_0^{(n)}(p_i; m_0, \lambda_0, \Lambda) = 0 \quad (3.6)$$

↓

$$\mu \frac{d}{d\mu} Z_\phi^{-n/2} G_R^{(n)}(p_i; m_0, \lambda_0, \Lambda) = 0. \quad (3.7)$$

The specific dependence of  $\lambda$ ,  $m$  and  $Z_\phi$  on the scale  $\mu$  defines three functions: the beta function ( $\beta$ ), the anomalous mass dimension ( $\gamma_m$ ) and the anomalous field dimension ( $\gamma_\phi$ ):

$$\begin{aligned} \beta(\lambda) &\equiv \mu \frac{\partial \lambda}{\partial \mu}, \\ \gamma_m(\lambda) &\equiv \frac{1}{m} \mu \frac{\partial m}{\partial \mu}, \\ \gamma_\phi(\lambda) &\equiv -\frac{1}{2} \mu \frac{\partial \ln Z_\phi}{\partial \mu}. \end{aligned} \quad (3.8)$$

Using now these three functions to rewrite Equation 3.7, one obtains the Renormalization Group Equations:

$$\left[ \mu \frac{\partial}{\partial \mu} + \beta \frac{\partial}{\partial \lambda} + \gamma_m m \frac{\partial}{\partial m} + n \gamma_\phi \right] G_R^{(n)}(p_i; m_0, \lambda_0, \Lambda) = 0. \quad (3.9)$$

Because  $G_R$  is a renormalized function, it does not depend on the regularization parameter  $\Lambda$ . Consequently, neither do  $\beta$ ,  $\gamma_m$  and  $\gamma_\phi$ . Besides, according to the form of Equation 3.9, these functions must be dimensionless, and so, in case they have a dependence on the renormalization scale it should be of the type:

$$\beta(\lambda, \mu/m), \quad \gamma_m(\lambda, \mu/m), \quad \gamma_\phi(\lambda, \mu/m).$$

Even though the three functions depend on the renormalized coupling constants, it is the beta function the one that shows the evolution with the renormalization scale. Mathematically, this function can have three behaviours when one considers small couplings and therefore the expansion at first order is valid:

(i)  $\beta(\lambda) > 0$ . In this case the coupling constant  $\lambda$  tends to zero in the infrared, and that allows the theory to make predictions at low energies. On the contrary,  $\lambda$  diverges in the ultraviolet.

(ii)  $\beta(\lambda) = 0$ .  $\lambda$  does not show any evolution, so it coincides with the naked value  $\lambda_0$ .

(iii)  $\beta(\lambda) < 0$ . The behaviour is the opposite to case (i) and the theories are called *asymptotically free* because there is no interaction at high energy.

If, instead, the couplings are strong, the first order approximation is not valid any more, and one should consider higher orders for  $\beta(\lambda)$ . Then, maxima and minima in  $\beta(\lambda)$  arise and so, also fixed points  $\lambda_*$  so that  $\beta(\lambda_*) = 0$ . If at high energies  $\lambda$  tends to  $\lambda_*$ , we say that there is a fixed point in the ultraviolet, and if the tendency is at low energies, the fixed point is in the infrared.

## 3.2 Renormalization Group Equations for the cosmological constant

The results just introduced are well known in a flat space, but when working in a curved space-time the formalism shows some problems. The bases for the generalization are clear: in the action representing a flat space-time one must change partial derivatives for the covariant ones, the Minkowski metric for a generic one, and  $d^4x$  for  $d^4x\sqrt{-g}$ . With these transformations on the fields of the Standard Model, the addition of the Hilbert-Einstein action, and the other terms necessary for renormalization, one obtains an action 3.2 for the vacuum in a curved space-time.

The cosmological constant appearing in Equation 3.1 is nothing else but a naked parameter that absorbs part of the divergences when the theory is renormalized.

When one uses the dimensional regularization and the renormalization scheme

### 3.2. Renormalization Group Equations for the cosmological constant 43

$\overline{\text{MS}}$ , the renormalization group equation for the cosmological constant can be written as:

$$\mu \frac{d}{d\mu} \left( \frac{\Lambda}{8\pi G} \right) = \beta_{\Lambda}(\overline{\text{MS}}) = \frac{m^4}{2(4\pi)^2}. \quad (3.10)$$

In the same way, the Newton constant  $G$  is also a parameter which has been renormalized and follows its own RGE:

$$\mu \frac{d}{d\mu} \left( -\frac{1}{16\pi G} \right) = \beta_G(\overline{\text{MS}}) = \frac{m^2}{(4\pi)^2} \left( \xi - \frac{1}{6} \right), \quad (3.11)$$

where  $\xi$  is the parameter introduced by the non-minimal part of the action.

The renormalization scale  $\mu$  has a difficult interpretation already in a flat space-time within the  $\overline{\text{MS}}$  scheme, because it is only an auxiliary parameter in the dimensional regularization. Furthermore, the beta function usually fails at low energies. On the other hand, the mass dependent schemes do give a meaning to  $\mu$ , and since at high energies both beta functions must agree, the comparison should let us interpret the renormalization scale even in the  $\overline{\text{MS}}$  scheme. The  $\overline{\text{MS}}$  scheme gets easier results, but besides the mentioned problems, it does not show the decoupling of the massive degrees of freedom (Appelquist-Carazzone theorem [11]).

Knowing these difficulties, it seems essential to calculate the RGE within a mass dependent scheme. However, up to now, calculations in a curved space-time are made perturbatively on the metric of a flat space-time. Consequently, non-perturbative effects cannot be seen and results are not universal. Actually, in Ref. [92] the RGE for  $\Lambda$  and  $G$  have already been calculated within a mass dependent scheme, and they obtained a null  $\beta$ -function. That was attributed to a problem in the calculation methodology, as the ultraviolet limit did not coincide with the result in the  $\overline{\text{MS}}$  scheme.

These are some of the reasons why usually one calculates the  $\beta$ -function with the  $\overline{\text{MS}}$  scheme which should be correct at high energies, and later, one poses hypotheses about the renormalization scheme and the degree of compliance of the Appelquist-Carazzone theorem. In the following, we will use this methodology, but before, a general form for Equation 3.10 can be given.

Let us consider the beta function of Equation 3.10, which has been obtained within the  $\overline{\text{MS}}$  scheme, and therefore, should show the correct behaviour at high energies. However, at low energies, the  $\beta$ -function depends on the mass and one should check whether massive degrees of freedom are important or not. We have seen that we cannot calculate it with a mass dependent renormalization scheme, but we can look for a general form. This kind of procedures introduce a series of terms of the form  $\mu/M$ , as it happens with the  $a_i$  terms in the vacuum action 3.2 (see [92]). Hence, one can expect a similar decoupling for the cosmological constant, so that its  $\beta$ -function has  $\mu^2 M^2$  terms:

$$\begin{aligned} \frac{d\Lambda}{d \ln \mu} &= \frac{1}{(4\pi)^2} \left( \sum_i A_i m_i^4 + \mu^2 \sum_j B_j M_j^2 + \mu^4 \sum_j C_j + \mu^6 \sum_j \frac{D_j}{M_j^2} + \dots \right) \\ &\equiv \sum_{n=0}^{\infty} \sum_i \alpha_{in} \mathcal{M}_i^4 \left( \frac{\mu}{\mathcal{M}_i} \right)^{2n} \equiv \beta_{\Lambda}(\mathcal{M}_i, \mu/\mathcal{M}_i). \end{aligned} \quad (3.12)$$

where  $m_i$  are the light degrees of freedom with  $\mu > m_i$ ,  $M_j$  are the heavy ones with  $\mu < M_j$ , and  $i$  and  $j$  represent the massive fields.  $A, B, C$  and  $D$  are constant terms, whereas the index  $n$  is the order of the development.

From the comparison between this equation in the ultraviolet and the one obtained in the  $\overline{\text{MS}}$  scheme, one can obtain the explicit form for the constant  $A_i$  corresponding to particles with mass  $m_i$  and spin  $J_i$ ,

$$A_i = (-1)^{2J_i} (J_i + 1/2) n_{J_i} N_c, \quad (3.13)$$

with  $n_{\{0,1,1/2\}} = (1, 1, 2)$  and  $N_c = 1, 3$  for particles without and with colour respectively.

In Equation 3.12 there are not odd powers because  $\mu$  appears in calculations bilinearly in the contractions with the metric tensor. Covariance, for instance, forbids the first term linear in  $\mu$  and the development starts with  $\mu^2$ . The decoupling is produced according to the Appelquist-Carazzone theorem, and it introduces an inverse power suppression by the heavy masses. However, the form of the cosmological constant is different from all the other parameters in the Standard Model, having a dimensionality of energy to the fourth. That makes the first orders,  $n = 1, 2$ , be

different, since the beta function itself has a particular dependence proportional to  $M^4$ . Higher orders are suppressed in the usual way, but the difference in the second order provides the cosmological constant with a characteristic soft decoupling.

This equation is not univocally defined yet, one must specify a concrete meaning for the renormalization scale within the cosmological framework. There are mainly the differences in this choice that originate several cosmological scenarios.

### 3.3 Cosmological scenarios

Considering the Renormalization Group Equations for the cosmological and Newton constants in the Einstein's equations has motivated various cosmological models, which are variants of the standard FLRW. Most of them are consequence of the theory just introduced, although results with a non-perturbative quantum gravity have been obtained too. These are added for completeness at the end of the section.

#### 3.3.1 Perturbative solution to the Renormalization Group Equations

Before particularizing for the different cosmological scenarios, one should look at the necessary RGEs.

From the beginning, the  $a_i$  terms in the vacuum action have been discarded for the study of the current Universe, that is, at low energies. Besides, in Ref. [175] it is demonstrated that the evolution of  $G$  is irrelevant within the perturbative theory, since  $1/G \sim M_{Pl}^2$  is very large and so, in comparison, its running is not observed. Its situation is the opposite that for the cosmological constant, and its RGE does not need to be used. Finally, in respect to the induced term ( $\Lambda_{ind}$ ), its RGE is completely independent from the one of  $\Lambda_{vac}$ , but the decoupling is expected to occur in the same way, and therefore, the same form can be used for the total and physical cosmological constants ( $\Lambda_{ph} \equiv \Lambda$ ) as it is also demonstrated in [175].

Once it is realised that the only necessary contribution for the current Universe is the one coming from  $\beta_{\Lambda_{ph}}$ , let us see different approaches to its form.

### 3.3.1.1 Scenario 1: $m_i < \mu, \quad \mu \sim \rho_c^{1/4}(t)$

In Ref. [174], Shapiro and Solà suppose that the light degrees of freedom are the only ones that contribute to  $\beta_\Lambda$ . This way, Equation 3.12 keeps only the first term proportional to  $A_i$ . But in order to know which are these degrees of freedom one has to first define the renormalization scale  $\mu$ . Accepting that  $\mu$  is the typical energy scale in the Universe, it can be taken as the critical energy at any time:

$$\mu \sim \rho_c^{1/4}(t). \quad (3.14)$$

Nowadays,  $\rho_c^0 \approx (3\sqrt{h_0} \cdot 10^{-3} eV)^4$ , so the renormalization condition is specified at  $\mu_c = (\rho_c^0)^{1/4} \approx 10^{-3} eV$ . With this energy scale and considering the Standard Model of Particles, the only active degrees of freedom are the lightest neutrinos, and therefore, the  $\beta_\Lambda$  function in Equation 3.12 can be rewritten as:

$$\frac{d\Lambda}{d\ln\mu} = \frac{-4}{(4\pi)^2} \sum_{\nu} m_{\nu}^4, \quad (3.15)$$

where the sum is only for the lightest neutrinos: the electronic one and possibly an sterile one.

In this particular case, one can explicitly calculate the RGE both for  $\Lambda_{ind}$  and  $\Lambda_{vac}$ , which, in fact, result to be identical. Equation 3.15 is the sum of both.

The direct integration of Equation 3.15 implies a growing cosmological constant towards the future. The expected behaviour is just the opposite, and this is why it is sometimes included a light scalar field  $S$  that is still unknown, but would have an energy similar to the light neutrinos and would contribute positively to  $\beta_\Lambda$ :

$$\frac{d\Lambda}{d\ln\mu} = \frac{1}{2(4\pi)^2} m_S^4 - \frac{4}{(4\pi)^2} \sum_{\nu} m_{\nu}^4, \quad (3.16)$$

$$\Lambda(\rho) = \Lambda_0 + \frac{1}{(4\pi)^2} \left( \frac{1}{2} m_S^4 - 4 \sum_{\nu} m_{\nu}^4 \right) \ln \frac{\rho}{\rho_0}. \quad (3.17)$$

### 3.3.1.2 Scenario 2: $M_i > \mu$ , $\mu \sim \rho_c^{1/4}(t)$

The authors in [16] consider that although the contribution of particles with  $M > \mu$  is suppressed, this is still dominant over the one of particles with  $m < \mu$ . So, the heaviest particles dominate the running at any scale, and the development in 3.12 must be kept until  $n = 3$ .

After defining a renormalization scheme, Guberina et al. [93] obtain within the Standard Model of Particles the following beta function  $\beta_\Lambda$ :

$$\frac{d\Lambda}{d \ln \mu} = \frac{1}{2(4\pi)^2} \sum_i \sigma_i m_i^4 \frac{\mu^2}{\mu^2 + m_i^2}, \quad (3.18)$$

where the sum is over the  $i$  massive degrees of freedom, and  $\sigma_i = +1, -1$  for bosons and fermions respectively.

Now, Equation 3.18 is integrated, and after approximating the neutrinos to be massless (which in this case is a valid approximation due to the large mass difference with the other particles in the Standard Model) the running of the cosmological constant is given, up to  $n = 2$ , by:

$$\Lambda(\mu) = \Lambda_0 + \frac{1}{(4\pi)^2} \left[ \mu^2 \frac{1}{4} \left( m_H^2 + 3m_Z^2 + 6m_W^2 - 4 \sum_i N_i m_i^2 \right) + \mu^4 \left( \frac{1}{2} \sum_i N_i - \frac{5}{4} \right) \right]. \quad (3.19)$$

However, the  $\mu^2$  term would imply a huge evolution in no way supported by observations, and therefore this term is set to zero. That imposes a value to the Higgs' mass as a function of the other fields in the Standard Model:

$$m_H^2 = 4 \sum_i N_i m_i^2 - 3m_Z^2 - 6m_W^2 \approx (550 \text{ GeV})^2. \quad (3.20)$$

Despite of this mass being a bit high, it is within the current accepted interval of mass for the Higgs. Anyway, that does not avoid needing too much tuning to make this cosmological constant compatible with observations. Besides, the condition 3.20 is equivalent to  $\mu^2 \sum_j B_j M_j^2 = 0$  in the development obtained according to scheme

in 3.2. These  $B_j$  are not exactly the same appearing in Equation 3.19 and therefore, the Higgs' mass is different for different schemes.

In the same way as it happened in Scenario 1, the energy scale is given by  $\mu \sim \rho^{1/4}$ .

### 3.3.1.3 Scenario 3: $M_i > \mu$ , $\mu \sim R^{1/2} \sim H(t)$

The main variation in this scenario is a change in the renormalization scale. In Reference [174], it was already proposed:

$$\mu \sim R^{1/2} \sim (G\rho)^2 \sim H(t), \quad (3.21)$$

where  $R$  is the scalar of curvature and  $H$  the Hubble parameter with current value  $H_0 \sim 10^{-33} eV$ . With the hypothesis of *Scenario 1*, that would imply the absence of any active degree of freedom<sup>2</sup>, and so the cosmological constant would not suffer any running. This is why it is assumed here that due to the soft decoupling in the cosmological constant, the heaviest particles with  $M \sim M_{Pl}$  are those truly responsible for the running. Even the masses close to the possible Great Unification scale ( $M_{GUT} \sim 10^{16} GeV$ ) would cause a inappreciable running when compared to the one produced at Planck scale. With these premises, the order  $n = 0$  in Equation 3.12 is strictly zero, and from  $n = 2$  on the terms are irrelevant in front of the dominant contribution of  $n = 1$  [176]:

$$\frac{d\Lambda}{d\ln \mu} \simeq \frac{1}{(4\pi)^2} \sum_i \mu^2 B_i M_i^2. \quad (3.22)$$

with  $M_i \sim M_{Pl}$ . Since for  $B = \mathcal{O}(1 - 10)$  and  $M_i \sim M_{Pl}$ :

$$\beta_\Lambda^0 \simeq \frac{BH_0^2 M_{Pl}^2}{(4\pi)^2} \sim \frac{B (1.5 \cdot 10^{-42} GeV \times 1.2 \cdot 10^{19} GeV)^2}{(4\pi)^2} \sim 10^{-47} GeV^4 \sim \Lambda_0, \quad (3.23)$$

---

<sup>2</sup>In the Standard Model of Particle Physics the lightest particles are neutrinos with  $m_\nu \geq 10^{-3} eV$ .

and two such different scales like the one given by the Planck mass and the Hubble constant determine the correct order of magnitude of the cosmological constant.

The fact that this choice of the renormalization scale provides such a low value makes the evolution to remain soft during most of the life of the Universe. The cosmological constant grows towards the past, and for example, in the Fermi epoch:

$$\Lambda_F \simeq H_F^2 M_{Pl}^2 \sim \left( \frac{T_F^2}{M_{Pl}} \right)^2 M_{Pl}^2 \sim M_F^4, \quad (3.24)$$

whereas in the Planck epoch  $\Lambda_{Pl} \sim M_{Pl}^4$ . In fact, the RGE is only valid until the Planck scale. After that point, it is necessary a complete quantum gravity theory, and since even the metric would be highly fluctuating then, it has no sense to speak about the Hubble parameter. So, “only” up to the Planck epoch, the running of the cosmological constant is described by:

$$\frac{d\Lambda}{d\ln H} = \frac{1}{(4\pi)^2} \sigma H^2 M^2, \quad (3.25)$$

$$\Lambda(H) = \Lambda_0 + \frac{\sigma}{2(4\pi)^2} M^2 (H^2 - H_0^2). \quad (3.26)$$

where  $\sigma = +1, -1$  correspond to the different cases where bosons or fermions dominate at high energies, and it has been defined  $M \equiv \sqrt{|\sum_i B_i M_i^2|}$ .

#### 3.3.1.4 Comparisons

Once it has been obtained the dependence of the cosmological constant with the energy scale, one can see the magnitude of the effect graphically.

In Figure 3.1, it has been represented the evolution of the cosmological constant as a function of both the critical density ( $\rho_c$ ) and the redshift ( $z$ ) for the three scenarios. It must be noted that the renormalization scales are different, but the relation between the Hubble parameter and the critical density (Eq.3.27) makes possible that the results are expressed just as a function of one of them, in this case  $\rho_c$ .

$$\rho_c(z) = \frac{3M_{Pl}^2}{8\pi} H(z)^2. \quad (3.27)$$

Scenario 1 is, given a particle physics model, a case without free parameters. The problem is that the mass of the light neutrinos is not a very well known parameter. Furthermore, in order to obtain the observed behaviour, an extra scalar field must be added to the beta function  $\beta_\Lambda$ , being in this way positive and producing a growing cosmological constant in the past. Following the values in [174], the figure has been plotted with  $m_\nu = 0.002 \text{ eV}$  and  $m_S = 4 m_\nu$ .

A similar thing happens in Scenario 2. However, here the Standard Model of particle physics fully determines the evolution:

$$\eta \equiv \frac{1}{2} \sum_i N_i - \frac{5}{4} = 10.75. \quad (3.28)$$

On the other hand, in Scenario 3, masses close to the Planck mass scale are completely unknown, waiting for a theory that predicts these values. In Figure 3.1 it has been used  $\nu = 0.1$ , where the parameter  $\nu$  is defined later in this chapter (Eq. 3.35) as the ratio between these masses and the Planck one.

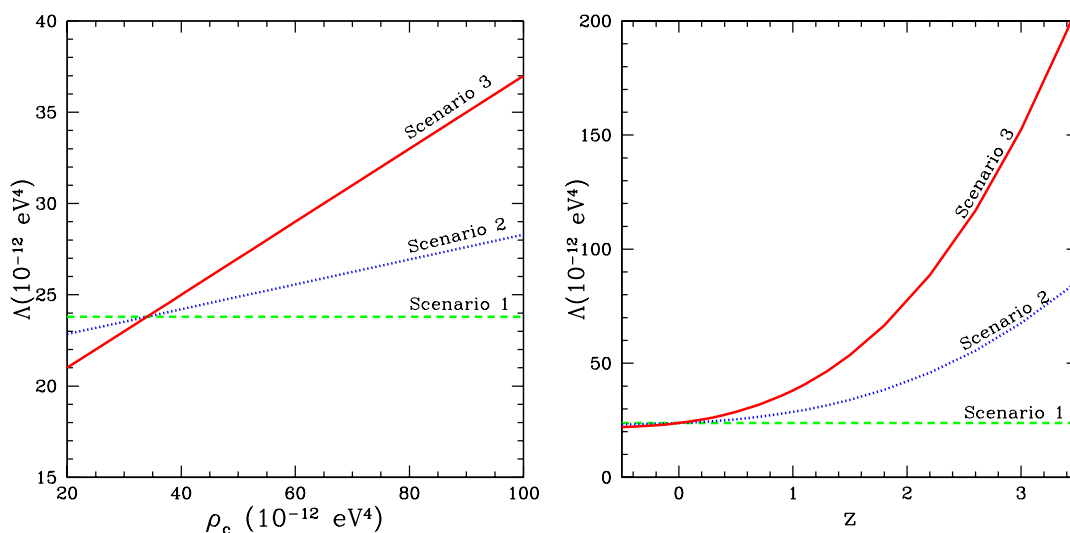


Figure 3.1: Evolution of the cosmological constant as an effect of the RGE in the three scenarios introduced in this section. The same evolution is shown as a function of the critical density ( $\rho_c$ ) and the redshift ( $z$ ).

All the models shown here forecast growing values of the cosmological constant towards the past and a decline in the future, even though it has been omitted a version of Scenario 1 without the extra scalar field and Scenario 3 with a negative  $\nu$ , both of them with the opposite behaviour. For the first model, Scenario 1, no running is observed at the scale of the other two. Since its cause are the less massive particles, its effect is much smaller than in the other cases, and the logarithmic evolution in  $\rho_c$  predicted by Equation 3.17 remains hidden six orders of magnitude below the others. The slope in Scenario 2, much more evident, is univocally determined by its RGE when the  $\mu^2$  term is tuned to be null. In Scenario 3, the slope is different according to the value of the index  $\nu$ . Even if in the figure one can observe a stepper function than the one in the previous scenario, the slope could be much smaller, and even insignificant if  $\nu$  were really small. The discussion of this third case is detailed in Section 3.4, all of it devoted to see the consequences of a cosmology dominated by the most massive particles situated close to the Planck scale as analysed in [75].

As a practical issue with a view to the second part of the thesis, these evolutions have also been represented as a function of redshift in Figure 3.1. This parameterization is very useful when cosmological distances are applied in order to characterize the models and determine the cosmological parameters.

### 3.3.2 Non-perturbative solution to the Renormalization Group Equations

This approach is quite different from the ones just shown, since the exact Renormalization Group Equations for quantum gravity are used under the assumption of the existence of a fixed point in the infrared [31, 24]. That allows the Renormalization Group Equations to be solved not perturbatively, but in an approximate way by means of the truncation method. In this manner, it is seen that the couplings  $G$  and  $\Lambda$  also acquire a dependence on the scale.

#### 3.3.2.1 Scenario 4: $\mu \sim 1/t \sim H(t)$

The existence of a fixed point ( $g_*$  and  $\lambda_*$  for  $G$  and  $\Lambda$  respectively) allows to establish a dependence with the scale close to that point:

$$\begin{aligned} G(\mu) &= g_*/\mu^2, \\ \Lambda(\mu) &= \lambda_*\mu^2. \end{aligned} \tag{3.29}$$

On the other hand, Bonanno et al. [31] consider that the energy scale is inversely proportional to the cosmic time,

$$\mu = \xi/t, \tag{3.30}$$

where  $\xi$  is a positive constant. Since  $H \propto 1/t$  in the FLRW cosmology, this election is not essentially different from 3.21.

Under these hypotheses, the system of differential equations for a flat FLRW cosmology is solved in [24]. An only attractor is found at  $t \rightarrow \infty$ :

$$\begin{aligned} G(t) &= \frac{3}{8}(1+w)^2 g_* \lambda_* t^2, \\ \Lambda(t) &= \frac{8}{3(1+w)^2} \frac{1}{t^2}, \end{aligned} \tag{3.31}$$

where  $w$  is the barotropic index of the equation of state  $p(t) = w\rho(t)$  corresponding to the dominant component.

It is worth to mention that, contrary to the other scenarios, the Newton constant also experiments an evolution here which should be taken into account when depicting the dynamics of the Universe.

### 3.3.3 Renormalization scale

As it has been seen in these four scenarios, four different renormalization scales have been proposed ( $\rho^{1/4}$ ,  $R^{1/2}$ ,  $H$  and  $t^{-1}$ ), which, in the cosmological framework, can be reduced to  $\rho^{1/4}$  and  $H$ . Nevertheless, that results in a great ambiguity as to the parameter with respect to which the evolution of the Universe is described.

A method to resolve the ambiguity has been proposed in [17]. They impose general covariance on the Einstein's equations (Eq. 2.5), and so, both sides of the equations must be conserved. Once established  $\Lambda(\mu)$  and  $G_N(\mu)$ , that relates  $\mu$  to the matter density  $\rho_M$ . In a similar way as the effect of the RGE on the density of matter is determined in this thesis, the authors in [17] use the relation in order to determine  $\mu$  as a function of  $\rho_M$ . However, the background is different: we do not assume the validity of the usual evolution of  $\rho_M(z)$  but it is derived from the equations, whereas in [17], the relation is considered to be universal.

Anyway, this method to determine  $\mu$  agrees within certain limits with the natural choices of the previous section. For the scenarios corresponding to the perturbative solution of the RGE, the  $\mu$  value can be approximated to  $H$  under some hypotheses, whereas for the ones based on quantum gravity with a fixed point in the infrared one gets  $\mu \propto 1/t$  only in a flat universe.

## 3.4 Cosmology in Scenario 3

In order to see how the dynamics of the Universe is affected by the evolution of the cosmological constant, the usual system of equations must be solved together with the Renormalization Group Equation for the cosmological constant, and, if necessary, with the Renormalization Group Equation for the gravitational constant. Thus, in this section the equations deduced in Section 2.3 are joined together with the ones deduced in the previous sections, in particular for Scenario 3.

### 3.4.1 Cosmological equations

In the previous sections, it has been obtained the RGE for the cosmological constant at low energies as a function of the energy scale, that is to say, in this scenario, as a function of the Hubble parameter  $H(t)$ . On the other hand, the conservation Equation 2.39 (*CE*) was expressed in terms of the cosmic time, whereas the variable for the Friedmann equation 2.42 (*FE*) was the redshift. By simply using the chain rule and doing some combinations among equations, the system of these three independent equations as a function of redshift reads:

$$CE, \quad a = \frac{1}{1+z}, \quad \dot{a} = aH \quad \Longrightarrow \quad \frac{d\Lambda}{dz} + \frac{d\rho}{dz} = \frac{3\rho}{1+z}, \quad (3.32)$$

$$RGE \quad \Longrightarrow \quad \frac{d\Lambda}{dz} = \frac{d\Lambda}{d \ln H} \frac{d \ln H}{dH} \frac{dH}{dz} = \frac{(4\pi)^2}{2} \sigma M^2 \frac{dH^2}{dz}, \quad (3.33)$$

$$FE \quad \Longrightarrow \quad \frac{dH^2}{dz} = \frac{8\pi G}{3} \left( \frac{d\Lambda}{dz} + \frac{d\rho}{dz} \right) + 2H_0^2 \Omega_K^0 (1+z). \quad (3.34)$$

This is the set of cosmological equations that, once it is solved, describes the dynamics of a universe with an evolving cosmological constant.

Let us define now two dimensionless parameters,  $\nu$  and  $\kappa$ , from which only one is independent, but which are useful in order to analyse the model:

$$\nu \equiv \frac{\sigma}{12\pi} \frac{M^2}{M_P^2}, \quad (3.35)$$

$$\kappa \equiv -2\nu\Omega_K^0. \quad (3.36)$$

With these definitions and inserting Equation 3.34 into 3.33 and then the result into 3.32, one obtains a differential equation for the density of matter,

$$\frac{d\rho}{dz} - \frac{3(1-\nu)\rho(z)}{1+z} - \kappa\rho_c^0(1+z) = 0, \quad (3.37)$$

which can be integrated with the initial condition such that for  $z = 0$  the density of matter be  $\rho = \rho_M^0$ :

$$\rho(z; \nu) = \left( \rho_M^0 + \frac{\kappa}{1-3\nu} \rho_c^0 \right) (1+z)^{3(1-\nu)} - \frac{\kappa}{1-3\nu} \rho_c^0 (1+z)^2. \quad (3.38)$$

Introducing now this result into the continuity equation 3.32, the evolution of the cosmological constant energy density is achieved:

$$\Lambda(z; \nu) = \Lambda_0 + \rho_M^0 f(z) + \rho_c^0 g(z), \quad (3.39)$$

where the initial condition is  $\Lambda(z = 0) = \Lambda_0$  and

$$f(z) = \frac{\nu}{1 - \nu} \left[ (1 + z)^{3(1-\nu)} - 1 \right], \quad (3.40)$$

$$g(z) = -\frac{\kappa}{1 - 3\nu} \left\{ \frac{z(z + 2)}{2} + \frac{\nu}{1 - \nu} \left[ (1 + z)^{3(1-\nu)} - 1 \right] \right\}. \quad (3.41)$$

Both in Equation 3.38 and 3.39, the parameters  $\nu$  and  $\kappa$  play an important role. The latter denotes the spatial curvature of the Universe: if  $\nu > 0$  the sign of  $\kappa$  agrees with the sign of the curvature  $k$ , for  $\kappa > 0$  ( $\sigma > 0$ ) the universe is closed, whereas for  $\kappa < 0$  ( $\sigma < 0$ ) the universe is open. On the contrary,  $\nu < 0$  makes  $k$  and  $\kappa$  be of the opposite sign. For  $\kappa = 0$  the universe is flat, and the second terms of the right hand side of Equations 3.38 and 3.39 disappear. The other parameter  $\nu$  acts as a *cosmological index* and shows the deviation of the density with respect to its value in a FLRW cosmology without the effects of renormalization, since for  $\nu = 0$  also  $\kappa = 0$ , and so, the standard results are recovered.

Let us examine now how the dynamics of the Universe changes with the cosmological index  $\nu$ .

### 3.4.2 Cosmological index $\nu$

The energy density evolution equations for  $\rho(z)$  and  $\Lambda(z)$  vary enormously according to the value of  $\nu$ . At low redshift, discrepancies are tolerable since the initial condition is imposed at  $z = 0$ . However, at high redshift, some behaviours are very different from the cosmological constant case and are incompatible with current observations.

#### 3.4.2.1 Case $\nu < 0$

In this interval the cosmological constant becomes negative and grows towards the past ( $z \rightarrow \infty$ , but still in the matter dominated epoch where equations have been

solved), whereas the density of matter tends towards  $\rho_M \rightarrow +\infty$ . Going to the future ( $z \rightarrow -1$ ) both densities diminish in absolute value, approaching to zero the matter component and to a  $\nu$ -dependent value the cosmological constant. In a flat universe the concrete value is just:

$$\Lambda(z = -1) = \Lambda_0 + \left| \frac{\nu}{1 - \nu} \right| \rho_M^0. \quad (3.42)$$

This way the cosmological constant ends by being positive, being now of the imposed sign  $\Lambda(0) = \Lambda_0$ , and negative in the past. The transition between the negative and positive cosmological constant was produced at redshift:

$$z_{tr} = \left[ 1 + \left( 1 + \frac{1}{|\nu|} \right) \left( \frac{\Omega_\Lambda^0}{\Omega_M^0} \right) \right]^{\frac{1}{3(1+|\nu|)}} - 1. \quad (3.43)$$

Just to give some numbers, let us consider a universe with  $\Omega_M^0 = 0.3$ ,  $\Omega_\Lambda^0 = 0.7$  and  $\nu = -0.1$ , then the transition occurs at  $z_{tr} = 1.7$ . For the same cosmology, lower values of  $\nu$ ,  $\nu = -0.05$ , mean transitions at higher redshift,  $z_{tr} = 2.4$ . So, the physics which is deduced from the  $\nu < 0$  case is admissible as long as  $|\nu|$  is not excessively large, considering that then the transition redshift would be low enough so as to be detected.

#### 3.4.2.2 Case $\nu = 0$

All the conclusions obtained for a universe with a truly constant cosmological constant are recovered.

#### 3.4.2.3 Case $0 < \nu < 1$

In this range, both the density of matter and of cosmological constant become positive and tend to infinite towards the past. In the future, the cosmological constant will achieve a positive, and in general different from zero, value, whereas the density of matter tends to zero.

Let us come back to the flat case where the asymptotic regimes are more easily obtained. Similar to Equation 3.42, now the cosmological constant will reach the value:

$$\Lambda(z = -1) = \Lambda_0 - \frac{\nu}{1 - \nu} \rho_M^0. \quad (3.44)$$

So, depending on the value of  $\nu$ , the asymptotic limit will be positive or negative. It can be shown that this characteristic remains the same for some values of the curvature.

Note here that this behaviour is the desired one in string theories or M-Theory, where it is necessary a negative or null cosmological constant in order to define the asymptotic states of the so-called S matrix. This kind of theories will then be able in the future to predict a value for  $\nu$  as a requirement of the theory itself.

#### 3.4.2.4 Case $\nu = 1$

This is not a very desirable case, since in a flat universe the density of matter would be the same at each redshift. The situation improves when it is considered a positive curvature, but it gets even worse in a universe with negative curvature, where the density of matter in the past tends to  $\rho_M \rightarrow -\infty$ .

For a positive curvature ( $k > 0$ ) and  $\nu > 0$  one obtains  $\kappa > 0$ . With these signs, Equation 3.38 describes an evolution for the density of matter which goes from a positive large value in the past to a very small value in the future. On the other hand, the cosmological constant begins by being also large and positive, goes through zero and grows again in modulus towards large negative values. The transition occurs at:

$$z_{tr} \simeq \exp(-\Omega_\Lambda^0/3\Omega_M^0) - 1. \quad (3.45)$$

For a slightly curved universe completely compatible with current CMB observations,  $\Omega_M^0 = 0.30$  and  $\Omega_\Lambda^0 = 0.71$ , one obtains  $z_{tr} = -0.54$ . Therefore, we should wait to the far future in order to reach the transition epoch.

### 3.4.2.5 Case $\nu > 1$

This last section encompasses the most observationally disfavoured case. A value of  $\nu$  greater than one implies that as the modulus of the cosmological constant grows, also does the density of matter due to the energy balance between  $\Lambda$  and  $\rho$ . So, we would live in a universe with an increasing density of matter even though expanding, reminding of Hoyle's Universe (although in that case he supposed an steady universe) where matter was created.

## 3.4.3 Primordial nucleosynthesis restrictions

The impact of a running cosmological constant is also evident beyond the matter dominated era. In particular, the nucleosynthesis epoch is a very well known period which is altered by this running. But this pillar of the Standard Model of Cosmology is a very solid one, and any new cosmological alternative should respect it unless it introduces a complete landscape as consistent as the current one for describing the Universe.

In order to see how our knowledge of the primordial nucleosynthesis restricts the possibility of an evolving cosmological constant, it is necessary to solve the cosmological equations in this epoch. That means that the equation of state of matter ( $p_M = 0$ ) has to be changed by the one of radiation ( $p_R = \rho_R/3$ ). This way, the continuity equation converts into:

$$\dot{\Lambda}_R + \dot{\rho}_R + 4H\rho_R = 0. \quad (3.46)$$

Following the same steps as in the matter dominated era, the density of radiation can be expressed as:

$$\rho_R(z; \nu) = \left( \rho_R^0 + \frac{\kappa}{2 - 4\nu} \right) (1 + z)^{4(1-\nu)} - \frac{\kappa}{2 - 4\nu} (1 + z)^2. \quad (3.47)$$

However, for radiation, it is more appropriate to express the result as a function of the temperature  $T$  of the thermal bath of radiation, being  $(1 + z) \propto T$ ,

$$\rho_R(T; \nu) = \frac{\pi^2}{30} g_* T^4 \left( \frac{T_0}{T} \right)^{4\nu} + \frac{\kappa}{2-4\nu} \left[ \left( \frac{T}{T_0} \right)^{4(1-\nu)} - \left( \frac{T}{T_0} \right)^2 \right], \quad (3.48)$$

where  $T_0 \approx 2.75 \text{ K} = 2.37 \times 10^{-4} \text{ eV}$  is the current CMB temperature and the number of ultrarelativistic degrees of freedom,  $g_*$ , is of order one ( $g_* = 2$  for photons and  $g_* = 3.36$  with also neutrinos). In a similar way, the cosmological constant density is:

$$\Lambda_R(T; \nu) = \Lambda_0 + \rho_R^0 f_R(T) + \rho_c^0 g_R(T), \quad (3.49)$$

with

$$f_R(T) = \frac{\nu}{1-\nu} \left[ \left( \frac{T}{T_0} \right)^{4(1-\nu)} - 1 \right], \quad (3.50)$$

$$g_R(T) = -\frac{\kappa}{2-4\nu} \left\{ \frac{T^2 - T_0^2}{T_0^2} - \frac{\nu}{1-\nu} \left[ \left( \frac{T}{T_0} \right)^{4(1-\nu)} - 1 \right] \right\}. \quad (3.51)$$

The first limitation from these equations comes from the fact that the density at the nucleosynthesis epoch cannot be much different from the standard one since its value is known with high precision [200, 135]. Therefore, the  $\nu$  index has to be small enough:

$$|\nu| \ll 1. \quad (3.52)$$

Furthermore, the density of cosmological constant must be less than the density of matter at the nucleosynthesis epoch in order to allow atomic nuclei to be formed with the abundances they are observed. Imposing the difference between both to be at least one order of magnitude, it is obtained again the same restriction:

$$\frac{\Lambda_R(T)}{\rho_R(T)} \simeq \frac{\nu}{1-\nu} \simeq \nu \ll 1, \quad (3.53)$$

where the development is valid in a flat universe.

This limit obtains a stricter constrain from the CMB fluctuations and galaxy studies, which impose a maximum of  $\nu_{max} = 2.3 \times 10^{-3}$  [136]. Density perturbations further constrain the limit to  $|\nu| < 10^{-4}$  [77].

### 3.4.4 Behaviour in the physical range $|\nu| \ll 1$

Once it has been determined the most probable range for  $\nu$ , all the subsequent analysis is restricted to this interval. It is then useful to define the most natural value for this index, that obtained for  $\sigma = +1$  and  $M = M_P$ :

$$\nu_0 \equiv \frac{1}{12\pi} \approx 2.6 \times 10^{-2}. \quad (3.54)$$

The various functions and parameters will be represented for the first multiples of  $\nu_0$ .

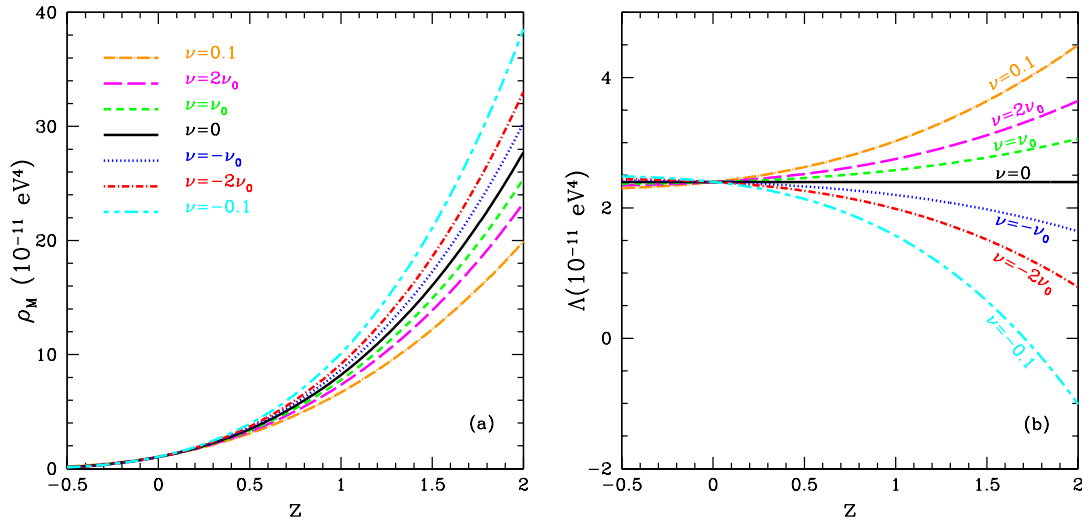


Figure 3.2: Density of matter (a) and cosmological constant (b) in a flat universe with  $\Omega_M^0 = 0.3$  and  $\Omega_\Lambda^0 = 0.7$ . Different kinds of lines show a different deviation from the standard model with  $\nu = 0$ .

Figure 3.2 shows the variation of the density of matter (a) and cosmological constant (b) in a flat universe with  $\Omega_M^0 = 0.3$  and  $\Omega_\Lambda^0 = 0.7$ . The redshift interval

starts in a point in the future,  $z = -0.5$ , and ends where the furthest supernova data are expected to be detected,  $z = 2$ . So, variations in this range should be detected observationally.

As a result of demanding a non-null  $\beta_\Lambda$ , it appears a correlation between the evolution of  $\rho_M(z; \nu)$  and  $\Lambda(z; \nu)$ . These two quantities are important in cosmology since the luminosity distance is a function of them, and their form is relevant in the determination of the cosmological parameters (Eqs. 2.51 and 2.42 in Chapter 2).

Comparing with the standard cosmological model ( $\nu = 0$ ), it is seen that for a negative cosmological index the density of matter grows faster towards the past, whereas for a positive value, the growth is slower than usual. Looking at the future, the distinction is not appreciable: the density of matter tends to zero regardless the value of  $\nu$ . The opposite happens for the cosmological constant. It is for a positive  $\nu$  (negative) that the cosmological constant increases (decreases) towards the past, whereas in the future it reaches a constant positive value. It is worth remembering that all these comments refer to  $|\nu| \leq 0.1$ , since as it has been seen, wider ranges imply other behaviours.

Figure 3.3 reproduces the same functions as Figure 3.2 for a non-null curvature. The results are qualitatively the same, but the features are stronger already at lower  $\nu$ 's. Particularly, it is for closed universes with  $\nu < 0$  that the greatest evolution in the cosmological constant is generated, and so, this is the most favoured case to be compared with observations.

Looking at the evolutions of the cosmological constant and the density of matter one can wonder if these high values of the cosmological constant could alter the structure formation. Nevertheless, in this model the cosmological constant remains always under the density of matter, and for  $\nu \ll 1$  it has been seen that primordial nucleosynthesis is not damaged either (see Section 3.4.3). In fact, the equality between matter and cosmological constant has been produced recently. For a flat universe with the parameters used in Figure 3.2 ( $\Omega_M^0 = 0.3$  and  $\Omega_\Lambda^0 = 0.7$ ), it is obtained the equality redshift  $z = (0.29, 0.31, 0.32, 0.34, 0.36)$  for  $\nu = (-2\nu_0, -\nu_0, 0, +\nu_0, +2\nu_0)$  respectively. For larger values of  $\nu$  still within the limit 3.53, the transition redshifts are low:  $z = (0.27, 0.43)$  for  $\nu = (-0.1, +0.1)$ , and the structure formation is never altered. The variation of the equality redshift with  $\nu$  is represented by the lower curve in Figure 3.7 (b).

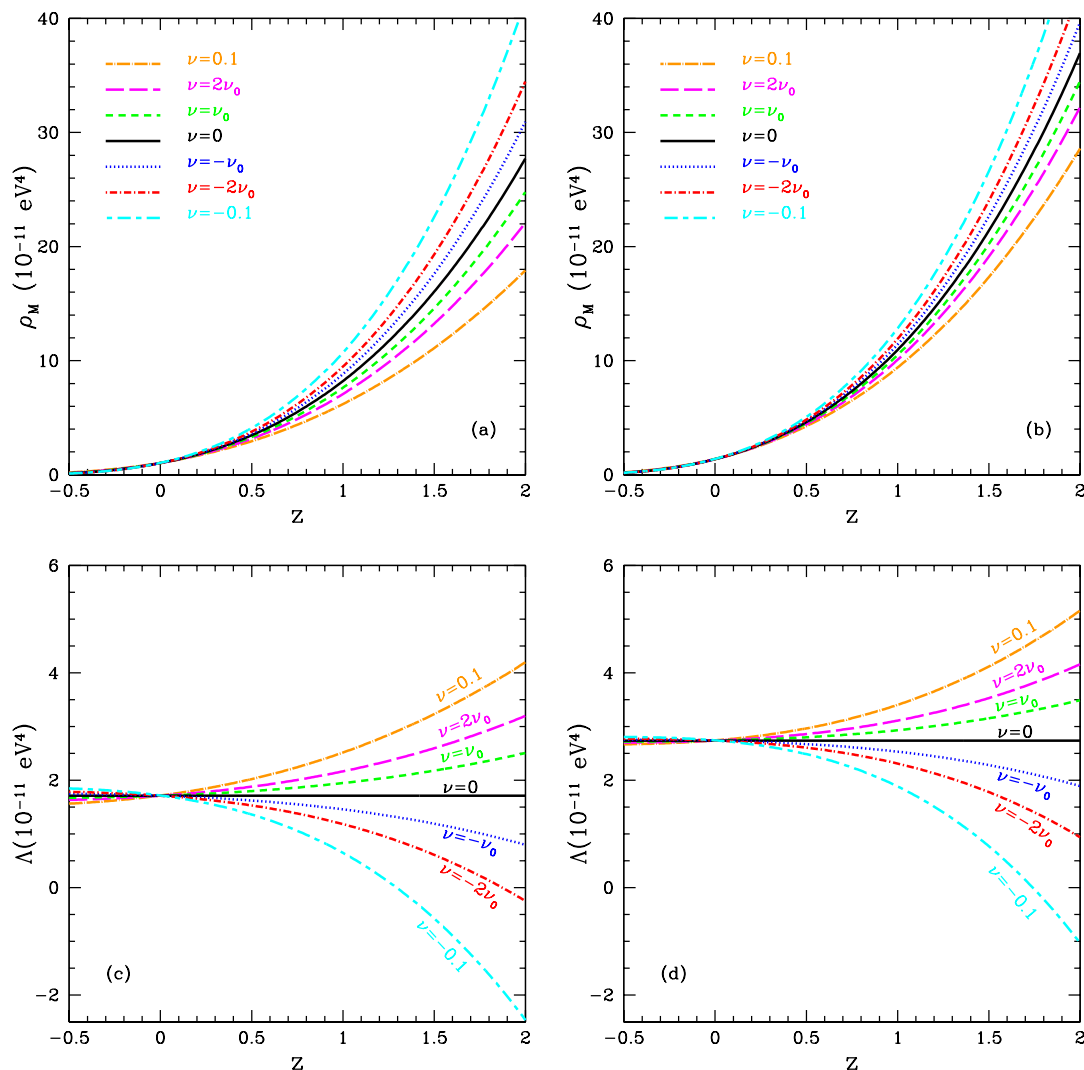


Figure 3.3: Evolution of the density of matter and cosmological constant for an open universe with  $\Omega_M^0 = 0.3$  and  $\Omega_\Lambda^0 = 0.5$  (left) and for a closed universe with  $\Omega_M^0 = 0.4$  and  $\Omega_\Lambda^0 = 0.8$  (right).

It has been already mentioned that the functions  $\rho_M(z; \nu)$  and  $\Lambda(z; \nu)$  are the most interesting ones for cosmology, since they are the only observables. In order to see the effect that the running of the cosmological constant has in the luminosity distance, it can be calculated the percentage of variation of the function. Again in the flat case, the development of the cosmological constant at first order in  $\nu$  is:

$$\Lambda(z) \simeq \Lambda_0 + \nu \rho_M^0 [(1+z)^3 - 1] . \quad (3.55)$$

Then, the effect of the variation is given by

$$\delta_\Lambda \equiv \frac{\Lambda(z; \nu) - \Lambda_0}{\Lambda_0} = \nu \frac{\Omega_M^0}{\Omega_\Lambda^0} [(1+z)^3 - 1] . \quad (3.56)$$

This effect is important at high redshifts from the point of view of Type Ia supernovae. At  $z = 1.5$  and with a cosmology  $\Omega_M^0 = 0.3$ ,  $\Omega_\Lambda^0 = 0.7$  and  $\nu = \nu_0$  the effect is  $\delta_\Lambda = 16\%$ . Considering  $\nu = 0.1$ , still in the acceptable range of  $\nu$  ( $\nu = 0.1$  implies an effective mass scale of  $M \lesssim 2 M_P$ ) the deviation grows up to 48%. These results should be perfectly distinguishable with future supernova experiments such as SNAP [179].

The deviation for  $\delta_\Lambda$  for the first multiples of  $\nu_0$  is drawn in Figure 3.4 (a). The second graphic in the same figure represents the variation rate of  $\Lambda(z)$  with redshift normalized to the current critical density (Fig. 3.4 (b)), that is another way of seeing how the cosmological constant varies with respect to a truly cosmological constant. In fact, this function is nothing but the Taylor development to first order near  $z = 0$ , and so, it is another observable function.

Any of these curves is symmetric with  $\nu$  at high redshifts. As it is observed in the form of Equation 3.39, the running is greater for  $\nu < 0$  than for  $\nu > 0$ , and that is reflected in both figures.

### 3.4.5 Other characteristics

The density of matter and cosmological constant are not the only magnitudes being affected by the  $\nu$  dependence. The deviations appearing with respect to the Standard Model are also significant in the Hubble parameter, the cosmological parameters  $\Omega_M^0$  and  $\Omega_\Lambda^0$ , and the deceleration one, for instance.

#### 3.4.5.1 Hubble parameter

Once it has been obtained the redshift evolution of the matter and cosmological constant densities, the evolution law of the Hubble parameter can be recovered by simply introducing these evolutions into Equation 2.42 or by integrating expression 3.33. With any of the options, the result is given by:

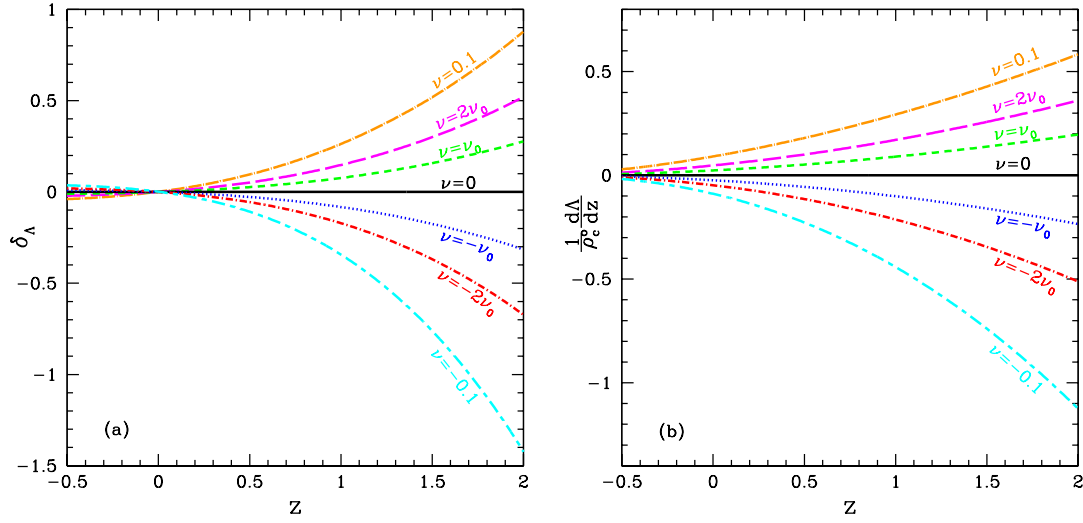


Figure 3.4: (a) Deviation  $\delta_\Lambda$  and (b) variation rate  $(1/\rho_c^0) d\Lambda/dz$  in a flat universe with  $\Omega_M^0 = 0.3$  and  $\Omega_\Lambda^0 = 0.7$ . Curves are not symmetric with  $\nu$  due to the form of  $\Lambda(z)$  (Eq. 3.39).

$$H^2(z; \nu) = H_0^2 \left\{ 1 + \Omega_M^0 \frac{(1+z)^{3(1-\nu)} - 1}{1-\nu} + \frac{1 - \Omega_M^0 - \Omega_\Lambda^0}{1-3\nu} \left[ (1+z)^2 - 1 - 2\nu \frac{(1+z)^{3(1-\nu)} - 1}{1-\nu} \right] \right\}. \quad (3.57)$$

Clearly, this expression is a generalization, and so, for  $\nu = 0$  it is recovered the standard result:

$$\begin{aligned} H^2(z) &= H_0^2 \left\{ 1 + \Omega_M^0 [(1+z)^3 - 1] + (1 - \Omega_M^0 - \Omega_\Lambda^0) [(1+z)^2 - 1] \right\} \\ &= H_0^2 \left[ \Omega_M^0 (1+z)^3 + \Omega_K^0 (1+z)^2 + \Omega_\Lambda^0 \right]. \end{aligned} \quad (3.58)$$

Since it has been seen that the cosmological index  $\nu$  is restricted by physics and observations and that the most physical region is that with  $\nu \ll 1$ , Equation 3.57 can be developed in this range with the guarantee that the result is valid. Then, the behaviour in the future is easily modeled: the Hubble parameter always tends, independently of the curvature, to a constant value in the future which depends on  $\nu$ :

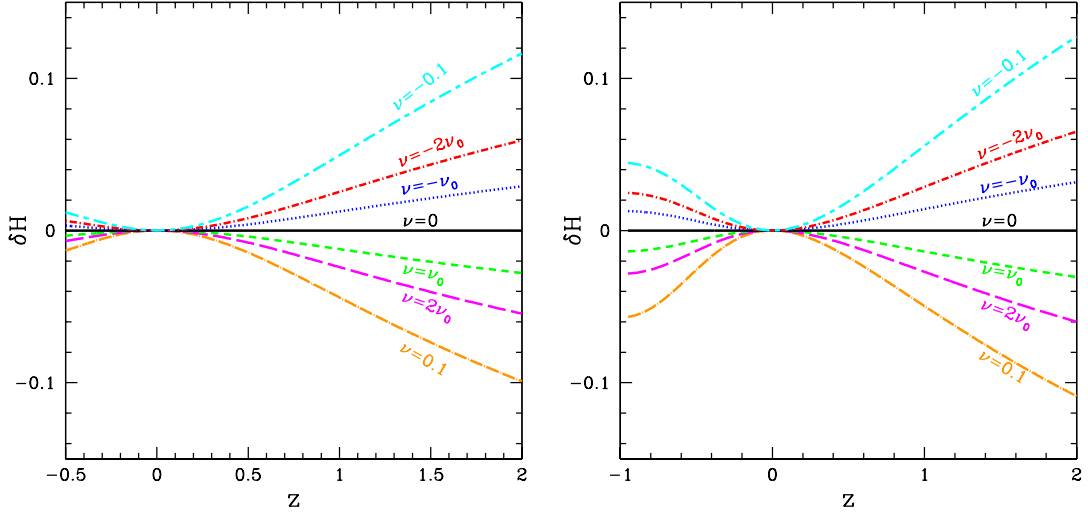


Figure 3.5: Deviations of the Hubble parameter for the different  $\nu$ 's indicated on the curves, with respect to a universe with cosmological constant. Figure on the left shows a flat universe with  $\Omega_M^0 = 0.3$  and  $\Omega_\Lambda^0 = 0.7$ , whereas the curvature is negative in the right one ( $\Omega_M^0 = 0.3$  and  $\Omega_\Lambda^0 = 0.5$ ).

$$H^2(z = -1; \nu) = H_0^2 \left[ 1 - \frac{\Omega_M^0 + \Omega_K^0}{1 - \nu} \right] \simeq H_0^2 [\Omega_\Lambda^0 - \nu (\Omega_M^0 + \Omega_K^0)]. \quad (3.59)$$

At every redshift the function  $H(z, \nu)$  is related with  $\Lambda(z, \nu)$ , and so it appears a deviation with respect to the  $\Lambda(z) = \Lambda_0$  case. This variation could be observable. Let us consider an example which can show that. For a flat universe ( $\kappa = 0$ ) and still in the  $\nu \ll 1$  limit, one can define at first order in  $\nu$

$$\Delta(z; \nu) \equiv H^2(z; \nu) - H^2(z) \simeq -\nu H_0^2 \Omega_M^0 \{1 + (1+z)^3 [3 \ln(1+z) - 1]\}, \quad (3.60)$$

and so, the relative deviation between this model and the standard one, which represents the different rate at which  $H(z; \nu)$  approaches the constant value given by 3.59 in comparison to that of  $H(z; \nu = 0)$ , is:

$$\delta H(z; \nu) \equiv \frac{H(z; \nu) - H(z)}{H(z)} = \frac{1}{2} \frac{\Delta(z; \nu)}{H(z)}$$

$$= -\frac{1}{2} \nu \Omega_M^0 \frac{1 + (1+z)^3 (3 \ln(1+z) - 1)}{1 + \Omega_M^0 [(1+z)^3 - 1]}. \quad (3.61)$$

That is a negative correction for  $\nu > 0$ . Therefore, the Hubble constant would always stay under the expected value in the Standard Model. The opposite would occur for  $\nu < 0$ . This behaviour is shown in Figure 3.5, first in the flat universe where the development 3.60 has been made, and then for an open universe with  $\Omega_M^0 = 0.3$  and  $\Omega_\Lambda^0 = 0.5$ . Even though the variations are really small ( $< 10\%$  for  $\nu < 0.1$ ),  $H$  is the parameter which experiences the least important variations, and so, it is not the optimal one to use in order to distinguish this kind of model from the real cosmological constant.

### 3.4.5.2 Cosmological sum rule

When the Friedmann equation (Eq. 2.42) is divided by the Hubble parameter itself, it is obtained the so-called *cosmological sum rule*. However, the running of the cosmological constant includes the  $\nu$  dependence also in this expression, and the usual law is modified:

$$1 = \Omega_M(z; \nu) + \Omega_\Lambda(z; \nu) + \Omega_K(z; \nu), \quad (3.62)$$

where

$$\Omega_M(z; \nu) \equiv \frac{\rho_M(z; \nu)}{\rho_c(z; \nu)}, \quad \Omega_\Lambda(z; \nu) \equiv \frac{\Lambda(z; \nu)}{\rho_c(z; \nu)}, \quad \Omega_K(z; \nu) \equiv \frac{-k}{H^2(z; \nu) a^2} \quad (3.63)$$

and  $\rho_c(z; \nu) \equiv 3 H^2(z; \nu) / 8 \pi G_N$  is the critical density at each time.

If, as observations seem to point out, the universe is flat, the cosmological sum rule reduces to  $\Omega_M(z; \nu) + \Omega_\Lambda(z; \nu) = 1$ , and it is, in principle “measurable”. Since observations can provide us with  $H_0$ ,  $\Omega_M^0$  and  $\Omega_\Lambda^0$ , the functions can be determined for each  $z$  and  $\nu$ .

$$\Omega_M(z; \nu) = \frac{8 \pi G \rho_M(z; \nu)}{3 H^2(z; \nu)} = \frac{\Omega_M^0 (1+z)^{3(1-\nu)}}{1 + \frac{\Omega_M^0}{1-\nu} [(1+z)^{3(1-\nu)} - 1]}, \quad (3.64)$$

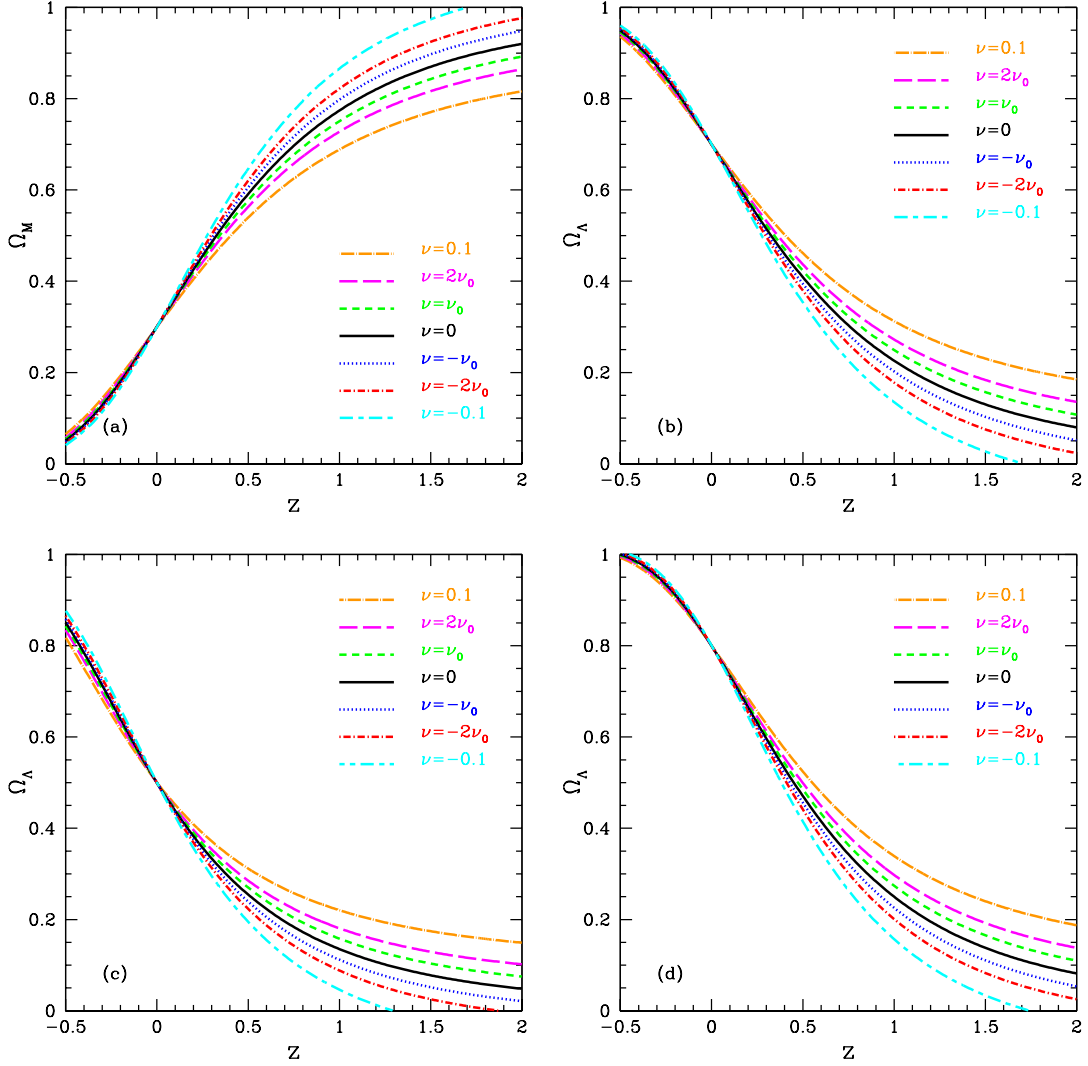


Figure 3.6: Redshift evolution of  $\Omega_M$  (a) and  $\Omega_\Lambda$  (b) for a flat universe with  $\Omega_M^0 = 0.3$  and  $\Omega_\Lambda^0 = 0.7$ . In the bottom panel it is shown the evolution of  $\Omega_\Lambda$  for an open universe with  $\Omega_M^0 = 0.3$  and  $\Omega_\Lambda^0 = 0.5$  (c) and for a closed universe with  $\Omega_M^0 = 0.4$  and  $\Omega_\Lambda^0 = 0.8$  (d).

$$\Omega_\Lambda(z; \nu) = \frac{8\pi G \Lambda(z; \nu)}{3H^2(z; \nu)} = \frac{\Omega_\Lambda^0 + \frac{\nu}{1-\nu} \Omega_M^0 [(1+z)^{3(1-\nu)} - 1]}{1 + \frac{\Omega_M^0}{1-\nu} [(1+z)^{3(1-\nu)} - 1]}. \quad (3.65)$$

From these equations it is easy to look at the behaviour in the two temporal limits: the past and the future,

$$\begin{aligned}\Omega_M(z = \infty) &= 1 - \nu, & \Omega_\Lambda(z = \infty) &= \nu, \\ \Omega_M(z = -1) &= 0, & \Omega_\Lambda(z = -1) &= 1,\end{aligned}\tag{3.66}$$

which, evidently follow the cosmological sum rule:

$$\Omega_M(z = \infty) + \Omega_\Lambda(z = \infty) = 1 = \Omega_M(z = -1) + \Omega_\Lambda(z = -1).\tag{3.67}$$

It is interesting to note that towards the future  $\Omega_\Lambda(z; \nu) \rightarrow 1$  and  $\Omega_M(z; \nu) \rightarrow 0$ , the same in this model and in the standard one. In fact,  $(\Omega_M = 0, \Omega_\Lambda = 1)$  is a fixed point towards which the cosmic fluid is driven, independently of the value of  $\nu$  ( $\nu = 0$  included). Towards the past, things are different. The asymptotic trend is  $\Omega_\Lambda(z \rightarrow \infty) \rightarrow \nu$ , and so,  $\Omega_\Lambda$  never reaches 0, differing from what happens in the standard case. All these behaviours are reflected in Figure 3.6 for a flat universe with  $\Omega_M^0 = 0.3$  and  $\Omega_\Lambda^0 = 0.7$ . The bottom panel in the same figure shows how  $\Omega_\Lambda$  tends to its limit faster or slower depending on the curvature.

### 3.4.5.3 Deceleration parameter

Another interesting parameter that describes the dynamics of the Universe is the deceleration parameter which has been first shown in Section 2.3.1 in the introductory chapter. Nowadays, there is a great amount of supernovae close to the point where the Universe passed from being decelerated to accelerated ( $z^*$ ) and therefore, it has become a unique observational feature to distinguish among models. This redshift is then model dependent, and in our case:

$$q(z; \nu) = -\frac{\ddot{a} a}{\dot{a}^2} = -\frac{\ddot{a}}{a H^2(z; \nu)} = \frac{1}{2} [\Omega_M(z; \nu) - 2\Omega_\Lambda(z; \nu)],\tag{3.68}$$

or equivalently,

$$q(z; \nu) = -1 - \frac{\dot{H}}{H^2} = -1 + \frac{1}{2} (1 + z) \frac{1}{H^2(z; \nu)} \frac{dH^2(z; \nu)}{dz}.\tag{3.69}$$

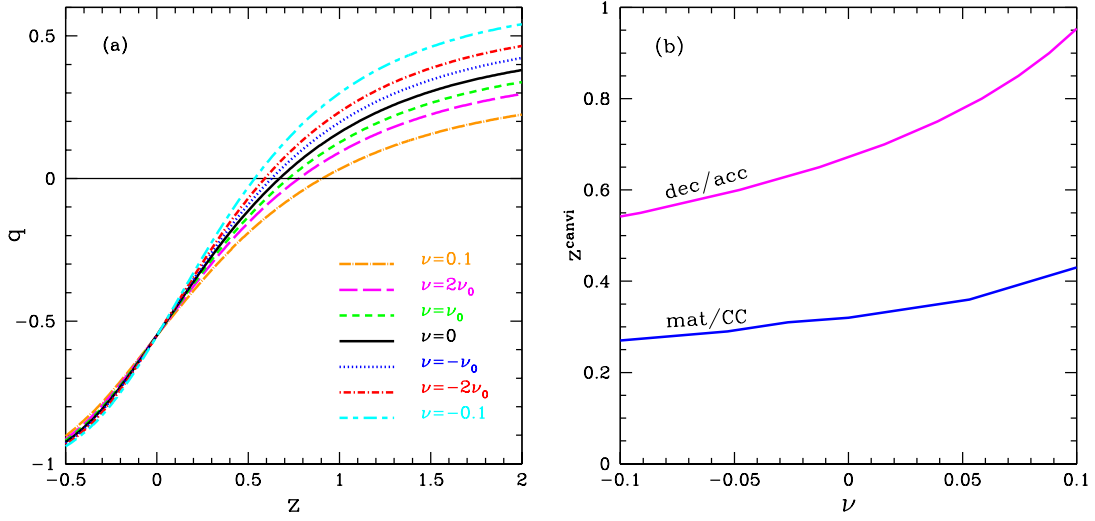


Figure 3.7: (a) Deceleration parameter and (b) transition redshift both for the deceleration/acceleration transition and the matter/cosmological constant one. The more positive  $\nu$  is, the farther we are now from the transitions.

In Figure 3.7 (a), one can observe the deceleration parameter for a flat universe with  $\Omega_M^0 = 0.3$  and  $\Omega_\Lambda^0 = 0.7$ . Though it is only shown the flat case, the characteristics are the same for any reasonable curvature, that is to say, for compatible values with CMB. The common trend is an increasingly accelerated universe coming from decelerating universes. The value of this deceleration in the remote past depends on the cosmological index  $\nu$ .

If we restrict to the flat case, which as we have seen is representative enough, and introduce the functions  $\Omega_M(z; \nu)$  and  $\Omega_\Lambda(z; \nu)$ , it can be obtained a development at first order in  $\nu$  that is useful to do some analytical calculations:

$$q(z; \nu) = -1 + \frac{3}{2} \frac{\Omega_M^0 (1+z)^3}{1 + \Omega_M^0 [(1+z)^3 - 1]} \quad (3.70)$$

$$\times \left\{ 1 - \nu \left[ 3 \ln(1+z) + \frac{\Omega_M^0 [(1+z)^3 - 1 - 3(1+z)^3 \ln(1+z)]}{1 + \Omega_M^0 [(1+z)^3 - 1]} \right] \right\}.$$

At  $z = 0$ , even with the inclusion of  $\nu$ , it is recovered the standard result for the cosmology in a flat FLRW universe:

$$q(0; \nu) = -1 + \frac{3}{2} \Omega_M^0 = \frac{\Omega_M^0}{2} - \Omega_\Lambda^0 \equiv q_0. \quad (3.71)$$

Doing the opposite and eliminating the dependence in  $\nu$ , it is defined the redshift at which the acceleration of the universe is zero  $z^*$  in the Standard Model:

$$q(z; 0) = -1 + \frac{3}{2} \frac{\Omega_M^0 (1+z)^3}{1 + \Omega_M^0 [(1+z)^3 - 1]}, \quad (3.72)$$

$$z^* = -1 + \sqrt[3]{2 \frac{\Omega_\Lambda^0}{\Omega_M^0}} \approx 0.67. \quad (3.73)$$

The numerical value corresponds to  $\Omega_M^0 = 0.3$  and  $\Omega_\Lambda^0 = 0.7$  and separates the decelerated universe from the accelerated universe. This point has nothing to do with the redshift which separates the universe dominated by matter from the universe dominated by the cosmological constant (Fig. 3.7 (b)). In fact, before the cosmological constant equals the matter, it is already important enough to produce acceleration, and the transition redshift matter/cosmological constant is posterior (Section 3.4.4 for numerical values) to the deceleration/acceleration one.

To fully characterize this model with a running of the cosmological constant, it is interesting to obtain the variation of  $z^*$  as a function of the index  $\nu$ . Since the acceleration begins for  $\Omega_M(z) < 2\Omega_\Lambda(z)$ , considering a flat universe implies the change of celerity at  $\Omega_\Lambda(z; \nu) = 1/3$ , or equivalently at

$$\frac{1}{2} (1+z^*)^3 - \frac{\Omega_\Lambda^0}{\Omega_M^0} = \nu \left\{ (1+z^*)^3 \left[ 1 + \frac{3}{2} \ln(1+z^*) \right] - 1 \right\}. \quad (3.74)$$

The solution to this transcendental equation has been drawn in the upper curve of Figure 3.7 (b). The more negative  $\nu$  is, the closer to us the transition has occurred, being the evolution non-symmetrical with respect to the standard case  $\nu = 0$ : whereas a positive value of  $\nu = +0.1$  makes a shift of 36% in  $z^*$ , the negative value  $\nu = -0.1$  only produces a variation of 21%. As it is being happening with most of the commented functions, this is consequence of the asymmetry with respect to  $\nu$  of the original function  $\Lambda(z)$ .

## Chapter 4

---

# Dark energy equation of state

---

Due to the difficulty of determination of the nature of dark energy and the large amount of theoretical candidates, many studies are focused on determining its equation of state. The other components of the Universe are fully characterised by it: the density is one third of the pressure for radiation, and for matter the pressure can be assumed to be null, for instance. However, for dark energy things are not so easy. Since we do not have any hint about what dark energy is, not even a constant proportionality can be assumed. In the following, and after introducing some general aspects of the equation of state, it is explored how very different dark energy models can mimic a standard equation of state. The problems of parameterizing such a general function as  $w(z)$  and its high degree of degeneracy are also discussed.

### 4.1 Basics

The equation of state for each component in the Universe is the relation between its pressure and its density, and it is a necessary ingredient in order to characterize the fluid. By knowing the equation of state, and therefore, the energy-momentum tensor which in our case is that of a perfect fluid, one can establish properties about the space-time evolution through the classical energy conditions. We start now by stating these conditions in the cosmological context and seeing its implications about the range where we expect the equation of state to lie. After that, it is explored the form of the equation of state of a quintessence field and take it as an archetype to later compare dark energy models with each other.

### 4.1.1 Classical energy conditions

The classical energy conditions impose restrictions over the form of the energy momentum tensor, which can be translated into the equation of state of a perfect fluid, such as dark energy in a FLRW universe. A complete discussion about it can be found in [43], here it is only mentioned how the most habitual conditions restrict the possible combinations of density and pressure of the dark energy component and the consequences into  $w(z)$ . A summary of the energy conditions reads:

Weak energy condition (WEC)	$\rho \geq 0$ and $\rho + p \geq 0$
Null energy condition (NEC)	$\rho + p \geq 0$
Dominant energy condition (DEC)	$\rho \geq  p $
Null dominant energy condition (NDEC)	$\rho \geq  p $ and $\rho = -p$
Strong energy condition (SEC)	$\rho + p \geq 0$ and $\rho + 3p \geq 0$

On the other hand, what is expected from the dark energy component is to be a source with positive energy density so that there is enough density to make the Universe flat or nearly flat, and also to be a source with negative pressure so that the expansion of the Universe is accelerating now<sup>1</sup>. In the  $(\rho, p)$  plane, this implies that we are interested in models of the 4th quadrant as indicated in Figure 4.1. Most of the energy conditions allow a component to have  $\rho \geq 0$  and  $\rho \geq |p|$ , what, as it will be seen, corresponds to the family of quintessence models (also k-essence and other alternatives can share this characteristic). In an homogeneous and isotropic universe, these requirements translate, for an equation of state of the form  $p = w\rho$ , into having  $-1 \leq w \leq 0$ . In this case, DEC assures that dark energy would always be stable as stated by the conservation theorem of Hawking and Ellis [100]. However, also models with  $\rho \geq 0$  and  $\rho < |p|$  have a positive density and negative pressure, but they do not obey any of the classical energy conditions. This is not a sufficient condition to assure that the dark energy component is not stable, but in most cases it is so. For a dark energy source with  $p = w\rho$  in a FLRW universe that implies  $w < -1$ , that is, a phantom component.

Phantom energies violate then all energy conditions. Since they do not obey DEC,  $p + \rho < 0$  and the density grows to infinity in a finite time, when also the scale

---

<sup>1</sup>In fact, it is necessary that  $p < -1/3\rho$  in order that the Einstein's equations describe an accelerating Universe. Therefore, a dark energy source must violate SEC.

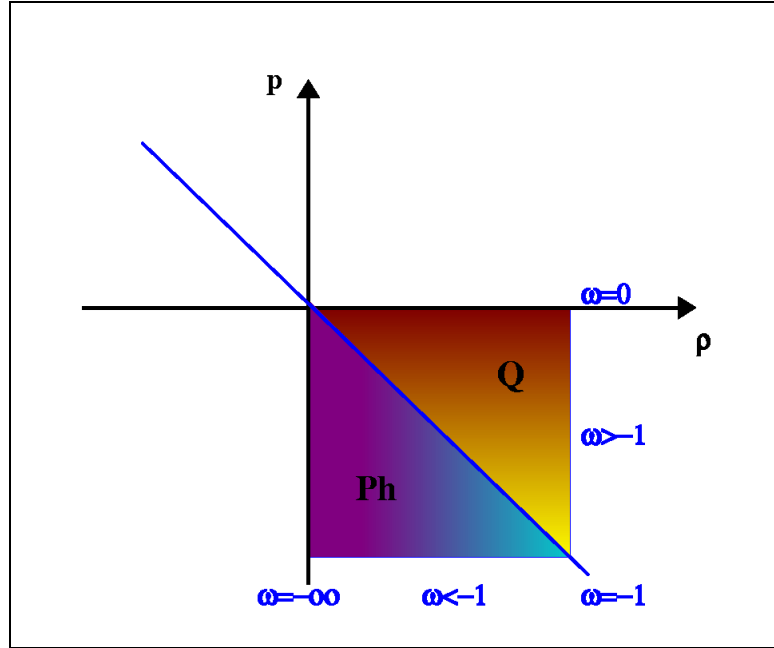


Figure 4.1: Pressure-density plane shadowing the region expected for a component that makes the Universe accelerate: positive energy density and negative pressure. This quadrant corresponds to two very different behaviours: quintessence-like behaviour ( $Q$ ) and phantom-like behaviour ( $Ph$ ). The parameter  $w$  is defined as the ratio  $w = p/\rho$ .

factor has grown to infinity. This singularity is known as *Big Rip*. The catastrophic end and the violation of the classical energy conditions sometimes motivate to limit the dark energy equation of state in the range  $-1 \leq w < -1/3$ . Nevertheless, as it is seen in the numerical analysis of this work, current data favour a supernegative equation of state. Since the relation  $p = w\rho$  can be just an effective parameterization of the component, and in fact, the classical energy conditions are not even clear demands of General Relativity (quantum systems for example do violate classical energy conditions), we do not restrict its value whenever it be possible to work without priors on  $w$ , and in any case, never to the small interval  $-1 \leq w < -1/3$ .

### 4.1.2 Quintessence

Although it has just been said that phantom fields are not going to be excluded as a reasonable source of dark energy, quintessence is introduced here as the archetype of an energy component with equation of state  $p = w\rho$ .  $K$ -essence and phantom fields are only mentioned here for comparison and completeness.

A quintessence field is a minimally coupled to gravity scalar field  $Q$  that evolves with time according to the Klein-Gordon equation as explained in the introductory chapter of this part:

$$\ddot{Q} + 3H\dot{Q} + V'(Q) = 0, \quad (4.1)$$

where dots indicate a derivative respect to time and primes respect to the field  $Q$ .

Somehow, quintessence is an extension or modification to General Relativity, since it introduces a new term in the Lagrangian density,  $\mathcal{L}_Q$ , and therefore, in the effective action. Even so, there is no fundamental theory with such an action that predicts the field, and it is for the time being a phenomenological theory which seems to describe the observations.

$$\mathcal{L}_Q = \sqrt{-g} \left( \frac{1}{2} \partial_\mu Q \partial^\mu Q - V(Q) \right). \quad (4.2)$$

The above Lagrangian density gives the energy-momentum tensor for quintessence, and hence its pressure and density, that for an homogeneous field (inhomogeneities should only be seen at very large scale) is:

$$\rho = \frac{1}{2} \dot{Q}^2 + V(Q), \quad p = \frac{1}{2} \dot{Q}^2 - V(Q). \quad (4.3)$$

From these quantities, it is straightforward to write the equation of state as:

$$w = \frac{p}{\rho} = \frac{\frac{1}{2} \dot{Q}^2 - V(Q)}{\frac{1}{2} \dot{Q}^2 + V(Q)}. \quad (4.4)$$

Such an equation of state mimics the observed cosmological constant-like behaviour ( $p \sim -\rho$ ) when the kinetic energy of the field is negligible compared to the potential energy ( $\dot{Q}^2 \ll V(Q)$ ). So, if the field is rolling down its potential, it must be now approaching the minimum. Further from this minimum and also further in time, the evolution of the field and the specific form of the potential play a role in the evolution of the equation of state. Nevertheless, if the slow-roll condition is fulfilled, the equation of state must lie in the range  $-1 < w < 0$  but the exact behaviour

can be very different (constant, slowly varying, rapidly varying or oscillatory [39]) according to the potential.

However, and although this mechanism generates the desired behaviour, the present-day density associated to the field is very much dependent on the initial conditions and so, instead of answering the question *Why the energy density of dark energy is so small today?*, it just changes the question to *Why the energy density of dark energy had to be exactly that in the past?*

An answer is partly given by a branch of quintessence models with *tracker fields* [212, 186]. The equation of motion of these fields allows an attractor solution, so that the evolution at late times of the field is quite independent of the initial conditions and it only dominates recently. In these cases, the  $Q$  field follows the evolution of the dominant component (first radiation and then matter) having its equation of state a value close to but less than the one of the dominant component, till  $w_Q \rightarrow -1$  and the acceleration shows. This scaling behaviour of dark energy justifies the coincidence between the current density of matter and the density of dark energy, and that irrespective of its initial value.

There exists a wide family of potentials that drive to an attractor, but choosing one or the other is still an ad hoc decision. A table with some of the studied quintessence potentials is shown below together with the motivation for its inclusion in the action (Table 4.1). Each of these potentials generates a different form for  $w(z)$  according to Equation 4.4, and, as seen in Figure 4.2, the forms are unrelated to each other. This plot has been obtained from Ref. [206] and it shows nine quintessence models including brane inspired potentials, pure exponentials, potentials with two exponentials, periodic potentials, Pseudo Nambu-Goldstone bosons (PNG), etc. (see Ref. [206] for details).

The minimally coupled to gravity  $Q$  field is the simpler option one introduces in order to fit the observations. However, the field could also interact with other components. In coupled quintessence models, the quintessence field is coupled to, for instance, dark matter and/or baryons [10]. The Lagrangian of the theory is then modified accordingly. On the other hand, the  $Q$  field is compatible with the inclusion of other sources. It has been noted in Chapter 3 that the cosmological constant is necessary for renormalizability within a Quantum Field Theory context, and therefore, even when working with a quintessence field, the cosmological constant should not be omitted. Its inclusion or that of any other independent source

$V(Q)$	Motivation	Reference
$V_0 \exp(-\lambda Q)$	Compactification of higher dimensional supergravities	Ratra & Peebles (1988) [156], Wetterich (1988) [207], Ferreira & Joyce (1998) [78]
$V_0/Q^\alpha$	SUSY QCD	Peebles & Ratra (1988) [142]
$m^2 Q^2$	PNG bosons	Frieman et al. (1995) [83]
$\cos(Q/f) + 1$	PNG bosons	Frieman et al. (1995) [83]
$V_0 \exp(\lambda Q^2)/Q^\alpha$	SUGRA	Brax & Martin (1999) [35]
$V_0(\cosh \lambda Q - 1)^p$	Field theory Condensed matter non-perturb. RGEs	Sahni & Wang (2000) [169]
$V_0 \sinh^{-\alpha}(\lambda Q)$	-	Ureña-López & Matos (2000) [198]
$V_0(e^{\alpha\kappa Q} + e^{\beta\kappa Q})$	Particle physics Slopes?	Barreiro, Copeland & Nunes (2000) [20]
$V_0(\exp M_p/Q - 1)$	Particle physics	Zlatev, Wang & Steinhardt (1999) [212]
$V_0[(Q - B)^\alpha + A]e^{-\lambda Q}$	Low energy limit of M-theory	Albrecht & Skordis (2000) [3]

Table 4.1: Potentials and motivation for their form for some of the quintessence models. See the references for the value and the meaning of the constants. The table is an extension of that given by Varun Sahni in Ref. [166].

of dark energy does not alter the equations for the quintessence component.

From Equation 4.4 and visually from Figure 4.2 one can see that, in general, the barotropic index is time dependent (equivalently redshift dependent). At the present epoch  $w$  is almost constant, but, when exploring the past of the Universe, the form of the potential dictates the evolution of the equation of state. To solve

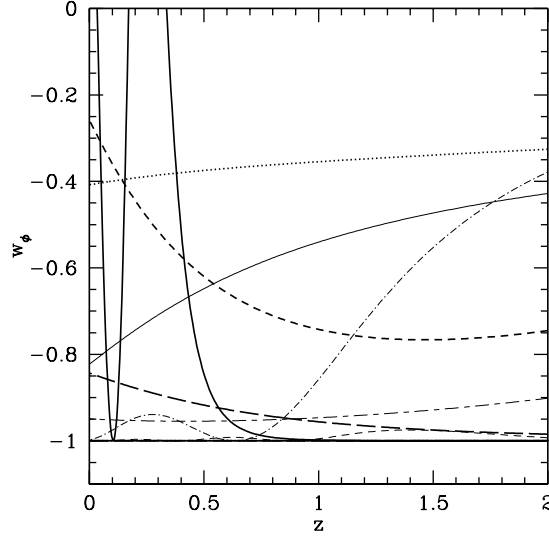


Figure 4.2: Equation of state for nine different quintessence models. Most of them correspond to potentials in Table 4.1 (see text). Plot extracted from Weller and Albrecht (2002) [206].

the Friedmann equations, it is enough to know that  $w = w(t)$ , and then, the specific form for each model can be inserted into the result. Introducing this dependence into the continuity equation for quintessence (Eq. 2.40) one obtains the evolution of its energy density:

$$\frac{d\rho_Q}{dt} + 3H(\rho_Q + p_Q) = (1+z)\frac{d\rho_Q}{dz} - 3[1+w(z)]\rho_Q = 0, \quad (4.5)$$

$$\rho_Q(z) = \rho_Q^0 \exp\left(3 \int_0^z dz' \frac{1+w(z')}{1+z'}\right). \quad (4.6)$$

This is the general expression for the energy density of a perfect fluid with  $p = w(z)\rho$  which can be put in the Hubble parameter. For a constant barotropic index, the energy density reduces to:

$$\rho_Q(z) = \rho_Q^0 (1+z)^{3(1+w)}, \quad (4.7)$$

and for a cosmological constant ( $w = -1$ ) one recovers a constant energy:

$$\rho_Q(z) = \rho_Q^0. \quad (4.8)$$

Applying this procedure for other components  $X$  rather than quintessence is what we call a quintessence-like setup for an  $X$  dark energy component. With this methodology, one can describe any source of dark energy as a density

$$\rho_X(z) = \rho_X^0 \exp\left(3 \int_0^z dz' \frac{1 + \tilde{w}(z')}{1 + z'}\right), \quad (4.9)$$

with an effective equation of state of the form  $p = \tilde{w}(z)\rho$  as it is explained in the following.

## 4.2 Mimicking the equation of state $p = w\rho$

Most of dark energy models can be described by an energy component which can be modeled as a perfect fluid with an equation of state of the form  $p = w\rho$ . However, there are some alternatives that either are not perfect fluids or their equation of state has a different dependence. The aim of this section is to express mathematically the most promising models as if they consisted of a perfect fluid with an equation of state of the form  $p = \tilde{w}\rho$ , although in the context of some of the models that does not have any physical sense.

This *pseudo-equation of state* or *effective equation of state*,  $\tilde{w}$ , depending on the case, allows to directly treat all the alternative models in a single Friedmann equation, that is to say, all of them are represented by:

$$H^2(z) = H_0^2 \left[ \Omega_M^0 (1+z)^3 + \Omega_X^0 \exp\left(3 \int_0^z dz' \frac{1 + \tilde{w}(z')}{1 + z'}\right) + \Omega_K^0 (1+z)^2 \right]. \quad (4.10)$$

This is important in observational cosmology, since each experiment can then contrast its data with a simple and very general equation and obtain a family of dark energy models compatible with their observations. Otherwise, one should test all the models one by one to see which is the most favoured one.

### 4.2.1 Evolving cosmological constant

The first example is one of the main models in this thesis, an evolving cosmological constant. Although a cosmological constant has always a real equation of state of the form  $p = -\rho$ , the fact that it evolves makes the conservation equation to be different from the one we assume for a dark energy  $X$  component. Therefore, it is defined a mathematical pressure  $\tilde{p}_\Lambda$  which fulfils the conservation law for an  $X$  component:

$$\frac{d\Lambda}{dt} + 3H(\Lambda + \tilde{p}_\Lambda) = 0. \quad (4.11)$$

Now, the functions  $\rho(z)$  and  $\Lambda(z)$  needed to solve that differential equation are those obtained from solving the system of Equations 3.32-3.33-3.34 adding the conservation law.

With this definition, one can determine the pseudo-equation of state  $p_\Lambda(z) = \tilde{w}_\Lambda(z)\Lambda(z)$  as the one that satisfies Equation 4.11:

$$(1+z)\frac{d\Lambda}{dz} - 3[1 + \tilde{w}_\Lambda(z)]\Lambda = 0, \quad (4.12)$$

$$\tilde{w}_\Lambda = \frac{1}{3}(1+z)\frac{1}{\Lambda(z)}\frac{d\Lambda(z)}{dz} - 1. \quad (4.13)$$

Particularizing for a flat universe where the equations are much simpler, and using Equation 3.39 in 4.13 is easy to see that:

$$\tilde{w}_\Lambda = \frac{\Omega_M^0 \nu (1+z)^{3(1-\nu)}}{\Omega_\Lambda^0 + \Omega_M^0 \frac{\nu}{1-\nu} [(1+z)^{3(1-\nu)} - 1]} - 1. \quad (4.14)$$

That introduces important changes with respect to the true  $w$  as seen in Figure 4.3. For a flat universe with  $\Omega_M^0 = 0.3$  and  $\Omega_\Lambda^0 = 0.7$  and  $\nu = \nu_0 \approx 0.026$ , a different value even at redshift zero is obtained:

$$\tilde{w}_\Lambda(z=0.0) = -0.99, \quad \tilde{w}_\Lambda(z=0.5) = -0.96, \quad \tilde{w}_\Lambda(z=1.0) = -0.91. \quad (4.15)$$

Towards the future (negative redshifts), the pseudo-equation of state tends to the true equation of state, whereas in the past either it mimics the behaviour of a phantom component or tends towards positive values depending on the sign of the cosmological index  $\nu$ . This is a first example that could be detected as a phantom source of dark energy, when, in fact, it is just an effective behaviour observed when the analysis is made on a quintessence-like setup.

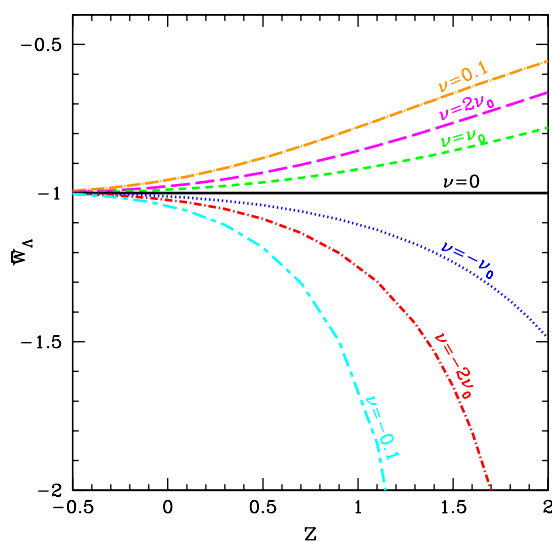


Figure 4.3: Evolution of a *pseudo-equation of state* produced by an evolving cosmological constant. This particular case corresponds to the model introduced in Section 3.3.1.3 for a flat universe with  $\Omega_M^0 = 0.3$  and  $\Omega_\Lambda^0 = 0.7$ , and different values of the cosmological index  $\nu$ .

### 4.2.2 Chaplygin gas

The Chaplygin gas case is much different from the previous one. It is a perfect fluid, but not with a common equation of state. The generalized Chaplygin gas equation of state [26] reads:

$$p_{Ch} = -\frac{A}{\rho_{Ch}^n}, \quad (4.16)$$

where  $A$  and  $n$  are positive constants and which reduces to the original Chaplygin gas model [117] for  $n = 1$ . With this equation of state, the conservation law for a

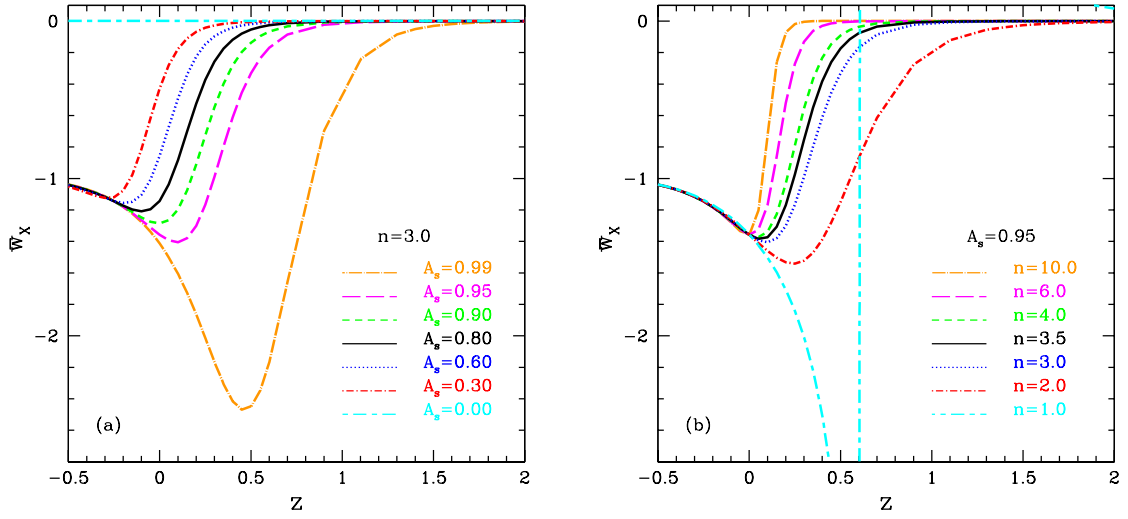


Figure 4.4: Evolution of the effective equation of state of a common dark energy component with  $p = \tilde{w}\rho$  when the universe is made of a Chaplygin gas. A flat universe with  $\Omega_M^0 = 0.3$  and  $\Omega_\Lambda^0 = 0.7$  is assumed. (a) Variation as a function of the parameter  $A_s$  with  $n = 3$  fixed. (b) Variation as a function of the parameter  $n$  with  $A_s = 0.95$  fixed.

dark energy component, Equation 4.5, leads to a density evolution:

$$\rho_{Ch} = \rho_{Ch}^0 [A_s + (1 - A_s)(1 + z)^{3(1+n)}]^{1/(1+n)}, \quad (4.17)$$

where  $\rho_{Ch}^0$  is the current energy density of the Chaplygin gas and  $A_s \equiv A/(\rho_{Ch}^0)^{1+n}$  is a dimensionless constant. This energy density tends to a “matter” dominated universe towards the past and to a “cosmological constant” dominated universe towards the future, and so, it has been proposed as a candidate to unify dark matter and dark energy [29, 26]. Due to that, a universe sourced with a Chaplygin gas does not have the usual contribution of dark matter, having a total energy density given by the sum:  $\Omega_b^0(z) + \Omega_{Ch}^0(z) + \Omega_k^0(z)$ , where  $\Omega_b^0(z)$  is used instead of the habitual sum of baryonic and dark matter  $\Omega_M^0(z) = \Omega_b^0(z) + \Omega_{DM}^0(z)$ . If we want to rewrite the equations of a Chaplygin gas in the way established in Section 4.1 we have to take the latter into account.

Once we know all the ingredients, the effective equation of state of this component

is derived by first considering  $\rho_X = \rho_{Ch} - \rho_M^2$ . Since matter is pressureless, the pressure remains the same  $p_X = p_{Ch}$ , and then via the ratio  $\tilde{w}_X = p_{Ch}/(\rho_{Ch} - \rho_M)$  one obtains:

$$\tilde{w}_X = -\frac{A_s}{[A_s + (1 - A_s)(1 + z)^{3(1+n)}] \left\{ 1 - \frac{\Omega_M^0}{\Omega_X^0 + \Omega_M^0} \frac{(1+z)^3}{[A_s + (1 - A_s)(1+z)^{3(1+n)}]^{1/(1+n)}} \right\}}. \quad (4.18)$$

This evolution is plotted in Figure 4.4. In both plots it is assumed a flat universe with  $\Omega_M^0 = 0.3$  and  $\Omega_\Lambda^0 = 0.7$ , and either  $A_s$  or  $n$  are fixed to the values obtained with the fits to SNe Ia magnitudes in [25]. Vertical lines appear because of the various zeros of the function  $\tilde{w}_X$ . In general, the apparent behaviour of this component would be that of dust in the past, passing through a phantom epoch where we still are, to finish with a cosmological constant-like behaviour.

### 4.2.3 Cardassian models

As it has been noted in Chapter 2, Cardassian models are a quite special kind of models since they can be seen from two points of view: as the interpretation of matter as an interacting fluid [90], or as the effects of observing a Universe which is a 3-dimensional brane in a higher dimensional universe [82]. The consequences in both cases are the same, the Hubble parameter is modified by the introduction of a new term. The Friedmann equation for this family of models is a general function of the density, for example:

$$H^2 = f(\rho) = \frac{8\pi G}{3}(\rho + C\rho^n), \quad (4.19)$$

where  $C$  and  $n$  are constants. Note that the density only accounts for matter and radiation, there is no vacuum or curvature. There exist various generalizations of this

---

<sup>2</sup>To be precise,  $\rho_X = \rho_{Ch} - \rho_b$  should be used. However, the baryonic energy density is a well known quantity  $\Omega_b^0 h^2 = 0.0224 \pm 0.0009$  (WMAP result with a varying spectral index [184]), and it is easier for calculations to consider the commonly used parameter  $\rho_M$  and then subtract the known value  $\rho_b$ .

simple model [80]. However, this first proposal is the one used here. This is also the easiest model to be compared with quintessence in the analysis: mathematically, it can represent a universe sourced with matter and an extra perfect fluid with density:

$$\rho_{Ca} = C\rho^n = \rho_{Ca}^0(1+z)^{3n}. \quad (4.20)$$

Obtaining the effective equation of state is then straightforward: since  $n$  is constant,  $\tilde{w}_{Ca} = n - 1$ . Therefore, any quintessence model with a constant equation of state is equivalent to have a Cardassian component with  $n = w + 1$ .

#### 4.2.4 Modified Gravity

Cardassian models can be seen as modifications of gravity because they add a new term in the action of the theory. Although General Relativity has been tested at small and intermediate scales, it has not been checked at large scales (of the order of the Hubble radius). So, up to now, gravity admits modifications at large distances and, under this point of view, Cardassian models are completely admissible. The family of models that depend on these modifications are called on the whole Modified Gravity Models. For them, the scalar of curvature appearing in the Hilbert-Einstein action is replaced by a function of it or of any other invariant:

$$S = -\frac{1}{16\pi G} \int d^4x \sqrt{-g} R \implies S = -\frac{1}{16\pi G} \int d^4x \sqrt{-g} f(R, R^{\alpha\beta} R_{\alpha\beta}, \dots). \quad (4.21)$$

This function  $f(R, R^{\alpha\beta} R_{\alpha\beta}, \dots)$  can have different contributions, but usually it only depends on the scalar of curvature  $R$  (whether it be as  $1/R$ ,  $\ln R$ ...) and not on other contractions. As the easiest example, we consider the inclusion of inverse powers of  $R$  [120, 42]:

$$f(R) = R - \frac{-\mu^{2(n+1)}}{R^n}. \quad (4.22)$$

For a positive integer  $n$ , it can be shown that the modification to the curvature behaves as if it were a source of dark energy with an equation of state of the form:

$$\tilde{w}_X = -1 + \frac{2(n+2)}{3(2n+1)(n+1)} \quad \text{for } n > 1. \quad (4.23)$$

That is a constant equation of state regardless of the dimension  $n$ . It spans from  $\tilde{w} = -2/3$  for  $n = 1$  to  $\tilde{w} = -1$  for  $n \rightarrow \infty$ , a range that, as it has been argued in Section 4.1, fulfils DEC and, therefore, represents a stable source of dark energy.

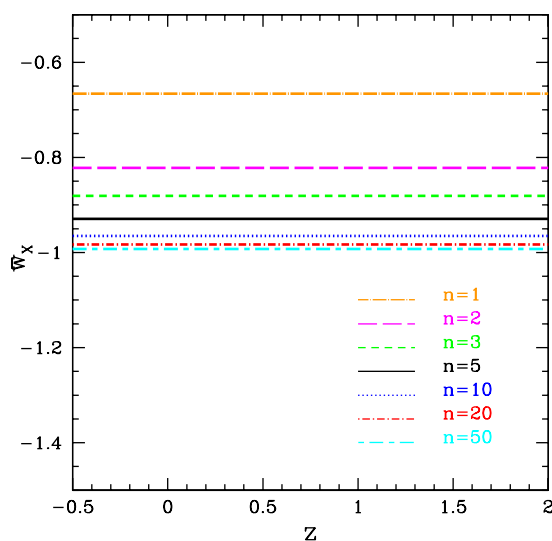


Figure 4.5: Different values of the effective equation of state according to the index  $n$ . Since  $n$  is constant,  $\tilde{w}$  is also always constant for this simple model. That is not true for more complicated models.

Other expressions for  $f(R)$  involve different dependences for  $\tilde{w}_X$ . Its constancy can be lost and even some models predict equations of state with  $\tilde{w} < -1$ .

#### 4.2.4.1 Braneworld cosmologies

One of the ways in which gravity is modified from the usual General Relativity is by the existence of extra dimensions as motivated by M-theory. If these extra dimensions are not compactified, ordinary matter must be confined onto a three-dimensional brane embedded into a bulk of a higher dimension. These kinds of universe are known as *Braneworlds*.

Modifying gravity implies a modification on the Friedmann equation as well, and

this modification can be hidden in a correction function  $L(\rho)$  which multiplies the usual density [49]:

$$H^2 = \frac{8\pi\ell_{\text{Pl}}^2}{3}\rho_\chi L^2(\rho_\chi) - \frac{k}{a^2}. \quad (4.24)$$

Therefore, braneworlds with extra dimensions are treated as a scalar field  $\chi$  with its own continuity equation on the brane:

$$\dot{\rho}_\chi + 3H(\rho_\chi + p_\chi) = 0. \quad (4.25)$$

Some models do really have this field on the brane. For others, it is just a representation within this framework. That is so for Cardassian [90, 82] and Dvali-Gabadadze-Porrati (DGP) models [64]. The function  $L(\rho)$  for some of these models is shown in Table 4.2.

From Equation 4.25 and 4.24, one can calculate the effective equation of state parameter as:

$$\tilde{w}_{\text{brane}} \equiv -\frac{1}{3} \frac{d(n \ln \rho_\chi)}{d \ln a} - 1, \quad (4.26)$$

where it has been introduced an index  $n$  defined as

$$n(\rho_\chi) \equiv 1 + 2 \frac{\ln L(\rho_\chi)}{\ln \rho_\chi}. \quad (4.27)$$

The barotropic index  $\tilde{w}_{\text{brane}}$  is sometimes constant, as for Cardassian models (Section 4.2.3), but it is in general time dependent and very different depending on the model. For instance, none of the branches of DGP models have a constant  $\tilde{w}(z)$ . The so-called positive branch is self-accelerating (+), and the negative one needs dark energy to produce acceleration (-). In the latter case, the *effective* equation of state goes through an epoch of phantom behaviour ( $w < -1$ ). For the former, the DGP model (+) in a flat universe, the effective equation of state was derived in

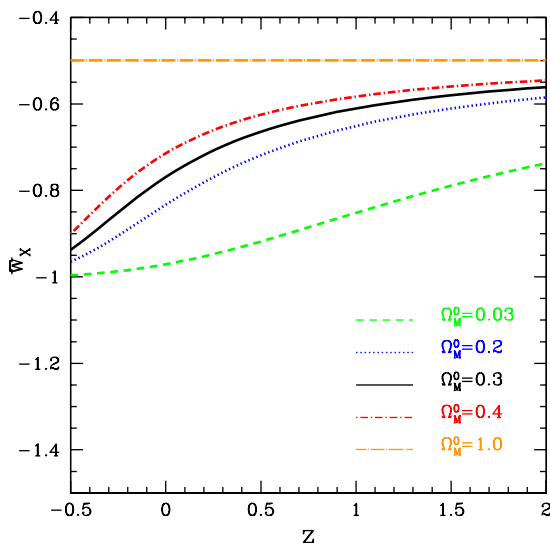


Figure 4.6: Effective equation of state in DGP (+) models. The value only depends on the density of matter, and so, cosmologies with a small  $\Omega_M^0$  have a more stressed dark energy behaviour, whereas the equation of state is closer to be matter-like for large  $\Omega_M^0$ .

Ref. [127] by considering an effective energy density of  $\rho_{eff} \equiv 3H/8\pi G r_c^{-3}$  with an standard conservation law. Therefore, it was obtained:

$$\tilde{w}(z) = \frac{\Omega_M^0 - 1 - \sqrt{(1 - \Omega_M^0)^2 + 4\Omega_M^0(1+z)^3}}{2\sqrt{(1 - \Omega_M^0)^2 + 4\Omega_M^0(1+z)^3}}. \quad (4.28)$$

This equation only depends on the density of matter, since the cosmological sum rule relates it to the scale  $r_c$  in a flat universe as  $4\Omega_{r_c} = (1 - \Omega_M^0)^2$ . Intuitively, one can understand this modification to gravity as a dark energy component that is important when the density of matter is small, but that is reduced for large  $\Omega_M^0$ , being then closer to zero, as the equation of state of matter is (Figure 4.6).

Although DGP and Cardassian models are the most treated and constrained by observations due to their simplicity, there is a wider family defined by the function  $L(\rho)$  as we have seen. It is interesting to note that this parameterization in terms of  $L(\rho)$  has allowed the authors of [49] to establish conditions under which the system achieves scaling solutions. That is an interesting condition for a dark energy model

---

<sup>3</sup>The constant  $r_c$  is the only parameter of the model, defined as the scale at which gravity starts to propagate into the bulk  $r_c = m_{(4)}^{Pl\ 2}/M_{(5)}^{Pl\ 3}$  ( $m_{(4)}^{Pl}$  is the Planck mass in 4D and  $M_{(5)}^{Pl}$  in 5D).

since then the energy density scales with the dominant energy component of the Universe and the coincidence problem can be solved.

Braneworld model	$L(\rho_\chi)$	Reference
Randall-Sundrum type II	$\sqrt{1 + (\rho_\chi/2\sigma)}$	Randall & Sundrum (1999) [154, 153]
Shtanov-Sahni	$\sqrt{1 - (\rho_\chi/2 \sigma )}$	Shtanov & Sahni (2003) [177]
Dvali-Gabadadze-Porrati	$(1/\sqrt{D\rho_\chi}) \times$ $(\mp 1 + \sqrt{1 + D\rho_\chi})$	Dvali, Gabadadze & Porrati (2001) [64]
Cardassian	$\sqrt{1 + B\rho_\chi^n}$	Freese & Lewis (2002) [82]

Table 4.2: Different braneworld models as described by the function  $L(\rho_\chi)$ .  $\sigma$  is the tension of the brane,  $D$  and  $B$  are positive constants and  $n < -1/3$ .

#### 4.2.4.2 Loop quantum cosmology

Loop quantum cosmology is a different approach that does not try to modify gravity by itself, but to unify it with quantum physics. As a result, gravitation is modified at small scale, at least, and therefore, we include it in this section. Besides, there have been some attempts to establish a correspondence between braneworlds and loop-inspired cosmologies [50].

The unification of general relativity and quantum physics is made non-perturbatively and without the need for a classical background. In this framework, the application of cosmological symmetries (isotropy and homogeneity) allows to develop the Friedmann equations from the effective Hamiltonian of the theory, where the inverse volume  $a^{-3}$  is quantized. Loop quantum cosmology as developed by Bojowald [30] differentiates three regimes: one below the Planck scale  $a_i \sim l_{Pl}$  where space-time is discrete, one over  $a_*$  where classical equations are recovered, and in the middle a semi-classical phase where quantum effects modify the standard Fried-

mann equations. Here, it is discussed the behaviour in this phase and its transition to  $a > a_*$ .

In a similar way as we have done with braneworld cosmologies, we do not deduce the set of equations, but only give their expression in order to treat the models as a component of dark energy. The justification and complete formulae can be found in [50] for example.

The quantification of  $a^{-3}$  in the momentum of an scalar field ( $a^{-3} \rightarrow D(q)a^{-3}$ ) introduces a correction function in its kinetic energy, and therefore, the Friedmann equation can be expressed as:

$$H^2 = \frac{8\pi l_{Pl}^2}{3} \left[ \frac{1}{2D(a)} \dot{\phi}^2 + V \right] - \frac{k}{a^2}. \quad (4.29)$$

Also the conservation equation is modified:

$$\ddot{\phi} + 3H \left( 1 - \frac{1}{3} \frac{d \ln D}{d \ln a} \right) \dot{\phi} + D \frac{dV}{d\phi} = 0. \quad (4.30)$$

Quantization results give for  $D(q)$ :

$$D(q) = \left\{ \frac{3}{2l} q^{1-l} [(l+2)^{-1} ((q+1)^{l+2} - |q-1|^{l+2}) - \frac{1}{1+l} q ((q+1)^{l+1} - \text{sgn}(q-1)|q-1|^{l+1})] \right\}^{3/(2-2l)}, \quad (4.31)$$

with  $q = a^2/a_*^2$ ,  $a_*^2 = a_i^2 j/3$ ,  $a_i = \sqrt{\gamma} l_{Pl}$ , the quantization parameter  $j$  taking half-integer (positive) values, and  $\gamma = \ln 2/\sqrt{3}\pi \approx 0.13$ .

The system of equations 4.29 and 4.30 allows to define an effective pressure  $p_{L,\text{eff}}$  and density  $\rho_{L,\text{eff}}$  so that they reproduce the standard equations:

$$\rho_{L,\text{eff}} = \frac{\dot{\phi}^2}{2D} + V, \quad (4.32)$$

$$p_{\text{L,eff}} = \frac{\dot{\phi}^2}{2D} \left( 1 - \frac{1}{3} \frac{d \ln D}{d \ln a} \right) - V. \quad (4.33)$$

So, the effective equation of state takes the form

$$\tilde{w}_{\text{LQC}} = \frac{2\dot{\phi}^2}{\dot{\phi}^2 + 2DV} \left( 1 - \frac{1}{6} \frac{d \ln D}{d \ln a} \right) - 1. \quad (4.34)$$

The similarity between Eq. 4.34 and Eq. 4.26 has motivated the authors of Ref. [50] to propose a relation between braneworlds and loop-inspired cosmologies, as it has been said before. However, the correspondence cannot be one-to-one, since loop quantum cosmology models have two free functions ( $V(\phi)$  and  $D(a)$ ) and from braneworlds it is only needed to know the expression of  $L(\rho_\chi)$ . Therefore, there is a family of loop-inspired models for every braneworld.

### 4.3 Parameterizing the equation of state

After this brief route along some of the multitude of dark energy models, we have seen the variety of redshift evolutions that  $w(z)$  can follow. The selection did not pretend to be exhaustive, yet representative of the main approaches. Only quintessence models by themselves cover the whole  $(w, z)$  plane (remember Figure 4.2). If, besides, it is allowed the possibility for the equation of state of being an effective representation of a different theoretical model, as discussed in the previous section, the possibilities for the form of the dependence  $w(z)$  spectacularly rise.

It is evident, then, that there is not any ideal parameterization of  $w(z)$  that describes all of the possibilities. At this point, one should decide which strategy to follow so as to be as general as possible. The optimal solution would be to determine  $w(z)$  in a non-parametric way which would be valid for all dark energy models. We develop this option in Chapter 7 as one of the main contributions to this thesis. However, there are also arguments on the side to try to parameterize  $w(z)$  in a way that it can be adapted to the majority of the models. We will see the pros and cons of each choice as we dig into the analysis and the results. First of all, we give some of the most common developments in the literature.

### 4.3.1 Common developments

The first try to do is to consider a constant equation of state. Cosmological models have in general a large number of free parameters to be fitted from observations, so the less parameters introduced artificially the better. In the case of using extragalactic distances, the number is significantly smaller than in other methods such as CMB, but still the cosmological parameters ( $\Omega_M^0$ ,  $\Omega_\Lambda^0$  and  $\Omega_K^0$ ) together with those corresponding to dark energy and those related to the standardization of the astrophysical objects used must be determined. That already represents degeneracy in the results with respect to variations of the parameters. Therefore, a constant equation of state is, in principle, preferable if there is no justified reason to consider evolution. Anyway, even if evolution is present, a constant equation of state can be interpreted as an effective or average value<sup>4</sup> along the studied redshift range:

$$w(z) = w_0, \quad (4.35)$$

$$w_0 \equiv \frac{\int_0^z w(z) \Omega_X^0(z)}{\int_0^z \Omega_X^0(z)} \quad (\text{constant average equation of state}). \quad (4.36)$$

A cosmological constant; topological defects such as domain walls, strings or textures; a Cardassian model; a  $f(R)$ -modification of gravity, and some others are completely determined by a constant value. For evolving models, one can define the average  $w_0$ , but the integration through  $z$  makes it impossible to go back to the original model from the *observed* constant value. There is as well the problem of deciding the redshift range where to calculate it.

It seems then that the information obtained from  $w_0$  is not enough to distinguish among all the models. An additional hint is given by knowing the sign of the evolution. Cooray and Huterer (1999) [48] introduced the first derivative in dark energy studies:

$$w(z) = w_0 + w'z. \quad (4.37)$$

---

<sup>4</sup>We prefer *average* rather than *effective* to distinguish this meaning to the *effective* used in the previous section.

Their aim was to study quintessence as an evolving field, and not only as a constant or average value as it was done in previous analyses. Just from the sign of the derivative, one can already distinguish between quintessence tracker models ( $w' > 0$ ) and k-essence ( $w' < 0$ ).

Nowadays, that is not the most used development for the equation of state. The linearity in  $z$  makes that at high redshift  $w(z)$  becomes ridiculously high [124]. The difference is not very meaningful for SNe data, which at most reach  $z \approx 2$ , but for CMB ( $z \approx 1100$ ) the value of  $w$  has no physical sense. A couple of years after the introduction of the linear development, Chevallier and Polarski (2001) [45] proposed another development: it was a linear Taylor expansion as well, but now in the scale factor  $a$  instead of the redshift  $z$ . The development was popularized later by Linder (2003) [125]:

$$w(z) = w_0 + w_a \frac{z}{1+z}. \quad (4.38)$$

Recently, the fit of this function with one of the latest SNe Ia data sets was used in Ref. [160] to argue that its use is equivalent to a strict prior on the form of  $w(z)$ . That was justified by the difference both in uncertainty and form of  $w(z)$  with this development and with another one with more freedom ( $w(z) = \sum_i^4 w_i \ln^i(1+z)$  in this case). What is evident is that if the equation of state happened to be sinusoidal or cubic with  $z$  for example, it would not be well approximated by a linear function. On the other hand, more parameters such as the four  $w_i$  from [160] increase the uncertainty in the determination enormously. The trade-off between restricting too much the function and having an excessive number of parameters is a very difficult problem to solve when parameterizing the equation of state.

Other forms have been suggested by different authors. Some of them, as the one introduced by Efstathiou (1999) [65] adapt to a kind of dark energy models in particular (tracker fields in this case):

$$w(z) = w_0 + w_l \log(1+z). \quad (4.39)$$

Others, as that of Rapetti et al. (2005) [155], also consider the redshift  $z_t$  at which there is the transition between the present value  $w_0$  and the early value  $w_1$ :

$$w(z) = \frac{w_0 z_t + w_1 z}{z + z_t}. \quad (4.40)$$

All of them are different parameterizations of the same behaviour. Therefore, when there is no reason to prefer one development in front of another, we will trust that, usually, the simplest solution tends to be the best one. In the following, we consider two kinds of expansions: the constant (or average) one 4.37 and Linder's development 4.38.

## 4.4 Degeneracy

The determination of the equation of state of dark energy via extragalactic distances is an extremely degenerate problem. Besides the ambiguity in the theoretical model behind a result,  $w(z)$  suffers from two main sources of numerical degeneracy:

- Degeneracy because of uncertainties in the cosmological parameters. Fitting more than one parameter at the same time always introduces degeneracy due to correlations among them.
- Degeneracy due to the mathematical form with which the equation of state is related to the distance, a double integral that smooths a possible evolution.

The first point is usual in all the problems of determining free parameters and it is addressed via the introduction of priors for some of them. Also the combination of the results of various methods with different degeneracy directions allows to break the large degeneracy of one method alone. The combination is better the more different are their main directions of degeneracy. This is what is called *perpendicular methods* in the Scheme 4.7. The concrete priors and combinations are going to be commented while obtaining the results.

The second point is intrinsic to the method and cannot be avoided when using this approach that necessarily involves a double integral. In the following section, we see the degree of degeneracy that this point introduces in the result.

Furthermore, these two sources of degeneracy in the obtained value of the equation of state are not yet the whole problem. Once an  $w(z)$  is determined, it appears

a second problem of assigning a theoretical model behind the numbers. As it has been seen in the previous section, that is a third point:

- Degeneracy due to all the different models that produce the same effective equation of state.

This source cannot be reduced either mathematically or observationally. If all the models can be expressed by the same effective equation of state, and some of them are equivalent, to choose one or the other given a particular result can only be justified by the theoretical preference for one of the models.

Figure 4.7 shows an scheme of these steps and of the problems one finds when trying to conclude and explain a form for the equation of state from observational data such as SNe Ia magnitudes.

#### 4.4.1 Degeneracy in the luminosity distance

Let us attack now the source of degeneracy specifically associated with the main method used in this thesis to determine the equation of state, that coming from the luminosity distance. In the following, we give some rough numbers to quantify the problem.

The expression of the luminosity distance as a function of the cosmological parameters is given by Equations 2.51 and 2.49. As it can be seen, the distance is related to the equation of state via a double integral. We define the inner integral in the luminosity distance as the function  $J(z)$ :

$$J(z) \equiv \int_0^z dz' \frac{1+w(z')}{1+z'}. \quad (4.41)$$

And then, the normalized density of dark energy is simply:

$$\Omega_X(z) = \Omega_X^0 \exp(3J(z)). \quad (4.42)$$

Very different forms of the equation of state  $w(z)$  can lead to a similar  $J(z)$ . In fact, the equality of the several  $J(z)$  does not need to be exact in order to obtain

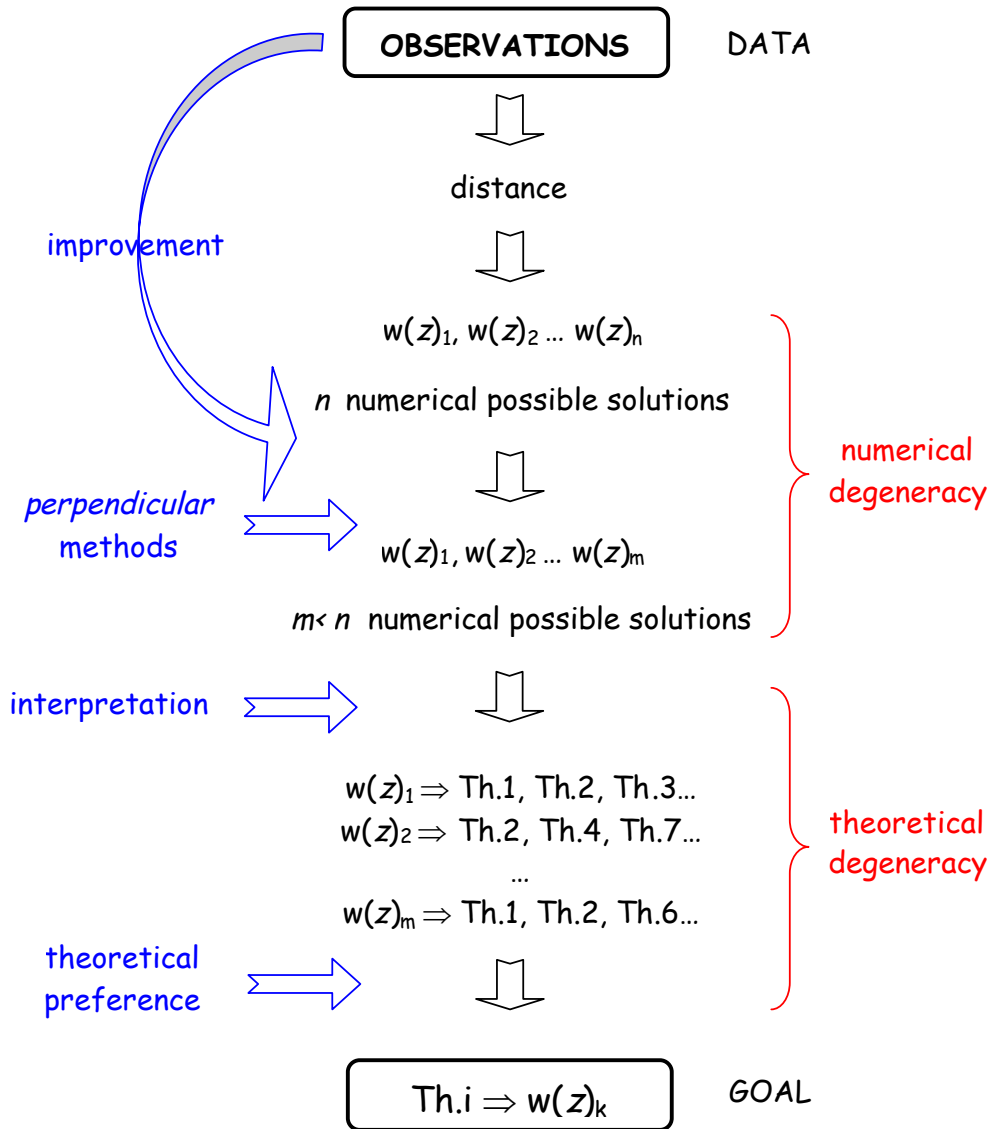


Figure 4.7: Steps in the determination and explanation of the equation of state from observations of extragalactic sources. A fit to the distance is highly degenerated, and one tries to solve it by using priors and combining methods. That breaks part of the numerical degeneracy, but there is still the problem of knowing which of the theoretical models that predict the measured equation of state is the real one.

differences in the luminosity distance that are smaller than the dispersion from current data.

In the following, we always suppose an exact knowledge of  $\Omega_M^0$  in a flat universe,

so we do not observe the large degeneracy with small variations of  $\Omega_M^0$  or with the inclusion of curvature  $\Omega_K^0$ . We are forgetting about the first point in the previous section to concentrate on the second one. Besides, we are only taking into account the effects of the first integral in redshift in order to obtain some analytical expressions (otherwise it would be impossible) and so, we are losing again part of the degeneracy.

To study this concrete source of degeneracy, we can particularize for a development of the equation of state at first order in the scale factor  $a$  (Eq. 4.38), and calculate  $J(z)$ :

$$J(z) = -w_a \frac{z}{1+z} + (1 + w_0 + w_a) \ln(1+z). \quad (4.43)$$

Just to give an example, we can observe with which evolving models a constant equation of state is degenerate (named  $w_c$  to distinguish it from the constant term in the evolution equation):

$$(1 + w_c) \ln(1+z) \equiv -w_a \frac{z}{1+z} + (1 + w_0 + w_a) \ln(1+z) \quad (4.44)$$

$$\implies \frac{w_a}{w_0 + w_a - w_c} = \frac{1+z}{z} \ln(1+z). \quad (4.45)$$

If we consider data ranging from  $z = 0$  to  $z = 2$  (as supernova of Type Ia are distributed) we can average the dependence on redshift and use a constant value, which is enough to obtain degenerate models. From now on we mean by *degenerate* models that the difference between their respective luminosity distance curves is smaller than the data capability to distinguish between them.

$$0 < z < 2 \implies \frac{1+z}{z} \ln(1+z) \approx 1.25_{-0.25}^{+0.40} \approx \frac{5}{4}. \quad (4.46)$$

From Eq. 4.45 and Eq. 4.46 we deduce the rough equality:

$$w_c \simeq w_0 + \frac{w_a}{4}. \quad (4.47)$$

The same just done for Linder's development can be done for the linear expansion in redshift (with notation  $w(z) = \tilde{w}_0 + w'z$ ), with a result:

$$w_c \simeq \tilde{w}_0 + \frac{w'}{3}. \quad (4.48)$$

In short, different combinations of the equation of state parameters which fulfil the following equality have a similar enough  $J(z)$  to be degenerate in the luminosity distance:

$$w_c \simeq w_0 + \frac{w_a}{4} \simeq \tilde{w}_0 + \frac{w'}{3}. \quad (4.49)$$

With these averages (Eq. 4.46 for instance), we are able to find models which differ in the luminosity distance typically by less than a 3%. Data uncertainty for the best future SNe surveys such as SNAP is supposed to allow a distinction at 1% level. So, not all the models obtained with this methodology are degenerate for oncoming data. However, this does not mean that the degree of degeneracy of the equation of state is low since, as we have said before, we are not considering part of the degeneracy.

Let us consider now five models with an equation of state of the form of 4.38. Three of them are degenerate with a cosmological constant model as indicated by the criterion 4.49:

$$\text{Model 1} \quad w_0 = -1.0, \quad w_a = +0.0 \quad (4.50)$$

$$\text{Model 2} \quad w_0 = -1.2, \quad w_a = +0.8 \quad (4.51)$$

$$\text{Model 3} \quad w_0 = -0.7, \quad w_a = -1.2 \quad (4.52)$$

The other two show a distinct evolution both of the equation of state and the luminosity distance. We call them *non-degenerate* models.

$$\text{Model 4} \quad w_0 = -0.7, \quad w_a = +0.0 \quad (4.53)$$

$$\text{Model 5} \quad w_0 = -1.1, \quad w_a = -0.8 \quad (4.54)$$

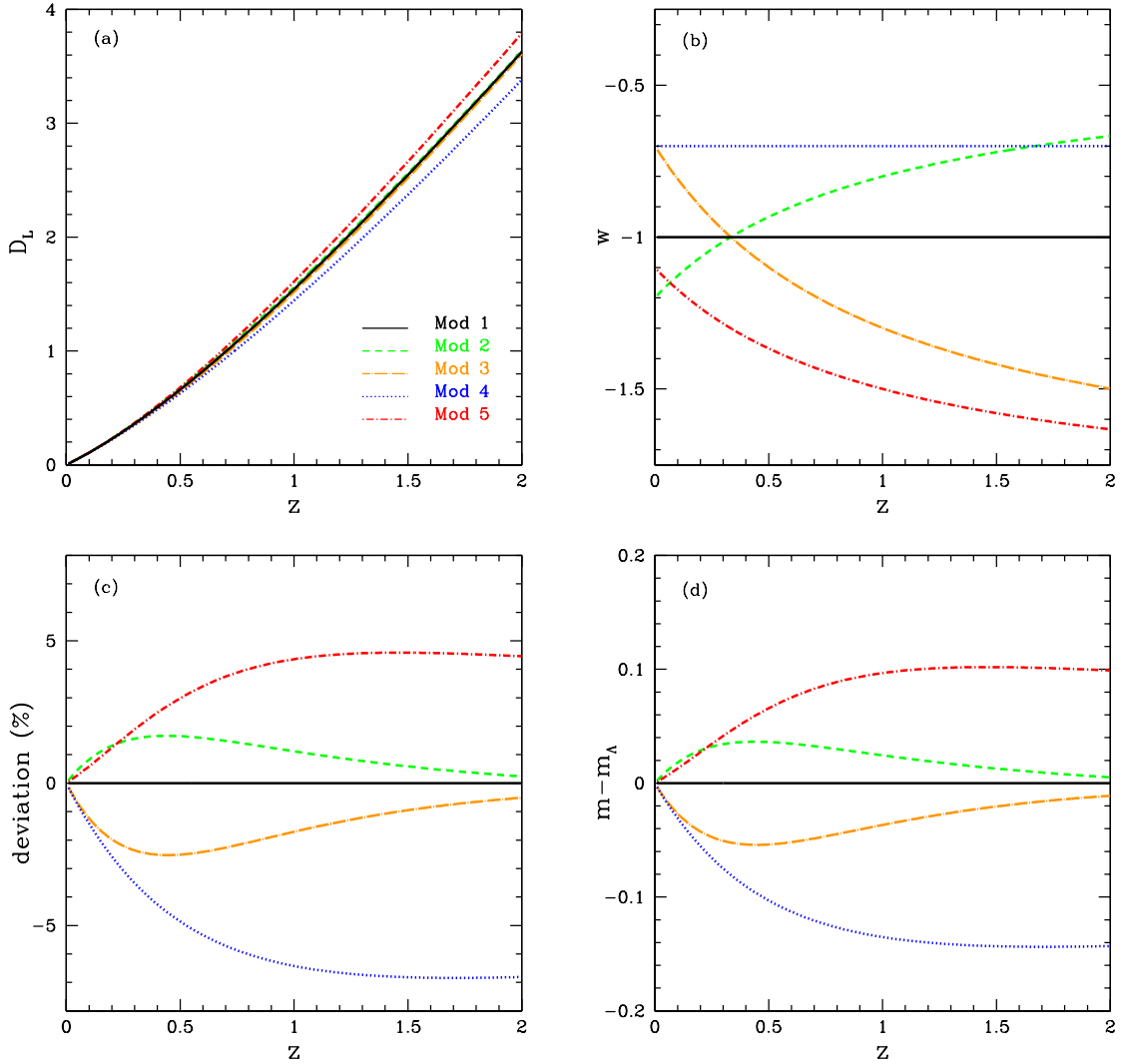


Figure 4.8: Degeneracy caused by dark energy. (a) Luminosity distance vs redshift for the five different models showed for exemplification purposes in Section 4.4.1 and the form of their equation of state (b). (c) Percentage of deviation of the luminosity distance of those models with respect to the cosmological constant one ( $w_0 = -1$ ,  $w_a = 0$ ). (d) The same as in (c) but for magnitudes. Lines in the four graphics correspond to the labels in (a).

Figure 4.8 shows a representation of these different cosmologies. In Fig. 4.8 (b) it has been plotted the form of the equation of state, whereas the corresponding luminosity distances are in Fig. 4.8 (a). We have also made two definitions in order to observe the variation among models. Figure 4.8 (c) shows the deviation in the

luminosity distance with respect to a cosmological constant model ( $w_0 = -1$ ,  $w_a = 0$ ) which can be defined as

$$\text{deviation}(\%) = \frac{D_L - D_L^\Lambda}{D_L} \times 100. \quad (4.55)$$

This deviation can be translated into magnitudes (Fig. 4.8 (d)) via the relation:

$$m - m_\Lambda = -5 \log \left( 1 - \frac{D_L - D_L^\Lambda}{D_L} \right). \quad (4.56)$$

Considering the current intrinsic dispersion of SNe ( $\sim 0.15 \text{ mag}$ ), all these models would be degenerate, and data cannot distinguish among them. However, if future experiments such as SNAP achieve an *effective dispersion* (only because of systematics) of 0.02, then differences of 1% in luminosity distance will be, in principle, distinguishable. Models 1, 2 and 3 would be in the limit of distinguishability, but methods as the one proposed in Chapter 7 could take advantage of intermediate redshifts, where differences are larger, to discriminate among them. It is interesting to notice that although models have been chosen according only to criteria referring to the inner integral, the plots in Figure 4.8 account for the whole degeneracy.

In conclusion, nowadays the degree of numerical degeneracy is important, but it is expected to diminish appreciably as the dispersion in SNe Ia magnitudes diminishes. In Chapter 5, some alternative methods to combine these results with those from other extragalactic distances are shown, and it is seen that the combination breaks part of the degeneracy. Anyway, equivalences among theoretical models cannot be avoided and a better understanding of what dark energy is, is needed in order to bet for one of the theoretical options given the *best* numerical  $(w_0, w_a)$  solution. Up to now, then, theoretical degeneracy cannot be broken, although there is the tendency to prefer the cosmological constant, given the lack of well-founded motivations to discard it in favour of a more complicated model.

## **Part II**

### **Observational constraints**



## Chapter 5

---

# Cosmic distances and standard candles

---

All the theoretical cosmological models introduced in the first part of the thesis need to be compatible with astrophysical observations and, among them, extragalactic distances are a very important tool to test these models. This chapter describes the determination of cosmic distances both to astrophysical objects and to some key points in the past of the Universe. Most of the chapter is devoted to summarize the details of the main tool used in our calculations, Type Ia supernovae.

### 5.1 The cosmic distance ladder

The only direct way to measure distances is by trigonometric parallaxes. The measure is based on the different position that seems to have a star due to the movement of the Earth around the Sun. However, at large distances, parallax angles become too small to be measured, and the method, although very precise, is only valid up to a scale of some kiloparsecs.

All the remaining methods must be calibrated with this first step of the ladder, and in some cases, with previous steps to the method itself as well. Secondary indicators are typically stellar clusters, main sequence stars and some standard candles which are described in the next section. At really large distances various techniques are used: the Tully-Fisher relation, the planetary nebula luminosity function, the

globular cluster luminosity function, the surface brightness and luminosity fluctuations, etc. Type Ia supernovae, although being a standard candle, is also a very powerful tool to measure extragalactic distances at high redshift, and it is shown in Section 5.2 that there are other extragalactic distance indicators that can reach even higher redshifts. However, none of these other tools have achieved the precision of SNe Ia yet.

### 5.1.1 Standard candles

A standard candle is an object with known intrinsic luminosity. The dilution of this luminosity from its position to ours is given in an euclidean space-time by the inverse square law of distances. Assuming isotropic emission, the flux that we receive from a candle is given by the geometric definition which relates the received flux  $\mathcal{F}$  with the absolute luminosity  $\mathcal{L}$ :

$$\mathcal{F} \equiv \frac{\mathcal{L}}{4\pi d_L^2}. \quad (5.1)$$

For a known  $\mathcal{L}$ , the measure of  $\mathcal{F}$  allows to determine the luminosity distance to the source. That is only a definition in our four-dimensional Universe. Although it corresponds to the physical distance in an euclidean space, it loses meaning in a curved space (the meaning of distances in cosmology and in particular of the luminosity distance has been explained in detail in Section 2.3.2). The relation is often defined in astronomy in terms of the apparent magnitude  $m$  and expressed as a function of redshift,  $z$ :

$$m(z, H_0, \Omega_M^0, \Omega_X^0) = \mathcal{M} + 5 \log_{10} [H_0 d_L(z, H_0, \Omega_M^0, \Omega_X^0)]. \quad (5.2)$$

That is the *magnitude-redshift relation*, where terms have been defined in order to collect all the dependence on the current value of the Hubble parameter into a zero point

$$\mathcal{M} \equiv M - 5 \log_{10} H_0 + 25. \quad (5.3)$$

Notice that the combined expression  $D_L(z, \Omega_M, \Omega_\Lambda) = H_0 d_L(z, H_0, \Omega_M, \Omega_\Lambda)$  entering the argument of the logarithm on the r.h.s. of Equation 5.2 is Hubble constant-free. In this way all the cosmological model dependence is encoded in the luminosity distance function  $d_L(z, H_0, \Omega_M, \Omega_\Lambda)$  (Eq. 2.51). This fact is important for using a particular kind of standard candles, Type Ia supernovae, to determine the cosmological parameters and test different cosmological models. Actually, we have formulated the magnitude-redshift relation in the way used for that purpose, but it can be found in alternative forms when used with other candles.

Before supernovae, in a lower step of the ladder, Cepheid variables are used to determine distances. They show a period-luminosity relation: shorter period Cepheids are less bright and vice versa. They are suitable for distances shorter than  $\sim 50 Mpc$ , beyond which they are not visible any more. That corresponds more or less to a redshift  $z \sim 0.01$ , the redshift at which there already are the sets of nearby supernovae. Cepheids rely on trigonometric parallaxes, and the next step, SNe Ia, must rely on distances from Cepheids [9].

## 5.2 Extragalactic sources as distance indicators

Traditionally, distances have been determined by means of the standard candles just mentioned, but the yearn for reaching higher redshifts is entailing the use of other extragalactic sources which are not as well behaved as the previous ones.

Fanaroff-Riley Type IIb radio galaxies (*FR IIb*), for instance, can be calibrated in such a way so that they can be used for cosmological purposes. In Refs. [54, 55], their dimensionless coordinate distance was calculated together with that of Type Ia supernovae and both were used as complementary tools. A similar thing happens with compact radio sources which were analysed in [95, 122] where it was delimited the suitable range of data to be calibrated.

Higher redshifts can be reached by quasars and gamma-ray bursts, but although they have also been used as candles, their calibration is still dubious. These objects are better used for cosmology without the need to be standard candles, such by means of the Lyman- $\alpha$  forest for quasars [114] or by means of the number of counts for gamma ray bursts [19].

As a matter of fact, the calibration of none of the above sources has achieved a degree of acceptance comparable to supernovae. Type IIP supernovae can be calibrated via the expanding photosphere method or the luminosity-velocity relation, but nowadays, the best calibrable standard candles are Type Ia supernovae. Although SNeIIP can reach higher redshifts their dispersion is wider and less understood. Due to the importance of SNeIa in modern observational cosmology, we dedicate the second part of the chapter to present the behaviour of these objects.

### 5.3 Key distances for cosmology

Besides the distances measured from extragalactic sources, it is worth mentioning some distances that for some reason can be especially well measured, and therefore, can help to constrain the behaviour of the Universe at that point and its evolution.

In this thesis we do not enter the physics behind each method, we just use their final result to combine it with the one we obtain with SNeIa. We see that the complementarity of the results improves the constraints on all the parameters.

#### 5.3.1 Low redshift, 2dFGRS

The 2dF Galaxy Redshift Survey (*2dFGRS*) [193] was a spectroscopic survey that observed mainly galaxies up to a redshift of  $z \sim 0.2$ . That allowed to determine the growth parameter in a mean redshift,  $z = 0.15$ , and its dependence on the cosmological parameters is now used to constrain them.

For a general cosmological model, one has to solve the differential equation for the linear fluctuation growth factor (see [119] for the methodology). However, for a constant dark energy equation of state, the growth parameter can be written as

$$f(z_G, \Omega_M^0) = \left( \frac{\Omega_M^0}{\Omega_M^0 + (1 - \Omega_M^0)(1 + z)^{3w}} \right)^{0.6}. \quad (5.4)$$

The observational result from the 2dFGRS survey is  $f(z = 0.15) = 0.51 \pm 0.11$  according to the redshift space distortion parameter obtained in [101] and the linear bias in [199].

As it happens with Baryonic Acoustic Oscillations (BAO), the major constraint on the growth factor goes to the density of matter  $\Omega_M^0$  and not to dark energy. However, that is interesting when joining this results with SNeIa, because, as we will see, the confidence regions are almost perpendicular. But BAO constraints also go in the same direction and are more precise, so to study the cosmological parameters we prefer using BAO rather than the growth parameter of 2dFGRS.

### 5.3.2 Intermediate redshift, BAO

At a slightly higher redshift than 2dFGRS, at a mean redshift of  $z = 0.35$ , baryonic acoustic oscillations have been measured [70]. Their constraints are important for the equation of state, although up to now, the method used here relies on a constant equation of state. We use the baryonic acoustic oscillation peak detected in the SDSS luminous red galaxy survey. A convenient parameter defined in a way independent from the Hubble constant is  $A(z)$ . It depends on the dilation  $D_V(z)$  and is defined as:

$$A = \frac{D_V(z)}{cz} \sqrt{\Omega_M^0 H_0^2}, \quad (5.5)$$

where

$$D_V(z) = \left( D_M(z)^2 \frac{cz}{H(z)} \right)^{\frac{1}{3}}, \quad (5.6)$$

and  $D_M(z)$  is the comoving angular diameter distance given by  $D_M = d_A(1+z)$ . So, in a FLRW universe,  $A$  is written as a function of any given cosmology as:

$$A(z_B, \Omega_M^0, \Omega_X^0) = \frac{\sqrt{\Omega_M^0}}{(H(z_B)/H_0)^{1/3}} \left[ \frac{1}{z_B \sqrt{|\Omega_K^0|}} \text{sinn} \left( \sqrt{|\Omega_K^0|} \int_0^{z_B} \frac{H_0 dz'}{H(z', \Omega_M^0, \Omega_X^0)} \right) \right]^{2/3}. \quad (5.7)$$

The result obtained by Eisenstein et al. in [70] for  $z_B = 0.35$  is  $A = 0.469 \pm 0.017$ .

In the same way, we add future expectations also for BAO. The slope of the

confidence region changes with redshift: the lower the redshift, the better the determination of the density of matter, and the opposite happens for the dark energy parameters. We assume a future survey with a 2% uncertainty in the angular distance  $D_V$  at a mean redshift of  $z = 0.55$ . Considering a cosmological constant fiducial model with  $\Omega_M^0 = 0.3$  and  $\Omega_\Lambda^0 = 0.7$ , it is obtained  $D_V(z = 0.55) = 1995 \pm 40 \text{ Mpc}$  and therefore  $A(z = 0.55) = 0.452 \pm 0.009$ . Confidence regions for both the current value and the incoming one are shown in Figure 5.1.

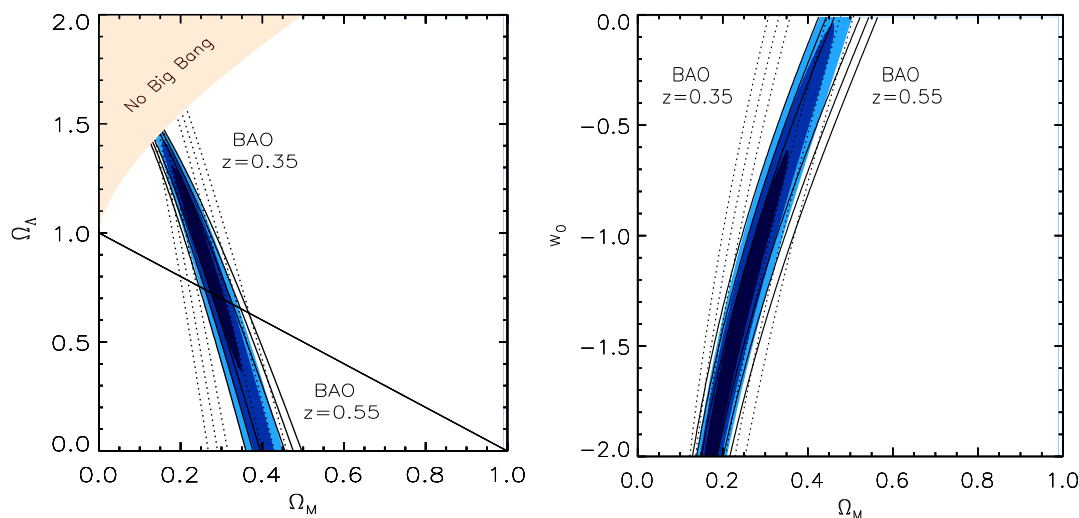


Figure 5.1: Confidence regions showing BAO constraints on the cosmological parameter plane ( $\Omega_M^0, \Omega_\Lambda^0$ ) and for a constant equation of state ( $w_0, \Omega_M^0$ ). Dashed lines represent the current constraint at  $z = 0.35$  from [70], solid lines show future expectations at  $z = 0.55$  with a 2% uncertainty in the angular distance  $D_V$ . Filled in blue  $1\sigma$ ,  $2\sigma$  and  $3\sigma$  joint confidence regions.

### 5.3.3 Very high redshift, CMB

CMB fluctuations are produced at very high redshift,  $z \approx 1089$ , so the CMB gives information about the youth of the Universe. To introduce this information, we use the shift parameter  $R$  which determines the whole shift of the CMB angular power spectrum [32].  $R$  is given as a function of the cosmological parameters by

$$R(z_C, \Omega_M^0, \Omega_X^0) = \frac{\sqrt{\Omega_M^0}}{\sqrt{|\Omega_K^0|}} \text{sinn} \left( \sqrt{|\Omega_K^0|} \int_0^{z_C} \frac{dz' H_0}{H(z', \Omega_M^0, \Omega_X^0)} \right), \quad (5.8)$$

where  $z_C = 1089$ . From the observations of CMB including WMAP, CBI and ACBAR, the shift parameter is constrained to be  $R = 1.716 \pm 0.062$  [184, 202]. The last constraints of WMAP3 improve this result up to  $R = 1.70 \pm 0.03$  [183, 203].

However, due to the precision with which CMB fluctuations favour a flat universe (or very close to), normally the information from CMB is introduced by assuming a flat universe. That, of course, breaks part of the degeneracy present among cosmological parameters and dark energy, and eases calculations for complex models where the number of independent parameters is high. Nevertheless, one has to be conscious of the loss of generality and be cautious about the conclusions.

## 5.4 Supernovae as standard candles

The use of Type Ia supernovae as standard candles is widely accepted in cosmology. However, as it will be seen, they are not perfect standard candles and, therefore, SNe Ia must be calibrated. This section gives an idea about the main physics of SNe Ia, which is basic to understand their behaviour as standard candles. Also the chief methods to calibrate the data are shown, and some comments about different sources of uncertainties and systematics are given, paying special attention to the treatment of the redshift uncertainty as the analysis of its particular effect is part of this thesis.

### 5.4.1 Supernovae

Phenomenologically, a supernova is a stellar explosion that produces a *huge* luminosity. During a few days, these kinds of explosions reach the same luminosity as the whole host galaxy and the closest ones are even observable with naked eye. Physically, not all supernovae are the same, and behind the same name very different processes are hidden. However, the first classification was made not due to the differences in their nature but by observational criteria.

During the thirties, the study of extragalactic *nebulae* allowed to discover several of these blasts. Walter Baade and Fritz Zwicky started using the term *supernova* for them [15], and a systematic search began. All of the first observed supernovae were lacking in hydrogen, but later similar objects with hydrogen lines in their



Figure 5.2: Classification scheme of supernovae. The main characteristic of each type is shown in brackets. *S* indicates that the distinction is in the spectrum and *LC* in the light curves.

spectrum were observed. In 1941, Rudolph Minkowski together with Baade classified supernovae according to that characteristic: Type I SNe are those without hydrogen whereas Type II SNe show hydrogen features in their spectrum. Afterwards, other subgroups were made and Zwicky even added new groups (Type III, IV and V) which had no continuity. Nowadays, the common classification is still based on Minkowski's one and can be seen in Figure 5.2. This table shows how different types of supernovae are related to differences in their spectra or light curves. Also the intrinsic distinction, that is, the explosion mechanism, is highlighted. A finer distinction based on that is being revised as new objects are discovered [197].

Most of the supernova types classify *core collapse* supernovae, which are typically the death of massive stars ( $8M_{\odot} < M_{*} < 80M_{\odot}$ ). The life of a star is a succession of stages of fusion where once an element is exhausted, the core contracts until the pressure and temperature are sufficient to begin the next stage and halt the contraction. When all the elements are exhausted and there is nothing else to be burned exothermically, the core is only supported by the degeneracy pressure

of electrons. But this pressure is not enough, and the core of the star collapses homologously. When the density in the inner part is of the order of that of the atomic nucleus the collapse suddenly stops, but the outer parts are still falling and bounce against this barrier. Although the exact mechanism is not completely understood yet, these shock waves make the outer parts to be expelled and the inner core remains as a compact object.

A crucial fact for the classification of core collapse supernovae is that massive stars lose a large amount of mass due to stellar winds. Therefore, when a star reaches the last stages of its life, it may have lost some of its external layers. If this is not the case, Type II supernovae are produced and we can observe hydrogen in the spectrum close to the explosion epoch. If the object only loses the first layer composed by hydrogen, the spectrum lacks hydrogen and we have a Type Ib supernova. More massive stars lose the following layers as well, and so, Type Ic supernovae do not show helium features in their spectra.

Another relevant aspect that causes differences among the observed explosions is the fact that stars are not always isolated, but half of them are gravitationally tied and form binary systems. The evolution of the stars, then, is not identical to that of an individual object. In a binary system, both members could produce a common envelope before the explosion, and if so, part of the common envelope will be lost because of friction. According to the mass of the remaining hydrogen-rich envelope, we can distinguish three kinds of Type II supernovae: Type IIb SNe with  $M_{env} < 1M_{\odot}$ , Type IIL SNe with  $M_{env} < 2 - 3M_{\odot}$  and Type IIn SNe with  $M_{env} > 4 - 5M_{\odot}$ . The first classification was made again through the observational features, and the letter which indicates the subtype within Type IIs is related either to the spectrum or the light curve. Type IIL SNe have a *L*inear ascent in magnitude during more than two months after the maximum of the light curve and Type IIP SNe show a *P*lateau after maximum. The other two subtypes were established later according to the features in their spectrum. Type IIn SNe have *n*arrow lines maybe due to the fact that the stars are embedded in a dense interstellar medium which absorbs part of the radiation. On the contrary, Type IIb SNe have *b*road lines and show almost no hydrogen features, being possibly the evolutive link with Type Ib/c SNe, since at late times their spectra are similar. Figure 5.3 and Figure 5.4 show these differences in the spectra and light curves respectively.

The other mechanism to generate supernovae, a *thermonuclear explosion*, is only

seen for Type Ia supernovae, which are observed as very bright and homogeneous explosions without hydrogen in their spectra. These supernovae are the main tool used in this thesis. Therefore, we use the rest of the chapter to describe in more detail these explosions.

### 5.4.2 Physics of Type Ia supernovae

Type Ia supernovae are thought to be thermonuclear explosions in binary systems, where one of the stars is a carbon-oxygen white dwarf (C-O WD). This star has burned the hydrogen and when it finishes also the helium, it does not reach a temperature high enough to initiate the combustion of carbon, becoming a white dwarf mainly composed by carbon and oxygen. If the mass of the WD is close to the Chandrasekhar mass<sup>1</sup>, and if there is any mechanism that makes this mass exceed the Chandrasekhar limit (as for instance the accretion in a binary system), the remaining combustions will take place in the degenerate environment in an explosive way.

It is unlikely that ignition occurs in a core of degenerate helium, since the observed energy and abundances do not agree with predictions. A mix of oxygen, neon and magnesium is not suitable either: a very high density is needed in order to start the ignition, and then probably a gravitational collapse would result. A core of degenerate carbon and oxygen seems to be the most adequate progenitor. However, as it has been said, this object must add mass to surpass Chandrasekhar's limit and hence, it must be part of a binary system. Different scenarios have been proposed (see for example [103] for a review), mostly belonging to two classes: Single Degenerate scenarios [209] where only the C-O WD is degenerate, and Double Degenerate scenarios [110] where both objects are white dwarfs. In the latter, the two WDs follow an orbit around the centre of mass which shrinks due to the emission of gravitational waves. The most massive white dwarf accretes mass from the less massive one during the process, and eventually it explodes. However, some simulations show that although the sum of the masses of both objects is close to the Chandrasekhar mass, the merging can lead to a collapse instead than to a thermonuclear explosion, and so nowadays they are not favoured.

---

<sup>1</sup>The Chandrasekhar mass is the maximum mass that a white dwarf can have being supported by the pressure of degenerate electrons.

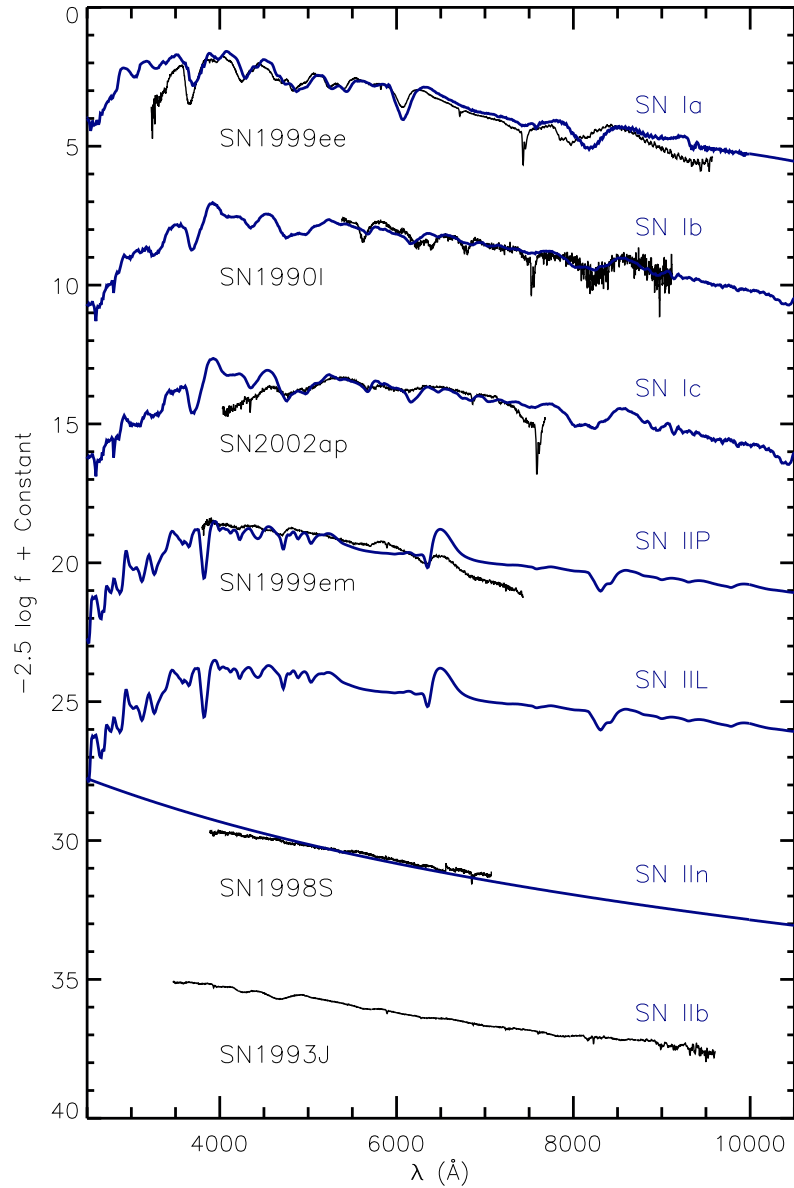


Figure 5.3: Composite figure with the spectral templates for all types of supernovae (blue line), and for real objects (black line). The use of templates is, however, not accurate for the non-homogeneous groups. Templates have been obtained from Peter Nugent [137] and the spectra of individual supernovae from the SUSPECT archive [188].

Also recent observations seem to point instead towards a Single Degenerate scenario [165], where there is a wider range of models depending on the companion star [41]. In these cases two possible ways of starting the ignition are considered:

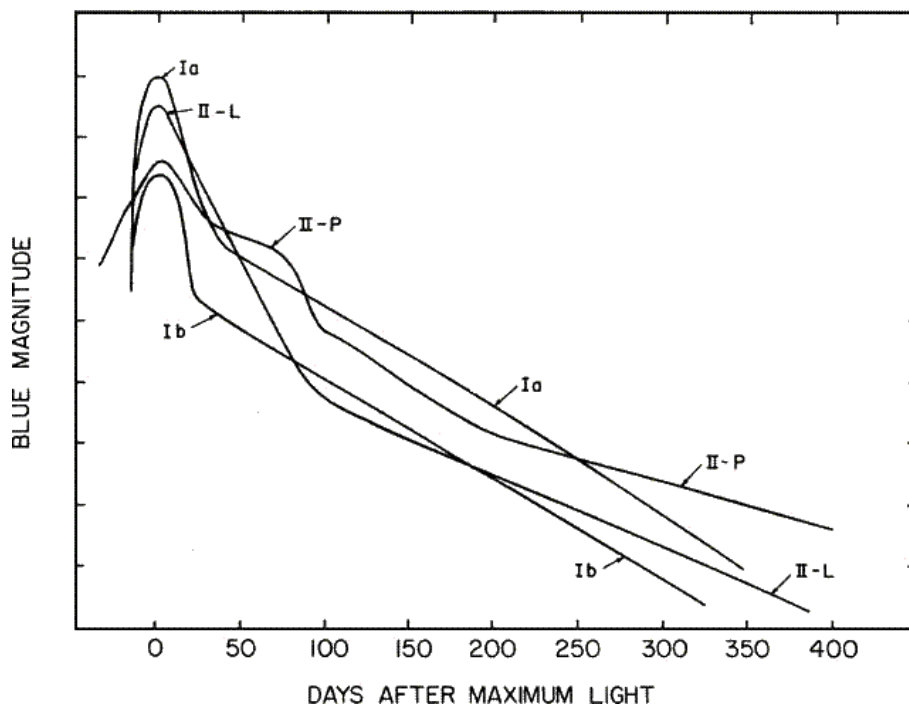


Figure 5.4: Schematic light curves for different types of supernovae (Source: Ref. [208]).

- Chandrasekhar explosions, where the WD accretes mass until it reaches the Chandrasekhar's limit and explodes,
- and Sub-Chandrasekhar explosions, where the WD also accretes mass from the companion star but now it forms a layer of helium that, when burning, can ignite the core of C-O before reaching the limit of mass.

For the normal SNeIa, the most popular option is a Chandrasekhar explosion generated by intermediate accretion rates ( $\sim 10^{-7} M_{\odot} yr^{-1}$ ). According to simulations, these explosions produce both iron peak and intermediate-mass elements as observed in the spectra. But not only the progenitor is important to reproduce observations, and the explosion mechanism is another unknown of the SNeIa paradigm. Deflagration models seem not to generate the correct quantity of these elements, but that could be solved with delayed detonation models [84] which produce the observed luminosity as well.

If eventually the choice outlined in this section turns out to be the true mechanism, it would explain the high similarities in all the observed supernovae, at least in the normal ones, since all of them would originate from a core with mass

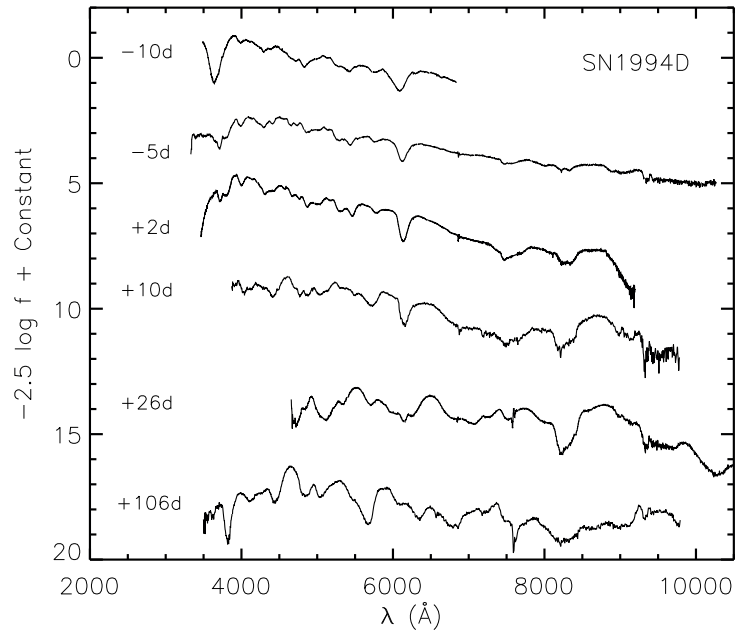


Figure 5.5: Spectroscopic evolution of a normal SNe Ia, SN1994D, at chosen epochs from -10 days to 126 days. Spectra have been obtained from the SUSPECT archive [188].

$M_{Ch} \approx 1.4 M_{\odot}$ . On the other hand, for the subluminous SNe Ia it is sometimes resorted to sub-Chandrasekhar models of explosion, which would account for the smaller amount of energy released.

### 5.4.3 Observational features

The only way to contrast the different scenarios introduced in the previous section is by using the information coming from the measured energy, either from the spectra or the light curves. They are also important to characterize the objects, since, in fact, spectra and light curves hold all the information we can obtain from SNe Ia. Therefore, these are the only tools we have at our disposal to understand the nature of the phenomenon.

### 5.4.3.1 Spectra

The most distinctive feature of Type Ia supernovae is the SiII absorption line in the early spectra at a wavelength  $\lambda \approx 6150 \text{ \AA}$ , together with the lack of hydrogen that defines all Type Is. An observed supernova is often classified as SNe Ia mainly because of these lines.

The spectra of SNe Ia evolves as the explosion proceeds. Close to the maximum, the spectra show important emission and absorption lines. It is easy to see intermediate mass elements such as O, Mg, Si, S, Ca, etc. in neutral or first ionization states. At short wavelengths, some elements from the iron peak are observed as well. Figure 5.5 shows that the strongest lines are those of silicon (corresponding to SiII at  $6355 \text{ \AA}$  in rest frame) and the H and K lines of CaII at  $3934 \text{ \AA}$  and  $3968 \text{ \AA}$  also in rest frame. The P-Cygni profile of these lines allows to obtain the expansion velocity of the photosphere at the time of creation of the line. For the SiII line velocities of order  $10000 \text{ Km/s}$  are obtained, and they are even higher for the CaII lines ( $v \approx 13000 \text{ Km/s}$ ). These high velocities diminish fast as we go farther from the luminosity peak.

As time goes by, the nucleus of the white dwarf becomes richer in iron, and therefore, the iron lines become stronger although the intermediate mass elements are still important. Approaching the nebular phase, the spectra starts to be dominated by forbidden emission lines from first several ionization states of iron, and cobalt multiplets. The evolution of the latter shows the radioactive decay of cobalt in the last stages of the supernova. Calcium lines (CaII H & K and the triplet close to the infrared) are still visible as it happens in all the stages of the evolution of the supernova.

This is the general behaviour for 80% of SNe Ia, but the remaining 20% can show different features. Referring to the spectra, some of them do not have the silicon line, and sometimes, even the calcium and sulphur lines are absent. In these cases, all the spectroscopic evolution as well as the light curves must be taken into account to classify the object. Typical examples of that are the superluminous SN1991T and the subluminous SN1991bg. On the other hand, spectra at low and high redshift do not differ significantly.

### 5.4.3.2 Light curves

Spectra are the key elements to classify supernovae as Type Ia, but the homogeneity of light curves allows to use them as standard candles, or, at least, as *calibrable* standard candles. So, the study of the light curves is of paramount importance in cosmology.

The common trend for SNe Ia and the comparison with the other types can be seen in Figure 5.4. In the case of core collapse supernovae, the light curve can differ appreciably from one object to another, but for these thermonuclear explosions the shape is standard. After the explosion there is a sudden increase of luminosity, which, after more than a week, reaches the maximum. The decrease has two differentiated slopes: a first fast one with an increase in magnitude of about  $0.1 \text{ mag/day}$ , and less than a month later the slope suddenly changes to  $0.01 \text{ mag/day}$ . Also the absolute magnitude at maximum is characteristic. Using 111 SNe Ia from the Asiago Supernova Catalog, the authors in Ref. [157] found a Gaussian distribution with mean  $M_B = -19.46$  and a dispersion of 0.57 for normal supernovae.

These similarities among observations must occur because all of them come from the explosion of very similar objects. When the C-O WD explodes having a mass  $M \sim M_{Ch}$ , the surface increases fast but the temperature remains almost constant. At the beginning, the sphere is opaque and the nuclear energy released when explosively burning carbon and oxygen results into the Fe-peak elements. That makes the object expand, the density diminishes and, therefore, so does the opacity, allowing every time more flux to leave the supernova. This epoch lasts less than 20 days, and it appears in the light curve as a very fast increment of luminosity.

The more the ejecta expand, the more transparent they become to the  $\gamma$ -radiation. Besides, the radioactive decay is also diminishing exponentially, and the light curve starts to fall. The maximum is usually modelled with a parabola ( $\propto t^2$ ), although the behaviour is different depending on the energy band. To give an example, the maximum in the infrared is about five days before the maximum in the B band, and after it, there is a monotonous decay in ultraviolet and visible, but not in infrared, where it is produced a second maximum.

The chain  $^{56}\text{Ni} \rightarrow ^{56}\text{Co} \rightarrow ^{56}\text{Fe}$  describes the slopes in the observed light curves, and it can account for the differences observed with different filters. Other radioactive elements synthesized during the explosion and with longer half-lives ( $^{57}\text{Co}$ ,  $^{55}\text{Fe}$ ,

$^{44}\text{Ti}$ ...) are responsible for the light curve even thousands of days after the explosion, when, in most of the cases, there are no observations.

From the cosmological point of view, the most important feature in the light curve is, in principle, its maximum (usually in B). Since it must highly depend on the quantity of nickel available, the understanding of the model of synthesis of elements during the explosion is decisive to understand the homogeneity of the group. Especially, if as we are seeing with the increasing number of observations, by subluminous and superluminous events are not as rare as they were thought to be.

## 5.5 Standardizing Type Ia supernovae

As soon as the amount of observed SNe Ia started to be statistically significant, it became evident that there was a dispersion in the luminosity peak, decline rate, colour and even spectrum of SNe Ias. This dispersion is not only accounted for subluminous and superluminous supernovae, but it is also seen among the normal ones.

It is obvious that all the observed quantities have a dispersion just because of being measured. However, it was soon realised that there was a correlation between the luminosity at maximum and the decline rate (as seen in the upper plot of Figure 5.6). This intrinsic dispersion adds to the statistical one and once it is understood, the objects can be calibrated and only show the statistical dispersion.

Although during the 70's such a relation was found observationally [152], it was in 1993 when Mark M. Phillips established the empirical relation between the luminosity at maximum and the linear decline rate [149]. He fitted the curve in three bands (B, V and I) without excluding any peculiar object, and, after applying the correction

$$M_{corr}^{max} = a + b\Delta m_{15}(B), \quad (5.9)$$

he found a reduction on the dispersion of the absolute magnitude  $M$  of almost a 50%. In the previous equation  $a$  and  $b$  are free parameters and  $\Delta m_{15}(B)$  is the increment in magnitude in B from the maximum up to 15 days after it.

According to the *Phillips relation*, brighter SNe Ia are slower (wider light curves), whereas the dimmer ones show a faster decline (narrower). A naive interpretation of this result is based on the amount of  $^{56}\text{Ni}$ . The more  $^{56}\text{Ni}$  synthesized, the higher the temperature is, and, therefore, the iron peak elements will be in a higher ionization state. That makes the opacity larger and so, more radiation is trapped. Releasing all this energy is then slower and the light curve shows wider.

This is the origin for most of the methods to calibrate SNe Ia. Some of them describe the light curves as a single parameter family of curves. Others widen the relation to two or even three parameters, considering for example the colour as extra parameter. All of the methods introduce a correction to the observed magnitude which accounts for the difference between the observed supernova and what is considered a standard one. In the following, a brief explanation for the most commonly used methods is given, with a special emphasis on the stretch factor method, which is the one chosen for calculations in this thesis.

### 5.5.1 $\Delta m_{15}$ template fitting

This method is a straightforward application of the Phillips relation. From a set of very well measured SNe Ia one can measure  $\Delta m_{15}(B)$  and obtain two things: the relation  $M_B - \Delta m_{15}$ , and templates for several values of  $\Delta m_{15}$  by averaging their light curves. Then, the observed points of new supernovae can be compared to these templates, and via a  $\chi^2$  minimization one finds the  $\Delta m_{15}$  and two shifts: one giving the magnitude of the peak and the other one the phase [98, 99].

The first representative results were obtained from 18 low redshift SNe Ia discovered by the Calán/Tololo survey close to the maximum. The relation between  $\Delta m_{15}$  and that maximum was found to be, with respect to a standard supernova with  $\Delta m_{15} = 1.1$ ,

$$M_{B,corr} = -(19.26 \pm 0.05) + (0.86 \pm 0.21)(\Delta m_{15} - 1.1). \quad (5.10)$$

Therefore, the correction term  $\Delta_{B,corr}^{1.1}$  can be written as  $(-0.86 \pm 0.21)(\Delta m_{15} - 1.1)$  and the apparent magnitude should be corrected with [147]:

$$m_{B,corr} = m_B + \Delta_{B,corr}^{1.1}. \quad (5.11)$$

### 5.5.2 Stretch factor

The *Supernova Cosmology Project* introduced in 1997 another parameterization to calibrate the supernovae, the stretch factor. In order to represent the faster and the slower SNeIa, this method stretches linearly the time axis and transforms all the light curves into a single standard one (the composite curve) [146, 147]. That procedure is only valid during the first four weeks and in the  $B$  and  $V$  bands, since at other wavelengths there is a secondary maximum about 20 and 40 days after the absolute one.

The free parameter that represents the method is the width factor  $w = s(1 + z)$ , which accounts for the contribution due to the time dilation (factor  $1 + z$ ) and for the stretch factor  $s$  itself. Usually, the stretch factor is interpreted as a parameter that encodes the variation of the opacity with temperature following the explanation of the Phillips relation given in Section 5.5.

In a similar way as it happened with the  $\Delta m_{15}$  template fitting method, one must construct a series of templates for the light curves in each band. However, in this case, the templates correspond to a fiducial supernova with  $s = 1$ , and the observed supernova is compared to the template by stretching the time axis. This comparison allows to determine not only the stretch but also the magnitude of the peak and the time of the maximum. Peter Nugent's templates in UBVRIJHK bands can be found in [137].

The effect of the width of the light curve translates into the magnitude as:

$$m_{B,corr} = m_B + \alpha(s - 1). \quad (5.12)$$

$\alpha$  is a positive parameter to be determined by minimization of the dispersion to a given cosmology and is calculated for a set of SNeIa (see Section 6.1.4), whereas as it has been seen  $s$  is a measured property of each SNeIa.

Up to now, two methods based in the same principle have been explained. The

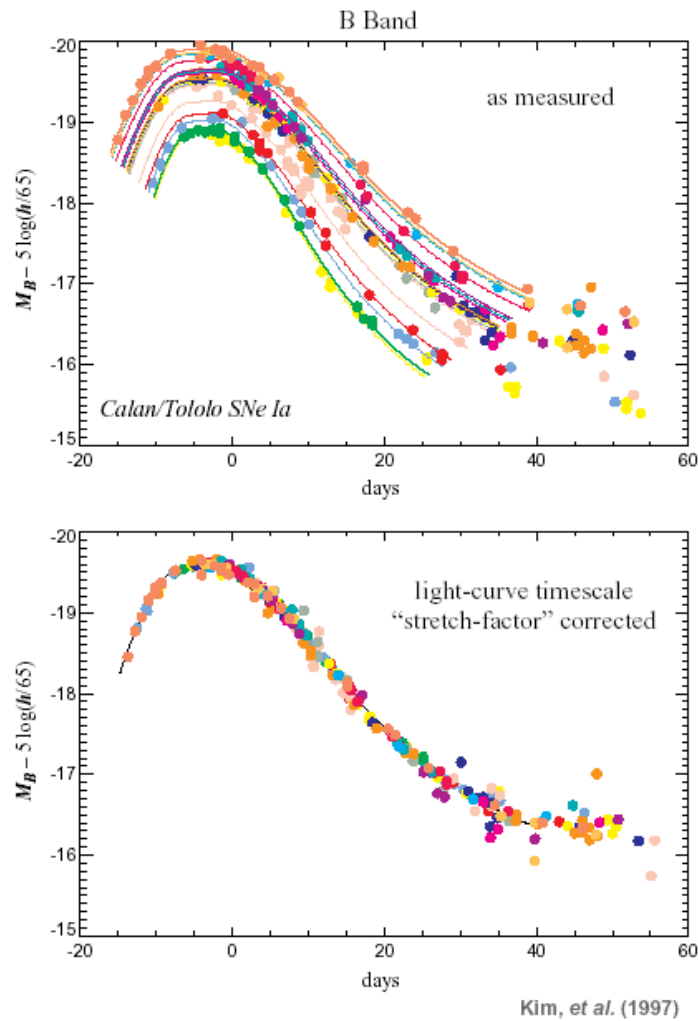


Figure 5.6: Light curves of the nearby SNe Ia from the Calán/Tololo survey. In the upper panel it is apparent the dispersion and the relation between the maximum brightness and the width of the light curves. The lower panel shows the composite curve after applying the stretch factor correction.

stretch factor is highly correlated with  $\Delta m_{15}$ , but yet the two parameters are not equivalent. In Ref. [9], it was calculated the following relation between both methods with 58 nearby SNe Ia:

$$\Delta m_{15}(B) = (1.98 \pm 0.16)(s^{-1} - 1) + (1.13 \pm 0.02). \quad (5.13)$$

This dispersion between methods is in general not very important, and the same cosmological conclusions are obtained after correcting the SNe Ia with any of them, but one has to be consistent and stick always to the same one.

### 5.5.2.1 Adding the extinction correction

As it is explained in Section 5.6.2, the extinction is commonly added to the magnitude in a way independent of the standardization. However, it can be included in the light curve fitting as the *Supernova Legacy Survey* do by modifying the stretch correction [97, 14] (see also an alternative method introduced in next section):

$$m_{B,corr} = m_B + \alpha(\hat{s} - 1) - \beta c. \quad (5.14)$$

If one adds this correction to the fit, the obtained stretch factor  $\hat{s}$  can be different from the one without  $s$ -correction because of the addition of the new term, even though the definition of the stretch is the same. The extinction correction is here a linear function defined as  $c = (B - V)_{Bmax} + 0.057$ , where one measures the colour excess with respect to a fiducial SN with  $(B - V) = -0.057$  at the maximum in B band. This term includes both the host galaxy extinction and any possible intrinsic colour variation.

Just as before,  $\hat{s}$  and  $c$  are characteristics of each supernova, whereas  $\alpha$  and  $\beta$  are obtained from the fit to the light curves.

### 5.5.3 Multicolour Light Curve Shape (MCLS)

The main contribution of this method developed by the *High-Z Team* is the use of different bands and colours to quantify the reddening as well [159, 158]. It incorporates the observed evidence that fast decliners are usually redder in  $(B - V)$  and slow decliners are bluer.

The MCLS equations in principle describe the light curves as a linear family of the peak luminosity. Adding a second order term, it is also described the fact that a SN fainter is redder than the fiducial one by the same amount as a bright SN is bluer with respect to the fiducial one.

First order :

$$\begin{aligned} m_V &= M_V + R_V \Delta + \mu_V \\ m_{B-V} &= M_{B-V} + R_{B-V} \Delta + E(B - V) \end{aligned}$$

$$\begin{aligned} \text{Second order :} \quad m_V &= M_V + R_V \Delta + Q_V \Delta^2 + \mu_V \\ m_{B-V} &= M_{B-V} + R_{B-V} \Delta + Q_V \Delta^2 + E(B-V). \end{aligned} \quad (5.15)$$

Where the parameters of the model to be determined are:  $\Delta = M_V(\text{SN}) - M_V(\text{SN}_{\text{fid}})$ , the distance modulus  $\mu_V$ , the colour excess  $E(B-V)$  and time at maximum  $t_0$ . As before one obtains them by an iterative minimization of  $\chi^2$ , considering an initial value for the correlation values between  $\Delta$  and the light curve shape (both the linear ones  $R$ , and the quadratic ones  $Q$ ), the absolute magnitude  $M_V$  and the colours  $M_{B-V}$ . Templates giving  $M_V$ ,  $R$  and  $Q$  to compare with are obtained from nearby SNe Ia.

Nowadays, an improvement of this method called MLCS2k2 is being used [115]. It generalizes the MCLS equations, improves the treatment of reddening and allows the use of the U band information. The new equations for each band  $X$  (where  $X$  stands for any of UBVRI) are:

$$m_X(t - t_0) = M_X^0 + \mu_0 + \zeta_X(\alpha_X + \beta_X/R_V)A_V^0 + P_X \Delta + Q_X \Delta^2. \quad (5.16)$$

The method uses information from spectra about the extinction ( $\zeta_X$ ,  $\alpha_X$  and  $\beta_X$ ), from the photometry ( $m_X(t)$ ), uses the templates ( $M_X^0$ ,  $P_X$  and  $Q_X$ ) and finally gives  $t_0$ ,  $R_V$ ,  $A_V^0$ ,  $\Delta$  and  $\mu_0$ . The correction to the magnitude is then included in the equations themselves.

#### 5.5.4 Bayesian Adapted Template Match (BATM)

This method [196] is based on the use of a set of nearby SNe Ia with well known light curves in various colours and for a wide range of luminosities. These light curves are moved to a determined redshift, with an arbitrary host extinction, and finally observed through the filters used in the real observations. In this way, instead of comparing the observed light curve with the template at the redshift of the template, is this one that is moved to the redshift of the SNe Ia. This avoids to calculate the K-corrections for an object which is still unknown or to use the extinction of the host galaxy which is also a controversial parameter.

### 5.5.5 Colour-Magnitude Intercept Calibration (CMAGIC)

If SNe Ia are standard candles, not only the magnitude at maximum should be characteristic, but also at any other time that can be identified by any reason. Wang et al. [201] showed that, during more or less the first month past maximum, the magnitude at a given value of the colour index has a very small dispersion, and, besides, during this period the relation between the magnitude in B and the  $(B - X)$  colour in an X band (X equals to V, R or I) is linear:

$$m_B = B_{BX} + \beta_{BX}(B - X), \quad (5.17)$$

with  $B_{BX}$  and the slope  $\beta_{BX}$  constants for each supernova.

The innovation of CMAGIC is then the working space being the colour-magnitude plane. The authors claim that that reduces the scatter with respect to the previous alternatives in a method that, besides, does not need to use any template.

## 5.6 Uncertainties and systematics

A lot of work is being devoted to calibrate SNe Ia as explained in the previous section. However, that calibration can be affected by different sources of systematics. At the time of precision cosmology, when a great amount of data is starting to be collected, the control of uncertainties and systematics is vital to obtain not only accurate but also precise results.

Next, a summary of the usually considered systematics is listed, with the inclusion of the treatment of the redshift uncertainty, which is usually underestimated or just ignored. We show its importance at low redshift and in future photometric surveys.

### 5.6.1 Time dilation and K-correction

In this section, we consider the two main corrections that have to be applied to the raw data in order to transform all SNe Ia into rest frame and be able to compare

them.

*Time dilation* is a contribution due to the fact that cosmological redshifts are produced because of the expansion of the Universe. Then, observed light curves are dilated by a factor  $(1+z)$  as predicted by General Relativity. The effect acts in the same way as the stretch factor does.

The *K-correction* is a more elaborated contribution. It accounts for the differences between the wavelengths at which the supernova emits and the ones we receive because of the expansion of the Universe. The correction is needed when one wants to convert the observed data into rest frame, since there is a difference between the shape of the filter of the received band and of the emitting band. This is a nonlinear correction to each point in the light curve, and it is obtained iteratively when fitting the light curve, since its value depends on the epoch and the stretch. A concrete method for determining K-corrections is explained in [134].

In general, each point of the light curve is translated into the blue rest frame by applying:

$$m_B(t) = m_X \left( \frac{t'}{s(1+z)} \right) + K_{BX} \left( \frac{t'}{1+z} \right), \quad (5.18)$$

where  $X$  is the observed band,  $t$  is the rest frame time scale,  $t'$  is observed time scale and  $z$  the redshift of the supernova.

## 5.6.2 Galaxy and host extinction

The reddening in the Galaxy is an additive contribution to the magnitude, and, contrary to the one in the host galaxy, is considered to be known. The colour excess due to Galactic extinction can be obtained from the dust map of the Galaxy given by Schlegel, Finkbeiner & Davis in [170]. Using the interstellar extinction law with  $R_B = 4.14$ ,  $R_V = 3.1$ ,  $R_R = 2.33$  or  $R_I = 1.48$ , one can calculate the absorption made by the Galaxy in the direction of the supernova ( $A_X$ ).

The extinction in the host galaxy or even in the intergalactic medium is a more delicate matter. The absorption of the intergalactic medium is not considered as the highest redshift SNeIa do not show specially high colour excesses. The distribution

of reddenings is more or less the same at low and high redshift, so dispersion in reddening should be attributed to differences in the host galaxies or the position of the supernovae within them and not to the intergalactic medium.

The way of treating the host galaxy extinction is not standard, and each collaboration does it in a different manner. For most supernovae the colour excess estimate is compatible with no extinction, so all the analyses make the first calculations without any host galaxy extinction correction. That is justified for SNe Ia lying in early-type galaxies, where the amount of gas and dust is much smaller than in late-type galaxies. Confirming that, Sullivan et al. [187] showed with a set of 39 distant SNe Ia that those hosted in late-type galaxies were  $0.14 \pm 0.09 mag$  fainter than those in early-types.

However, at least spiral and irregular galaxies when used for cosmological purposes should be corrected, but still, the determination of the colour excess  $E(B - V)$  at high redshift is not easy. Future large surveys will allow us to use just clearly unreddened SNe Ia, but for the moment low extinction subsamples include data with values as large as  $E(B - V) = 0.1$ , which can dim the supernova by more than  $0.4 mag$ .

A range of possibilities appears when trying to correct from host galaxy extinction. Some authors correct only for  $E(B - V) > 0$ , which is in fact natural taking into account that physically dust cannot make a supernova bluer. Others impose a prior on the extinction and fit its value together with the light curve parameters. Even other methods fit it without imposing any prior. As already noted in [119], for instance, different ways of correcting for host galaxy extinction can lead to biases in the results and differences in the determination of the cosmological parameters. Therefore, a better understanding of this source of uncertainty is necessary.

As for Galactic extinction, the absorption due to the host galaxy affects the magnitude in an additive way, the same for all the points of the light curve:

$$m_B = m_B^{ne} - A_{Gal.} - R_B E(B - V)_{Host}, \quad (5.19)$$

where  $m_B^{ne}$  is the magnitude in B without considering the effect of extinction,  $A_{Gal.}$  is the absorption made by the Galaxy and  $A_B = R_B E(B - V)_{Host}$  is the absorption of the host galaxy.

### 5.6.3 Gravitational lensing

The magnification and demagnification of SNe Ia due to gravitational lensing is assumed to be compensated for large sets of supernovae. So, its effect is not supposed to alter the conclusions although there are some individual SNe Ia clearly lensed such as SN1997ff [116].

In fact, the effect is only significant at high redshift. The dispersion due to lensing at  $z = 1.5$  is estimated to be a 7% [94]. However, the same authors show a method to reduce it up to a 3%. On the other hand, the uncertainty has nowadays a very small repercussion on the cosmological parameters mainly because of two reasons. First, because most of the data are not at high redshift, and second because current sets seem to be unbiased and have a magnification distribution compatible with a mean equal to unity. Therefore, usually there is no correction due to gravitational lensing.

### 5.6.4 Sample contamination and selection effects

Obtaining good quality spectra is crucial for avoiding any *sample contamination*, since as it has been said, the identification of the silicon, calcium and the lack of hydrogen lines in the spectra is the main tool to classify supernovae as Type Ias. Usually, at low redshift, spectra have enough quality. On the other hand, at high redshift SNe Ia are the brightest observed supernovae, and therefore, the contamination of other objects must be negligible. Problems about sample contamination could arise in photometric surveys, where spectra will not be available even at low redshift. This should be prevented by combining this kind of surveys with parallel observations to obtain spectra.

The Malmquist bias is one of the major *selection effects* in astronomy (for flux-limited surveys the detection of brighter objects is favoured). In the case of SNe Ia, the cosmological parameters are only modified if the Malmquist bias acts in a different way at low and high redshift. Of course, that has to be checked for every survey specification, but with current sets and surveys it has been estimated not to exceed 0.03 *mag*.

### 5.6.5 Redshift uncertainty

Among all the effects that condition the measurement of the magnitude of a supernova, that caused by the uncertainty in redshift is usually the less taken into account. Nowadays, most of the ongoing supernova surveys obtain redshifts from the spectrum either of the supernova or of the host galaxy. This is a very precise measure of the redshift and therefore, for cosmological purposes, usually redshifts are assumed to have no error. However, in Ref. [107] it was already noticed that, at low redshift, even small uncertainties are important for the determination of the cosmological parameters.

In a first approximation at low redshift, the magnitude-redshift relation can be written as  $m = \mathcal{M} + 5 \log_{10}(cz)$ . Therefore, an uncertainty  $\delta z$  translates into magnitude as  $\delta m = 5 \log_{10}(e) \delta z / z$ . At low redshift, peculiar velocities ( $v \approx 300 \text{ Km/s} \Rightarrow \delta z \approx 0.0001$ ) are more important than the uncertainty in spectroscopic redshifts. That introduces an uncertainty of  $\delta m \approx 0.005$  usually added in quadrature to the magnitude uncertainty in the  $\chi^2$  tests.

But that analysis is not enough. Some of the incoming surveys which are supposed to observe a large number of SNeIa will not be able to obtain spectra for all of them. In these cases, redshifts are going to be estimated from photometry (photo- $z$ 's), and therefore redshift uncertainties will be large enough to be taken into account. Simulations done in Ref. [194] show a scatter of  $\sigma_z < 0.1$  in photo- $z$ 's with respect to the spectroscopic ones for field galaxies. Averaging neural network and template fitting determinations they obtain a dispersion of  $\sigma_z = 0.073$ , which at  $z = 0.5$  could cause an error in the magnitude of  $0.3 \text{ mag}$  for a concordance cosmology. It is in these cases that a complete analysis is necessary.

The effect that the uncertainty in the redshift has on the magnitude depends both on the underlying cosmology and the calibration of the supernova. In [107] the different contributions were treated separately. However, the most important contribution comes from the propagation of errors in Equation 5.2, above all at redshifts lower than 1. That is given by:

$$\delta m = \frac{\partial m}{\partial z} \delta z, \quad (5.20)$$

and from the theoretical magnitude-redshift relation (Eq. 5.2), the derivative can be

written as

$$\frac{\partial m}{\partial z} = 5 \log e \left[ \frac{1}{1+z} + \frac{H_0}{H(z)} \sqrt{|\Omega_K^0|} \operatorname{tann}^{-1} \left( \sqrt{|\Omega_K^0|} \int_0^z \frac{H_0}{H(z')} dz' \right) \right], \quad (5.21)$$

where in a similar way as defined in Section 2.3.1:

$$\operatorname{tann} x \equiv \begin{cases} \tan x & \text{for } \Omega_K^0 < 0 \\ x & \text{for } \Omega_K^0 = 0 \\ \tanh x & \text{for } \Omega_K^0 > 0 \end{cases}. \quad (5.22)$$

This uncertainty is slightly dependent on the underlying cosmology but, of course, the dominant source is the error in the redshift measure,  $\delta z$  (see Figure 5.7). For a relatively low error,  $\delta z = 0.01$ , it can be seen that supernovae at  $z < 0.1$  are very much affected, but the effect is less than 0.05 magnitudes at  $z > 0.5$ , much less than the intrinsic dispersion of SNe Ia. However, as  $\delta z$  increases, also increase both the redshift under which the propagated error is crucial and the asymptotic  $\delta m$  at high redshift. At the error level of the expected photo- $z$ 's,  $\delta z = 0.08$ , supernovae at  $z < 0.5$  have uncertainties larger than 0.4 magnitudes, and even at high redshift the uncertainty is comparable to the intrinsic dispersion. This could be an important point limiting the use of photometric surveys for the determination of the cosmological parameters. Especially, if we consider that the distribution of photo- $z$ 's is not just Gaussian but has wider tails with catastrophic photo- $z$ 's errors such as  $\delta z/(1+z) > 0.15$ .

The effect of this source of error on the cosmological parameters and on the equation of state of dark energy, together with the importance of catastrophic photo- $z$ 's and the inclusion of some spectroscopic redshifts in the survey are widely treated in Chapter 8.

## 5.7 Data samples

During the elaboration of this thesis the set of SNe Ia data used to estimate the cosmological parameters has been growing noticeably. However, the size of this set grows more slowly than new observations do, mainly because different reduction techniques and template fitting methods prevent a direct combination of the results.

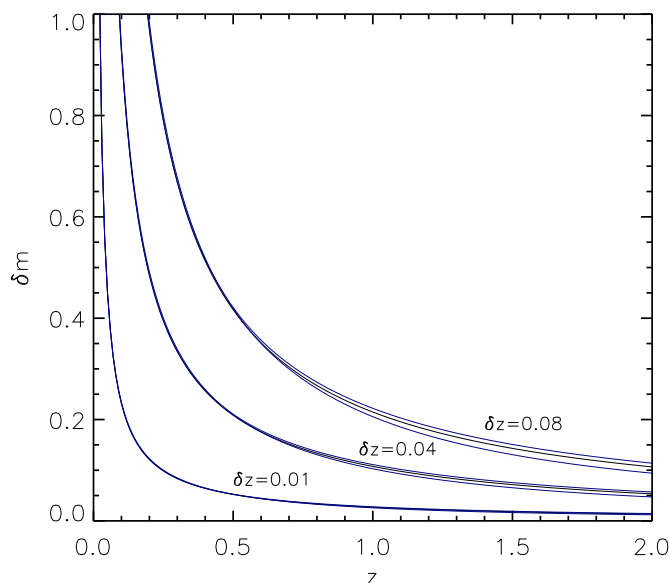


Figure 5.7: Uncertainty in the magnitude,  $\delta m$ , due to the error in the redshift measure,  $\delta z$ , as a function of redshift. For each  $\delta z$  three different cosmological constant cosmologies have been plotted:  $(\Omega_M^0, \Omega_\Lambda^0) = (0.2, 0.6)$ ,  $(0.3, 0.7)$  and  $(0.4, 1.0)$ . This source of uncertainty is very important at low- $z$ , and also at increasing redshifts for increasing  $\delta z$ 's.

Chronologically, the first significant set was that of Perlmutter et al. (1999) for the Supernova Cosmology Project (P99, [145]). For their main fit they used a set that included 16 low-redshift supernovae from the Calán/Tololo survey and 38 high-redshift supernovae, all of them calibrated via the stretch factor method. By the same time, also the High-Z Supernova Search Team published a high-redshift set calibrated via the Multi-Colour Light Curve Shape (MLCS) method (Riess et al. (1998), R98, [158]). The low-redshift sample was the same in both cases, but high-redshift samples involved different instruments and methodologies. At the end of the past century, that led to two independent evidences of the necessity of an energy component that accelerates the expansion of the Universe.

From that time, both teams have been enlarging those samples and improving their respective methods; new collaborations have been created to increase the number of observed SNe Ia as well. The larger sets or new data for the old ones can be found in:

- The compilation of 230 SNe Ia of Tonry et al. (2003) [196] (T03) (with subsets

of 172 and 130 data used for the cosmological fits);

- Knop et al. (2003) [119] (K03) with new calibrations for the SNe Ia of P99 plus eleven high redshift SNe observed with the Hubble Space Telescope (65 SNe Ia with a subset of 54 used in the main fit);
- The analysis of 22 new high redshift SNe Ia for a total of 222 objects in Barris et al. (2004) [21] (B04);
- State of the art at the beginning of 2004 in Riess et al. (2004) [161] (R04). A gold set with 156 SNe Ia is defined from different sources;
- Nine high redshift SNe Ia from the ESSENCE (Equation of State: SuperNOvae trace Cosmic Expansion) project in Krisciunas et al. (2005) [121] (K05);
- Five new SNe Ia at  $z \approx 0.5$  in Clocchiatti et al. (2005) [47] (C05); and
- The 73 SNe Ia from the SNLS (SuperNova Legacy Survey) in Astier et al. (2005) [14] (A05).

At the time of writing the thesis, the largest set of SNe Ia is the gold set from Riess et al. (2006) [160] (R06). It is a new state of the art with 182 SNe Ia, which, as in previous compilations, come from various recalibrated and restricted samples plus 17 new SNe observed with the Hubble Space Telescope. The set covers from redshift 0.023 (high enough to avoid the possible existence of the Hubble Bubble) to the highest redshift supernova at  $z = 1.77$ , with a mean of  $\langle z \rangle = 0.54 \pm 0.35$ . However, it has been recently claimed in Ref. [131] that this set is not statistically homogeneous and that a careful analysis of systematics should be done. It is a set joining two decades of data and the differences in the treatment of systematics through time may show up.

Also the ESSENCE collaboration has built up a set with their data and the SNLS supernovae published in Wood-Vasey et al. (2007) [211] (VW07). The full set has 162 SNe Ia in the redshift range  $0.015 < z < 0.96$ , being in this case the mean redshift lower than for Riess' data:  $\langle z \rangle = 0.38 \pm 0.27$ . Figure 5.8 shows the Hubble diagram together with the redshift histogram for the two sets, where one can observe the difference between both distributions. As it will be seen in next chapters, the two samples do not lead to compatible results within  $1\sigma$  intervals. Therefore, some work in the direction of building a complete homogeneous new sample from these two is being done [56].

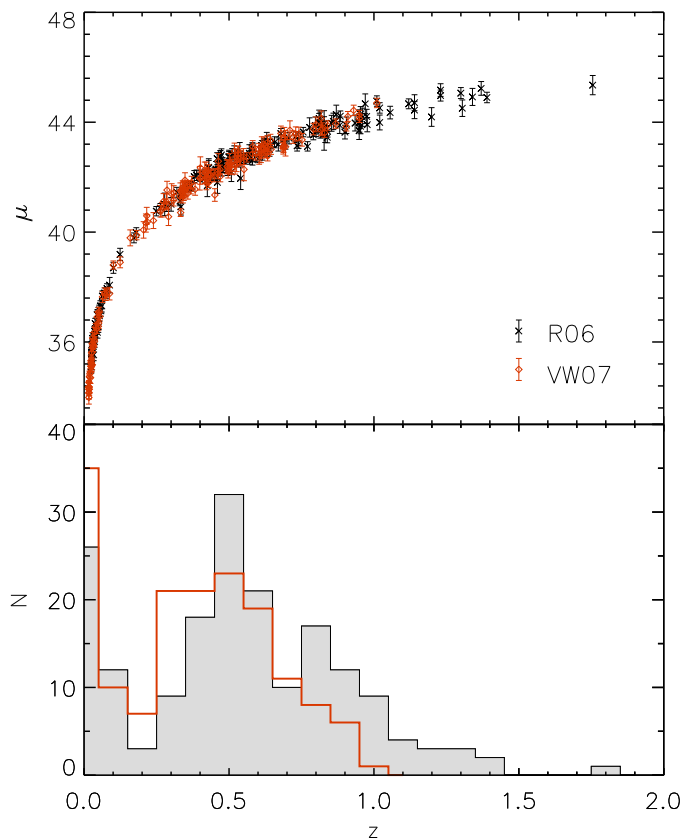


Figure 5.8: Hubble diagram and redshift histogram for the compilation of 182 SNe Ia from Riess et al. (2006) [160] (black crosses, R06) and the 162 SNe Ia from Wood-Vasey et al. (2007) [211] (red diamonds, VW07).

### 5.7.1 Bootstrap resampling

Before ending this section we present a statistical method used to generate new sets of data from the original ones just introduced.

The bootstrap method is a Monte Carlo-based method. Its distinctive feature is that it is aimed to extract statistical information from a data set by generating different realizations of the original data set, instead of by considering the model behind the data to be parameterized by random variables.

The generation of each of these distributions of  $n$  elements is quite easy: one just has to generate  $n$  random variables distributed as integers, with a flat distribution from 1 to  $n$ . These random integers are the ones which select the members of the

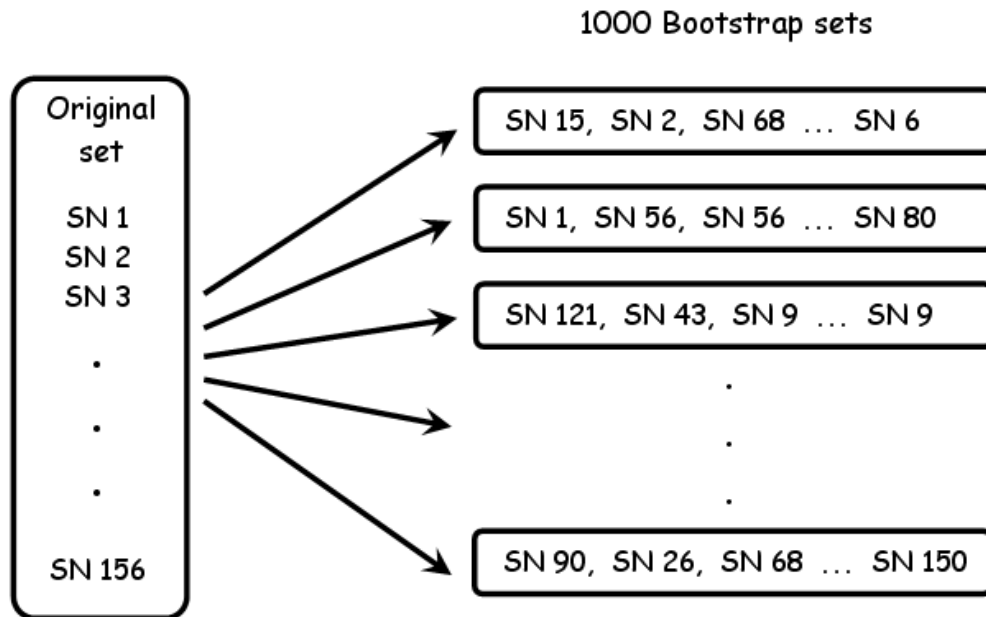


Figure 5.9: Outline of the generation of 1000 data sets via bootstrap resampling from the original set, in this case that of Riess et al. (2004) [161].

data set to be considered. In this way, we are sampling with replacement, since some of the values are taken more than once. The Fortran subroutine `bootspbec.f` has been used for that purpose.

Bootstrap resampling is used later in the analysis to estimate  $1\sigma$  uncertainties in the equation of state.



## Chapter 6

---

# Looking for the underlying cosmology

---

This chapter is dedicated to obtain the most probable values of the cosmological parameters and of those parameterizing the dark energy density. SNeIa are used together with priors coming from different cosmological experiments, to determine the discrete parameters described in the theoretical part of the thesis, paying special attention to running cosmological constant models and to common developments of the equation of state.

### 6.1 Parameter estimate: the maximum likelihood method

The maximum likelihood technique developed by R.A. Fisher in the 1920s is one of the most used methods to estimate parameters given a data set.

The method considers that observations  $X_i$  are random variables coming from an unknown population which can be described via a probability density function ( $\phi(\mathbf{X}, \theta)$ , *pdf*). This *pdf* depends on the variables  $X_i$  and the parameters  $\theta_i$ , and gives the probability of the data given the parameters. But, in order to estimate the best set of parameters from the data, it must be interpreted in the opposite way. Within this interpretation, the function is called *likelihood function*, because it says how likely is a set of parameters given the data:

$$L(\theta|\mathbf{X}) \equiv \phi(\mathbf{X}, \theta). \quad (6.1)$$

From this point of view, the likelihood function cannot be integrated to obtain probabilities of the parameters, because  $\theta_i$  are not random variables as  $X_i$  are. However, even though the likelihood function is not strictly a probability function, it still has some nice properties. If  $L(\theta_A|\mathbf{X}) > L(\theta_B|\mathbf{X})$ , then  $\theta_A$  is more plausible than  $\theta_B$  for the parameter  $\theta$ . The maximum likelihood method is based on that property, and it simply looks for the parameters  $\theta_i$  which make maximum  $L(\theta|\mathbf{X})$  for the observations  $\mathbf{X}$ .

The concept of likelihood is well understood within a Bayesian framework. According to the Bayes' theorem, the posterior probability is related to the prior probability through the conditional probability of the data given the parameters, and that is nothing but the likelihood:

$$P(\theta|\mathbf{X}) = \frac{P(\mathbf{X}|\theta)P(\theta)}{P(\mathbf{X})} \propto L(\theta|\mathbf{X})P(\theta). \quad (6.2)$$

This relation is important, since it allows to use the *a priori* information on the parameters and marginalize over those without direct interest.

### 6.1.1 $\chi^2$ as a maximum likelihood method

Differences in maximum likelihood methods arise from the choice of the probability functions used. The  $\chi^2$  function, defined as the square of the ratio between the *true* error and the measured one, showed to be an adequate choice:

$$\chi^2 = \sum_i \left( \frac{y_i - y(x_i, \theta)}{\sigma_i} \right)^2. \quad (6.3)$$

Let us suppose that a theoretical model relates observations to some unknown parameters  $y(x_i) = y(x_i; \theta)$ . One can model the data  $y_i$  with a Gaussian *pdf* if errors on data are independent and normally distributed around the true model  $y(x_i, \theta)$ . Moreover, if data are independent, the joint *pdf* is given by the product of the individual probability of each datum:

$$\phi(\mathbf{Y}, \theta) \propto \prod_i \exp \left( -\frac{1}{2} \left[ \frac{y_i - y(x_i, \theta)}{\sigma_i} \right]^2 \right). \quad (6.4)$$

The set of parameters maximizing this function maximizes its logarithm as well, and therefore one can write:

$$\ln \phi(\mathbf{Y}, \theta) \propto \sum_i \left( -\frac{1}{2} \left[ \frac{y_i - y(x_i, \theta)}{\sigma_i} \right]^2 \right) = -\frac{1}{2} \chi^2. \quad (6.5)$$

If errors have a constant standard deviation ( $\sigma_i = \sigma$ ), one obtains the least squares estimator; for different standard deviations one obtains the  $\chi^2$  estimator. Maximizing the likelihood is then equivalent to minimize the  $\chi^2$ .

As for this thesis, observations are mainly pairs of magnitude and redshift values and parameters are both the cosmological parameters and the ones related to the dark energy equation of state. The magnitude-redshift relation links the observations with the unknown parameters (Section 5.1.1).

### 6.1.2 Goodness-of-fit

The goodness-of-fit in a  $\chi^2$  fit can be qualitatively estimated by comparing the  $\chi^2$  value to the number of degrees of freedom. It is expected that for large data sets, these two terms become equal. However, strictly speaking, the lower  $\chi^2$  is, the better the fit, because the difference between the theoretical and observed data is smaller.

On the other hand, one can give the  $p$ -value as a quantitative measure for the goodness of the fit. The  $p$ -value is the probability that one obtains a larger  $\chi^2$  by chance for that number of degrees of freedom. Usually, one only discards models for low values of  $p$ , let us say  $p < 0.05$  for instance. In our case, this lower limit is not going to be a problem, since all tested models have much higher probabilities. And that is the true problem: most of the tested theoretical models are equally good at modeling the data.

P(%)		dofs			
		1	2	3	4
68.27	$1\sigma$	1.00	2.30	3.53	4.72
90.00	-	2.71	4.61	6.25	7.78
95.44	$2\sigma$	4.00	6.17	8.02	9.70
99.00	-	6.63	9.21	11.3	13.3
99.73	$3\sigma$	9.00	11.8	14.2	16.3
99.99	-	15.1	18.4	21.1	23.5

Table 6.1:  $\Delta\chi^2$  as a function of the number of degrees of freedom (dofs) and the desired level of probability when errors are normally distributed.

### 6.1.3 Confidence regions

For Gaussian errors, the minimum  $\chi^2_{min}$  determines the best parameters. Besides, contours of constant  $\chi^2$  represent contours of constant probability and  $\Delta\chi^2 = \chi^2_{level} - \chi^2_{min}$  regions can be interpreted as confidence regions.

In fact, that is true even for non-Gaussian errors, but then the relation between the value of  $\Delta\chi^2$  and the confidence level should be determined, via Monte Carlo simulations for instance. On the other hand, normal errors allow a straightforward integration of the probability:

$$P[\theta_1 \leq \theta \leq \theta_2] = 1 - \alpha, \quad (6.6)$$

where  $1 - \alpha$  is the desired percentage of probability for the value of the parameter  $\theta$  to lie in the interval  $[\theta_1, \theta_2]$ . For a single parameter,  $\Delta\chi^2 = 1$  gives  $1\sigma$  intervals, i.e., there is a 68.27% of probability that the true parameter lies within this range. The corresponding values of  $\Delta\chi^2$  for more degrees of freedom and higher probability levels can be found in Table 6.1.

In our results, only confidence intervals for one parameter or degree of freedom and confidence regions for two parameters are given. Analysis in a higher dimensional parameter space are unavoidable in cosmology, but we either analytically marginalize over the nuisance parameters (see Section 6.1.4) or project the higher dimensional confidence region onto a two-dimensional space of interest (numerical

marginalization). In order to do the projection, one can minimize the  $\chi^2$  with respect to the *extra* parameters and use the ordinary  $\Delta\chi^2$  for two degrees of freedom with the results. In the case of three parameters that just means:

$$\chi^2(\theta_1, \theta_2) = \min_{\theta_3} \{ \chi^2(\theta_1, \theta_2, \theta_3) \} . \quad (6.7)$$

### 6.1.3.1 Monte Carlo errors

It has been seen that the  $\chi^2$  methodology allows for a direct estimate of confidence intervals when the observational errors are normally distributed. However, that is not always true and in those cases different approaches must be considered.

The bootstrap resampling technique introduced in the last chapter gives rise to a very powerful way (but also very time-consuming) of determining confidence levels. Once  $n$  data sets have been generated, one can find the best parameters for every set. This samples the parameter space, and for a large enough number of results one obtains the probability distribution in that space. Confidence intervals are then calculated just by counting the percentage of results within the interval.

## 6.1.4 Priors and marginalization

*A priori* information on the unknown parameters can be easily incorporated into the information given by the data through the Bayes' theorem (Eq. 6.2).

Since the likelihood and the  $\chi^2$  are related via  $L = \exp(-1/2 \chi^2)$ , the addition of a Gaussian prior on a parameter  $L(\theta|\mathbf{X})P(\theta)$  simply adds a term to the  $\chi_0^2$  without the prior:

$$\chi^2 = \chi_0^2 + \frac{(\theta - \theta_{prior})^2}{\sigma_{prior}^2}, \quad (6.8)$$

where the *a priori* information is  $\theta_{prior} \pm \sigma_{prior}$ .

Again according to the Bayes' theorem, the product of the likelihood and the prior is a well defined probability and, therefore, one can integrate it over a param-

eter  $\theta$  (marginalize) in order to obtain the probability of the other ones regardless of  $\theta$ .

That is especially useful for nuisance parameters which are not relevant to the problem. In the case of cosmology with supernova magnitudes, the zero point  $\mathcal{M}$  and the width-brightness parameter  $\alpha$  as defined in Equations 5.2 and 5.12 are of this kind. In Refs. [89, 58], the marginalization over  $\mathcal{M}$  and  $\alpha$  was done analytically assuming flat priors, and the resulting  $\chi^2$  was found to be:

$$\begin{aligned}
\chi_{\alpha\text{-int}}^2(\Omega_M, \Omega_\Lambda, w) &= -2 \ln \left[ \int_{-\infty}^{\infty} d\alpha \exp \left( -\frac{1}{2} \chi_{\mathcal{M}\text{-int}}^2(\Omega_M, \Omega_\Lambda, w, \alpha) \right) \right] \\
&= A - \frac{B^2}{C} - \frac{(F - \frac{BE}{C})^2}{D - \frac{E^2}{C}}, \tag{6.9} \\
A &= \sum_{i=1}^n \frac{(5 \log_{10} [d_L(\Omega_M, \Omega_\Lambda, w, z_i)] - m_i)^2}{\sigma_i^2}, \\
B &= \sum_{i=1}^n \frac{5 \log_{10} [d_L(\Omega_M, \Omega_\Lambda, w, z_i)] - m_i}{\sigma_i^2}, \\
C &= \sum_{i=1}^n \frac{1}{\sigma_i^2}, \\
D &= \sum_{i=1}^n \frac{(1 - s_i)^2}{\sigma_i^2}, \\
E &= \sum_{i=1}^n \frac{(1 - s_i)}{\sigma_i^2}, \\
F &= \sum_{i=1}^n \frac{(5 \log_{10} [d_L(\Omega_M, \Omega_\Lambda, w, z_i)] - m_i)(1 - s_i)}{\sigma_i^2},
\end{aligned}$$

where the parameter  $w$  represents whatever parameter describing dark energy and  $\chi_{\mathcal{M}\text{-int}}^2(\Omega_M, \Omega_\Lambda, w, \alpha)$  is defined by:

$$\chi_{\mathcal{M}\text{-int}}^2(\Omega_M, \Omega_\Lambda, w, \alpha) = -2 \ln \left[ \int_{-\infty}^{\infty} d\mathcal{M} \exp \left( -\frac{1}{2} \chi^2(\Omega_M, \Omega_\Lambda, w, \mathcal{M}, \alpha) \right) \right]. \tag{6.10}$$

The zero point in the case one uses distance modulus is encoded in the Hubble constant. Usually, the standardization correction is already included in the distance

modulus as calculated via the MCLS2k method [115]: therefore, only  $H_0$  must be marginalized.

### 6.1.5 Implementation and numerical issues

The most probable parameters are found as those giving the maximum likelihood or equivalently the minimum  $\chi^2$ . Thanks to the limited number of parameters to study, there has been no need to use a minimization algorithm that introduces the danger of getting stuck in a false minimum. The  $\chi^2$  is calculated in a grid of points covering the whole space of possible values for the unknown parameters with a Fortran program. The only numerical issue to worry about is the integration of the luminosity distance, which is calculated with a ten points Gaussian-Legendre integration as implemented in the QGAUS() subroutine in [151].

The first order system of ordinary differential equations that conform the set of cosmological equations in Scenario 1 is solved numerically. For that purpose it has been used the package RKSUITE [34] based on Runge-Kutta methods.

## 6.2 Cosmological constant

Now, we use this methodology to estimate various parameters. The cosmological constant is the simpler source of dark energy and it only introduces one extra parameter,  $\Omega_\Lambda^0$ , with respect to a matter dominated universe. Other theoretical models such as the DGP ones (Section 4.2.4.1) share this characteristic, but in that case it cannot be considered as a source of dark energy but as a modification of General Relativity. The cosmological constant deserves, then, a special attention and should not be discarded in front of more complex models unless it is clearly ruled out by observations or a better theoretical model is found.

In summary, a universe with a cosmological constant evolves according to three cosmological parameters:  $\Omega_M^0$ ,  $\Omega_\Lambda^0$  and  $\Omega_K^0$ . The equation of state is fixed to  $w(z) = -1$ . The use of SNeIa magnitudes introduces two nuisance parameters in the analysis,  $\mathcal{M}$  and  $\alpha$ ; for data sets with distance moduli instead of magnitudes, the zero point is given by  $H_0$ . In the following, these are marginalized when necessary, as explained in the previous section. The full dynamics of the Universe is

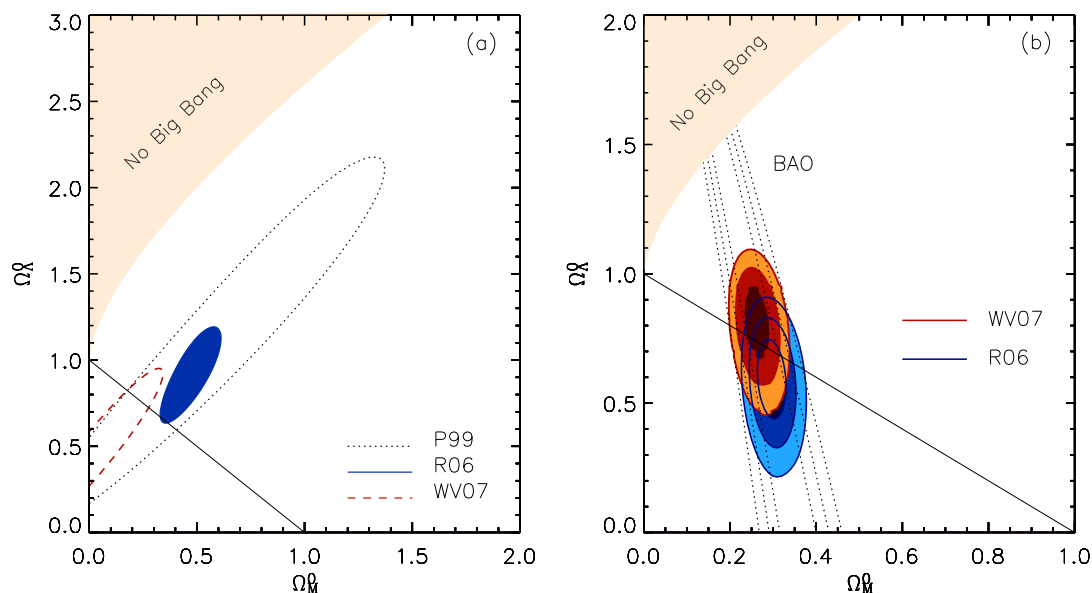


Figure 6.1: Confidence regions for the cosmological parameters obtained for a cosmological constant model from two SNe Ia data sets: R06 [160] and VW07 [211]. (a)  $1\sigma$  regions comparing present-day results with those at the end of the 90s (Perlmutter et al. (1999) [145]). (b)  $1\sigma$ ,  $2\sigma$  and  $3\sigma$  regions when joining BAO constraints (dotted black lines in the plot). Note the scale difference between plots.

in this case described by the three cosmological parameters which are linked by the cosmological sum rule. If the geometry of the Universe appeared to be flat, only one independent parameter would be enough to reveal its past and future evolution, a delight for physics and mathematics!

With almost 200 SNe Ia, the precision on the cosmological parameters is enough to rule out with high confidence most of the allowed space. However, the accuracy provided by different data sets makes their results incompatible at the  $1\sigma$  level. Figure 6.1 shows the confidence regions for  $\Omega_M^0$  and  $\Omega_\Lambda^0$  after marginalizing over  $H_0$ . In the left panel it is plotted the  $1\sigma$  contour for two current sets: R06 made of 182 SNe Ia [160] and VW07 built up from 162 SNe Ia [211]. Results with one of the first supernova data sets used for cosmology (54 SNe Ia in P99 [145]) are included as well for comparison. The uncertainties in the parameters have diminished a factor of four since then, but due to the differences between sets, SNe Ia by themselves cannot elucidate the curvature of the Universe. Besides, whereas one of the sets favours a low density universe, the other one opts for a high density one. That has

set	$\Omega_M^0$	$\Omega_\Lambda^0$	$H_0^\dagger$	$\chi^2$	$p$
– SNe –					
R06	$0.48_{-0.10}^{+0.06}$	$0.94_{-0.19}^{+0.17}$	63.5	156.4	0.89
sR06	$0.66_{-0.19}^{+0.17}$	$1.18_{-0.31}^{+0.27}$	63.8	129.5	0.93
VW07	$0.03_{\ddagger}^{+0.21}$	$0.48_{-0.15}^{+0.32}$	65.3	125.7	0.98
flat curvature					
R06	$0.35_{-0.04}^{+0.04}$	$0.65_{-0.04}^{+0.04}$	$62.6_{-0.8}^{+0.9}$	158.6	0.87
VW07	$0.22_{-0.04}^{+0.05}$	$0.78_{-0.05}^{+0.04}$	$65.9_{-0.9}^{+1.0}$	126.6	0.98
– SNe + BAO –					
R06	$0.30_{-0.03}^{+0.02}$	$0.60_{-0.11}^{+0.11}$	62.7	159.9	-
VW07	$0.26_{-0.02}^{+0.02}$	$0.81_{-0.09}^{+0.09}$	65.8	126.9	-

†  $[H_0] = Km/s/Mpc$ .

‡ Outside the physically allowed region.

Table 6.2: Cosmological parameters obtained for a cosmological constant model from two supernova data sets: R06 [160] and VW07 [211], with and without BAO constraints. sR06 is a subsample of R06 only made of SNeIa with  $z < 0.95$ .  $1\sigma$  errors are found after marginalizing over  $H_0$ , except in the flat case.

consequences not only on the required dark energy content, but also on the amount of dark matter needed to account for the full  $\Omega_M^0$ .

We homogenize this discrepancy in the matter density by including BAO constraints.  $1\sigma$ ,  $2\sigma$  and  $3\sigma$  confidence regions can be seen in Figure 6.1 (b), and Table 6.2 contains the best fit and  $1\sigma$  errors for individual parameters. Still, both sets are not fully consistent with each other but they agree in the  $1\sigma$  limit around the concordance model:  $\Omega_M^0 = 0.28$ ,  $\Omega_\Lambda^0 = 0.72$ .

SNeIa are not very sensitive to the curvature of the Universe, but other cosmological methods such as CMB measurements are. WMAP3 data [183] with a Hubble constant of  $72 \pm 8 Km/s/Mpc$  [79] quantify the curvature of the Universe to be  $\Omega_K^0 = -0.014 \pm 0.017$ . In practice, this is small enough to assume a flat universe when considering a larger number of parameters related to dark energy. In case one considers a flat universe with a true cosmological constant, the best fit is  $\Omega_M^0 = 0.35 \pm 0.04$  for R06 data and  $\Omega_M^0 = 0.22 \pm 0.05$  with VW07 set. According to  $\chi^2$  values (see Table 6.2) neither the curved fit nor the flat fit are preferred in front

of the other one.

Discordance among results obtained with the two sets is inherent to these data. We checked it by constructing a subsample of R06 only made of the 157 SNeIa with  $z < 0.95$  (sR06). In this way, the redshift distribution of the new set with mean  $\langle z \rangle = 0.44 \pm 0.27$  is not so different from that of VW07 ( $\langle z \rangle = 0.38 \pm 0.27$ ) as the original R06 sample ( $\langle z \rangle = 0.54 \pm 0.35$ )<sup>1</sup>. We fit the cosmological parameters with this subsample and obtain  $\Omega_M^0 = 0.7 \pm 0.2$  and  $\Omega_\Lambda^0 = 1.2 \pm 0.3$ . These results agree at  $1\sigma$  with those of the full sample. However, these are still at a distance of  $3\sigma$  from the best fit of VW07. Therefore, we expect the differences between sets not to be due to differences in redshift distributions, but due to differences in instruments, calibration or standardization methods. Waiting for the union of both sets with a single light-curve fitting methodology [56], in the following we continue giving both results.

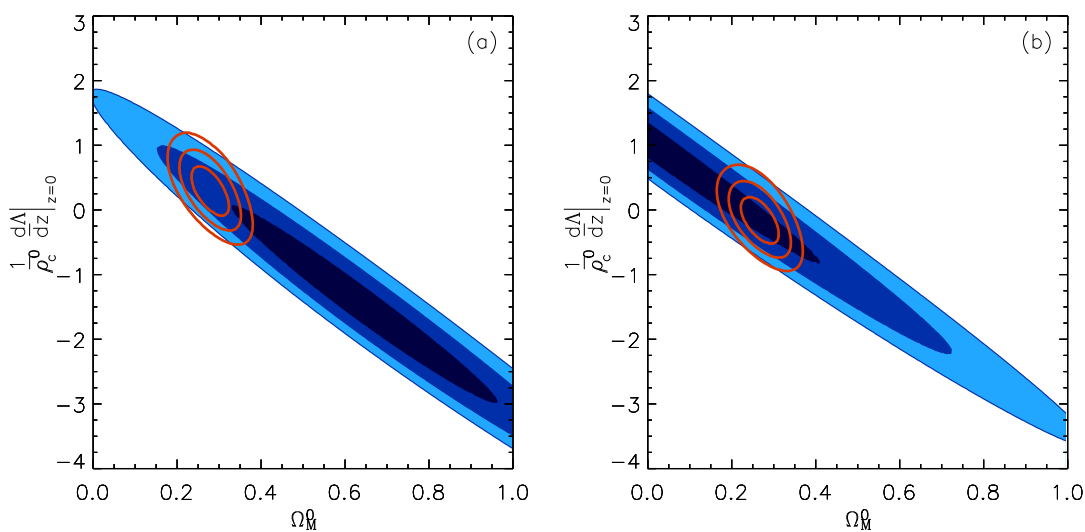


Figure 6.2: (a) Confidence regions showing  $1\sigma$ ,  $2\sigma$  and  $3\sigma$  contours in the  $(\Omega_M^0, (1/\rho_c^0)d\Lambda/dz|_{z=0})$  plane for a general evolving cosmological constant in a flat universe. Results correspond to the 182 SNeIa in R06 [160]. Solid red lines include a prior on the density of matter  $\Omega_M^0 = 0.27 \pm 0.03$  as well. (b) The same as (a) but for the 162 SNeIa in VW07 [211].

<sup>1</sup>Histograms for the redshift distributions were shown in previous chapter, Figure 5.8.

## 6.3 Running cosmological constant

The current impossibility to justify theoretically the existence of the measured cosmological constant has motivated many alternatives. Before digging into those predicting a running of the cosmological constant it is worth checking whether the running, or in general the evolution of a dark energy source, is compatible with observations.

Let us first rewrite the Hubble parameter by introducing a Taylor development to first order of an evolving cosmological constant:

$$H^2(z) = H_0^2 \left[ \Omega_M^0 (1+z)^3 + \Omega_\Lambda^0 + \frac{1}{\rho_c^0} \frac{d\Lambda}{dz} \Big|_{z=0} z + \Omega_K^0 (1+z)^2 \right]. \quad (6.11)$$

Next, we restrict ourselves to a flat universe and determine the confidence regions in the  $(\Omega_M^0, (1/\rho_c^0)d\Lambda/dz|_{z=0})$  space. We would expect the first derivative  $d\Lambda/dz$  to give us some general hints about the evolution of the dark energy component.

As seen in previous results, the fits for the two data sets are very different, but both of them are compatible with no evolution at  $1\sigma$  level. The correlation between the first derivative and the matter density is high, as observed from the inclination of the ellipses in Figure 6.2. A prior on  $\Omega_M^0$  improves then the determination of  $(1/\rho_c^0)d\Lambda/dz|_{z=0}$ . We use a prior of  $\Omega_M^0 = 0.27 \pm 0.03$ , which is equivalent to the use of BAO constraints. In this section we use directly the prior on  $\Omega_M^0$  instead of BAO, since its value was calculated for models of dark energy with a constant equation of state. Although the cosmological constant is a particular case of those models, that is not the case of running cosmological constant models. Including this prior on  $\Omega_M^0$ ,  $1\sigma$  uncertainties diminish by a factor 5, but no better conclusions can be obtained from current data. Results are still marginally compatible with a cosmological constant, but now a positive evolution is preferred from R06 data and a negative one from VW07.

Table 6.3 contains the best fit values for this general evolution and the three following different scenarios.

set	$\Omega_M^0$	$\theta$	$H_0^\dagger$	$\chi^2$	$p$
– General –					
R06	$0.6_{-0.2}^{+0.2}$	$d\Lambda = -1_{-1}^{+1}$	63.6	156.5	0.89
VW07	$0.0_{\ddagger}^{+0.3}$	$d\Lambda = +1.0_{-1.2}^{+0.2}$	65.4	125.7	0.98
prior $\Omega_M^0 = 0.27 \pm 0.03$					
R06	$0.28_{-0.03}^{+0.03}$	$d\Lambda = +0.2_{-0.2}^{+0.3}$	63.6	159.8	-
VW07	$0.27_{-0.03}^{+0.03}$	$d\Lambda = -0.2_{-0.2}^{+0.2}$	65.4	126.8	-
– Scenario 1 –					
R06	$0.20_{-0.08}^{+0.10}$	$\tau^\S = -16_{-12}^{+11}$	63.5	156.5	0.89
VW07	$0.37_{-0.17}^{+0.26}$	$\tau^\S = +18_{-21}^{+24}$	65.3	125.8	0.98
prior $\Omega_M^0 = 0.27 \pm 0.03$					
R06	$0.27_{-0.04}^{+0.02}$	$\tau^\S = -8_{-5}^{+4}$	63.5	157.1	-
VW07	$0.27_{-0.03}^{+0.03}$	$\tau^\S = +8_{-7}^{+7}$	65.3	126.1	-
– Scenario 2 –					
R06	$0.35_{-0.04}^{+0.04}$	$\eta = +11_{-55}^{+5}$	60.4	158.6	0.86
VW07	$0.22_{-0.04}^{+0.05}$	$\eta = -6_{-19}^{+36}$	67.2	126.6	0.97
fixed $H_0$					
R06	$0.35_{-0.04}^{+0.04}$	$\eta = -5_{-5}^{+5}$	63.5	158.6	0.87
VW07	$0.22_{-0.04}^{+0.05}$	$\eta = +3_{-5}^{+4}$	65.3	126.6	0.98
– Scenario 3 –					
R06	$0.22_{-0.07}^{+0.09}$	$\nu = -0.5_{-0.3}^{+0.3}$	63.5	156.5	0.89
VW07	$0.35_{-0.14}^{+0.15}$	$\nu = +0.6_{-0.7}^{+0.8}$	65.3	125.7	0.98
prior $\Omega_M^0 = 0.27 \pm 0.03$					
R06	$0.26_{-0.02}^{+0.03}$	$\nu = -0.3_{-0.1}^{+0.2}$	63.5	156.8	-
VW07	$0.27_{-0.03}^{+0.03}$	$\nu = +0.3_{-0.3}^{+0.3}$	65.3	126.0	-

†  $[H_0] = Km/s/Mpc$ .

§  $[\tau] = 10^{-9}eV^4$ .

‡ Outside the physically allowed region.

Table 6.3: Best fits for the different models with a running of the cosmological constant presented in this thesis. See text for the definition of each parameter. Data sets and  $1\sigma$  errors as in Table 6.2.

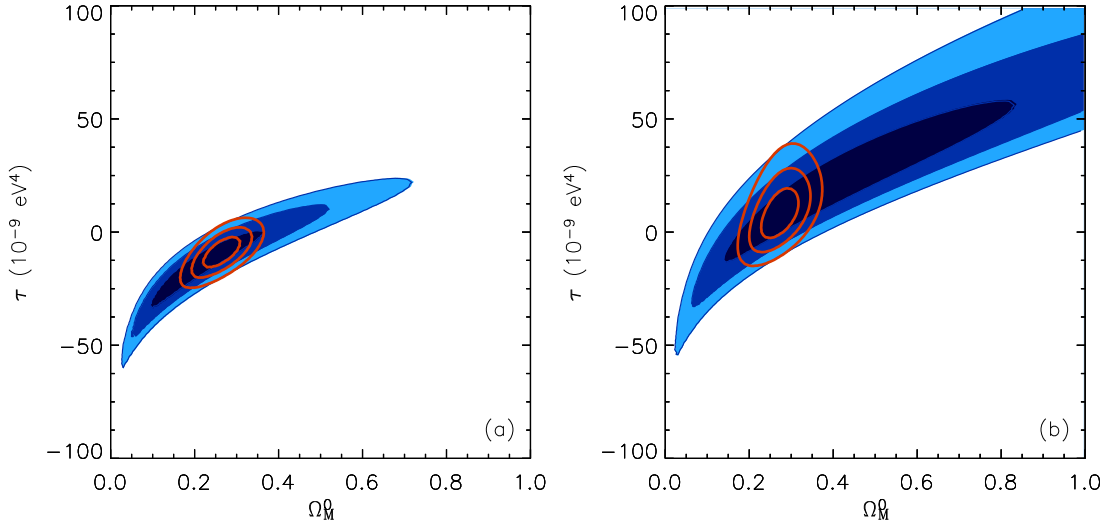


Figure 6.3: As Figure 6.2 but for a concrete evolution, that of Scenario 1 represented by  $\tau$  as defined in Equation 6.12.

### 6.3.1 Scenario 1

In this scenario, the lightest degrees of freedom are the only ones causing the running of the cosmological constant. As explained in Section 3.3, only considering the lightest neutrinos would force a larger cosmological constant in the future. In order not to be restricted to only this behaviour, an extra scalar field  $S$  was introduced. Let us define the parameter  $\tau$  as the combination of these fields appearing in Equation 3.16:

$$\tau \equiv \frac{1}{2}m_S^4 - 4 \sum_{\nu} m_{\nu}^4. \quad (6.12)$$

The sign of  $\tau$  corresponds to the sign of the  $\beta$ -function, and therefore, to the sign of the running of  $\Lambda$ .

Riess et al. (2006) data, which in general favour a larger amount of dark energy, support here a cosmological constant decreasing towards the past. With such a negative  $\beta$ -function, the existence of the  $S$  field is not mandatory. The best fit without this field constrains the mass of the lightest neutrinos to  $m_{\nu} = 0.007 \pm 0.006 \text{ eV}$  with SNeIa data alone and  $m_{\nu} = 0.006 \pm 0.005 \text{ eV}$  when also using prior information on the matter density. Of course, any lower value for the neutrino's

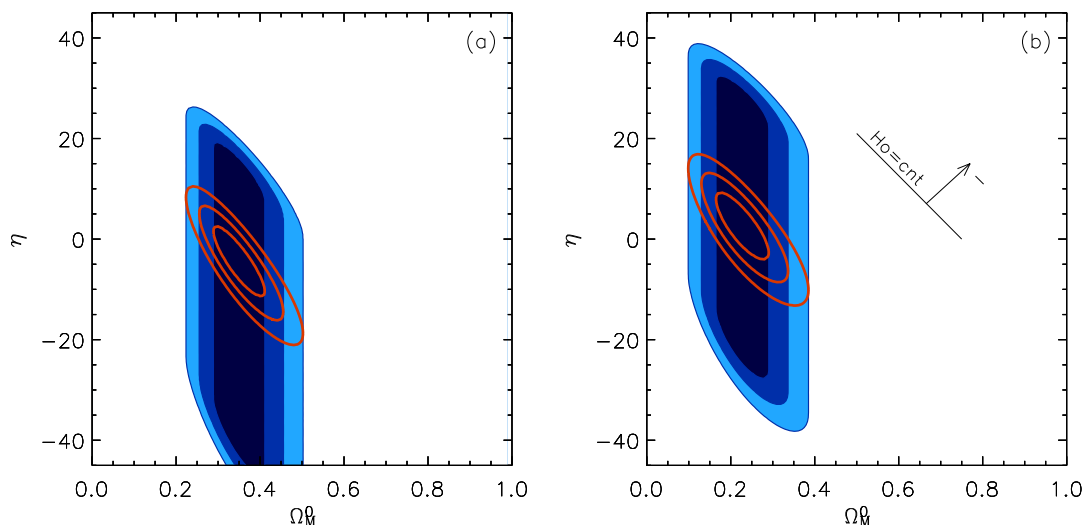


Figure 6.4: As Figure 6.3 but for the parameter  $\eta$  representing the running in Scenario 2. Results are highly degenerate with respect to the value of  $H_0$ ; panel (b) shows the direction of degeneracy. Solid red lines indicate here regions with  $H_0$  fixed to the best fit values in Table 6.2.

mass is allowed as long as one admits the existence of the sterile field.

On the other hand, the underlying running reflected by Wood-Vasey et al. SNe Ia is positive, meaning a larger cosmological constant in the past and a smaller one in the future. Being the  $\beta$ -function positive, only the combination of the masses of the lightest neutrinos and the sterile field can be determined. In this case, the effective mass represented by  $\tau$  is of order  $m_{eff} = 0.01 \pm 0.01$  eV. Therefore,  $m_S^4 = 2(8m_\nu^4 - m_{eff}^4)$ , that allowing a relatively large mass of the  $S$  field.

Figure 6.3 shows the confidence regions in the  $(\Omega_M^0, \tau)$  space. As before, the value of  $\tau$  highly depends on  $\Omega_M^0$ , and so, the prior knowledge on  $\Omega_M^0$  is important to break the degeneracy. That constrains the amount of evolution, but as seen with the quoted masses it translates weakly onto the mass determination due to the relation  $\tau \propto m^4$ .

### 6.3.2 Scenario 2

Within the same context as Scenario 1, Scenario 2 also characterizes a running of the cosmological constant, but now caused by the heaviest particles. For the Standard

Model of Particle Physics, the running is fully determined by:

$$\eta \equiv \frac{1}{2} \sum_i N_i - \frac{5}{4} \quad (= 10.75 \text{ for SM}). \quad (6.13)$$

But one can accept modifications to the Standard Model and consider  $\eta$  a free parameter.

Contrary to Scenario 1, this kind of evolution allows to determine the density of matter with a precision similar to that obtained with a prior in previous scenarios. Unfortunately,  $\eta$  is not determined with the same accuracy.

The value of  $\eta$  is highly degenerate with that of the Hubble constant. In fact, for VW07 data, the  $\chi^2$  for  $\eta = 10.75$  (SM value) with the best fit value for the density of matter is only affected in the third decimal place with respect to the true minimum for  $\eta = -6$ . The Hubble constant, however, is changed from  $67.2 \text{ Km/s/Mpc}$  to  $63.6 \text{ Km/s/Mpc}$ .

With these results there is no need to include any prior on the density of matter, but prior information on the Hubble constant is necessary to break the degeneracy. Figure 6.4 shows the confidence regions for this scenario with SNe Ia alone and fixing  $H_0$  as well.  $H_0$  is fixed to the best fit values in Table 6.2 for each data set. These values are common to all the scenarios, and this one is the only one that departs from the usual values.

Although the  $\eta$  parameter is always compatible with no effective running, fixing  $H_0$  is essential to obtain the same behaviour as with other scenarios: a negative running for R06 data and a positive one for VW07.

### 6.3.3 Scenario 3

The last scenario changes the renormalization scale and, although the heaviest degrees of freedom cause the running as in Scenario 2, considering  $H(z)$  as the renormalization scale changes the form of the  $\beta$ -function. Now, the  $\beta$ -function is proportional to the cosmological index introduced in Chapter 3:

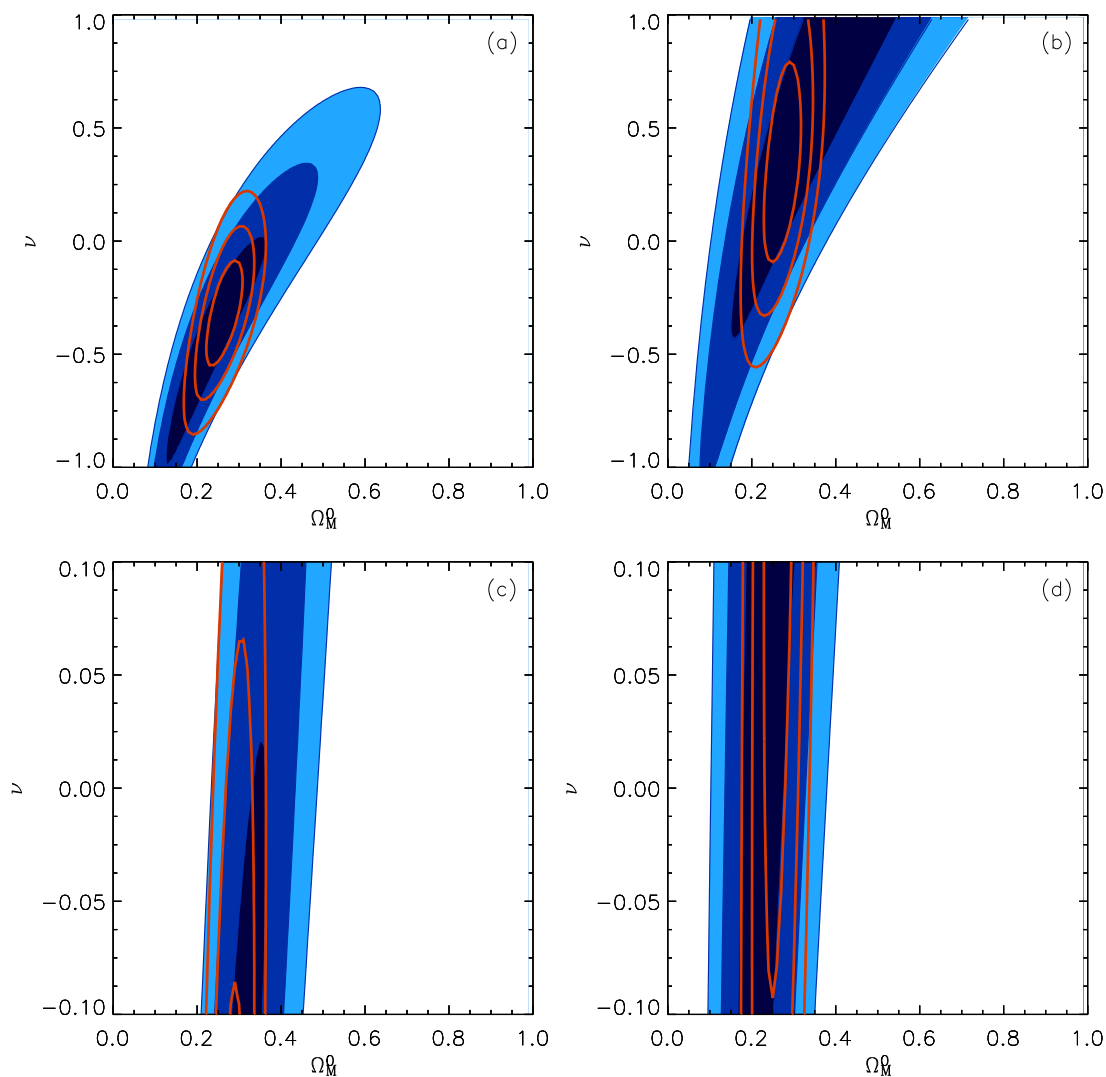


Figure 6.5: As Figure 6.3 but for the cosmological index  $\nu$  representing the running in Scenario 3. Panels (c) and (d) show a zoom in the physically acceptable range of  $\nu$  for R06 and VW07 respectively.

$$\nu \equiv \frac{\sigma}{12\pi} \frac{M^2}{M_P^2}. \quad (6.14)$$

As explained in Section 3.4, a natural value for this parameter would be  $\nu_0 = 0.026$ ; and the physical range for it  $|\nu| \ll 1$ , for example  $-0.1 < \nu < 0.1$ .

Current data, either of the sets, cannot achieve the precision needed to constrain this parameter in that interval. As seen in Figure 6.5, the confidence regions fully

cover its range and, in the range of interest, the density of matter is well determined, so no prior on it can better constrain  $\nu$  up to the needed precision. Besides,  $\nu$  is very slightly degenerate with  $H_0$ , and fixing its value does not reduce uncertainties significantly, but we would pay the price of depending on the  $H_0$  value.

VW07 data are compatible at  $1\sigma$  level with no evolution but prefer positive  $\nu$ 's. On the other hand, the absence of evolution is only true at  $2\sigma$  level and negative  $\nu$ 's are preferred with R06 sample. Notice that the absence of evolution does not necessarily indicate the incorrectness of the model, but it could be a sign of a lack of particles close to the Planck scale.

These are the general trends for the three scenarios as well: VW07 set is more conservative with respect to an evolving source than R06 is. In summary, current SNe Ia data are not able to put serious constraints on particle physics parameters, and particle physics models with the standard and expected values for the free parameters do not describe observations satisfactorily.

From the point of view of a  $\chi^2$  analysis, all those theoretical models are equally qualified to describe the data, and the  $p$ -values shown in Table 6.3 do not suggest that any model should be discarded by any of the sets. Besides, all of them have the same number of unknown parameters, and therefore, none of the criteria based on Ockham's razor to choose between models can differentiate them. The running cosmological constant models are in the same situation as dark energy sources with a constant equation of state, in the sense that two independent parameters are needed in order to represent their behaviour. Let us see now how well can do SNe Ia with this other branch of cosmological models.

## 6.4 Constant dark energy source

The cosmological constant is a constant dark energy source with  $w_0 = -1$ , but as seen in Section 2.3.3 other kinds of sources have a constant barotropic index too. For these models,  $w(z) = w_0$  is not a parameterization nor an approximation, it is a true value. However, it has the meaning of an effective value at  $z = 0$  for any evolving model.

SNe Ia data by themselves do not constrain  $w_0$  with great accuracy. The con-

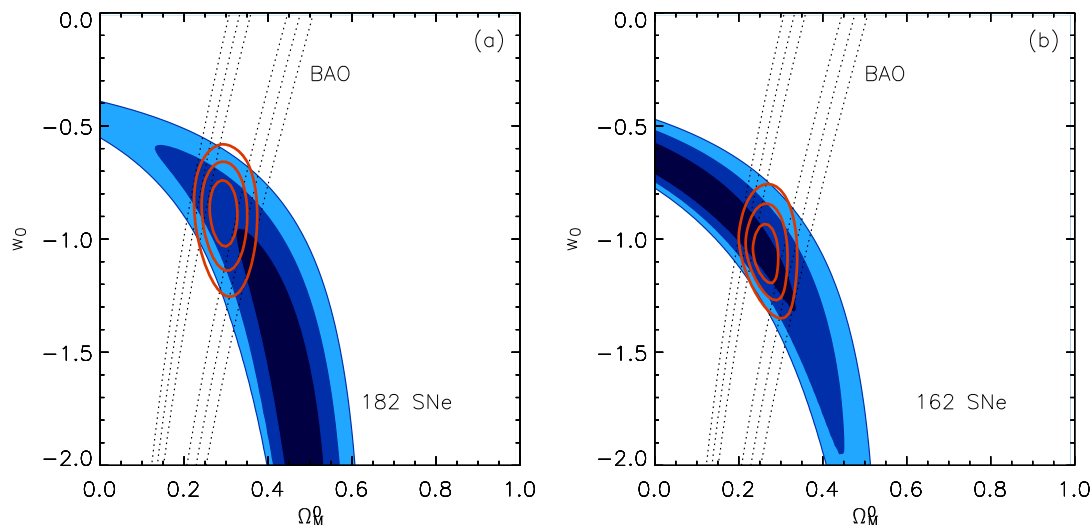


Figure 6.6: (a) Confidence regions showing  $1\sigma$ ,  $2\sigma$  and  $3\sigma$  contours in the  $(\Omega_M^0, w_0)$  plane for a constant equation of state in a flat universe. The results correspond to the 182 SNeIa in R06 [160]. Solid red lines enclose the same probability regions when joining SNe results with BAO constraints. (b) The same as (a) but for the 162 SNeIa in VW07 [211].

confidence region surface diminishes the closer we approach the cosmological constant value, but still the  $1\sigma$  uncertainty on  $w_0$  as obtained from current SNeIa data is almost a 50% of its value.

However, the banana-like shape of the confidence regions (see Figure 6.6) reveals that, for low matter densities, the prior knowledge on  $\Omega_M^0$  can break part of the degeneracy. Even more, BAO constraints, which have been specifically calculated for these models, are nearly perpendicular to SNe regions, being both methods great partners for the study and determination of  $w_0$ .

Figure 6.6 with its counterpart Table 6.4 shows  $1\sigma$ ,  $2\sigma$  and  $3\sigma$  confidence regions in the  $(\Omega_M^0, w_0)$  space for the two sets of SNeIa: BAO as reported in Ref. [70] and the combination of both. Just like for the running cosmological constant models, we consider a flat universe so that results are comparable. With the inclusion of BAO constraints (red solid contours in the plot) the uncertainty on  $w_0$  falls down to a 10% and the cosmological constant stays in the  $1\sigma$  limit for both SNe sets. In Scenario 1, 2 and 3, the cosmological constant was at most at  $2\sigma$  of the best fit; the uncertainty on  $\tau$ ,  $\eta$  and  $\nu$  ( $\theta$  in general) never approached this 10% and in most

set	$\Omega_M^0$	$w_0$	$H_0^\dagger$	$\chi^2$	$p$
– SNe –					
R06	$0.46_{-0.08}^{+0.05}$	$-1.7_{-0.7}^{+0.5}$	63.8	156.6	0.89
VW07	$0.0_{\ddagger}^{+0.2}$	$-0.65_{-0.40}^{+0.05}$	65.3	125.7	0.98
– SNe + BAO –					
R06	$0.29_{-0.02}^{+0.02}$	$-0.88_{-0.10}^{+0.11}$	62.7	159.7	-
VW07	$0.26_{-0.02}^{+0.02}$	$-1.08_{-0.08}^{+0.10}$	65.8	126.9	-

†  $[H_0] = Km/s/Mpc$ .

‡ Outside the physically allowed region.

Table 6.4: As in Table 6.2 but parameters correspond to a constant dark energy equation of state. A flat universe is assumed.

cases was of order 100%. With these sets then, SNeIa determine  $w_0$  much better than the *running parameters*,  $\theta$ , do.

The selected region in the  $(\Omega_M^0, w_0)$  plane is still wide enough to allow for most of the theoretical models discussed in previous chapters. Only cosmic strings and textures ( $w = -1/3$ ) are clearly ruled out already with SNe alone. The remaining topological defect, domain walls, is at  $2\sigma$  level when combining BAO constraints with R06 and at more than  $4\sigma$  with VW07 instead. Quintessence, k-essence, phantoms, Cardassian, DGPs and the remaining evolving models can all have an effective  $w_0$  close to  $-1$ , and therefore they can be accommodated with this results. However, this effective value hides all the information on the evolution with the integration through redshift. As for the running cosmological models, there is still no direct correspondence between  $w_0$  and the  $\theta$  parameter for each of them. In both cases, the evolution is encoded in one single parameter,  $w_0$  or  $\theta$ , but a constant  $\theta$  behaves as an evolving  $w(z)$ . This is clearly seen in Equation 4.14, where the pseudo-equation of state for Scenario 3 is detailed for a flat universe as a function of  $\nu$ .

The form of  $w(z)$  is essential then to improve our knowledge on the theory behind dark energy. With the determination of a constant  $w_0$ , one can only rule out models with a constant equation of state; not much or nothing can be said about the evolving ones.

## 6.5 Evolving equation of state

We have seen in Chapter 4 how different can be the evolution of the equation of state through redshift depending on the underlying theoretical model. Figure 4.2, extracted from Ref. [206], is a clear example and it does not include  $w(z) < -1$  models yet.

Those behaviours are impossible to parameterize with few parameters, and lots of parameters cannot be determined without excessive degeneracy with current observational data. That is the trade-off we were talking about in Section 4.3. The most one can aspire to is to try to know the global slope of the function and that is represented by its first derivative. However, the linear development on  $z$  increases (or decreases) indefinitely and that is not the desired behaviour at high redshift. As we also argued in Section 4.3, this thesis uses Equation 4.38, that is, a linear development on the scale factor  $a$ , although this parameterization is not free from criticisms [160]. A best choice, a continuous fit, is left to next chapter.

The parameterization in the scale factor with only two parameters is still not well determined by SNeIa. In order to constrain the  $(w_0, w_a)$  space, one has to impose some priors on the remaining parameters. In the following, we assume a flat universe as done for a constant equation of state and fix the Hubble constant to the best fit value in Table 6.4. Each set of SNeIa has its own zero point, and a similar value of  $H_0$  is repeatedly found for all the tests:  $63.5 \text{ Km/s/Mpc}$  for R06 and  $65.3 \text{ Km/s/Mpc}$  for VW07. Therefore, it seems justified to fix this value to improve the knowledge on the others. A prior on the density of matter diminishes the uncertainties as well. Note that in this case we are not using the BAO constraint but the Gaussian prior  $\Omega_M^0 = 0.27 \pm 0.03$ . As it happened with a running cosmological constant, BAO constraints are not explicitly calculated for an evolving equation of state, and so, we add this information directly on the matter density.

With these premises, one obtains the probability contours displayed in the top panel of Figure 6.7 for R06 (a) and VW07 (b) data. Again, almost every model with  $w_a < -4(1 + 2w_0)$  is allowed by SNeIa data alone, and both  $w_0$  and  $w_a$  are badly constrained. The addition of the extra parameter  $w_a$  is not rewarded by a gain in information, because current data cannot constrain  $w_0$  and  $w_a$  at the same time. That makes that  $w(z)$ s covering all the physically accepted plane are permitted (Fig. 6.7 (c), (d)).

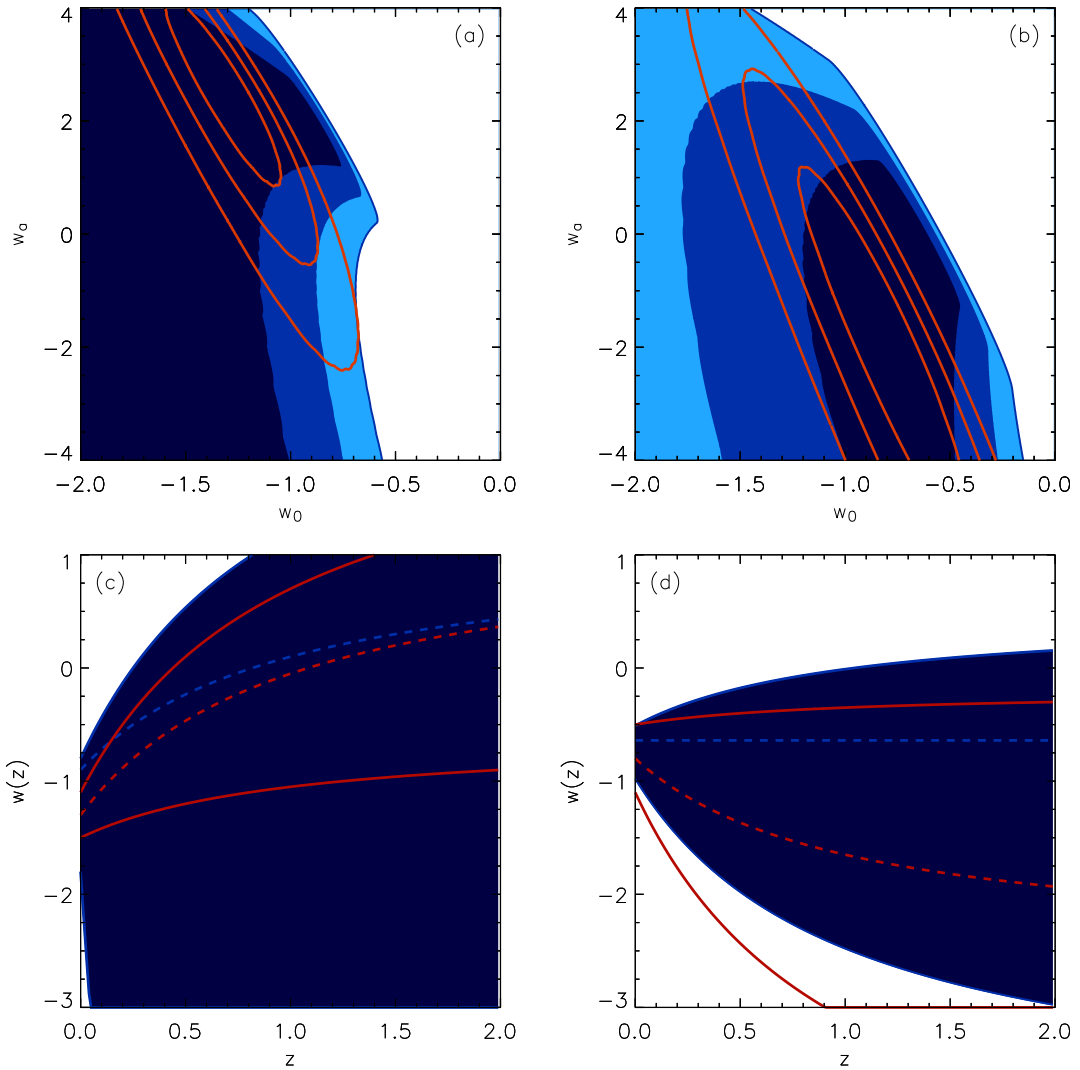


Figure 6.7: (a) Confidence region in the  $(w_0, w_a)$  plane for an evolving equation of state in a flat universe for the 182 SNe Ia in R06 [160]. The Hubble constant is fixed to the best fit value in Table 6.4 and the density of matter has been marginalized. Solid red lines show the contours when a prior  $\Omega_M^0 = 0.27 \pm 0.03$  is included before marginalizing. (b) The same as (a) but for the 162 SNe Ia in VW07 [211]. (c) and (d) Representation of the  $1\sigma$  results in the above panel for the full parameterized function  $w(z) \simeq w_0 + w_a z/(1+z)$ . Blue solid regions are determined by SNe Ia alone and red lines include the prior on the matter density.

Table 6.5 shows  $1\sigma$  determinations for the equation of state parameters from which the evolutions in Figures 6.7 (c) and (d) have been obtained. The cosmological constant is only ruled out (just at  $1\sigma$ !) when R06 data are used in combination with

set	$w_0$	$w_a$	$\chi^2$	$p$
– SNe –				
R06	$-0.9^{+0.1}_{-0.9}$	$2_{\ddagger}^{+2}$	156.5	0.88
VW07	$-0.64^{+0.13}_{-0.34}$	$0_{-3}^{+1}$	125.7	0.96
– SNe + $\Omega_M^0 = 0.27 \pm 0.03$ –				
R06	$-1.3^{+0.2}_{-0.2}$	$+2.5^{+1.1}_{-1.6}$	156.6	-
VW07	$-0.8^{+0.3}_{-0.3}$	$-1.7^{+2.0}_{-2.3}$	126.4	-

$\ddagger > 30$ .

Table 6.5: Best fit values for the parameters of an evolving equation of state  $w(z) = w_0 + w_a z / (1 + z)$ . It has been assumed a flat universe and the Hubble constant fixed to the best fit value in Table 6.4.  $1\sigma$  errors are found after we marginalize over  $\Omega_M^0$ .

the prior on the matter density. In spite of the lower mean redshift of the VW07 data distribution, this set is able to better constrain the  $w(z)$  space due to the smaller amount of evolution it demands. Within its  $1\sigma$  limits, one can accommodate the running cosmological constant Scenario 3 with the natural value  $\nu_0$ , or a Chaplying gas model with a large range of parameters  $A_s$  and  $n$ , for instance. On the other hand, R06 data together with BAO constraints seem more likely to be described by a DGP model or a modification to gravity with a moderate  $n$ . However,  $1\sigma$  intervals are wide enough to be consistent with almost all of them and, of course, with a constant dark energy source. Rapidly evolving sources such as sinusoidals are not well parameterized by this kind of development.

## 6.6 Near future results

In the previous sections we showed results from two sets in parallel, R06 and VW07. Both of them have different redshift distributions and lead to different conclusions, but also have been obtained and reduced in a different manner. Their union would increase the number of SNeIa at intermediate and high redshift, and that would surely settle and improve our knowledge.

A naive join of both sets by scaling the two samples to the same zero point

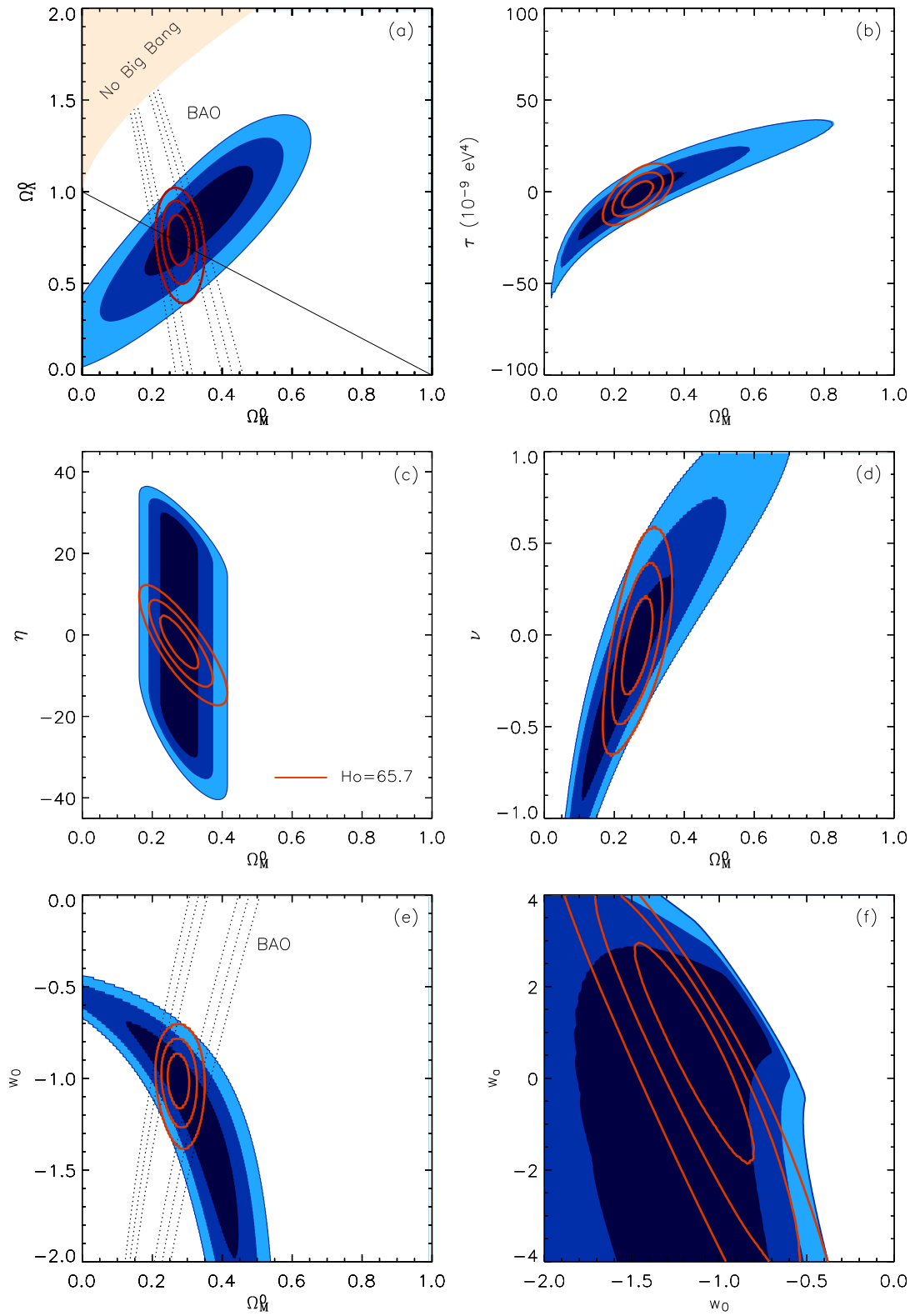


Figure 6.8: Dark energy parameters obtained with the data compilation in Ref. [56] (see text). Contours as in previous figures.

has been done in Ref. [56], but still light curve fitting methodology and calibration differ. The same authors are working on that direction. In this section, results for this full set of 192 SNe Ia are given, but maybe when you are reading these lines the two data sets are already homogeneously joined. Results are, then, just a measure of the improvement we will get, but should not be interpreted as serious constraints to the cosmological parameters and the equation of state.

In Figure 6.8 there is a summary of all the parameters reported from Section 6.2 to Section 6.5 for this last sample. As a general trend, results are halfway between R06 and VW07. The dominating set is VW07, but the area of the confidence region diminishes with respect to this set due to the extra high redshift supernovae. From these results, there is no observational necessity of any running, evolution or even a departure from a  $w_0 = -1$ . Even though confidence regions are still large enough not to clearly point out a single model, if the final combination of data sets results in agreement with the current compilation, indications would be symptomatic of a cosmological constant. Estimates for the parameters of the most promising dark energy models have been reported by Davis et al. (2007) in [56].

The size of the confidence regions depends on the number of data, their redshift distribution and the best fit position on the plane. For these data sets, the differences due to the number of data are not significant. The full compilation has sacrificed the increment on the number of data to a stricter selection of the supernovae to be used for cosmology. This increases the confidence in the results: there is a gain in accuracy and a small loss in precision. The improvement in precision can be obtained by enlarging high redshift samples.

## Chapter 7

---

# Reconstructing dark energy with an inverse method

---

After estimating the parameters of an evolving equation of state, the next step is to consider the evolution in a non-parametric way. In order to recover  $w(z)$  it is introduced a minimization algorithm, being the approach in this chapter completely different from the one in the previous analysis. The same methodology is applied to the running cosmological constant as well.

### 7.1 The problem

Science meets two kinds of problems: *forward* and *inverse* problems. Given a complete theory, the prediction of data is what is called the forward problem. The opposite direction, i.e., having some data try to guess an underlying theory, is the inverse problem.

Just for illustration purposes, one can consider General Relativity. A logical deduction is that the elliptical orbit followed by a planet is altered because of the curvature of space-time. Einstein calculated that its effect on the shift of the perihelion precession of Mercury should be of about 43 seconds of arc per century [67]. That was the difference between the result of Newton's theory and observations, and therefore it was a crucial test which General Relativity passed. The prediction of the perihelion shift is a typical example of a forward problem.

The main problem treated in this thesis is quite different: we face an inverse problem. We have some data, let us say SNe Ia magnitudes for definiteness, and we want to know what makes the observed values of those magnitudes be so. That is to say, which model of Universe would allow us to measure that amount of light from a supernova explosion produced at a given redshift.

In the previous chapter, we somehow mixed both problems. We defined a grid of possible models of the universe, and for each of them we calculated the magnitude that it would produce for each supernova. These results are then compared with observations, and the model which is more similar to observations is chosen as the model which best describes our Universe. So, we generated  $n$  forward problems to solve an inverse problem.

However, already with a  $\chi^2$  methodology as it was used, one can directly solve the inverse problem by minimizing the  $\chi^2$  function. This alternative procedure, which can be done in several different ways, does not need to solve  $n$  forward problems, but just to find any smart form of minimizing the function given the nature of the problem, and it is the one used when the previous trick is not computationally possible. And that happens when we want to fit a function in a non-parametric way. In the following section, it is introduced a minimization method developed to reconstruct the dark energy equation of state as a continuous function [73, 74].

## 7.2 Inverse problems

The approach to dark energy via the solution of the inverse problem is the usual way of attacking it. But one should take into account that inverse problems are usually ill-posed or ill-conditioned [189], that is:

- The solution does not necessary exist.
- The solution is not unique.
- The solution is not stable and small differences in data cause large differences in the result.

It has been shown in Section 4.4 that the determination of the equation of state of dark energy is an extremely degenerate problem. It is besides a non-linear problem

with an unknown function that, although normally parameterized for simplicity, should be determined in a non-parametric way. One can try to dodge all these difficulties by regularizing the problem, for example by adding *a priori* information or demanding a smooth solution. To do this, the use of probabilistic techniques is required.

### 7.2.1 A non-parametric non-linear inversion

A correct treatment of an inverse problem provides a powerful way to determine the values of functional forms from a set of observables. This approach is useful when the information along a certain coordinate, in our case information on  $w(z)$ , emerges in observables coupled with information at all other  $z$ . Dark energy is here addressed using a non-linear non-parametric inversion. Most frequently, when the parameters to be determined are a set of discrete unknowns, the method used is a least squares. One can minimize the  $\chi^2$  via methods based on singular value decomposition, gradient descents, Newton-like methods, conjugate gradient, Levenberg-Marquardt, etc. These possibilities are exact for linear problems and quite good for most linearizable problems which are not very far from linearity and do not have local minima. But the continuous case, where functional forms are to be determined, requires a general inverse problem formulation. The inverse method used here is a Bayesian approach to this generalization [189, 191].

For simplicity and according to recent observations, we consider a flat universe with only two dominant constituents (at present): cold matter and dark energy. Therefore, we characterize the cosmological model by the density of matter,  $\Omega_M^0$ , and by the index  $w(z)$  of the dark energy equation of state. The vector of unknowns  $\mathbf{M}$  has then a discrete and a continuous component:

$$\mathbf{M} = \begin{pmatrix} \Omega_M^0 \\ w(z) \end{pmatrix}. \quad (7.1)$$

On the other hand, the observational data are mainly SNe Ia magnitudes. We have a finite set of  $N$  magnitudes,  $m_i$ , and consider the magnitude-redshift relation (Eq. 5.2) in a flat universe relating the unknowns to the observational data:

$$m^{th}(z, \Omega_M^0, w(z)) = \mathcal{M} + 5 \log[D_L(z, \Omega_M^0, w(z))]. \quad (7.2)$$

All parameters and functions are defined as in previous chapters, but now the functional form of  $w(z)$  and the assumption of a flat universe imply:

$$H(z, \Omega_M^0, w(z)) = H_0 \sqrt{\Omega_M^0(1+z)^3 + \Omega_X^0(z)}, \quad (7.3)$$

$$\Omega_X^0(z) = \Omega_X^0 \exp\left(3 \int_0^z dz' \frac{1+w(z')}{1+z'}\right). \quad (7.4)$$

We redefine our data and convert the original SNe magnitudes to dimensionless distance coordinates  $y$ :

$$y_i \equiv \frac{10^{(m_i - \mathcal{M})/5}}{c(1+z_i)} = \int_0^{z_i} \frac{dz'}{\sqrt{\Omega_M^0(1+z')^3 + \Omega_X^0(z')}}}, \quad (7.5)$$

$$\sigma_{y_i} = \frac{\ln 10}{5} y_i \sigma_{m_i}. \quad (7.6)$$

With this definition we deal directly with a function  $y(\Omega_M^0, w(z))$ , the only part which depends on the cosmological model. To convert our  $m_i$  data to  $y_i$ , we can adopt the value obtained from low redshift supernovae and use  $\mathcal{M} = -3.40 \pm 0.05$ . Defined in this way,  $y_i$  is used in other analyses [55].

After the corresponding transformations, the observables are now described by a vector of  $N$  components,  $y_i$ , and by a covariance matrix ( $\mathbf{C}_y$ ). This method can handle correlated measurements, where non-diagonal elements  $C_{y_i y_j}$  are different from zero (observations  $i$  and  $j$  being correlated). But, at present, those have not been estimated for the composite samples of distance indicators. We would then use:

$$C_{y_i y_j} = \sigma_{y_i}^2 \delta_{ij}. \quad (7.7)$$

Similarly, the unknown vector of parameters is described by its *a priori* value,  $\mathbf{M}_0$ , and the covariance matrix ( $\mathbf{C}_0$ ). The function describing  $w(z)$  should be

smooth, both for regularizing the solution and for having a physical sense. This leads to non-null covariance between neighbouring points in  $z$  for  $w(z)$ . Thus, the covariance matrix  $\mathbf{C}_0$  has the form:

$$\mathbf{C}_0 = \begin{pmatrix} \sigma_{\Omega_M^0}^2 & 0 \\ 0 & C_{w(z),w(z')} \end{pmatrix}, \quad (7.8)$$

where a choice is made for the non-null covariance between  $z$  and  $z'$ ,  $C_{w(z),w(z')}$ . This choice is taken to be as general as possible. It would define the smoothness required in the solution by setting the correlation length between errors in  $z$  and  $z'$  (this gives the length scale in which the function can fluctuate between redshifts). The amplitude of the fluctuation of the function is given by the dispersion  $\sigma_w$  at  $z$ . In the Gaussian choice for  $C_{w(z),w(z')}$ ,  $\sigma_w$  is the  $1\sigma$  region where the solution is to be found.

Thus for a Gaussian choice,  $C_{w(z),w(z')}$  is described as

$$C_{w(z),w(z')} = \sigma_w^2 \exp\left(-\frac{(z-z')^2}{2\Delta_z^2}\right), \quad (7.9)$$

which means that the variance at  $z$  equals  $\sigma_w^2$  and that the correlation length between errors is  $\Delta_z$ . Another possible choice for  $C_{w(z),w(z')}$  is an exponential of the type:

$$C_{w(z),w(z')} = \sigma_w^2 \exp\left(-\frac{|z-z'|}{\Delta_z}\right), \quad (7.10)$$

while no difference in the results is found for those different choices of  $C_{w(z),w(z')}$ . In both functions, the amplitude  $\sigma_w$  could be considered to be redshift-dependent. However, the large ignorance associated with dark energy makes it absurd to focus on its uncertainty since, for instance, a large variation of  $w(z)$  at high redshift would invalidate our current (and small) knowledge of its present-day value.

This is all the information we have beforehand, and with that we are interested in determining the best estimator  $\tilde{\mathbf{M}}$  for  $\mathbf{M}$ . The probabilistic approach we use incorporates constraints from priors through the Bayes' theorem, i.e., the *a posteriori* probability density  $f_{post}(\mathbf{M}|\mathbf{D})$  for the vector  $\mathbf{M}$  containing the unknown model

parameters given the observed data  $\mathbf{D}$ , is linked to the likelihood function  $L$  and the prior density function for the parameter vector as:

$$f_{post}(\mathbf{M}|\mathbf{D}) \propto L(\mathbf{D}|\mathbf{M}) f_{prior}(\mathbf{M}). \quad (7.11)$$

The theoretical model described by the operator  $\mathbf{y}^{th}$ , which connects the model parameters  $\mathbf{M}$  with the predicted data  $\mathbf{D}_{predicted} = \mathbf{y}^{th}(\mathbf{M})$ , is to agree as closely as possible with the observed data  $\mathbf{y}$ . Assuming that both the prior probability and the errors in the data are distributed as Gaussian functions, the posterior distribution becomes:

$$f_{post}(\mathbf{M}|\mathbf{y}) \propto \exp \left[ -\frac{1}{2} (\mathbf{y} - \mathbf{y}^{th}(\mathbf{M}))^* \mathbf{C}_y^{-1} (\mathbf{y} - \mathbf{y}^{th}(\mathbf{M})) -\frac{1}{2} (\mathbf{M} - \mathbf{M}_0)^* \mathbf{C}_0^{-1} (\mathbf{M} - \mathbf{M}_0) \right], \quad (7.12)$$

where  $*$  stands for the adjoint operator. The best estimator for  $\mathbf{M}$ ,  $\tilde{\mathbf{M}}$ , is the most probable value of  $\mathbf{M}$ , given the set of data  $\mathbf{y}$ . The condition is reached by minimizing the misfit or objective function:

$$S \equiv \frac{1}{2} (\mathbf{y} - \mathbf{y}^{th}(\mathbf{M}))^* \mathbf{C}_y^{-1} (\mathbf{y} - \mathbf{y}^{th}(\mathbf{M})) + \frac{1}{2} (\mathbf{M} - \mathbf{M}_0)^* \mathbf{C}_0^{-1} (\mathbf{M} - \mathbf{M}_0), \quad (7.13)$$

which is equivalent to maximize the Gaussian density of probability when data and parameters are treated in the same way. According to the philosophy of the method, they are all parameters, whether directly measurable and described by their measured values and their uncertainties, or not directly measurable and described by *a priori* information. Note that the first term in the previous equation is exactly the misfit function in the  $\chi^2$  method, where the gaussianity assumption was made as well, and the second term is adding the *a priori* information on the parameters. Therefore, the usual least squares method does not consider this information on the non-measured parameters, although through the Bayes' theorem it can be easily

included. In our case, this Bayesian approach helps to regularize the inversion, and sometimes it is only due to the incorporation of the *a priori* information that one can obtain a solution. In general, one starts with scarcely restrictive priors but they become stricter if the algorithm does not converge. However, too strict priors compared to the *a priori* knowledge lead to biased results, and this fact must be always considered before choosing the priors.

The minimization of  $S$  has been done using a Newton method. That kind of methods use to define the direction of search as not only the direction of steepest ascent but also by the curvature defined by the Hessian of Equation 7.13. This allows a faster convergence of the algorithm at the cost of the difficulty to calculate the Hessian for large-sized inverse problems [189]. However, it is not necessary to know the Hessian exactly and in the following we will make the approximation

$$H_k = \left( \frac{\partial^2 S}{\partial M^2} \right)_k \simeq \mathbf{G}_k^* \mathbf{C}_y^{-1} \mathbf{G}_k + \mathbf{C}_0, \quad (7.14)$$

where it has been used that the second derivatives of Equation 7.5,  $\partial^2 y^{th} / \partial M_i \partial M_j \equiv \partial G^j / \partial M_i$ , are negligible in front of the first ones,  $G^j$ .

Despite this approximation, the problem of Eq. 7.2 or equivalently Eq. 7.5 is non-linear in the parameters, so the solution of the problem is reached iteratively. Before introducing the solution, let us define the operator  $\mathbf{G}$  represented by the matrix of partial derivatives of the dimensionless distance coordinate, which will simplify subsequent notation. Its kernel is denoted by  $g$  as defined in the next equations.

$$\mathbf{G} = \begin{pmatrix} \frac{\partial y_1^{th}}{\partial \Omega_M^0} & \frac{\partial y_1^{th}}{\partial w(z)} \\ \frac{\partial y_2^{th}}{\partial \Omega_M^0} & \frac{\partial y_2^{th}}{\partial w(z)} \\ \vdots & \vdots \\ \frac{\partial y_N^{th}}{\partial \Omega_M^0} & \frac{\partial y_N^{th}}{\partial w(z)} \end{pmatrix}, \quad (7.15)$$

with

$$\frac{\partial y_i^{th}}{\partial \Omega_M^0} = -\frac{1}{2} \int_0^{z_i} \frac{(1+z')^3 dz'}{H^3(z')} \equiv \int_0^{z_i} g_{\Omega_M}(z') dz', \quad (7.16)$$

$$\frac{\partial y_i^{th}}{\partial w(z)} = -\frac{1}{2} \int_0^{z_i} \frac{3\Omega_X^0(z') \ln(1+z') dz'}{H^3(z')} \equiv \int_0^{z_i} g_w(z') dz'. \quad (7.17)$$

With this definition, the solution is implemented as an iterative procedure where [189, 191]:

$$\begin{aligned} \tilde{\mathbf{M}}_{[k+1]} = \mathbf{M}_0 + \mathbf{C}_0 \mathbf{G}_{[k]}^* (\mathbf{C}_y + \mathbf{G}_{[k]} \mathbf{C}_0 \mathbf{G}_{[k]}^*)^{-1} \\ \left( \mathbf{y} - \mathbf{y}^{th}(\tilde{\mathbf{M}}_{[k]}) + \mathbf{G}_{[k]} (\tilde{\mathbf{M}}_{[k]} - \mathbf{M}_0) \right). \end{aligned} \quad (7.18)$$

Since we are working in a Hilbert space with vectors containing functional forms, the above operator products give rise to scalar products of the functions integrated over the domain of those functions. The expressions transform into having the products rewritten in terms of the kernels of the operators [190].

We indicate the scalar product by “ $\cdot$ ” and it is defined as it can be seen from this example:

$$C_w \cdot \frac{\partial y_j^{th}}{\partial w(z)} = \int_0^{z_j} dz' C_w(z, z') g_w(z'). \quad (7.19)$$

The components of the vector of unknowns  $\tilde{\mathbf{M}}$ , which in our case are both  $\Omega_M^0$  and  $w(z)$ , are then obtained in an explicit form from:

$$\tilde{M}_{[k+1]}(z) = M_0(z) + \sum_{i=1}^N W_{i[k]} \int_0^{z_i} C_0(z, z') g_{i[k]}(z') dz', \quad (7.20)$$

where

$$W_{i[k]} = \sum_{j=1}^N \left( S_{[k]}^{-1} \right)_{i,j} V_{j[k]}, \quad (7.21)$$

$$\begin{aligned} \mathbf{V} &= \mathbf{y} + \mathbf{G} (\mathbf{M} - \mathbf{M}_0) - \mathbf{y}^{th}(\mathbf{M}) \\ V_{i[k]} &= y_i + \int_0^{z_i} g_{i[k]}(z) (M_{[k]}(z) - M_0(z)) dz - y_i^{th}(z_i, \Omega_M^0, w(z)), \end{aligned} \quad (7.22)$$

$$\begin{aligned} \mathbf{S} &= \mathbf{C}_y + \mathbf{G} \mathbf{C}_0 \mathbf{G}^* \\ S_{i,j[k]} &= (C_y)_{i,j} + \int_0^{z_j} \int_0^{z_i} g_{i[k]}(z) C_0(z, z') g_{j[k]}(z') dz dz'. \end{aligned} \quad (7.23)$$

In the case of the dark energy equation of state and the matter density the expressions reduce to:

$$\Omega_{M[k+1]}^0 = \Omega_{M_0}^0 + \sigma_{\Omega_M^0}^2 \sum_{i=1}^N W_{i[k]} \frac{\partial y_i^{th}}{\partial \Omega_M^0 [k]}, \quad (7.24)$$

$$w_{[k+1]}(z) = w_0(z) + \sum_{i=1}^N W_{i[k]} \int_0^{z_i} C_w(z, z') g_{w[k]}(z') dz', \quad (7.25)$$

where it is denoted  $C_w(z, z') \equiv C_{w(z), w(z')}(z, z')$  and  $W_{i[k]}$  is given by the product (7.21) with:

$$V_i = y_i + \frac{\partial y_i^{th}}{\partial \Omega_M^0} (\Omega_M^0 - \Omega_{M_0}^0) + \frac{\partial y_i^{th}}{\partial w(z)} \cdot (w - w_0) - y_i^{th}(z_i, \Omega_M^0, w(z)) \quad (7.26)$$

$$S_{i,j} = \delta_{i,j} \sigma_i \sigma_j + \frac{\partial y_i^{th}}{\partial \Omega_M^0} C_{\Omega_M^0} \frac{\partial y_j^{th}}{\partial \Omega_M^0} + \frac{\partial y_i^{th}}{\partial w(z)} \cdot \left( C_w \cdot \frac{\partial y_j^{th}}{\partial w(z)} \right). \quad (7.27)$$

### 7.2.1.1 Control of the results

In order to test the accuracy of the inversion we use the *a posteriori* covariance matrix. It can be shown (see [190, 192]) that for the linear inverse problem with Gaussian *a priori* probability density function, the *a posteriori* probability density function is also Gaussian with mean Eq. 7.18 and covariance Eq. 7.28. Although its value is only exact in the linear case it is a good approximation here, since the luminosity distance is quite linear on the equation of state  $w(z)$  at low redshift.

$$\begin{aligned}\mathbf{C}_{\tilde{M}} &= (\mathbf{G}^* \mathbf{C}_y^{-1} \mathbf{G} + \mathbf{C}_0^{-1})^{-1} \equiv \mathbf{C}_0 - \mathbf{C}_0 \mathbf{G}^* \mathbf{S}^{-1} \mathbf{G} \mathbf{C}_0 \\ &= (\mathbf{I} - \mathbf{C}_0 \mathbf{G}^* \mathbf{S}^{-1} \mathbf{G}) \mathbf{C}_0.\end{aligned}\quad (7.28)$$

In an explicit form, the standard deviations from this covariance read:

$$\tilde{\sigma}_{\Omega_M^0} = \sqrt{C_{\tilde{\Omega}_M^0}} = \sigma_{\Omega_M^0} \sqrt{1 - \sum_{i,j} \frac{\partial y_i^{th}}{\partial \Omega_M^0} (S^{-1})_{i,j} \frac{\partial y_j^{th}}{\partial \Omega_M^0} \sigma_{\Omega_M^0}^2}, \quad (7.29)$$

$$\tilde{\sigma}_{w(z)}(z) = \sqrt{C_{\tilde{w}(z)}(z)} = \sqrt{\sigma_{w(z)}^2 - \sum_{i,j} C_w \cdot \frac{\partial y_i^{th}}{\partial w(z)} (S^{-1})_{i,j} \frac{\partial y_j^{th}}{\partial w(z)} \cdot C_w}, \quad (7.30)$$

where the symbols with tilde are the *a posteriori* values, whereas the symbols without it represent the *a priori* ones. It must be stressed that the uncertainty in the final  $w(z)$  does depend on the *a priori* assumption of the uncertainty. In fact, the very  $w(z)$  could depend on the prior. We go into that using Monte Carlo methods later in the analysis.

There are other parameters which help to interpret the results. From the form of Eq. 7.28 we see that the operator  $\mathbf{C}_0 \mathbf{G}^* \mathbf{S}^{-1} \mathbf{G}$  is related to the obtained resolution. This is usually called the *resolving kernel*  $K(z, z')$ . The more this term resembles the  $\delta$ -function the smaller the *a posteriori* covariance function is. In fact, in the linear case, the resolving kernel represents how much the results of the inversion differ from the true model. It represents the filter between the true model and its estimated value [18, 189]. In a useful way, it can also be expressed in terms of the *a priori* and the *a posteriori* covariance matrices:

$$\mathbf{K} = \mathbf{I} - \mathbf{C}_{\tilde{M}} \mathbf{C}_0^{-1}. \quad (7.31)$$

This expression is evaluated numerically to quantify the resolution and information generated in the inversion.

### 7.2.2 Discrete parameters: the parametric non-linear inversion

In the previous section we have obtained the results for a set of a continuous function and a discrete parameter, but we can also consider the case of various discrete parameters. It was pointed out that a successful parameterization for modeling a large variety of dark energy models is obtained by considering  $w(z)$  expanded around the scale factor  $a$ . Assuming a moderate evolution in the equation of state, we use the most simple and adequate (two-parameter) description of  $w(z)$ , Equation 4.38.

With this particular form for the function  $w(z)$ , commonly used to study the behaviour of dark energy, one can solve iteratively for  $w_0$  and  $w_a$  following the same methodology as before:

$$w_{0[k+1]} = w_0^0 + \sigma_{w_0}^2 \sum_{i=1}^N W_{i[k]} \frac{\partial y_i^{th}}{\partial w_0 [k]}, \quad (7.32)$$

$$w_{a[k+1]} = w_a^0 + \sigma_{w_a}^2 \sum_{i=1}^N W_{i[k]} \frac{\partial y_i^{th}}{\partial w_a [k]}, \quad (7.33)$$

where

$$\frac{\partial y_i^{th}}{\partial w_0} = -\frac{1}{2} \int_0^{z_i} \frac{3\Omega_X(z') \ln(1+z') dz'}{H^3(z')}, \quad (7.34)$$

$$\frac{\partial y_i^{th}}{\partial w_a} = -\frac{1}{2} \int_0^{z_i} \frac{3\Omega_X(z') [\ln(1+z') - \frac{z'}{1+z'}] dz'}{H^3(z')}. \quad (7.35)$$

The general *a posteriori* variance is also the same as in the continuous case, and for these parameters the explicit form reads:

$$\tilde{\sigma}_{w_0} = \sqrt{C_{\tilde{w}_0}} = \sigma_{w_0} \sqrt{1 - \sum_{i,j} \frac{\partial y_i^{th}}{\partial w_0} (S^{-1})_{i,j} \frac{\partial y_j^{th}}{\partial w_0} \sigma_{w_0}^2}, \quad (7.36)$$

$$\tilde{\sigma}_{w_a} = \sqrt{C_{\tilde{w}_a}} = \sigma_{w_a} \sqrt{1 - \sum_{i,j} \frac{\partial y_i^{th}}{\partial w_a} (S^{-1})_{i,j} \frac{\partial y_j^{th}}{\partial w_a} \sigma_{w_a}^2}. \quad (7.37)$$

The equations for  $\Omega_M^0$  are those of Section 7.2.1 (Eqs. 7.24, 7.16 and 7.29).

### 7.2.3 Implementation and numerical issues

Two main programs in **Fortran** have been developed in order to implement the set of equations in Section 7.2: **EoScont** and **EoSdisc** for the continuous and discrete cases respectively. The algorithm is just an iterative calculation of the set of equations with a collection of functions to calculate the cosmological magnitudes. These functions are the same as the ones used in the  $\chi^2$  program.

The method itself is a minimization method, so we do not have the problem of choosing an adequate minimization algorithm. The only numerical issues to be concerned about are then numerical integration, interpolation and matrix inversion.

For numerical integration it has been used the same **Fortran** routine as for the  $\chi^2$  program: a ten points Gaussian-Legendre integration as implemented in the **QGAUS()** subroutine in [151]. On the other hand, the best option for interpolating in the continuous case appeared to be the simplest one, a linear interpolation. Finally, the inversion of the matrix  $S$  and the one appearing in the covariance  $\mathbf{C}_{\tilde{M}}$  has been done with another **Fortran** subroutine (**INVERT()** subroutine in [151]) based on LU Decomposition. When using these programs within a Monte Carlo setting, random numbers were generated with the simple **RAND()** intrinsic function of **Fortran**.

## 7.3 Determination of a continuous $w(z)$

In this section we study the evolution of the dark energy equation of state in a generic way, and we do it by taking advantage of the ability of the method to reconstruct functions in a non-parametric form. Other methods to reconstruct  $w(z)$  from the dimensionless coordinate distance,  $y(z)$ , have been already used [168]. Their ground is the fact that  $w(z)$  can be expressed in terms of  $y(z)$  and its first and second derivatives [109]. So if we can obtain  $y(z)$ ,  $dy(z)/dz$  and  $d^2y(z)/dz^2$  from objects at cosmological distances [109, 87, 55] we also have the function  $w(z)$ . To do this it is necessary to fit, usually by bins,  $y(z)$  using a polynomial or a Padé approximant. So, with this method it is needed a basis to expand the function  $y(z)$  and then calculate the derivatives from the obtained coefficients. The uncertainties

can be large, because a function which fits well  $y(z)$  does not need to have the same derivatives as the physical  $y(z)$ .

The principal component analysis (PCA) has been used as well to fit  $w(z)$  [108, 106, 160]. This is a discrete reconstruction of  $w(z)$  at different redshifts which allows to see its evolution. By binning the data the method retrieves an uncorrelated measure of  $w(z)$  at each bin.

Finally, a recent analysis used a maximum entropy reconstruction technique (MaxEnt) [213]. Like for PCA, there is a binning,  $w$  is assumed constant at each bin and  $w(z)$  is decomposed into a sum of orthogonal functions. However, this is a Bayesian approach that shares some characteristics with the inverse method and adds *a priori* information on the equation of state through the Bayes' theorem. In their case, the prior is given by the information entropy of  $w$  relative to the model. The smoothness of the reconstruction is controlled by a regularization parameter.

As we have seen, our method is a Bayesian approach too. With the solution to a continuous inverse problem we have obtained a way to calculate the value of  $w$  at each redshift, so we must repeat the iterative process for every redshift where we want the solution. Several stopping criteria for the iterations have been tested:

- Based on the stability of the solution. One can stop the iterative process when the difference between iterations is  $|w_k(z) - w_{k-1}(z)| < \epsilon$ . However, that should be true at every calculated redshift, and, in practice, it is not the most efficient method when the number of points is large, for example the 31 redshifts used in our results.
- Minimum of  $S$ . Since one wants to minimize the misfit function  $S$ , a natural way of stopping the iterations is once  $S_{min}$  is reached. The possible criticism to this method is that one can get stuck in a local minimum. The probability of this happening can be minimized by starting from different points, which in our case is equivalent to choose different priors.
- Minimum of  $\chi^2$ . Finally, one could control the convergence by monitoring the  $\chi^2$ . Since this does not solve the objection made in the previous point, in our context it seems more reasonable to focus on  $S$ .

To reach the minimum of  $S$  with the settings described in the following, the number of iterations has been typically less than 10.

The next issue is to choose the prior. Using Ockham's razor one could take the cosmological constant as a start. The ideal uncertainty on it would be to take the latter as wide as possible, but, of course, that complicates (or even makes impossible) the convergence. We have seen in Chapter 4 that the classical energy conditions limit the range of the equation of state to  $-1 \leq w \leq -1/3$ . However, we admit that they are not necessarily fulfilled and we widen the range to  $-1.5 \leq w \leq -0.5$  (or  $-3 \leq w \leq 1$  in the Monte Carlo exploration) and so we include phantom fields as the possible source of dark energy. This is in fact necessary, since some observations favour  $w < -1$ . Also remark here that this is only a  $1\sigma$  interval, and therefore, there is a 32% of probability that the prior lies outside the range. The *a priori* space is then larger than the  $1\sigma$  region chosen. For the covariance function we use one of the form of Eq. 7.9 with the moderate variance  $\sigma_w = 0.5 - 1.0$  and a correlation length of  $\Delta_z = 0.05 - 0.10$  (see below). Larger covariances and/or larger correlation lengths cause the non-convergence of the algorithm. We have also tried other functional forms for the covariance, such as the one in Eq. 7.10, but no significant change or improvement has been found.

In the case of  $\Omega_M^0$ , we always suppose a good knowledge,  $\Omega_M^0 = 0.27 \pm 0.03$ . Large uncertainties complicate global convergence, but including this prior is similar to include BAO constraints. The geometry of the Universe is assumed to be flat, as equations have been deduced under this assumption. Its generalization is straightforward, but this way the dimension of the parameter space is reduced, in a way compatible with CMB results [183].

The last point to take into account is the number of redshifts where to give the solution. This number is limited by the resolution allowed by the data. Since all the used data sets have the same order of magnitude of supernovae, we can make a direct comparison with the same resolution in redshift. Redshift intervals have been chosen to be of  $\delta z = 0.06$ , then,  $w(z)$  is calculated in 30 points in the interval  $0 < z < 1.8$  according to the equations of Section 7.2 (Eqs. 7.24, 7.25, 7.29 and 7.30).

### 7.3.1 Current data

On the basis of the previous considerations, we apply the inverse method algorithm to two of the latest SNeIa data sets already used in the  $\chi^2$  analysis: the gold set of Riess et al. (2006), R06 [160] and the compilation of Wood-Vasey et al. (2007),

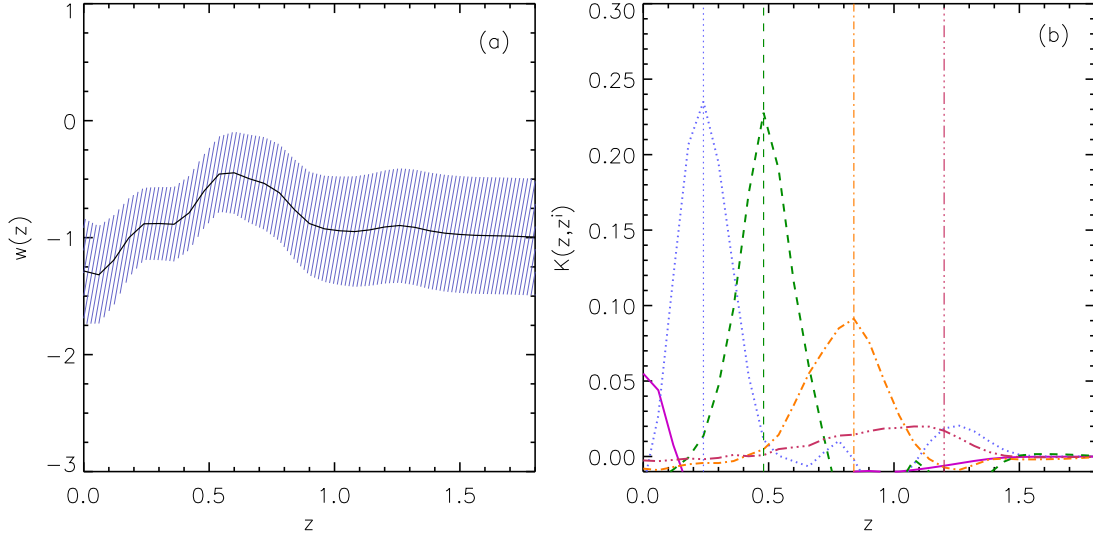


Figure 7.1: Reconstruction of  $w(z)$  using 182 SNe from the gold set of Ref. [160], R06. These results are obtained using Gaussian *a priori* covariances with amplitude  $\sigma_w = 0.5$  and  $\Delta_z = 0.08$ . For the density of matter the prior is set to  $\Omega_M^0 = 0.27 \pm 0.03$ . This fine grid calculation is plotted at redshift intervals of  $\delta z = 0.06$ . The left panel shows  $w(z)$  (solid line) and the  $1\sigma$  confidence interval (dashed shadow). On the right, different resolving kernels at  $z = 0, 0.24, 0.48, 0.84, 1.20$  are shown. The resolving kernels at high  $z$  show that there is no information to conclude on the evolution of the equation of state.

VW07 [211] (see Section 5.7).

In Figure 7.1(a) we have plotted the evolution of the barotropic index of the equation of state for R06 together with  $1\sigma$  intervals as given by Eq. 7.30; the (b) panel shows the resolving kernels at some representative redshifts  $z = 0, 0.24, 0.48, 0.84, 1.20$ . The resolving kernel becomes flatter at higher redshift, where the number of data is smaller, and so is the amount of information. At these redshifts, we recover exactly the prior, and the inverse method does not improve our *a priori* knowledge. At low and intermediate redshift, the slope of  $w(z)$  is positive in a way consistent with results in Section 6.5. Due to the prior of  $\Omega_M^0 = 0.27 \pm 0.03$ , this plot must be compared to  $w_0 = -1.3 \pm 0.2$ ,  $w_a = +2.5 \pm 1.4$  from Table 6.5. Obviously, the two results cannot be compared in a straightforward manner:  $w(z)$  only follows a function with a behaviour  $w_0 + w_a z / (1 + z)$  at low and intermediate redshift. At higher  $z$ , the descent towards the prior  $w(z)^0 = -1$  alters the form of the evolution. This is why the discrete parameterization shows a steeper evolution. The recovered

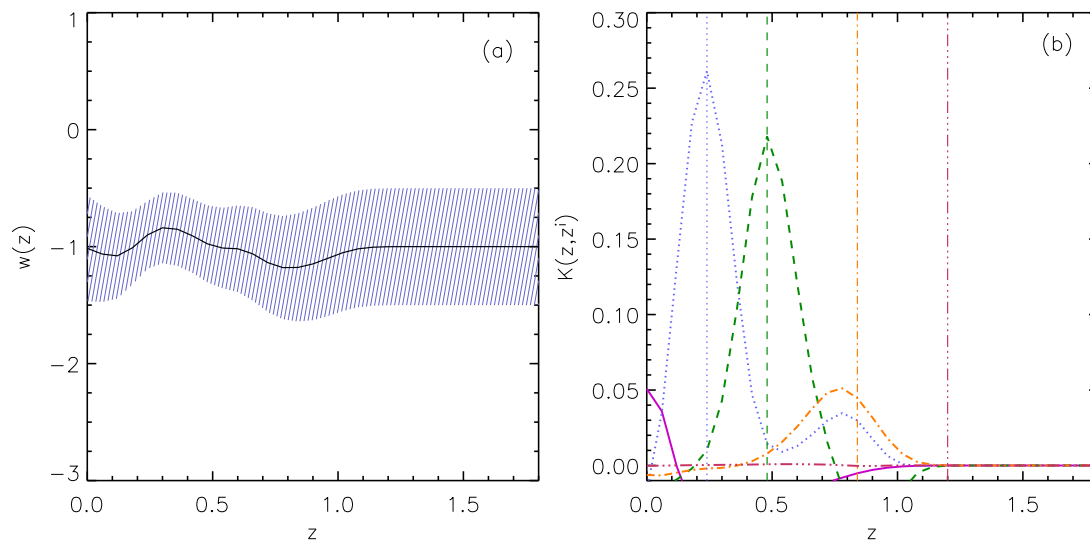


Figure 7.2: Reconstruction of  $w(z)$  (as in Figure 7.1) but with the 162 SNe compiled by the ESSENCE team ([211, 56]), VW07. Resolving kernels reflect the differences in the redshift distribution: higher at low redshift and lower at high with respect to R06, meaning a gain in information at low- $z$  but a loss at mid- $z$ .

$w(z)$  is compatible at  $1\sigma$  with a cosmological constant everywhere except in the interval  $0.5 < z < 0.8$  where the effect of the high redshift supernovae indicate a larger  $w$ . However, we discuss  $1\sigma$  intervals later with Monte Carlo errors.

Once again, R06 and VW07 results describe different behaviours. Through the ESSENCE compilation, the reconstruction is almost constant around  $w(z) = -1$ . The mean redshift of this data set is smaller than for R06 and so, resolving kernels tend to be flatter at lower redshift than before, but are slightly better at low redshift (Figure 7.2). There, the phantom divide crossing effect disappears, but the equation of state enters into the phantom regime at  $z > 0.6$ , where R06 data showed a bump towards positive  $w$ . The evolution at higher redshifts should not be trusted, since there are not enough data to improve the prior as firstly indicated by the shape of the resolving kernels. Anyway, the trend at low and intermediate redshift is the opposite in both cases, being in the VW07 reconstruction always  $1\sigma$  compatible with a cosmological constant.

As it has been mentioned when introducing the method, the  $1\sigma$  intervals given up to now do depend on the *a priori* chosen,  $\sigma_w$ . The maximum uncertainty is going to be the prior, so this  $\sigma_w$  must be interpreted as absolute ignorance. However, for

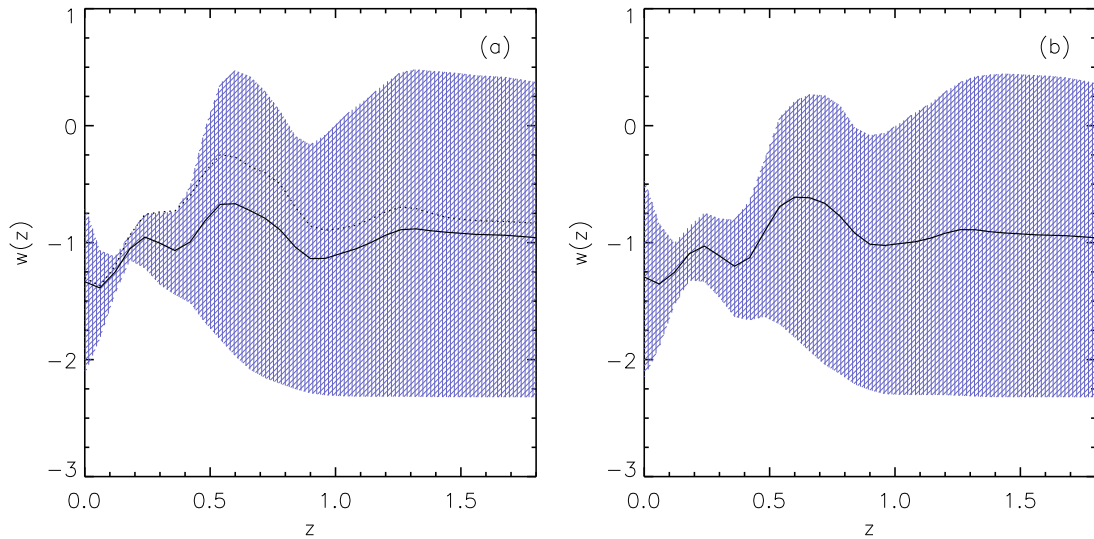


Figure 7.3: (a) Mean (solid line) and  $1\sigma$  Monte Carlo errors obtained from 1000 inversions of R06 data with random priors between  $-3 < w(z)^0 < 1$ . The dotted black line shows the inversion with a lowest  $S$ . (b) The same as (a) but now the 1000 sets are generated by bootstrap resampling from the original R06 set.

the convergence of the algorithm, one cannot set arbitrary high values for  $\sigma_w$ . To overcome this problem we have explored the  $w$  space of physical solutions, setting the prior on  $w(z)$  randomly between  $-3 < w(z)^0 < 1$ . After 1000 inversions with different priors in that range, we determine the absolute minimum and calculate the mean of those inversions and  $1\sigma$  intervals as the zone where 68.27% of the solutions lie. We checked that increasing the number of inversions does not change the results.

The final reconstruction can be seen in Figure 7.3(a) for R06 data and in Figure 7.4(a) for VW07. The inversions with a minimum  $S$  (dotted line) have priors close to  $w = -1$ :  $-0.83$  and  $-1.05$  respectively, and so, best fits are close to those in Figure 7.1 and Figure 7.2. The (b) panels in both figures add another contribution to the uncertainty. In these cases, reconstructions are made using 1000 data sets generated via bootstrap resampling of the original ones.

Within the Monte Carlo and bootstrap errors both sets are compatible at  $1\sigma$  with a cosmological constant. Although we get now some improvement, that was already observed in Figure 6.7(c) and (d). With that parameterization, we obtained the best fit values at present, and the error propagation at higher redshift made the confidence intervals huge. With this continuous determination, the best constrained

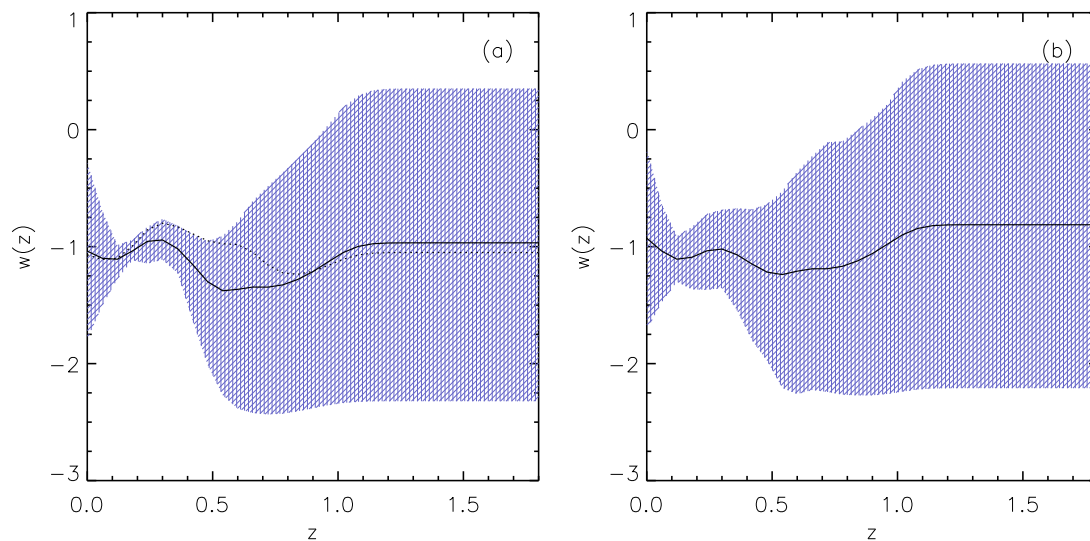


Figure 7.4: As in Figure 7.3 but for VW07 SNe Ia. The two data sets show its maximum discrepancy in the range  $0.5 < z < 1.0$ .

zone is that at intermediate redshift where the method exploits the larger number of supernovae. Therefore, the statement about the cosmological constant result should better be addressed using a reconstruction along redshift.

Results in Figure 7.3 agree with other reconstructions with R06 data such as the maximum entropy approach in [213] or the principal component analysis in [160]. In all cases the results are compatible with a cosmological constant, but the trend towards a higher  $w$  at  $z \approx 0.5$  is always present. The maximum entropy approach of Zunckel and Trotta (2007) shows a closer agreement with a cosmological constant for the SNLS data set (Ref. [14]). This sample is part of VW07, for which our inverse approach favours lower  $w$  as well. In our results, there is a departure from the cosmological constant towards the phantom side between  $0.5 < z < 1.0$  (Figure 7.4(b)) and even in a smaller range for the best inversions, but we have seen that the kernels in this interval indicate a bad resolution in the reconstruction. Anyway, the departure is at most  $0.25\sigma$ , and, therefore, not significant in a similar way as for R06 but with larger  $w$ s.

As it happened with the discrete parameterizations from previous chapter, we find no serious evidence for an evolving equation of state. On the light of current data sets, the cosmological constant is still the best bet, although lots of alternative dark energy models (too many!) cannot be discarded. Besides all the other

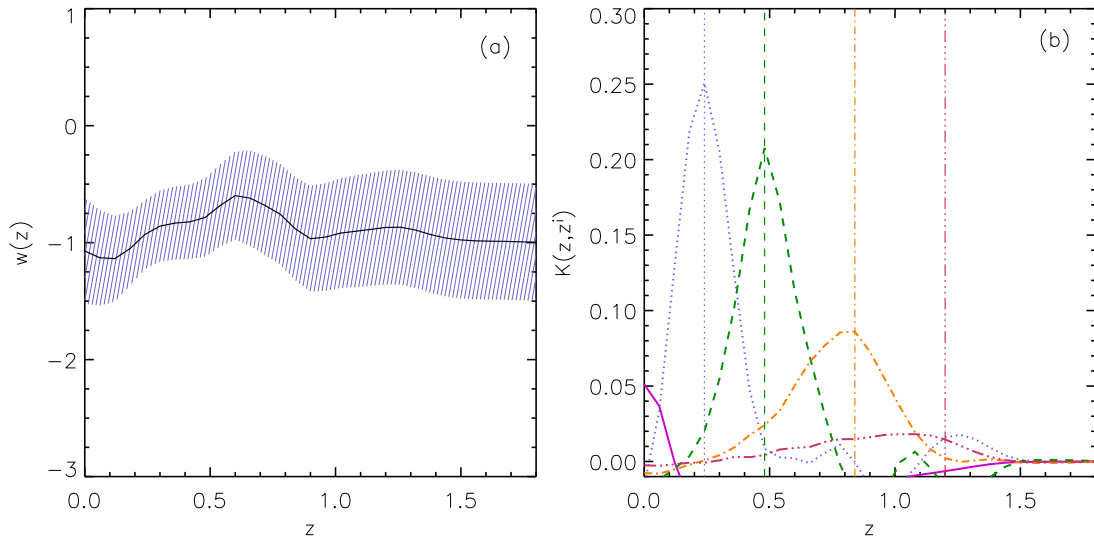


Figure 7.5: Reconstruction of  $w(z)$  (as in Figure 7.1) but with the 192 SNe from Davis et al. (2007) [56].

degenerate models which will never be ruled out, an evolving cosmological constant, quintessence fields, Cardassian models, DGPs, and others can be accommodated within  $1\sigma$  confidence intervals in the redshift range where there are enough data.

### 7.3.2 Near future results

Just as it was done in Chapter 6, we also include the confidence intervals obtained with the full compilation of SNe Ia of Ref. [56].

The presence of the highest redshift supernovae in R06 is enough to keep the ascent towards a larger  $w$  in the best inversion when only one realization of the data set is used (see Figs. 7.5 and 7.6 (a)). However, the bootstrap resampling of the set makes stronger the dominant sample, VW07, and for the mean of all the inversions the trend disappears (Fig. 7.6 (b)). In all the cases, the ascent is not significant within  $1\sigma$  intervals.

The reconstruction, then, resembles even more that of a cosmological constant than the ones for previous data sets, as it is expected from the separated behaviour. But the inclusion of more SNe Ia and the elimination of those with less credibility

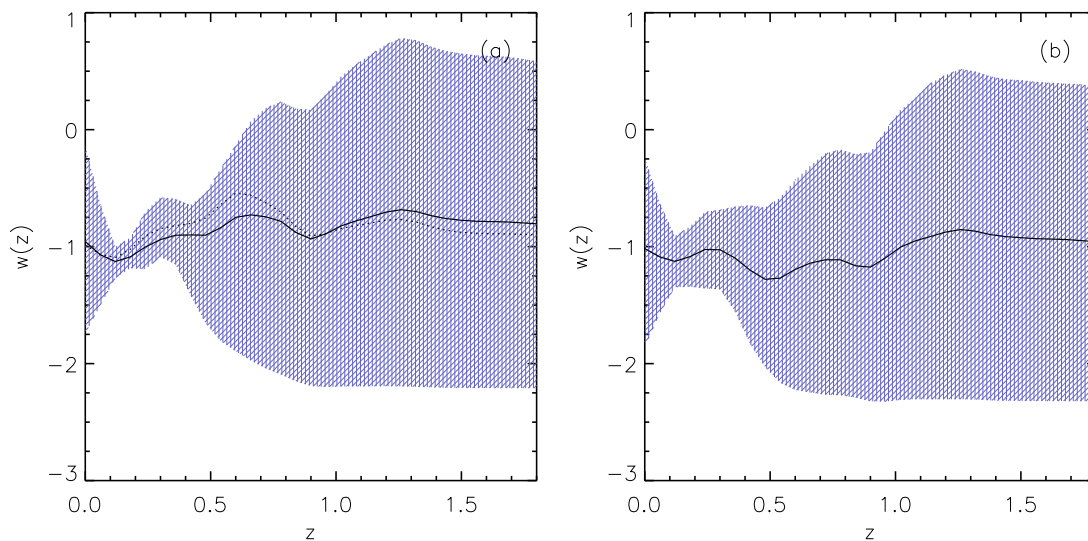


Figure 7.6: The same as in Figure 7.3, for the compilation in Ref. [56].

does not improve the size of the confidence intervals around the best  $w(z)$ . So, even though the combination of both samples does not help to obtain a more precise result, it is necessary to gain in accuracy given the difference in the general trends reflected by the two data populations.

## 7.4 Determination of a parameterized $w(z)$

Now, we leave the continuous reconstructions of  $w(z)$  to analyse the commonly used parameterization  $w(z) = w_0 + w_a z / (1 + z)$ . Although the present method has not been designed to perform parameterized fits, where other methodologies are more adequate, it can be easily extended to do that (Section 7.2.2).

The incorporation of priors on the equation of state, which are vital to regularize the inversion in the continuous case, loses part of its meaning now but they are still used in the same way they were used to include additional information in the  $\chi^2$  analysis.

As a first test, we directly apply Equations 7.32 and 7.33 to obtain the values which minimize the misfit function  $S$ . Table 7.1 shows the results for different choices of the *a priori* models. The uncertainties are given by Equations 7.36 and 7.37 as obtained with the inverse method. These are still dependent on the *a priori*

	$\Omega_M^0$	$w_0$	$w_a$	$S_{min}$
<i>Prior</i>	$0.27 \pm 0.03$	$-1 \pm 10$	$0 \pm 0$	
R06	$0.24 \pm 0.02$	$-0.94 \pm 0.12$	0	86.47
VW07	$0.28 \pm 0.02$	$-1.09 \pm 0.12$	0	67.64
D07	$0.29 \pm 0.02$	$-1.01 \pm 0.12$	0	81.47
<i>Prior</i>	$0.27 \pm 0.03$	$-1 \pm 10$	$0 \pm 10$	
R06	$0.25 \pm 0.02$	$-1.6 \pm 0.2$	$+4 \pm 1$	79.09
VW07	$0.27 \pm 0.02$	$-0.7 \pm 0.3$	$-3 \pm 2$	66.83
D07	$0.29 \pm 0.02$	$-1.1 \pm 0.3$	$+0.4 \pm 1.5$	81.45

Table 7.1: Priors, results and  $1\sigma$  errors for  $\Omega_M^0$ ,  $w_0$  and  $w_a$  as obtained from the inverse method in the discrete case and for three different SNeIa data sets: R06 [160], VW07 [211] and D07 [56].

uncertainty, but we are able to set much larger priors in the discrete case than before and, therefore, the dependence is less important. Together with the best fits for the parameters, we also include the value of  $S_{min}$ . This number is only useful for comparisons between inversions of different sets using the same priors, but it does not provide statistical information for the same reason we could not give  $p$ -values when adding a prior in the  $\chi^2$  analysis.

On the contrary than for the equation of state parameters, the inversion showed to be sensitive to the value of  $\Omega_M^0$ , and large covariances for its prior caused the non-convergence of the algorithm. This is why we used very strict priors in comparison to the ones for  $w_0$  and  $w_a$ ; we use  $\Omega_M^0 = 0.27 \pm 0.03$  as it is being done throughout the thesis.

Results for a constant equation of state with such a density of matter are compatible at  $1\sigma$  level with a cosmological constant, in a similar way as it happened with the  $\chi^2$ . However, when allowing an evolution, R06 data still prefers a positive evolution whereas it is negative for VW07. Notice that results with the same prior (Tables 6.5 and 7.1) do not lead exactly to the same minimum. We attribute this to the fact that the minimum valleys are extremely flat in some cases, and secondary minima close to the absolute one can appear. In any case, results for the equation of state of the two methods agree at  $1\sigma$  level.

The size of the uncertainties is of the same order of magnitude here and in

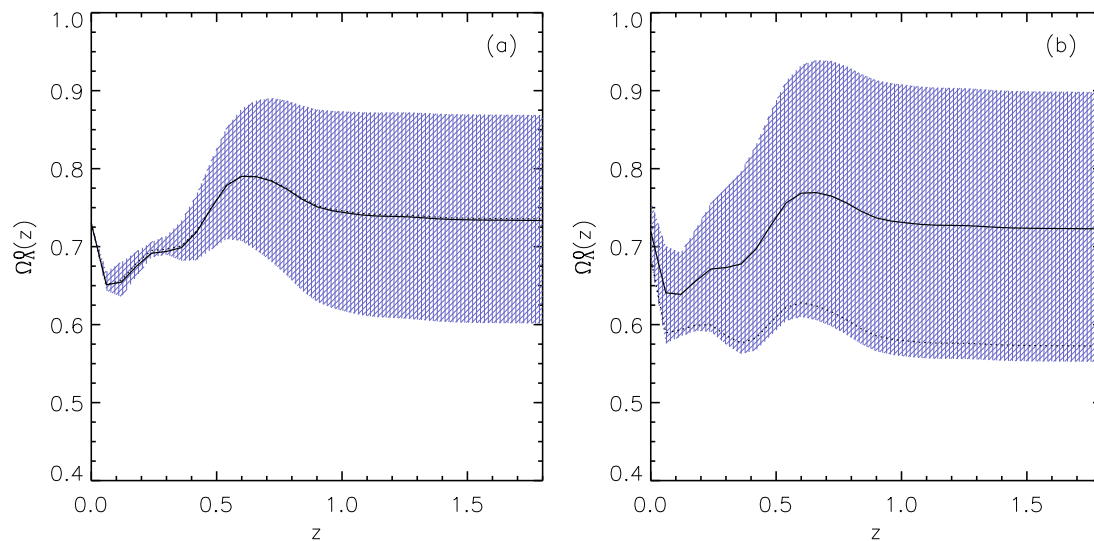


Figure 7.7: (a) Evolution of the cosmological constant along redshift obtained from R06 data. 1000 inversions with random priors in the range  $-0.2 < \Delta\Omega_{\Lambda}^0(z) < 0.2$  and a fixed  $\Omega_M^0 = 0.27$  have been used. The mean (solid line) and the inversion with a minimum  $S$  (dotted line) are almost superposed. (b) As (a) but with a softer prior on the matter density  $\Omega_M^0 = 0.27 \pm 0.03$ .

the  $\chi^2$  estimation, proving that, for wide enough priors, errors obtained with this methodology are independent of the *a priori* uncertainty. We also checked the effect by doubling the nominal value of  $\sigma = 10$  and obtain no change.

## 7.5 A running cosmological constant as an inverse problem

To finish this chapter, we return to continuous reconstructions and use the power of the inverse method to detect an evolution of the cosmological constant. Due to the context of this thesis, we interpret the unknown function as a running cosmological constant as introduced in Chapter 3, but it is, in fact, a general function which accounts for the dark energy density.

In Chapter 3, we showed equations for a running lambda in three different scenarios, but all of them were parameterized and depended only on discrete parameters. Here, we fit a general function for all the scenarios in a similar way as we did in

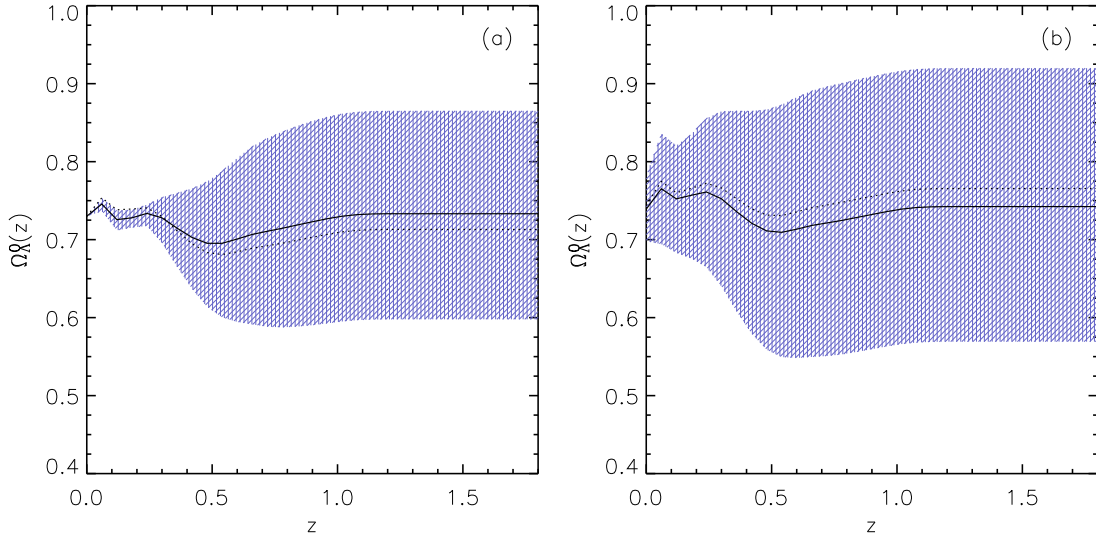


Figure 7.8: Evolution of the cosmological constant as in Figure 7.7 but for the VW07 data set.

the previous chapter (Eq. 6.11), but now there is no need to be content with a Taylor development to first order. Therefore, we want to determine a general function  $\Delta\Omega_\Lambda^0(z)$  such that

$$H^2(z) = H_0^2 [\Omega_M^0 (1+z)^3 + \Omega_\Lambda^0 + \Delta\Omega_\Lambda^0(z)] , \quad (7.38)$$

where we assume a flat universe (notice that in a flat universe  $\Delta\Omega_\Lambda^0(z=0) \equiv 0$ ). Following the notation of Part I the sum is  $\Omega_\Lambda^0(z) = \Omega_\Lambda^0 + \Delta\Omega_\Lambda^0(z)$ . The expression 7.18 can be used to iteratively calculate the form of the best  $\Omega_\Lambda^0(z)$  by substituting  $\partial y^{th}/\partial \Delta\Omega_\Lambda^0(z)$ .

In a flat universe, the value of the cosmological constant  $\Omega_\Lambda^0$  is fully determined by  $\Omega_M^0$ . In the following, we test two different situations: one with a fixed  $\Omega_M^0 = 0.27$  and, therefore, a fixed  $\Omega_\Lambda^0 = 0.73$ ; and another one allowing a small variation  $\Omega_M^0 = 0.27 \pm 0.03$  as in previous sections. If we knew the true density of matter, fixing its value would really allow us to see the evolution  $\Delta\Omega_\Lambda^0(z)$  alone. However, that is nowadays a too severe assumption and the small uncertainty at least must be considered.

The setup for the inversion is the same as for the barotropic index of the equation of state with two modifications related to the function. The uncertainty on the prior

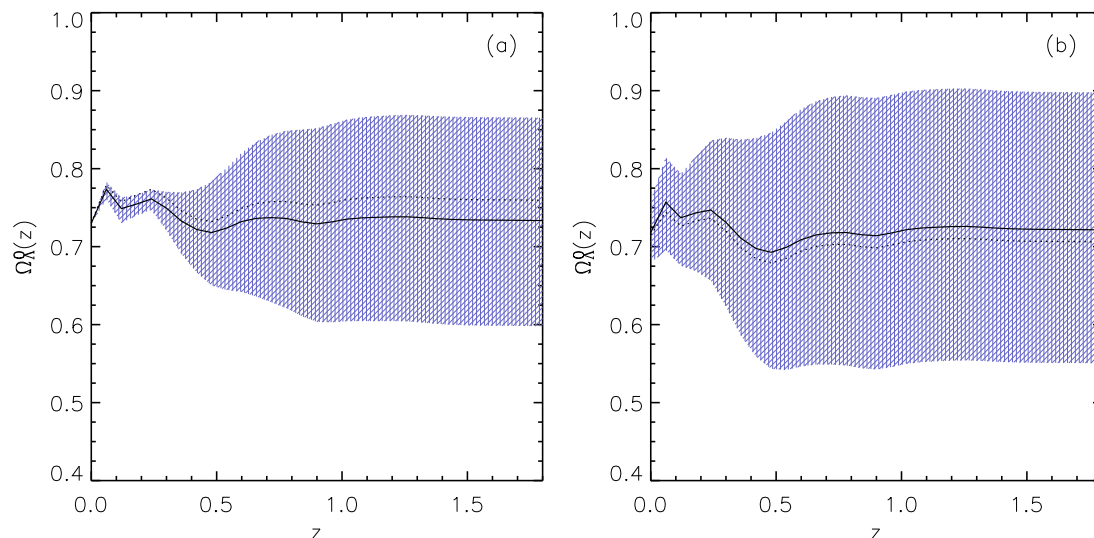


Figure 7.9: Reconstruction of  $\Omega_{\Lambda}^0(z)$  using 1000 sets as in Figure 7.7 and 7.8. The data compilation in D07 is used.

on  $\Delta\Omega_{\Lambda}^0(z)$  is set to  $\sigma(z) = 0.1$ , unless in the case of a fixed  $\Omega_M^0$  where we force the first point at redshift zero to have no uncertainty  $\sigma(z = 0) = 0$ . The Monte Carlo exploration of the  $\Omega_{\Lambda}^0(z)$ -space is made in the range  $-0.2 < \Delta\Omega_{\Lambda}^0(z) < 0.2$ . Since we are using the same data sets as in previous sections, we expect the same resolution, calculate the same number of points and obtain a similar interval where data can shed light into the problem.

With the 182 SNeIa in R06, one recovers the strongest evolution (Fig. 7.7) as we already noticed in the reconstruction of the equation of state. However, fixing  $\Omega_M^0 = 0.27$  proves to be a too strict prior. The best fit for the density of matter in the discrete  $\chi^2$  test was found in Chapter 6 to be  $\Omega_M^0 = 0.35$ , and this difference creates a jump between the first fixed point at  $z = 0$  and the first free point at  $z = 0.06$  in our reconstruction. As a matter of fact, this is the only data set which favours a model far from the conservative prior. Rather than a forced evolution, the inversion opts for a constant  $\Omega_{\Lambda}^0(z)$  but at a higher density of matter. This is represented in Figure 7.7 (b), where there is more freedom for  $\Omega_M^0$  and the reconstruction with the minimum  $S$  is found for a larger value of  $\Omega_M^0$  (dotted line in the plot).

For the other two samples, VW07 and D07, the result of the inversion is quite similar. A constant density cannot be discarded although at intermediate redshifts there is a soft trend with negative slope. As for the equation of state, one cannot

trust the reconstruction further in redshift than 0.6, since there the prior is recovered.

These reconstructions can be compared to the behaviour of the cosmological constant in the running scenarios. All models predict a smooth and monotonous evolution (see Figures 3.1(b) and 3.2(b)<sup>1</sup>) which need reliable reconstructions to higher redshifts so as to be tested. Up to now, the obtained smooth evolutions down to redshifts lower than 1 are compatible with the three scenarios of Chapter 3 as well as with most of dark energy models. Of course, an abrupt change in the equation of state would be much more informative, but after the results we have obtained in the two last chapters it seems that if we are not living in a Universe with a cosmological constant it at least behaves as if it were. So, in order to improve our knowledge we do need to improve our current data. We devote the following chapter to see which are our future perspectives according to the already planned supernova new experiments.

---

<sup>1</sup>A one to one comparison must be done after changing the  $y$ -axis to  $\Lambda/\rho_c^0$ .



## Chapter 8

---

# Future perspectives

---

As a final application of the methodology used throughout the thesis, this chapter exploits the higher quality of oncoming surveys' data for the study of dark energy. The degradation of the results due to photometric redshifts is especially analysed as a common drawback of most of future experiments, and some indications to minimize its effects are given.

### 8.1 Oncoming surveys

After the discovery of the accelerated expansion of the Universe [145, 158] a new satellite observatory (SuperNova Acceleration Probe, *SNAP* [179]) was proposed to determine the nature of the dark energy that causes the acceleration. That was in 1999, and, since then, the number of proposed SNeIa surveys has grown exponentially, and SNAP is now one of the competing missions to be launched within JDEM (Joint Dark Energy Mission).

Some of the experiments are designed as ground telescopes and can observe supernovae at low and intermediate redshift. For really high redshifts, where objects are too weak and redshifted to be seen from the Earth, satellites must be launched to space. Observing from space is a way to lower systematics as well, and some of the projects combine ground and space observations. In fact, these surveys are already reaching the time when the precision in the results is limited by systematics, hence the necessity of the improvement. Considering systematics and the intrinsic

dispersion of SNe Ia as two independent error sources, they sum up quadratically,

$$\sigma = \sqrt{\frac{\sigma_{intr}^2}{N} + \sigma_{sys}^2}, \quad (8.1)$$

where it has been assumed that systematic errors between supernovae are only correlated for supernovae in the same redshift bin:

$$\sigma_{sys,i,j}^2 = \begin{cases} \sigma_{sys}^2 & \text{for } i, j \in \text{bin } k \\ 0 & \text{otherwise} \end{cases}. \quad (8.2)$$

Since the intrinsic error diminishes with the number of supernovae, its effect is going to be negligible just with a few tens of objects per bin.

The assortment of acronyms in current literature is extensive: SNFactory [180], CSP [53], SDSSII [172], SNLS [181], ESSENCE [76], PANS [141], DES [59], LSST [126], Pan STARRS [140], SNAP [179], DESTINY [60], JEDI [113], ADEPT [2], DUNE [63], ALPACA [7], etc. Due to the importance of using complementary probes for cosmology, experiments are usually designed to combine two or more of the crucial tests. All of the above surveys have SNe Ia as one of the main science objectives, but usually they join SNe Ia with lensing or with baryonic acoustic oscillations.

We do not simulate all of the planned experiments, but select the most representative ones. As an archetype at high redshift we consider SNAP for tradition; LSST is taken as the ground-based experiment, because of the large amount of data it will gather ( $\sim 250000/\text{yr}$ ).

One can see that the order of magnitude of observations in SNe Ia surveys is increasing tremendously and that has deep consequences into the treatment and analysis of the data. The first generation of surveys only compiled a few supernovae, which were analysed by hand taking care of every single detail. Ongoing experiments already reaching a few hundreds of objects recur to automatic methods to classify, calibrate the light curve, treat the extinction, etc. Future massive surveys will need a completely automated process and even the storage of data will be complicated. That impressive amount of information assures very rich statistics so that only the best and selected objects will be used for cosmology.

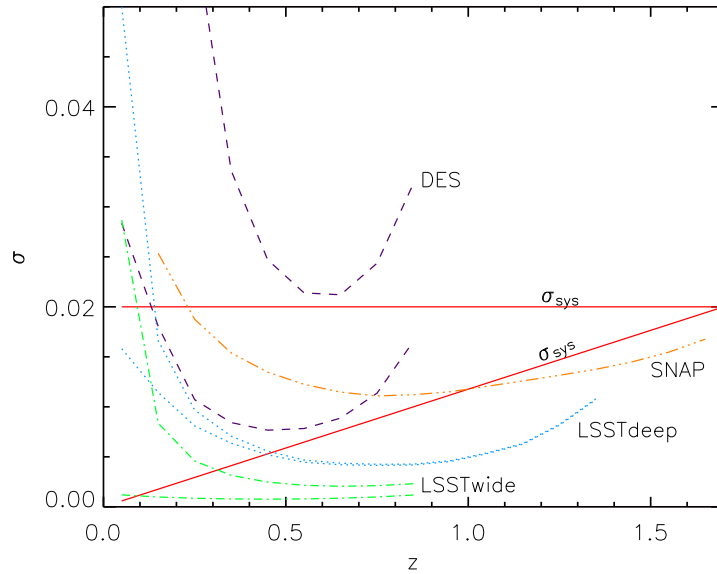


Figure 8.1: Uncertainties for different surveys as a function of redshift. Red solid lines indicate two different assumptions for systematic uncertainties. Dashed lines show the variation in the uncertainty due to the intrinsic dispersion according to the number of SNeIa of each survey. When two lines for the same mission are shown, the one with a larger uncertainty includes photo- $z$ 's errors as well (see text for values).

### 8.1.1 Generating data distributions

In order to simulate observations for the chosen experiments we generate Gaussian distributions in the redshift ranges announced by the collaborations. Data are binned in intervals of width  $\Delta z = 0.1$  and each interval is characterized by its mean redshift. Then, we calculate the magnitude for these supernovae within a given cosmological model. In each case, observational Gaussian errors are added to these values taking into account the systematic uncertainties and the intrinsic dispersion for SNeIa. After the corresponding calibrations, the intrinsic dispersion of supernovae is  $\sigma_{intr} = 0.15$ . For systematics, we either consider a constant  $\sigma_{sys}$  or a linear increment such as for instance [206]:  $\sigma_{sys} = z (0.02/1.7)$ . In some cases such as for low redshift samples systematics are ignored. The behaviour of other observational uncertainties, i.e., photo- $z$ 's in our case, is the same as for the intrinsic one. In the following, the specifications of the surveys are outlined.

$\langle z \rangle_{bin}$	$N(z)$			
	SNFactory	LSSTwide	LSSTdeep	SNAP
0.05	285	15785	90	0
0.15	15	23258	172	35
0.25	0	30733	344	64
0.35	0	36113	556	95
0.45	0	38351	832	124
0.55	0	36224	1132	150
0.65	0	30412	1269	171
0.75	0	23023	1312	183
0.85	0	16098	1286	179
0.95	0	0	1099	170
1.05	0	0	800	155
1.15	0	0	574	142
1.25	0	0	338	130
1.35	0	0	196	119
1.45	0	0	0	107
1.55	0	0	0	94
1.65	0	0	0	80
# SNe	300	250000	10000	2000
$\langle z \rangle$	0.05	0.45	0.75	—
$\sigma_{\langle z \rangle}$	0.03	0.30	0.30	—
limit		$z < 0.9$		

Table 8.1: Number of SNe Ia per bin for the surveys analysed in this chapter. Redshifts correspond to the centre of the bin. All distributions are drawn from a Gaussian with parameters as indicated in the bottom lines. The proposed SNAP distribution can be found in Ref. [118].

### SNFactory

The Nearby Supernova Factory is an ongoing survey at low redshift with expectations of discovering around 300 SNe Ia at  $0.03 < z < 0.08$  [5]. Besides of being an experiment designed to improve the calibration of SNe Ia, it will be the low redshift sample for some of the high redshift missions. In this case, we assume it is free of systematics, although peculiar motions or a different photometric calibration with respect to the high redshift set could damage the results. It has been simulated as

a Gaussian with mean  $\langle z \rangle = 0.05$  and  $\sigma_{\langle z \rangle} = 0.03$ . As for all the other cases, the number of supernovae per bin can be read in Table 8.1.

### LSST

The Large Synoptic Survey Telescope is a 8.4 *m* ground telescope with a 6.5 *m* effective diameter which will scan the sky continuously [195]. That will allow to detect around 250000 SNeIa per year and get a photometric point every five days in *r* band and every fifteen days in *g*, *b* and *i*. Only 10000 objects with  $z < 0.17$  and 10000 more with  $z < 0.30$  can be expected to have spectroscopic redshifts for this wide search. The enormous number of data is more than enough to use only selected objects for cosmology and to choose various subsets. The mean redshift of this survey is specified to  $\langle z \rangle = 0.45$  and it will detect supernovae at  $z < 0.9$  although its deep search will reach 1.4 with a mean of 0.75. The dispersion of the distribution is set to  $\sigma_{\langle z \rangle} = 0.30$ .

### SNAP/JDEM

The SuperNova Acceleration Probe collaboration aims to obtain spectra and photometry for 2000 supernovae within two years of mission [179]. The distribution of supernovae will have a maximum in the interval  $0.2 < z < 1.2$  where according to the present observed rates around 1800 supernovae should be found. A smaller number of data is expected to be gathered up to a redshift of 1.7 (see more details in [179]). In all the calculations we consider the fiducial SNAP simulation to be that of Ref. [118].

## 8.2 The best perspectives from Earth

Ground surveys encompass a wide redshift range, from the low redshift campaigns to the ones reaching redshift one, where the redshifted light meets with a too bright sky in the red.

A low redshift sample is always necessary to fix the zero point, and then a higher sample is needed in order to check the cosmology. The design of the surveys is of course different for different redshift ranges and, therefore, at least two different surveys are usually needed. In that case, we take SNFactory as the low-*z* sample

for the study of the equation of state. As an exception, the LSST wide survey with more than 15000 SNe at  $z < 0.1$  does not need an independent survey, in spite of the increment in the uncertainty due to photo- $z$ 's at low redshift.

### 8.2.1 LSST wide survey

Such a massive survey as LSST will be then self-sufficient and will obtain a low redshift anchor with an unprecedented quality without the necessity of an independent low- $z$  sample. However, not every supernova will have a spectroscopic redshift: the instrument itself could measure about 10000 spectra per year at  $z < 0.17$  if a fiber spectrograph were attached, and one could measure another 10000 at  $z < 0.30$  with LAMOST (Large sky Area Multi-Object Spectroscopic Telescope) for instance. We call such a distribution *wide A*. A distribution with all 20000 SNe Ia with spectroscopic redshifts at low- $z$  ( $z < 0.12$ ) is also used and referred to as *wide B*. For the remaining supernovae, only the photometric redshift will be available.

As seen graphically in Figure 8.1, the error in the magnitude for an spectroscopic survey ( $\delta z = 0$ ) with the characteristics of the LSST wide survey falls down to zero. Therefore, one obtains the minimum confidence regions for a survey reaching  $z = 0.9$  with this configuration. But that cannot be taken as a realistic result because of two reasons: photo- $z$ 's worsen the uncertainty on magnitudes, above all at low- $z$ , and systematics cannot be zero for a real experiment. The observational challenge is then to minimize both quantities.

Table 8.2 shows the uncertainties on the cosmological parameters and on the parameters describing the dark energy equation of state according to the accuracy in photo- $z$ 's determination. For an ideal error-free photo- $z$ , both of the cosmological parameters are determined with a 1% precision. The precision is good enough so that BAO constraints cannot improve the results. The same happens for a constant equation of state. The maximum difference between dark energy models close to a  $\Lambda$ -CDM where data have been simulated and those without dark energy is found at  $z \approx 0.5$ . Therefore, the large concentration of data around this redshift allows a precise determination of  $w_0$  as well as that of the combination of  $w_0$  and  $w_a$ . Even with this maximum precision, a small evolution cannot be discarded when pointing to a cosmological constant.

		LSSTwide			
Uncertainty:	Priors	$\sigma_{\Omega_M^0}$	$\sigma_{\Omega_X^0}$	$\sigma_{w_0}$	$\sigma_{w_a}$
$\sigma_{intr}=0.15,$ $\delta z = 0.00$	CC	0.004	0.008	-	-
	CC + BAO	0.004	0.008	-	-
	CC + BAO2	0.004	0.008	-	-
	flat	0.005	-	0.013	-
	flat + BAO	0.005	-	0.013	-
	flat + BAO2	0.004	-	0.012	-
	flat + $\sigma_{\Omega_M^0}$	-	-	0.02	0.32
$\sigma_{intr}=0.15,$ $\delta z = 0.08$	CC	0.018	0.049	-	-
	CC + BAO	0.013	0.035	-	-
	CC + BAO2	0.008	0.023	-	-
	flat	0.021	-	0.081	-
	flat + BAO	0.015	-	0.051	-
	flat + BAO2	0.009	-	0.033	-
	flat + $\sigma_{\Omega_M^0}$	-	-	0.08	0.60
$\sigma_{intr}=0.15,$ $\delta z = 0.08,$ 20000 SNe $\delta z = 0$ (wide A)	CC	0.017	0.042	-	-
	CC + BAO	0.012	0.032	-	-
	CC + BAO2	0.008	0.021	-	-
	flat	0.020	-	0.072	-
	flat + BAO	0.012	-	0.048	-
	flat + BAO2	0.009	-	0.032	-
	flat + $\sigma_{\Omega_M^0}$	-	-	0.07	0.58
$\sigma_{intr}=0.15,$ $\delta z = 0.08,$ $\delta z = 0 @ z < 0.12$ (wide B)	CC	0.012	0.018	-	-
	CC + BAO	0.010	0.015	-	-
	CC + BAO2	0.007	0.012	-	-
	flat	0.012	-	0.031	-
	flat + BAO	0.010	-	0.027	-
	flat + BAO2	0.008	-	0.020	-
flat + $\sigma_{\Omega_M^0}$	-	-	0.03	0.36	

Table 8.2:  $1\sigma$  uncertainties in the determination of the cosmological parameters and the dark energy equation of state according to the error in photo- $z$ 's for the LSST wide survey in a universe filled with cosmological constant. See text for the description of the four cases.

Photo- $z$ 's uncertainty degrades the results. For  $\delta z = 0.08$  the uncertainty on a constant equation of state increases from a 1% to an 8%, but the inclusion of current BAO constraints diminishes the error to 5%. Notice that this BAO constraint is that measured from observations in Ref. [70], therefore the underlying model does not need to be the same as that of the simulation, the result being an upper limit. BAO2 is a future expectation to be obtained at  $z = 0.55$  (see Section 5.3.2) calculated for the same fiducial model. The addition of BAO2 improves up to a 3% for  $\sigma_{w_0}$ , still more than doubling the results with  $\delta z = 0$ . These variations can be seen graphically in Figure 8.2. As for the variation of the equation of state, the uncertainties are doubled too. Hence the importance of the determination of photo- $z$ 's.

The value for  $\delta z = 0.08$  is that given through simulations for the DES survey [194] which is supposed to be LSST's precursor. However, the exact value can vary and improve with the experience gained with surveys previous to LSST. On the other hand, the error on photo- $z$ 's is less significant in the LSST wide survey than in more limited ones such as DES which has just a hundredth of LSST's data. Photo- $z$ 's uncertainties are random errors that reduce as a whole with an increasing number of supernovae. They are still important at low- $z$  where they can alter more than one magnitude the measured value of an individual object. The obtention of spectroscopic measurements randomly along redshift or only at high redshift to complement the survey does not improve the uncertainty on the unknown parameters. The best improvement is reached by measuring spectroscopic redshifts for the nearest SNe Ia. As explained above, current plans aim to obtain spectra for 20000 supernovae with  $z < 0.3$ . That only represents a 30% of the objects in that interval. But, at  $z = 0.3$ , the effective uncertainty due to the sum of the intrinsic dispersion and photo- $z$ 's is just  $\sigma = 0.005$ , well below systematics. When concentrating the efforts to measure spectra for supernovae at really low- $z$  were  $\sigma > 0.01$ , uncertainties in the parameters should decrease. That can be seen by comparing the results retrieved with distribution wide A and wide B (Table 8.2). 20000 spectroscopic redshifts distributed as in wide A do almost not improve determinations with respect to the whole sample with  $\delta z = 0.08$ . On the other hand, wide B reduces uncertainties to one half. It does not fully compensate the effect of photo- $z$ 's and results do not reach the precision of an equivalent spectroscopic survey. However, given the impossibility to obtain such a large number of spectra, wide B results demonstrate that efforts must be made in order to at least measure spectra in the low- $z$  range. Given this fact, we checked whether the inclusion of the SNFactory SNe Ia could help, but even with photo- $z$ 's with  $\delta z = 0.08$  results were exactly the same because there are 50 times more SNe Ia

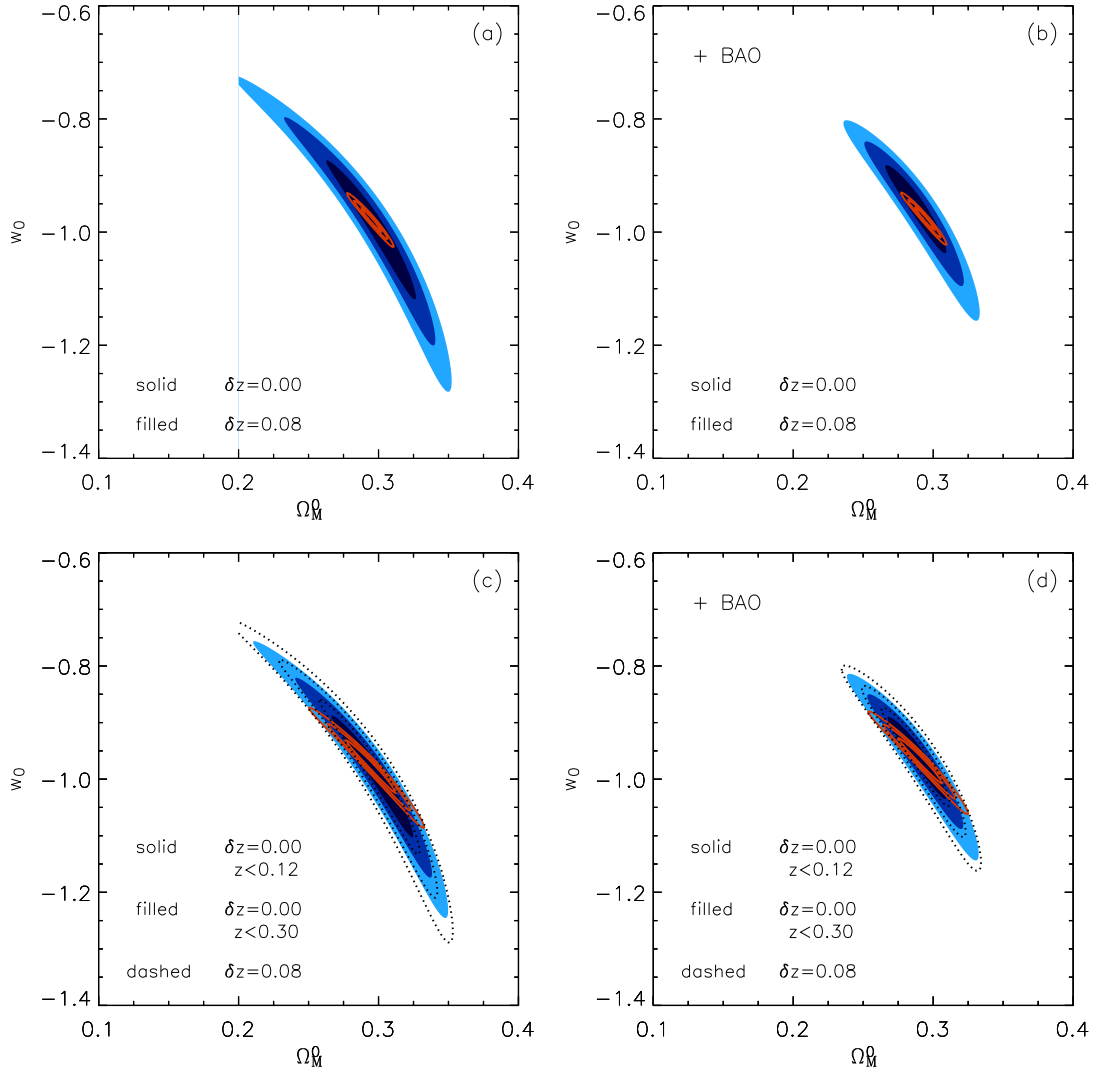


Figure 8.2:  $1\sigma$ ,  $2\sigma$  and  $3\sigma$  confidence regions in the  $(\Omega_M, w_0)$  plane with the addition of different sources of uncertainty related to photometric redshifts (see text). Systematics are not included. Results are obtained with 250000 LSST wide SNe Ia.  $1\sigma$  intervals for the individual parameters can be read in Table 8.2.

at  $z < 0.1$  with photometric redshift than with spectroscopic redshift.

The same argument of the number of supernovae per bin is valid for catastrophic errors as well. Its effect should be more important in a smaller survey such as DES, but even in that case there is no damage in the equation of state for a 2% of redshifts with catastrophic errors, and one needs a 10% to worsen  $w_0$  a 6%. Nevertheless, 10% is a big number compared to what is observed through simulations, and besides,

Uncertainty:	Priors	LSSTwideA				LSSTwideB			
		$\sigma_{\Omega_M^0}$	$\sigma_{\Omega_X^0}$	$\sigma_{w_0}$	$\sigma_{w_a}$	$\sigma_{\Omega_M^0}$	$\sigma_{\Omega_X^0}$	$\sigma_{w_0}$	$\sigma_{w_a}$
$\sigma_{sys} = 0.02$	CC	0.120	0.26	-	-	0.083	0.12	-	-
	CC + BAO	0.019	0.07	-	-	0.019	0.03	-	-
	CC + BAO2	0.014	0.06	-	-	0.010	0.02	-	-
	flat	0.153	-	0.43	-	0.087	-	0.21	-
	flat + BAO	0.020	-	0.08	-	0.019	-	0.05	-
	flat + BAO2	0.013	-	0.06	-	0.011	-	0.03	-
	flat + $\sigma_{\Omega_M^0}$	-	-	0.38	1.68	-	-	0.14	0.94
$\sigma_{sys} = 0.04$	CC	0.230	0.48	-	-	0.150	0.18	-	-
	CC + BAO	0.023	0.12	-	-	0.020	0.05	-	-
	CC + BAO2	0.020	0.11	-	-	0.012	0.04	-	-
	flat	0.210	-	0.70	-	0.190	-	0.42	-
	flat + BAO	0.023	-	0.12	-	0.020	-	0.06	-
	flat + BAO2	0.018	-	0.11	-	0.012	-	0.05	-
	flat + $\sigma_{\Omega_M^0}$	-	-	0.68	3.03	-	-	0.28	1.79

Table 8.3: Uncertainties in the determination of the cosmological parameters and the dark energy equation of state adding systematic uncertainties to a LSST deep survey set with both distributions wide A and wide B. The intrinsic dispersion  $\sigma_{intr} = 0.15$  is included as well.

catastrophic errors can be easily detected in a Hubble diagram, and so, most of these supernovae could be excluded beforehand.

The other factor to be concerned about when using a specific survey to constrain dark energy is systematics. A reasonable value for systematics on a ground survey is to take  $\sigma_{sys} = 0.02$ , although reaching this value is a technical challenge. We also check the precision of the determinations for the more conservative value of  $\sigma_{sys} = 0.04$ . Results for these two assumptions are tabulated in Table 8.3. Of course, the final uncertainty does depend on photo- $z$ 's as well. At low- $z$ , they are the dominant source of uncertainty, and for  $z < 0.2$  they still affect the result. This is evident for wide A distribution, but for wide B the improvement is due to the only contribution of systematics.

The addition of systematics worsens the determinations of the raw sample up to an order of magnitude. For the moderate value, the cosmological parameters are

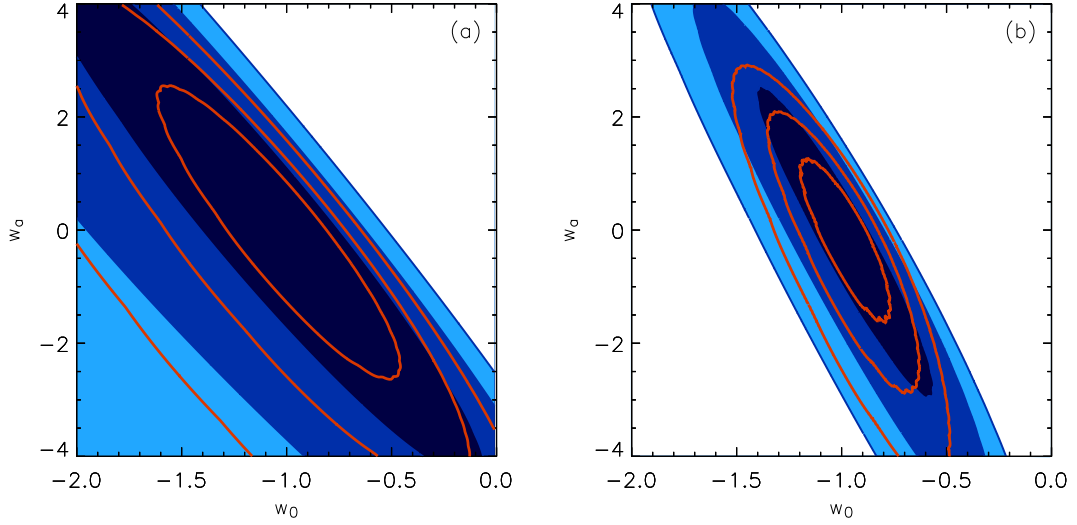


Figure 8.3: (a) Effect of photo- $z$ 's and systematics on  $1\sigma$ ,  $2\sigma$  and  $3\sigma$  confidence regions for the parameters describing the evolution of the equation of state as retrieved from the LSST wide A survey data. The contours have been obtained imposing a prior  $\sigma_{\Omega_M^0} = 0.03$  before marginalizing over. Solid filled regions add  $\sigma_{sys} = 0.04$  to results with wide A configuration. The solid red lines reduce systematics to  $\sigma_{sys} = 0.02$ . (b) The same as (a) with the addition of the 20000 spectroscopic redshifts for SNe Ia with  $z < 0.12$  (wide B).

determined with a precision close to that obtained with current data sets reaching much higher redshifts<sup>1</sup>. A similar thing happens with a constant equation of state, just the wideB configuration appreciably improves the determination of  $w_0$ . That is worse for the widest systematic uncertainty  $\sigma_{sys} = 0.04$ . However, even if the precision were not better than our actual knowledge, such a survey would let us gain in accuracy given the selfconsistency of the data. The parameter accounting for the evolution,  $w_a$ , is the most favoured by the high density of data, and using information about  $\Omega_M^0$  allows to obtain  $\sigma_{w_a} = 0.94$ . That is doubled with systematics, but keeping systematics around  $\sigma_{sys} = 0.02$  and taking care of photo- $z$ 's would be enough to diminish almost a factor two the current state of the art. In fact, the determination of all the parameters showed to be very sensitive to the distribution of spectroscopic redshifts even when systematics are added. The improvement of LSST wideB with respect to LSST wide A is close to divide by two the uncertainties for both levels of systematics before applying BAO constraints. Once they are used

<sup>1</sup>Notice that we are comparing current results where only statistical errors were given.

too, photo- $z$ 's are equally important for the parameters related to dark energy, but the determination of the density of matter is mostly conditioned by BAO.

The power of the LSST wide survey given an error model is limited by its redshift extent. This is why the deep configuration reaching  $z = 1.4$  with a careful determination of photo- $z$ 's is supposed to improve these results.

### 8.2.2 LSST deep survey

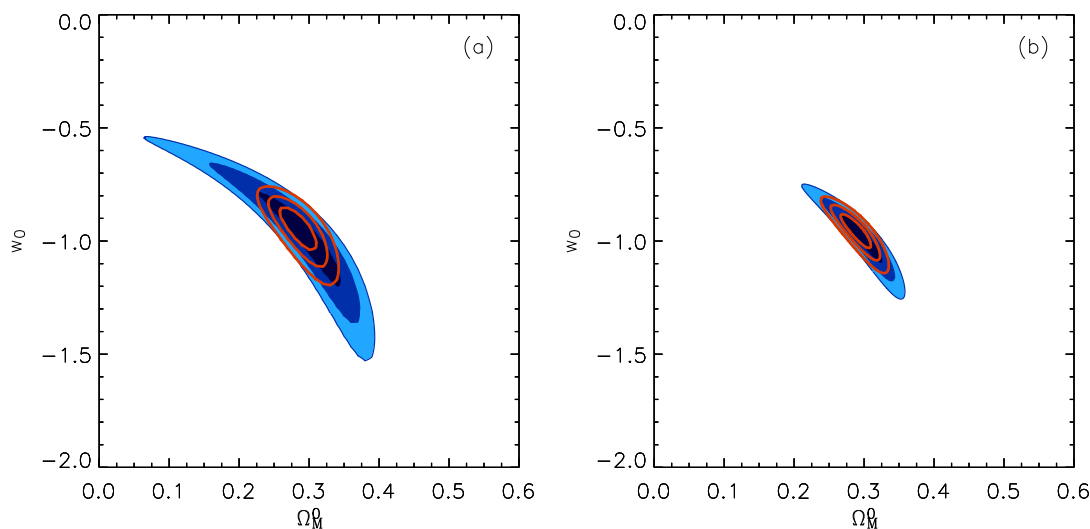


Figure 8.4: (a) Confidence regions for a constant equation of state. Blue filled contours make use of the LSST deep data with  $\delta z = 0.01$  and  $\sigma_{sys} = 0.02$ . Red lines include BAO constraints. (b) The same as (a) for the SNAP survey assuming  $\sigma_{sys} = 0.02 z/1.7$ .

The deep survey will obtain a smaller but not small number of supernovae with an expected uncertainty for photo- $z$ 's of  $\delta z < 0.01$ . That diminishes the difference between the uncertainty in the magnitude with and without photo- $z$ 's. However, the ground for the uncertainty is higher due to the more reduced number of data. The low- $z$  anchor is not completely determined by the survey itself now, and the inclusion of SNFactory triples the number of supernovae with  $\delta z = 0$  at the beginning of the Hubble diagram.

In compensation for the smaller number of data, the survey reaches a higher redshift. In fact, results without systematics and without any effort to get spectroscopic redshifts give uncertainties of the same order of magnitude for both surveys.

Uncertainty:	Priors	LSSTdeep				SNFactory + LSSTdeep			
		$\sigma_{\Omega_M^0}$	$\sigma_{\Omega_X^0}$	$\sigma_{w_0}$	$\sigma_{w_a}$	$\sigma_{\Omega_M^0}$	$\sigma_{\Omega_X^0}$	$\sigma_{w_0}$	$\sigma_{w_a}$
$\sigma_{sys} = 0.00$	CC	0.010	0.05	-	-	0.010	0.04	-	-
	CC + BAO	0.009	0.04	-	-	0.009	0.04	-	-
	CC + BAO2	0.007	0.03	-	-	0.007	0.03	-	-
	flat	0.017	-	0.07	-	0.015	-	0.06	-
	flat + BAO	0.010	-	0.06	-	0.012	-	0.05	-
	flat + BAO2	0.010	-	0.04	-	0.010	-	0.04	-
	flat + $\sigma_{\Omega_M^0}$	-	-	0.11	0.70	-	-	0.07	0.68
$\sigma_{sys} = 0.02$	CC	0.032	0.12	-	-	0.029	0.08	-	-
	CC + BAO	0.015	0.07	-	-	0.015	0.05	-	-
	CC + BAO2	0.011	0.05	-	-	0.015	0.04	-	-
	flat	0.105	-	0.21	-	0.040	-	0.14	-
	flat + BAO	0.020	-	0.08	-	0.015	-	0.06	-
	flat + BAO2	0.012	-	0.06	-	0.010	-	0.05	-
	flat + $\sigma_{\Omega_M^0}$	-	-	0.24	1.06	-	-	0.14	0.85
$\sigma_{sys} = 0.04$	CC	0.058	0.22	-	-	0.053	0.13	-	-
	CC + BAO	0.019	0.10	-	-	0.018	0.06	-	-
	CC + BAO2	0.015	0.07	-	-	0.011	0.05	-	-
	flat	0.095	-	0.37	-	0.073	-	0.23	-
	flat + BAO	0.018	-	0.10	-	0.017	-	0.07	-
	flat + BAO2	0.015	-	0.09	-	0.013	-	0.05	-
	flat + $\sigma_{\Omega_M^0}$	-	-	0.41	1.55	-	-	0.22	1.10

Table 8.4: Uncertainties in the determination of the cosmological parameters and the dark energy equation of state adding systematic uncertainties to the raw LSST deep survey both with and without the SNFactory set. Photo- $z$ 's with  $\delta z = 0.01$  and intrinsic dispersion  $\sigma_{intr}=0.15$  are included as well.

The improvement is only seen when considering systematics too. When adding systematics, those dominate over the statistics and the lower floor of statistics of the wide survey is hidden and surpassed by the higher redshift to be reached by the deep survey.

For a reasonable value of systematics,  $\sigma_{sys} = 0.02$ , the cosmological parameters are measured with two times more precision than with R06 data and more than

three times with respect to VW07. There is still room for improvement and the combination with BAO constraints divides the error by two both with and without the contribution from SNFactory.

The effect on a constant equation of state is more important. Already without the low- $z$  sample the uncertainty on  $w_0$  falls down to  $\sigma_{w_0} = 0.21$  as it also happened with the LSST wide B distribution, but the inclusion of SNFactory supernovae diminishes the error to  $\sigma_{w_0} = 0.14$ . As seen in Figure 8.4 (a), the perpendicularity between the SNe Ia and BAO contours still allows for a reduction of three times that value.

As for the evolution of dark energy,  $w_a$  is the hardest parameter to determine. The best configuration of LSST wide B reaching  $z = 0.9$  achieves  $\sigma_{w_a} = 0.94$ , increasing the limiting redshift up to  $z = 1.4$  improves its precision a 10%, and we see in the next section that a survey till  $z = 1.7$  would only go from  $\sigma_{w_a} = 0.85$  to  $\sigma_{w_a} = 0.81$  if there is not a simultaneous improvement on systematics. The blue confidence regions in Figure 8.5 represent  $1\sigma$ ,  $2\sigma$  and  $3\sigma$  regions in this case, when the prior  $\sigma_{\Omega_M^0} = 0.03$  is included as well. That can be compared to Figure 6.7 where red solid lines were calculated under the same assumptions for current data without the inclusion of systematics. The orange contours in the same plot are a first in-

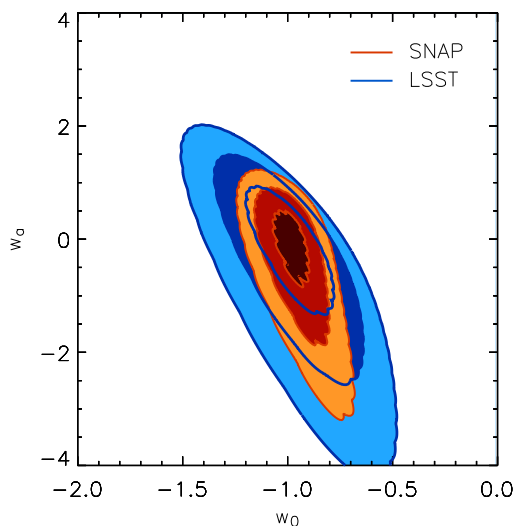


Figure 8.5: Confidence regions for the parameters describing the equation of state for LSST deep survey with  $\delta z = 0.01$  and  $\sigma_{sys} = 0.02$  (blue) and for SNAP with  $\sigma_{sys} = 0.02 z/1.7$  (orange). In both cases a prior  $\sigma_{\Omega_M^0} = 0.03$  has been included before marginalizing over.

dication that this announced improvement with the future most ambitious ground survey can be surpassed.

Table 8.4 summarizes the uncertainties for these cases and the degradations due to higher systematics. Note that also for  $\sigma_{sys} = 0.04$  the addition of an error-free low redshift sample (SNFactory with  $\delta z = 0$ ) represents in general a reduction of the uncertainty by half. That could be further reduced by obtaining spectroscopic redshifts for  $z < 0.2$  where statistical uncertainties dominate over systematics. Since that would represent less than 300 spectra for this configuration, results highly recommend the effort: for an evolving dark energy source and  $\sigma_{sys} = 0.02$ , the improvement provided by these 300 spectroscopic redshifts is equivalent to remove systematics.

### 8.3 Standard cosmology with space surveys, SNAP/JDEM

During the last years, SNAP has been a reference point for testing different theoretical models of dark energy and studying the discernability among them in the future. Therefore, the capabilities of the survey are widely known and we only introduce them here for completeness and in order to use the set later on to recover the continuous form of  $w(z)$  and determine the parameters in the running cosmological constant scenarios.

SNAP has at least three points in favour with respect to the ground surveys: the higher limiting redshift, the obtention of spectra for all its SNeIa observations and the lowering of systematics from space.

Results without systematics almost reproduce those for LSST deep survey because the higher ground floor for the uncertainty on the magnitude due to the smaller number of data is compensated by the higher limiting redshift of the survey. For the same level of systematics,  $\sigma_{sys} = 0.02$ , SNAP is already slightly better: when systematics dominate over statistical uncertainties it is the higher redshift that determines the power of the data set. But the true strength of the survey lies on the capability of improving systematics for observations from space. Whereas we considered  $\sigma_{sys} = 0.02$  to be an acceptable floor for systematics, the SNAP team

expects to diminish it, at least at low redshift, being a target to reach a limit such as  $\sigma_{sys} = 0.02 z/1.7$ .

The differences between SNAP and LSST deep, both with the inclusion of SNFactory data, have been reflected in Figures 8.4 and 8.5 for a constant and an evolving equation of state, respectively. The constant value of  $w$  with SNAP is an order of magnitude better constrained than with R06 data, diminishing by a half the uncertainty achieved with LSST deep. Similarly, the evolution  $w_a$  is improved by dividing by two its uncertainty. Once again, priors reduce the difference between surveys and this is why the gain in  $w_a$  is not so spectacular as for  $w_0$  when a prior on the density of matter is used. The same happens when adding BAO constraints to a constant equation of state: the improvement between both future surveys is only 1%.

All these results can be read from Table 8.5. Although most cosmologists are currently more concerned about dark energy than about the cosmological parameters, it is worth to point out as well the precision to be obtained with the new generation of experiments. According to the SNAP simulation, it will achieve  $\sigma_{\Omega_M^0} = 0.01$  and  $\sigma_{\Omega_X^0} = 0.04$  even with systematics. Cosmological parameters are vital to test flatness with SNe Ia and to obtain a measurement independent from CMB. This quality of the determination with present-day data would clearly indicate a closed spatial geometry with R06 data and an open geometry with VW07. Nowadays, both sets are at  $1\sigma$  compatible with a flat universe, as seen in Chapter 6.

In the following sections, we apply the standard survey's specifications:

- LSST deep:  $\sigma_{intr} = 0.15$ ,  $\delta z = 0.01$  and  $\sigma_{sys} = 0.02$ .
- SNAP:  $\sigma_{intr} = 0.15$ ,  $\delta z = 0.00$  and  $\sigma_{sys} = 0.02 z/1.7$ .

## 8.4 The continuous determination of the equation of state

After having seen the power of LSST and SNAP, we use these data so as to reconstruct  $w(z)$  in a continuous form, as done for current samples with the Inverse Method introduced in Chapter 7. In order to determine the uncertainty on the solution and at the same time check the strength of the method, we invert data

		SNFactory + SNAP			
Uncertainty:	Priors	$\sigma_{\Omega_M^0}$	$\sigma_{\Omega_X^0}$	$\sigma_{w_0}$	$\sigma_{w_a}$
$\sigma_{sys} = 0.00$	CC	0.010	0.033	-	-
	CC + BAO	0.009	0.031	-	-
	CC + BAO2	0.007	0.025	-	-
	flat	0.015	-	0.059	-
	flat + BAO	0.012	-	0.046	-
	flat + BAO2	0.008	-	0.033	-
	flat + $\sigma_{\Omega_M^0}$	-	-	0.07	0.65
$\sigma_{sys} = 0.02 z/1.7$	CC	0.015	0.041	-	-
	CC + BAO	0.012	0.035	-	-
	CC + BAO2	0.008	0.027	-	-
	flat	0.021	-	0.074	-
	flat + BAO	0.015	-	0.050	-
	flat + BAO2	0.009	-	0.034	-
	flat + $\sigma_{\Omega_M^0}$	-	-	0.08	0.69
$\sigma_{sys} = 0.02$	CC	0.019	0.054	-	-
	CC + BAO	0.013	0.041	-	-
	CC + BAO2	0.009	0.030	-	-
	flat	0.028	-	0.098	-
	flat + BAO	0.016	-	0.054	-
	flat + BAO2	0.009	-	0.037	-
	flat + $\sigma_{\Omega_M^0}$	-	-	0.10	0.81

Table 8.5: Uncertainties in the determination of the cosmological parameters and the dark energy equation of state for three different levels of systematics in the SNAP survey.

generated from two fiducial models, one of them degenerate with the cosmological constant. One can show that the method can reconstruct solutions which are degenerate with the cosmological constant at some  $z$ , having a relative difference in luminosity distance  $\Delta d_L(z)$  lower than 1% there, but differing from it at other  $z$ .

In Figure 8.6 (b), the short dashed line shows the equation of state of the fiducial dark energy model  $w(z) = -1.5 + 1.0z/(1+z)$ . The reconstruction has been overplotted together with  $1\sigma$  uncertainties as given by the inversion (Eq. 7.30), and it can be seen that we obtain an improvement over the prior at intermediate redshift.

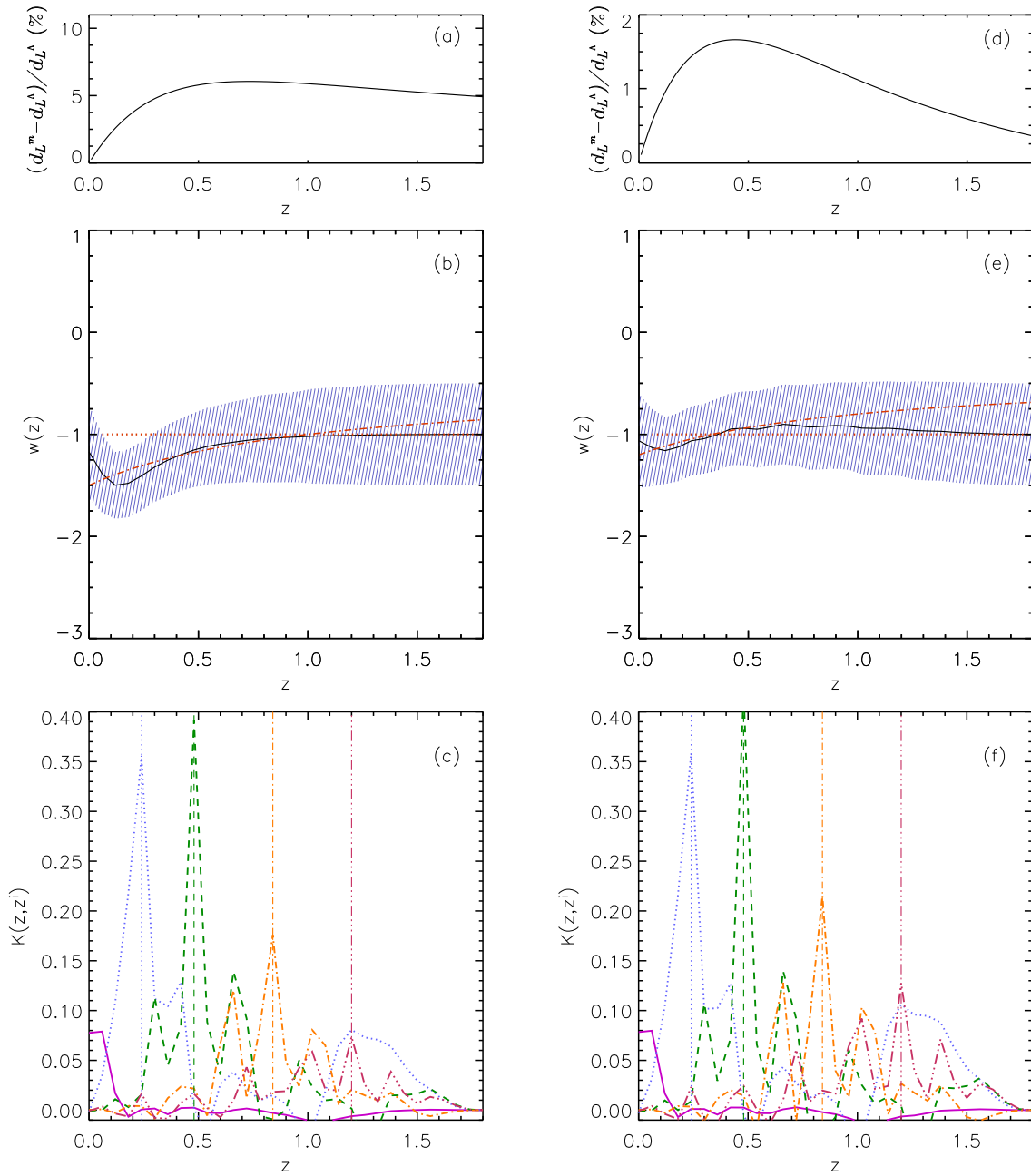


Figure 8.6: Reconstruction with SNAP and SNFactory data set. Gaussian covariance is as in Figure 7.1 and 7.2. In the upper panels it is shown the deviation in luminosity distance between model and the cosmological constant. The recovered  $w(z)$  is shown in the middle panels and the resolving kernels in the lower ones. On the left plots, the dot-dashed line is the fiducial dark energy model with  $w(z) = -1.5 + 1.0z/(1+z)$ . On the right plots the fiducial model is  $w(z) = -1.2 + 0.8z/(1+z)$  and is closer in luminosity distance to the prior (dotted line), taken to be the cosmological constant. See text for more comments.

The reconstruction differs from the cosmological constant at more than  $1\sigma$ . The resolving kernels also show that the intermediate  $z$  is the best resolved redshift range and it is so much more than for current data: at  $z = 0.5$  the kernel has grown from 0.2 to 0.4. As it happens for all data sets, redshift  $z = 0$  is worse determined than higher  $z$ . Multiple peaks appear in the resolving kernel and the kernel is wide at some  $z$ , which results in a degree of degeneracy of the function at those redshifts. This is a result to be expected as the dependence between the equation of state and the luminosity distance (as we have seen,  $w(z)$  is hidden within a double integral in redshift, and thus, its variation with redshift is smoothed) eludes the uniqueness of the result.

In Figure 8.6 (e), the synthetic sample corresponds to an equation of state  $w(z) = -1.2 + 0.8z/(z+1)$ . The corresponding difference in the luminosity distance between this model and the *a priori* one (cosmological constant) is less than a 2%, and despite this, the method is able to recover the real model at intermediate redshift, where the degree of information in  $w(z)$  is higher but also where the luminosity distance difference is larger than 1%. However, although the best inversion reconstructs the correct model, the cosmological constant is within  $1\sigma$  uncertainty along all  $z$  due to the closeness of the models. At high redshift, where there are fewer data and very small deviations in the luminosity distance, the prior is not improved. There, the SNAP sample meets its systematic error of 0.02 *mags*, and the limit of discernability of the models is shown in the impossibility to find variations in  $w(z)$  implying less than 1% in  $\Delta d_L$ . However, we can discriminate models against the cosmological constant which are 1% above the discernability at some  $z$ , while they might fall below it at other  $z$ .

As it was done in previous chapter, we complement the results obtained in a straightforward manner by the method with a Monte Carlo exploration of the space of solutions, in order to study the uncertainty on the result. To restrict ourselves to the equation of state, a prior on the density of matter  $\sigma_{\Omega_M^0} = 0.03$  is being imposed as well. Figure 8.7 shows the best inversion (dotted line) among 1000 with priors ranging  $-3 < w(z) < +1$  for the two data sets analysed in the sections above: LSST deep survey with  $\delta z = 0.01$  and  $\sigma_{sys} = 0.02$  and SNAP data with  $\sigma_{sys} = 0.02 z/1.7$ . In both cases, the intrinsic dispersion of SNe Ia is  $\sigma_{intr} = 0.15$  and the 300 SNFactory SNe Ia are added.

The solution is well determined up to  $z = 0.7$  for LSST and up to  $z = 0.9$  for

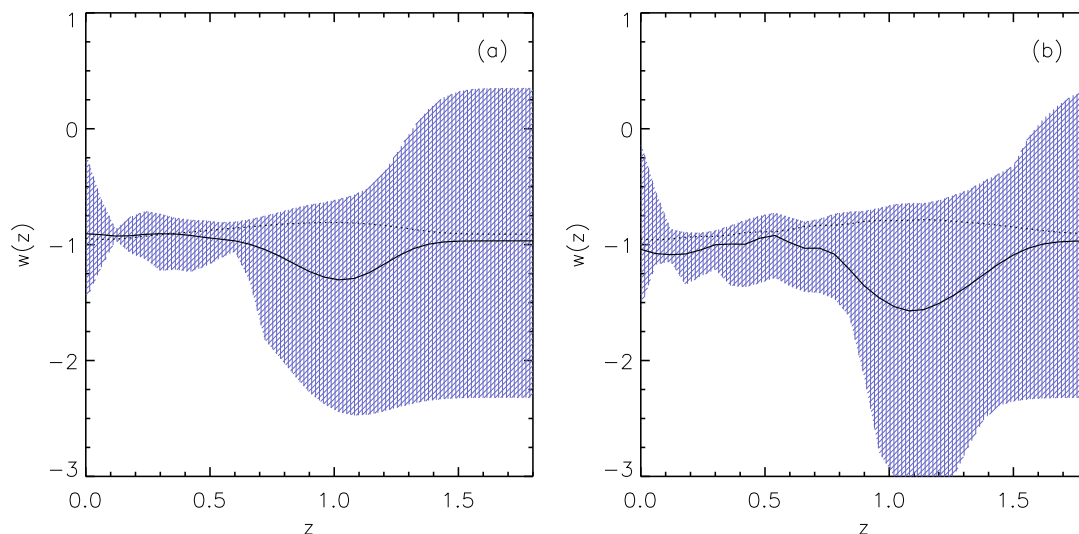


Figure 8.7: Reconstruction of  $w(z)$  and Monte Carlo errors obtained after 1000 inversions of LSST deep survey with  $\delta z = 0.01$  and  $\sigma_{sys} = 0.02$  (a) and SNAP data with  $\sigma_{sys} = 0.02 z/1.7$  (b). In both cases SNFactory SNeIa are added. The solid line shows the mean of all inversions and the dotted line the inversion with minimum  $S$ .

SNAP. From there on, the uncertainty on  $w(z)$  is highly asymmetric. Whereas the uncertainty remains moderate till  $z = 1.2$  (LSST) or  $z = 1.5$  (SNAP) for the positive side of the solution ( $w > -1$ ), the negative one ( $w < -1$ ) grows around  $z \approx 1$  and reaches  $\sigma_w^- = 2.4$  for SNAP.

This asymmetry is also found in the discrete parameterization and has a physical underlying reason. The dark energy density is a constant value when the dark energy source is a cosmological constant. In this case, the higher the redshift, the smaller and insignificant the dark energy density is as compared to the matter density. For  $w > -1$ , the density grows with redshift and the point where the matter density clearly dominates is delayed. On the contrary, for  $w < -1$ , the dark energy density decreases and it is negligible at a nearer redshift. This key redshift where dark energy starts to be insignificant can be determined via observations. However, once the matter density dominates, all the models with  $w < -1$  produce the same luminosity distance. At  $z = 1$ , the normalized values already are  $\Omega_M^1 \approx 2.4$  vs.  $\Omega_X^1 \approx 0.7$  and the variations of  $w$  get hidden behind  $\Omega_M^0$ .

In the plots, it seems that there is just a bump around  $z \approx 1$ . However, that is only the effect of the decrease of data at high redshift. The inversion recovers the prior where there is no enough information from SNeIa. That occurs around  $z = 1.2$

Priors	SNFactory + LSSTdeep		SNFactory + SNAP	
	$\sigma_{\Omega_M^0}$	$\sigma_\theta$	$\sigma_{\Omega_M^0}$	$\sigma_\theta$
- Scenario 1 -				
flat	0.055	$\sigma_\tau = 4.0 \cdot 10^{-9}$	0.028	$\sigma_\tau = 2.1 \cdot 10^{-9}$
flat + $\sigma_{\Omega_M^0}$	0.032	$\sigma_\tau = 2.6 \cdot 10^{-9}$	0.023	$\sigma_\tau = 1.8 \cdot 10^{-9}$
- Scenario 2 -				
flat + ZP fixed	0.012	$\sigma_\eta = 1.8$	0.007	$\sigma_\eta = 1.1$
flat + ZP fixed + $\sigma_{\Omega_M^0}$	0.012	$\sigma_\eta = 1.7$	0.007	$\sigma_\eta = 1.1$
- Scenario 3 -				
flat	0.045	$\sigma_\nu = 0.12$	0.023	$\sigma_\nu = 0.06$
flat + $\sigma_{\Omega_M^0}$	0.020	$\sigma_\nu = 0.09$	0.020	$\sigma_\nu = 0.05$

Table 8.6:  $1\sigma$  uncertainties for the free parameters appearing in the running cosmological constant scenarios obtained with LSST and SNAP. For both data sets, the low- $z$  sample SNFactory is included.

for LSST and  $z = 1.5$  for SNAP, points where the uncertainty in the positive part,  $\sigma_w^+$ , tends to fill the 68% of the explored area.

## 8.5 The running of the cosmological constant

Finally, we make use of the simulations for LSST and SNAP to determine the precision with which the parameters of the running cosmological constant models can be measured. The first results are obtained from the two samples generated from a theoretical model without any running.

Figure 8.8 shows the confidence regions for the parameters of the three scenarios and for the density of matter. The parameter related to the neutrino's mass in Scenario 1,  $\tau$ , is three times better determined with LSST than with R06, the current data set with minimum error. This improvement grows to six times when SNAP supernovae are used. The constraint on the density of matter is three times tighter as well, and that can be improved with the prior  $\sigma_{\Omega_M^0} = 0.03$ . For SNAP, there is almost no room for improvement, since the uncertainty on  $\Omega_M^0$  is already of the same order of magnitude as the prior. For LSST, however, the prior diminishes

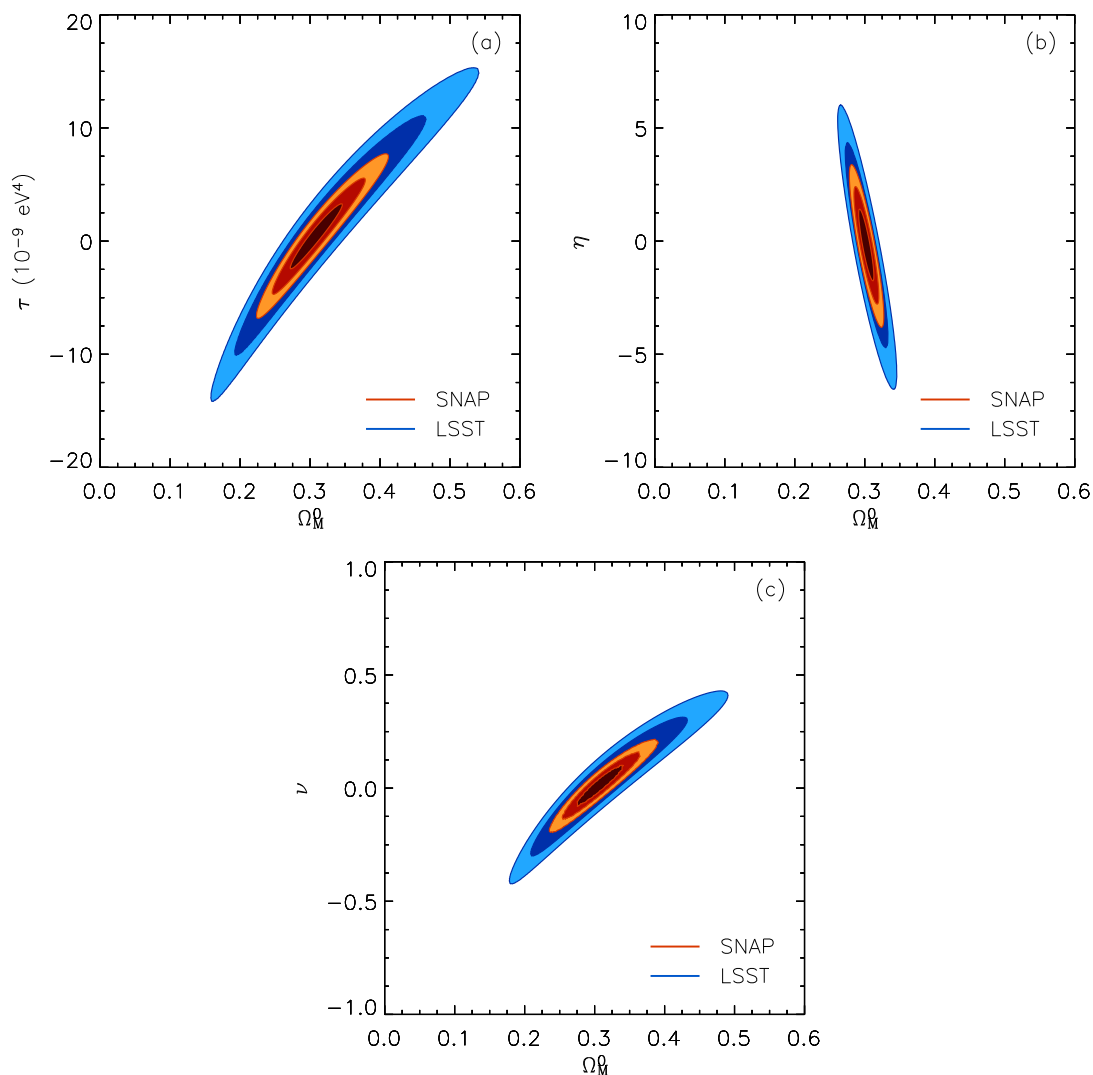


Figure 8.8:  $1\sigma$ ,  $2\sigma$  and  $3\sigma$  confidence regions for the distinctive parameters  $\theta$  of the running cosmological constant scenarios ( $\theta \equiv \tau$  for Scenario 1,  $\eta$  for Scenario 2 and  $\nu$  for Scenario 3) in the  $(\Omega_M^0, \theta)$  space. Blue contours enclose the probability regions obtained with the LSST wide survey and the orange ones correspond to SNAP.

by a half the uncertainties on both  $\Omega_M^0$  and  $\tau$  (see Table 8.6 for the concrete values).

The main problem of Scenario 2 was the degeneracy of  $\eta$  with the Hubble constant  $H_0$ . The degeneracy is not broken with the higher quality of the data and one must fix the zero point of the magnitude to constrain  $\eta$ . That, of course, relates the knowledge of  $\eta$  to the knowledge of  $H_0$ . Here, the inclusion of the prior  $\sigma_{\Omega_M^0} = 0.03$  is not necessary, and fixing  $H_0$  is enough to constrain  $\eta$  and reduce from 5 to 1 its

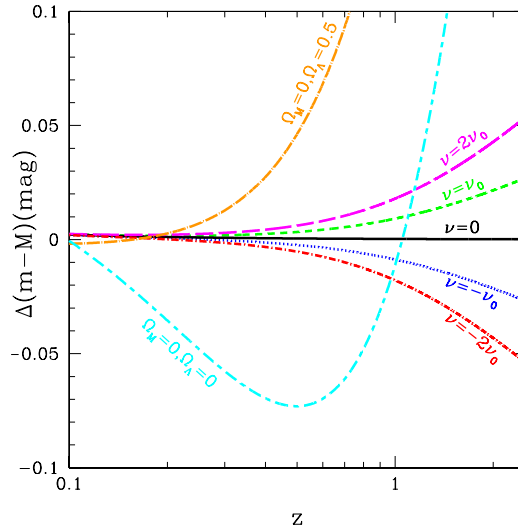


Figure 8.9: Deviations of the distance modulus  $m - M$  with respect to the case of a standard cosmological constant with  $\Omega_M^0 = 0.3, \Omega_\Lambda^0 = 0.7$ . Two fully academic situations are shown:  $(\Omega_M^0, \Omega_\Lambda^0) = (0, 0)$  –Milne’s open universe– and a pure de Sitter’s universe  $(0, 0.5)$ , both with no matter, in order to show the scope of the effects. Important differences appear for  $z \gtrsim 0.5$ . The other curves in the graphic show the case of Scenario 3 for various values of  $\nu$ . Differences become important at  $z \gtrsim 1$ .

uncertainty (SNAP). For the standard model of particles, though,  $\eta$  is fixed and one just has to check whether  $\eta = 10.75$  agrees with observations. In a universe filled with a constant cosmological constant, both LSST and SNAP are capable of clearly ruling out this kind of running caused by the particles of the standard model. In the same way, the standard running of Scenario 2 rules out the constant cosmological constant.

The third Scenario described the running of the cosmological constant via the parameter  $\nu$ . The SNAP survey data can be fit to obtain  $\sigma_\nu = 0.06$ . As we said, a typical value for  $\nu$  would be  $\nu_0 = 0.026$  and even smaller values are needed to be compatible with complementary observations [136, 77]. So, a strong evolution would be needed in order for it to be ruled out by SNAP in front of the cosmological constant. However, larger values such as  $\nu = 0.1$  cannot be theoretically discarded. If the universe behaves as experiencing a running proportional to  $\nu = 0.1$  for example, it could be detected by this survey and would be in the limit of detection of a large ground survey such as LSST.

Priors	Fiducial ( $\Omega_M^0, \theta$ )	SNFactory + SNAP	
		$\sigma_{\Omega_M^0}$	$\sigma_\theta$
- Scenario 1 -			
flat	(0.2, $\tau = -5.0 \cdot 10^{-9}$ )	0.025	$\sigma_\tau = 2.5 \cdot 10^{-9}$
flat	(0.3, $\tau = 0.0 \cdot 10^{-9}$ )	0.028	$\sigma_\tau = 2.1 \cdot 10^{-9}$
flat	(0.4, $\tau = +5.0 \cdot 10^{-9}$ )	0.042	$\sigma_\tau = 2.5 \cdot 10^{-9}$
- Scenario 2 -			
flat + ZP fixed	(0.2 $\eta = -2.25$ )	0.006	$\sigma_\eta = 1.1$
flat + ZP fixed	(0.3 $\eta = 0$ )	0.007	$\sigma_\eta = 1.1$
flat + ZP fixed	(0.4 $\eta = +1.25$ )	0.010	$\sigma_\eta = 1.2$
- Scenario 3 -			
flat	(0.2 $\nu = -0.2$ )	0.020	$\sigma_\nu = 0.08$
flat	(0.3 $\nu = 0.0$ )	0.023	$\sigma_\nu = 0.06$
flat	(0.4 $\nu = +0.2$ )	0.033	$\sigma_\nu = 0.06$

Table 8.7:  $1\sigma$  uncertainties for the parameters of the three running cosmological constant scenarios as a function of the position of the underlying model in the parameter space. The SNAP data set with  $\sigma_{sys} = 0.02 z/1.7$  is used.

We must take into account, however, that the SNAP distribution of data is optimized in order to distinguish models that have their maximum difference at redshifts closer than 1. Models with a running cosmological constant differ from the ones without such running at higher redshift ( $z > 1$ ) and the difference grows with  $z$ . For evolving equation of state models, we saw that than the maximum variation from a cosmological constant can be seen at  $z \approx 0.5$  (Figure 4.8 (d)). Thus, as we see in Figure 8.9, we need a sizeable group of supernovae at the highest redshift reachable by SNAP while the strong concentration of data around  $z = 1$  is needed to distinguish models with and without cosmological constant.

We can, therefore, try other distributions designed from the idea that the difference between models grows with redshift, as it indeed happens in the present case. For testing, we generate a distribution with 2000 SNeIa such as SNAP, but now most of them (1750) are equally distributed between  $1 < z < 2$ , and only 250 SNeIa (plus the SNFactory) are used at  $z < 1$ . The uncertainty on  $\nu$  diminishes with this modified distribution to  $\sigma_\nu = 0.02$ , showing the importance of the very high redshift supernovae. Increasing the number of data with  $z > 1$ , by using three

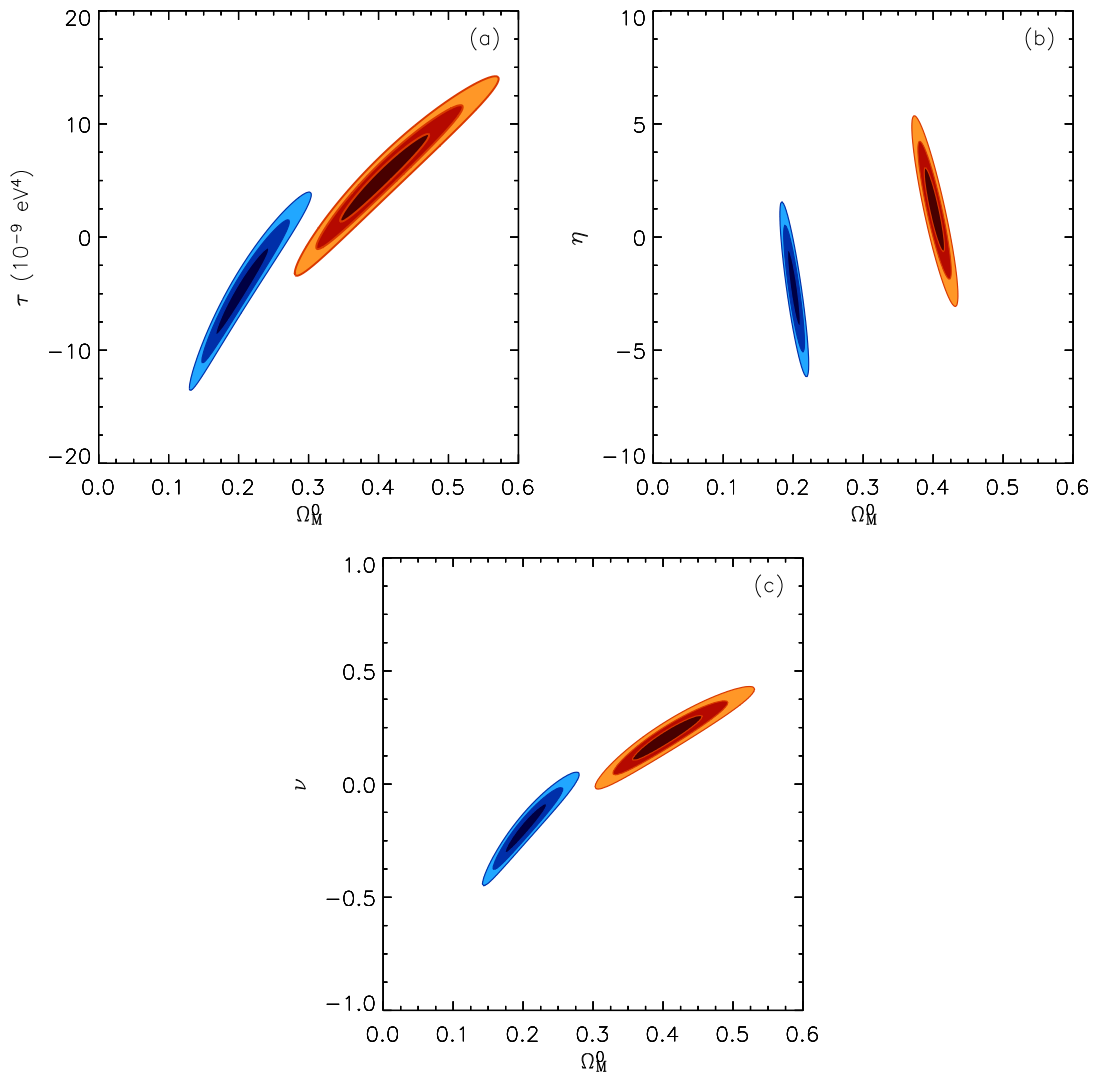


Figure 8.10: As Figure 8.8 but data simulations use fiducial models other than a cosmological constant without evolution. See Table 8.7 for the concrete values.

years of SNAP observations for example, improves the determination too, but not in such a spectacular way. With those 6000 SNe Ia one gets  $\sigma_\nu = 0.04$ .

The improvement with very high redshift objects is shared by the three running scenarios, but not by other dark energy models. A (moderate) growing cosmological constant can be detectable up to a higher redshift, but as commented before, some dark energy sources are already negligible at redshifts close to  $z = 1$ . A data distribution such as the one introduced before would be useless in these cases.

As a last point, we check the stability of the uncertainties given. All the previous

results correspond to a fiducial model of cosmological constant. But the size of the confidence regions, and, therefore, the uncertainty on the individual parameters can depend on their position in the parameter space. We calculated the determination of the three parameters  $\theta$  in other points as shown in Figure 8.10. The obtained variations are not very important, but the ellipse's surface tends to be minimum for models without evolution. The values for each fit and the fiducial models used in the simulations are shown in Table 8.7. For models close enough to a cosmological constant to be consistent with current observations, the uncertainty on the recovered parameters is not going to improve or worsen in a significant way with respect to the assumption of a cosmological constant.

## Chapter 9

---

# Conclusions

---

*A journey of a thousand miles begins with one small step.*

Chinese proverb

This thesis tries to be a contribution to the solution of the dark energy problem. The name itself, *dark energy*, shows the nature of the problem: complete lack of knowledge. By dark, one means to describe *something* which seems to fit observations but that we neither see nor know its nature. Usually, it is treated as a new energy contribution. Why not? Everything seems to be energy. Our mind is prepared and willing to know new kinds of energy. However, this is not the only possible explanation. Other parallel approaches such as modifications to gravity should not be discarded at our current level of knowledge. And other more exotic, or easier, or revolutionary alternatives should be proposed and tested. There currently are lots of different ways being travelled towards the desired answer, but we seem to be still far from the end of the way. Maybe we have not found the correct way yet. But in this thesis we follow one of them and try to take a step.

In the theoretical part at the beginning of the thesis, we introduced Einstein's field equations with special attention to the role of the cosmological constant and to the possibility that this is a time dependent term. The Friedmann equations are deduced and all the machinery is prepared and adapted to include an evolving cosmological constant as a source of dark energy.

Having the standard background adapted, the first step has been to motivate a

family of models for which the cosmological constant naturally arises as an evolving term. This gives us the chance to justify why the current value of the cosmological constant is precisely so, provided that one finds the reason for its initial value. This justification would solve one of the open problems in cosmology.

In the framework of a quantum field theory with fields on a curved space-time (semiclassical approximation), the action of the theory includes a term of interaction with the gravitational field. In order for the theory to be renormalizable, this term adds a cosmological constant  $\Lambda_{vac}$  in the Hilbert-Einstein action, and new terms on higher order derivatives of the metric. After the regularization process, the initial scale invariance is broken, and the dependence of the theory from the scale is encoded in the renormalization group equations. The  $\beta$ -function in particular is the equation giving the evolution of the cosmological constant (and Newton's constant) with the renormalization scale  $\mu$ .

Calculations of the  $\beta$ -function proved to be difficult in a curved space-time, and the attempts made up to now have proceeded perturbatively on the metric of a flat space-time. Therefore, the approach followed has been to calculate  $\beta_\Lambda$  via the  $\overline{\text{MS}}$  scheme with the corresponding difficulty in its physical interpretation, and afterwards to pose hypotheses about the meaning of the renormalization scale and the decoupling process of the massive degrees of freedom. That makes us consider three main different cosmological scenarios:

Scenario	Active dof	Particles	$\mu$
1	$m_i < \mu$	neutrinos	$\rho_c^{1/4}(t)$
2	$M_i > \mu$	SM	$\rho_c^{1/4}(t)$
3	$M_i > \mu$	Plank	$H(t)$

The domination of the massive degrees of freedom  $M_i$  is possible in the case of the cosmological constant because, thanks to its dimensionality, it experiences the so-called soft decoupling.

The consequences of Scenario 3 have been specially worked out as a part of the thesis. The cosmological equations depend on an extra single parameter function of the masses  $M$  close to the Plank scale:  $\nu = \sigma M^2 / 12 \pi M_P^2$ . The evolution of  $\rho(z; \nu)$  and  $\Lambda(z; \nu)$  depends on it, and so does the luminosity distance. For these parameters to be compatible with observations and the Big Bang model, the cosmological index

$\nu$  must be limited to the range  $|\nu| \ll 1$ , being  $\nu_0 = 1/12\pi \approx 0.026$  a natural value obtained for  $M \sim M_P$ .

Within this range, one can see that for a negative cosmological index the density of matter grows faster towards the past, whereas for a positive value, the growth is slower than for a standard cosmological model with  $\nu = 0$ . The distinction will not be appreciable in the future: the density of matter tends to zero regardless of the value of  $\nu$ . For the cosmological constant density the behaviour is the opposite. It is for a positive  $\nu$  (negative) that the cosmological constant increases (decreases) towards the past, whereas it reaches a constant positive value in the future. Evidently, the change on  $\rho(z; \nu)$  and  $\Lambda(z; \nu)$  with respect to the standard case causes variations on other related parameters such as the Hubble parameter, the deceleration parameter and the transition redshift where the Universe goes from being dominated by matter to being dominated by the cosmological constant. All of them parameters which should help to detect observationally the running from close measurements.

On the other hand, tests of these models should not be restricted to small redshifts. An unexplored consequence of this work is the possibility that the high order terms added to the action for renormalizability reasons (Eq. 3.2) would be the cause of inflation. That would complete a very elegant manner of generating inflation and, at the same time, explain the current accelerated expansion. However, we did not work on that aspect, but only on using mainly SNeIa observations to study close redshifts ( $0 < z < 2$ ) and compare this family of theoretical models with other kinds of dark energy sources.

A dark energy component is usually characterized by its equation of state, generally  $p(t) = w(t)\rho(t)$ . That accounts for quintessence, the archetype we use to represent a dark energy source. But mathematically, most sources can be rewritten as a perfect fluid component with a pseudo-equation of state of the form  $p = \tilde{w}(z)\rho$ . This allows to treat every model in a single Friedmann equation with the dark energy density defined by  $\tilde{w}$  (Eq. 4.10). We have deduced or compiled the quantity  $\tilde{w}(z)$  for some of the most promising dark energy candidates: a Chaplygin gas, Cardassian models, modifications to General Relativity including braneworld cosmologies, loop quantum cosmology models and running cosmological constant models. This is expected to make easier the task of identifying the true model from observations. But it is too a first indication of the large degeneracy problem we meet with dark energy: if every model can be expressed as a perfect fluid with  $\tilde{w}$ , any quintessence

model having  $w = \tilde{w}$  is degenerate with all other models characterized by the same  $\tilde{w}$ .

The degeneracy of  $w(z)$  has other contributions as well. The mathematical form with which the equation of state is related to the luminosity distance (a double integral) smooths the possible evolution. On the other hand, when determined jointly with other unknowns, the correlations among them increase the degeneracy of the equation of state with changes in the cosmological parameters. The latter is a common problem addressed by including priors and combining determinations from different methods. The former is characteristic of using extragalactic distances and affects our results from SNe Ia. Besides, the dispersion of supernovae or the level of systematics in future surveys will limit the detectable discernability among models and thus define the practical meaning of degeneracy.

Taking all these limitations into account, we use two current SNe Ia data sets to determine the best values for the cosmological parameters and those related to dark energy: 182 SNe Ia from Riess et al. (2006) [160] (R06) and 162 SNe Ia from Wood-Vasey et al. (2007) [211] (VW07). Both sets differ in their mean redshift and the calibration applied to SNe Ia. Because of this, the global conclusions obtained with both samples are mostly inconsistent at  $1\sigma$  level before adding complementary priors, and whereas R06 favours a high density universe, VW07 favours a low density one. When a flat universe is imposed following CMB results, the discrepancy translates into dark energy. R06 tilts towards a universe filled with a vanishing dark energy source in the past, but VW07 prefers an increasing energy density. We showed that the difference in the mean redshift ( $\langle z_{R06} \rangle = 0.54 \pm 0.35$  vs.  $\langle z_{VW07} \rangle = 0.38 \pm 0.27$ ) is not responsible for this difference in the results. Hence, we attribute the discrepancies to the variety of calibration techniques used, not only between both sets but also among subsamples of a same set as it happens in R06.

For completeness we use both samples. The parameters for a standard cosmology with a constant equation of state or an evolving one parameterized by  $w_0$  and  $w_a$  have been determined by several methods in papers from the collaborations publishing the data, for instance. Some alternative theories for dark energy have been tested as well and compared with the standard parameterization. Here, we pay special attention to running cosmological constant models. Parameter  $\tau$  of Scenario 1 is marginally compatible at  $1\sigma$  with no running, being results with VW07 data closer to a cosmological constant and results with R06 favouring a negative evolution. This

negative evolution allows to put an upper limit to the mass of the lightest neutrinos of  $m_\nu = 0.007 \pm 0.006$  eV. For the positive evolution, the dominant mass must be the scalar field and the evolution behaves as produced by an effective mass of  $m_{eff} = 0.01 \pm 0.01$  eV. The degeneracy of  $\tau$  with  $\Omega_M^0$  is important, and the addition of the prior  $\Omega_M^0 = 0.27 \pm 0.03$  diminishes the uncertainty to a half. Although the best fit for  $\tau$  is now closer to no evolution than without the prior, the true cosmological constant or the absence of an effective running is at more than  $1\sigma$  from the best fit.

In Scenario 2, the parameter accounting for the running,  $\eta$ , is highly degenerate with the Hubble constant (in general with the zero point magnitude). That makes information necessary on  $H_0$  to break the degeneracy. Fixing its value, the cosmological constant stays within  $1\sigma$  intervals, but the value predicted by the Standard Model of particle physics,  $\eta = 10.75$ , is out by more than  $2\sigma$  with R06 and at the limit with VW07. That makes this scenario observationally less appealing than the other two.

For Scenario 3, things are very similar to Scenario 1. The behaviour of  $\nu$  and  $\tau$  is exactly the same, but  $\tau$  encodes the information as  $\tau \propto m^4$  and the knowledge on  $\tau$  allows to put informative constraints on the mass. In the case of  $\nu$ , the theoretical model predicts a value  $\nu_0$  very close to zero, and current data do not reach the precision needed to point out this value in front of no running, for instance. R06 data rule out  $\nu_0 = 0.026$  at more than  $1\sigma$  and negative evolutions are preferred. For VW07, that  $\nu_0$  is perfectly compatible, but uncertainties of more than 10 times its value make it hard to constrain it. Anyway, a positive but stronger evolution is favoured by this set. Notice that even a clear obtention of  $\nu = 0$  could not be indicating the incorrectness of the theory, but just a lack of particles close to the Planck scale.

We see that, overall, current SNe Ia data are not able to put serious constraints on particle physics parameters, and particle physics models with the standard and expected values for the free parameters do not fully describe those observations satisfactorily and that opens the possibility of some new physics. Nevertheless, even the obtained sign of the running depends on the data set, and one must wait for future surveys to pin it down from accurate results. For the time being, a naive combination of the two data samples (Davis et al. (2007), D07, [56]) is also used to gain a more general view of the problem. Results in this case are halfway between R06 and VW07. From them, there is no observational necessity for any running,

evolution or even a departure from a  $w_0 = -1$ . If it is not cosmological constant, it must behave, at least effectively, as if it were. Actually, the running must exist if the cosmological constant is considered within a quantum field theory, but its effect would be now very small. However, confidence regions are still far from being narrow enough to obtain the desired precision and future surveys are needed in order to give informative results on the running.

When comparing these results to the ones obtained for a constant equation of state, we realise that present-day data lead to much tighter constraints for  $w_0$  than for  $\theta$ . Both R06 and VW07 together with the BAO prior constrain  $w_0$  with a precision of 10% and the cosmological constant always stays within the  $1\sigma$  interval. In Scenarios 1, 2 and 3, the cosmological constant is sometimes at  $2\sigma$  of the best fit and the uncertainty on  $\tau$ ,  $\eta$  and  $\nu$  never approaches 10%; it is, in most cases, of the order of 100%. The justification lies on the behaviour of the dark energy density. For the two families of models, the evolution is encoded in one single parameter, but the physics are different because a constant  $\theta$  behaves as an evolving  $w(z)$ . This fact makes that differences due to the running with respect to the true cosmological constant to become important at high redshift. On the other hand, the differences can be seen already at redshift zero for a constant equation of state. Therefore, much higher redshift data are needed in order to detect the former models as compared with the latter ones.

Before addressing how our constraints on the dark energy representations can improve with future samples, we found it worth to check if a continuous determination of  $\Lambda(z)$  and  $w(z)$  can give more information, at least on the general trends, than the discrete developments. Besides  $w(z)$ , commonly retrieved by other methods, we also reconstruct  $\Lambda(z)$  in order to directly accommodate the running cosmological constant models. To do that, one needs a mathematical method that allows to recover continuous functions from a finite set of discrete data. Inverse methods usually address these problems, and here we adapt a non-linear non-parametric Bayesian approach for the reconstructions.

This inverse method considers data and unknown parameters or functions in the same way. Data are directly measurable and described by their measured values and their uncertainties; unknowns are not directly measurable and described by *a priori* information. If both quantities are assumed to be gaussianly distributed, the misfit function to minimize is composed of two terms representing Gaussian probability

densities. One of them corresponds to the information given by the data and it is the same as in the  $\chi^2$  minimization. The second one introduces the *a priori* information on the unknown parameters, as done before in the discrete parameterizations via the Bayes' theorem. This is why it is a Bayesian approach, necessary in this case to regularize the inversion. The minimization of the misfit function has been done using a Newton method with an approximation to the Hessian that neglects the second order terms. That leads to an iterative equation for every parameter or function to be determined and an expression for its uncertainty once the minimum has been reached.

Priors always play a role within this method. The solution and its uncertainty do depend on the prior, but the dependence weakens for wide priors. However, wide priors do not always allow the convergence of the algorithm. This difficulty must be overcome by a Monte Carlo exploration of the space of solutions whenever strict priors are used. For the barotropic index of the equation of state, we use  $-1.5 \leq w(z) \leq -0.5$  and extend the range to  $-3 \leq w(z) \leq 1$  in the Monte Carlo exploration. When reconstructing  $\Lambda(z)$  we use an *a priori* variation of  $-0.1 < \Delta\Omega_\Lambda^0(z) < 0.1$  and increase the explored space of solutions to  $-0.2 < \Delta\Omega_\Lambda^0(z) < 0.2$ .

With this set-up and the R06 sample,  $w(z)$  grows from a phantom value towards  $w(z = 0.6) \gtrsim -0.5$ . At higher redshifts, one recovers the prior or the mean of the *a priori* range depending on the case. A function called resolving kernel tells us about the zone where data are capable of improving the information over the prior. For R06 data, kernels are almost flat at  $z \gtrsim 0.6 - 0.7$  indicating the absence of information. The same occurs at  $z = 0$ . In the range of interest, the method retrieves a positive evolution as obtained in the discrete parameterization. However, Monte Carlo errors make the result compatible with a cosmological constant at  $1\sigma$  almost over the whole redshift range. That is more restrictive for VW07 supernovae and the reconstruction only shows oscillations around a constant value of the equation of state of  $w(z) = -1$ .

Under the point of view of the cosmological constant density (or dark energy density) the same results are reproduced. For VW07, a constant density cannot be discarded although at intermediate redshifts there is a soft trend with negative slope hidden within  $1\sigma$  uncertainties and the degeneracy with respect to  $\Omega_M^0$ . The positive evolution of  $\Omega_\Lambda^0(z)$  is seen for R06 data as in all the other checks we are doing with them. For this function, results depart from the prior only at  $z \lesssim 0.6 - 0.7$  too. The

changes in the slope at higher redshifts are then meaningless as they only appear to allow the function to tend to the prior. Therefore, it is very difficult to detect any of the running cosmological constant scenarios from these results, since their effect only becomes important at higher redshifts.

The precision allowed by present-day data does not permit to identify clearly a characteristic behaviour of any single dark energy model. With discrete parameterizations, we are limited to determine the functions from their current values and, at most, a first derivative at redshift zero. Part of the improvement of the continuous method is to really calculate the value of the function at other redshifts where data can be more sensitive and obtain different precisions at different ranges according to the amount of information there. Each supernova is used in the calculations at every redshift, having more weight on the result those closer to that redshift. This is why there is no gain in information at  $z \gtrsim 0.7$ . The lack of large samples at high redshift not only affects the determination at those points, but at lower redshifts as well, because the contribution of extra data close to them is scarce. And this is why functions are much better determined at  $z = 0.2$  than at  $z = 1.2$  even if both points are gaps in the density of data. Of course, this is also why  $z = 0$  is worse determined than intermediate redshifts.

In order to extend the redshift range where SNeIa contribute to a gain in information, supernova samples should significantly increase at high redshift. And, even then, the determinations will not be as good as at low and intermediate redshifts because dark energy itself is less relevant to the contents and dynamics of the Universe. With future samples, uncertainties will globally decrease though, because the number of data will proportionally increase along  $z$ . So as to quantify the improvement, we use simulations for two oncoming surveys: LSST as a leading survey from Earth and SNAP from space.

Even though LSST is going to observe 250000 SNe per year (around 10000 in the deep survey), it is a photometric survey and only photo- $z$ 's will be available for most of the data. That is a common drawback for the majority of the massive ground surveys, and the uncertainty due to photo- $z$ 's really damages the determination of the cosmological parameters and dark energy. The redshift uncertainty translates into the magnitude as a decreasing function of the redshift (Fig. 5.7). At low- $z$ , the uncertainty on the magnitude can be larger than 1 *mag*, and the redshift at which it becomes negligible depends on the dispersion of photo- $z$ 's. Therefore, to minimize

the effect of photo- $z$ 's, one must reduce the dispersion of photo- $z$  with respect to the spectroscopic redshifts and, besides and more importantly, fully eliminate the lowest redshift photo- $z$ 's in favour of spectroscopic redshifts.

Making this effort on the photo- $z$ 's treatment, LSST deep survey would improve current determinations on the evolution of the dark energy equation of state,  $w_a$ , reducing in two (R06) or three (VW07) times its uncertainty and reach  $\sigma_{w_a} = 0.7$ . This result would be of the same order as with SNAP, which, although reaching a higher redshift, has a smaller number of data. Without any guarantee of measuring spectra for the low- $z$  subsample, SNAP gets better results, not only because of the higher redshift but because of the better control of systematics as well. Therefore, a constant equation of state can be measured with a precision of  $\sigma_{w_0} = 0.07$  and an evolving one up to  $\sigma_{w_0} = 0.08$  and  $\sigma_{w_a} = 0.7$ . One can compare these uncertainties with those to be obtained with LSST wideB configuration:  $\sigma_{w_0} = 0.14$  and  $\sigma_{w_a} = 0.94$ , very similar to those with LSST deep. In all the cases, these uncertainties are appreciably reduced when adding BAO constraints to the constant equation of state parameterization.

As for the running cosmological constant models, the best results are obtained with SNAP data, almost dividing by two the uncertainties corresponding to LSST deep. For SNAP, the uncertainty on the  $\theta$  parameters for the three scenarios are:  $\sigma_\tau = 2.1 \cdot 10^{-9}$  for Scenario 1,  $\sigma_\eta = 1.1$  for Scenario 2 and  $\sigma_\nu = 0.06$  for Scenario 3. That improves current determinations between 5 and 10 times, depending on the scenario and on the data set. However, as we have said, this family of models differs from a true cosmological constant only at high redshift, because evolutions are soft and small. Other data distributions which take this fact into account and have most of the data at  $z > 1$  would improve the determinations significantly. For example, Scenario 3 with a moderate running given by  $\nu_0 = 0.026$  cannot be detected even with SNAP ( $\sigma_\nu = 0.06$ ). However, such alternative distributions could reach  $\sigma_\nu = 0.02$ , allowing an observational distinction between the running model and a true cosmological constant at more than  $1\sigma$  level. Otherwise, only stronger runnings could be detected. We checked whether the size of the confidence region around the best fit depends on the position in the plane, and, although the point representing no effective evolution has the minimal uncertainty, changes are not important enough so as to make that small runnings can be detected with SNAP alone.

Finally, but not less important, the continuous determination of  $w(z)$  takes advantage of the higher limiting redshift and density of data of the oncoming surveys. The reconstruction is well determined up to  $z = 0.7$  for LSST and up to  $z = 0.9$  for SNAP. From there on, the uncertainty on  $w(z)$  is highly asymmetric. Whereas the uncertainty remains moderate for the positive side of the solution till  $z = 1.2$  (LSST) or  $z = 1.5$  (SNAP), where data still improve the *a priori* information, the negative one grows significantly. This is due to the large degeneracy among models with  $w < -1$  at high redshift. Further than this point, even these large surveys are not able to improve the *a priori* knowledge.

With the simulations of LSST and SNAP, we have reproduced (*preproduced* in fact) the best expectations one can have for the study of dark energy with SNe Ia within the next ten years. Waiting for new alternative methods both physical and mathematical, the gain in precision and accuracy will allow us to limit the possible values for  $w$  or  $\Lambda$ , but that is not going to answer the question of *what dark energy is*, if results are so close to a cosmological constant as it seems. We are very far from being able to learn the form of the function in a similar way to that of the spectrum of the CMB radiation which univocally determines a blackbody emission with a temperature of  $2.725K$ . For dark energy, neither the determinations can achieve this degree of precision nor there is a real physically motivated theory behind. Tight results departing from a cosmological constant would be easier to interpret, and maybe they would fit one of the proposed theories and they would surely rule out most of the existing ones. Tight results around a cosmological constant get us into trouble: we have no idea of what the cosmological constant is physically, at least not if it does not change by  $10^{55}$  orders of magnitude.

That opens three possible lines of work. *(i)* Work on theories to understand the meaning of the cosmological constant since it is the most reasonable answer given by observations. *(ii)* Test departures from the cosmological constant with alternative theoretical models or validate them with an unquestionable agreement with observations. *(iii)* Address the accelerated expansion through new ideas other than dark energy and attack the problem from another side.

Of course, all of them should be followed, as only time will tell us if we are in the correct way. Perhaps we are about to correctly interpret the meaning of the cosmological constant. Or maybe we are now just like Ptolemy tuning the untunable to describe through the epicycles that which is otherwise easily described

when changing the perspective. Let us just hope that we do not need 15 centuries to realise that we are in the wrong way... in case we are!



## Appendix A

---

# Notation

---

In the following, we include a list with the notation used in the thesis. It has been divided according to the part it belongs to, and distinguished between symbols and abbreviations and acronyms. A change in the chapter is indicated within each section with a wider line spacing. Besides, as a general convention we use:

$\mu, \nu$	Greek indexes (integers from 1 to 4)
$i, j, k$	Latin indexes (integers from 1 to 3)
	Latin indexes (integers from 1 to n)
$\sim$	Same order of magnitude
$\approx$	Truncation or rounding in numbers
$\cong$	Approximation in formulae

### A.1 Part I

#### Symbols

$ds$	Line element
$g_{\mu\nu}$	Metric
$x$	Temporal and spatial coordinates
$\phi$	Gravitational field (Einstein equations)
	Scalar field

---

$G_{\mu\nu}$	Einstein's tensor
$G_N$	Newton constant
$\rho$	Density
$T_{\mu\nu}$	Energy-momentum tensor
$R$	Scalar of curvature
$R_{\mu\nu}$	Ricci tensor
$R_{\mu\nu\alpha\beta}$	Riemann tensor
$\lambda$	Constant (original cosmological constant) Wavelength
$\Lambda$	Cosmological constant
$\Lambda_{ind}$	Induced cosmological constant
$\Lambda_{vac}$	Vacuum cosmological constant
$\Lambda_{eff}$	Effective cosmological constant
$V_H$	Higgs potential
$Q$	Quintessence field
$V(Q)$	Quintessence potential
$K$	K-essence field
$V(K)$	K-essence potential
$P$	Phantom field
$V(P)$	Phantom potential
$t$	Time coordinate
$c$	Speed of light
$r$	Radial comoving coordinate
$\theta$	Polar comoving coordinate
$\varphi$	Azimuthal comoving coordinate
$\chi$	Physical comoving coordinate
$d\Omega$	Angular differential
$k$	Curvature
$a$	Scale factor
$H_0$	Hubble constant
$h_0$	Dimensionless Hubble constant
$H$	Hubble parameter
$q_0$	Deceleration parameter
$z$	Redshift
$\nu$	Frequency
$d_{prop}$	Proper distance

---

$d_L$	Luminosity distance
$d_A$	Angular distance
$\mathcal{F}$	Flux
$\mathcal{L}$	Luminosity
$E$	Energy
$p$	Pressure of a perfect fluid
$\rho$	Density of a perfect fluid
$U_\mu$	Quadrivelocity
$w$	Barotropic index
$\rho_c^0$	Present-day critical density
$\rho_c$	Critical density
$\Omega^0$	Present-day normalized density with $\rho_c^0$
$\Omega^0(z)$	Normalized density with $\rho_c^0$
$\Omega(z)$	Normalized density with $\rho_c(z)$
$\eta_{\mu\nu}$	Minkowsky metric
$h_{\mu\nu}$	Perturbation Metric
$S$	Action
$a_i$	Constants
$m$	Mass/Renormalized mass
$\lambda$	Coupling constant/Renormalized coupling constant
$m_0$	Naked mass
$\lambda_0$	Naked coupling constant
$\Lambda$	Regularization parameter
$\mu$	Renormalization scale
$Z$	Renormalization constant
$G$	Green function
$G_0$	Naked Green function
$G_R$	Renormalized Green function
$p_i$	Momentum of the $i$ particle
$\beta$	Beta function
$\gamma_m$	Anomalous mass dimension
$\gamma_\phi$	Anomalous field dimension
$\xi$	Constant
$g_*$	Number of degrees of freedom for relativistic particles
	Fixed point

$\lambda_*$	Fixed point
$m_i$	Masses of the light degrees of freedom
$M_i$	Masses of the heavy degrees of freedom
$\mathcal{M}_i$	Masses of the light and heavy degrees of freedom
$A, B, \dots$	Constants
$J$	Spin
$\sigma$	Sign related to bosonic/fermionic domination
$M_{Pl}$	Planck mass
$m_S$	Scalar field mass
$m_\nu$	Neutrino mass
$m_H$	Higgs mass
$m_W$	Wino mass
$m_Z$	Zino mass
$\eta$	Defined constant
$\nu$	Constant: cosmological index
$\nu_0$	Cosmological index with $M = M_{Pl}$ and $\sigma = +1$
$\kappa$	Constant related to curvature
$z_{tr}$	Transition redshift (from positive to negative cosmological constant)
$z^*$	Transition redshift (from positive to negative acceleration)
$\delta_\Lambda$	Variation of $\Lambda$ with respect to a constant cosmological constant
$\delta H$	Variation of $H$ with respect to the standard Hubble parameter
$\tilde{w}(z)$	Effective barotropic index
$A, A_s$	Constants
$C$	Constant
$l_{Pl}$	Planck length
$L(\rho)$	Correction function (braneworlds)
$n(\rho)$	Index function (braneworlds)
$\chi$	Scalar field
$r_c$	Scale at which gravity changes its behaviour
$\sigma$	Brane tension
$B, D$	Constants
$D(a)$	Quantization of the operator $a^{-3}$ (LQC)
$a_i$	Below this scale factor space-time is discrete (LQC)
$a_*$	Scale factor at which classical equations are recovered (LQC)
$l$	Quantum number

---

$w_0$	Constant or average barotropic index
$w_c$ $\tilde{w}_0$	Alternative symbols for the constant or average barotropic index
$w'$	Derivative with respect to $z$ of the barotropic index
$w_a$	Derivative with respect to $a$ of the barotropic index in a linear expansion
$w_l$	The same but for a logarithmic expansion
$w_1$	Early value of the barotropic index
$z_t$	Redshift at which there is the transition from $w_0$ to $w_1$

## Abbreviations and acronyms

CMB	Cosmic Microwave Background radiation
COBE	Cosmic Background Explorer
WMAP	Wilkinson Microwave Anisotropy Probe
CDM	Cold Dark Matter
WIMP	Weakly Interactive Massive Particles
SNe Ia	Type Ia Supernovae
BAO	Baryonic Acoustic Oscillations
ISW	Integrated Sachs Wolfe effect
SDSS	Sloan Digital Sky Survey

GUT	Grand Unified Theory
FLRW	Friedman-Lemaître-Robertson-Walker
M	Matter
R	Radiation
S	Cosmic strings
W	Domain walls
T	Textures
Q	Quintessence
K	K-essence
	Curvature
Ph	Phantom
Ca	Cardassian
$\nu$	Neutrino
X	Unknown dark energy component

QFT	Quantum Field Theory
HE	Hilbert-Einstein
vac	Vacuum
MS	Minimal subtraction scheme
$\overline{\text{MS}}$	Modified minimal subtraction scheme
RGE	Renormalization Group Equations
F	Fermi epoch
CE	Conservation equation
FE	Friedmann equation
WEC	Weak energy condition
NEC	Null energy condition
DEC	Dominant energy condition
NDEC	Null dominant energy condition
SEC	Strong energy condition
SUSY	Supersymmetry
PNG	Pseudo Nambu Goldstone bosons
SUGRA	Super Gravity
DGP	Dvali-Gabadadze-Porrati
LQC	Loop quantum cosmology

## A.2 Part II

### Symbols

$\mathcal{M}$	Zero point magnitude in the blue band
$M$	Absolute magnitude
$d_L$	Luminosity distance
$D_L$	Hubble constant free luminosity distance
$f(z)$	Growth parameter
$A(z)$	Dimension less parameter measured by BAO

---

$D_V(z)$	Dilation
$D_M(z)$	Comoving angular diameter distance
$R(z)$	Shift parameter
$\lambda$	Wavelength
$v$	Velocity
$\Delta m_{15}(B)$	B magnitude increment from the maximum up to 15 days after it
$a$ $b$	Free parameters in Phillips relation
$M_B$	Absolute magnitude in B band
$s$ $\hat{s}$	Stretch factor
$w$	Width factor
$\alpha$	Free parameter in stretch correction
$c$	Colour excess in the extinction correction
$\alpha$ $\beta$	Free parameters
$\Delta$	Difference in magnitude with respect to a fiducial SN
$\mu$	Distance modulus
$t_0$	Time at maximum of the light curve
$R$	Linear correlations in MCLS method
$Q$	Quadratic correlations in MCLS method
$\zeta_X$ $\alpha_X$ $\beta_X$	Extinction parameters in an $X$ band
$B_{BX}$ $\beta_{BX}$	Constants in CMAGIC method
$K_{BX}$	K-Correction from $B$ to $X$ band
$R_X$	Slope of the extinction law in an $X$ band
$A_X$	Absorption in an $X$ band
$A_{Gal}$	Galactic absorption
$X_i$	Random variables
$\theta_i$	Unknown parameters
$\phi(\mathbf{X}, \theta)$	Probability density function
$L(\theta \mathbf{X})$	Likelihood function
$P$	Probability
$p$	$p$ -value
$\mathbf{M}$	Vector of unknowns in the inverse methodology
$y$	Dimensionless distance coordinate
$\sigma_y$	Uncertainty on the dimensionless distance coordinate

$C_{y_i y_j}$	Covariance components of data
$\mathbf{M}_0$	<i>A priori</i> vector of unknowns
$\mathbf{C}_0$	<i>A priori</i> covariance matrix
$C_{w(z), w(z')}$	Covariance of $w(z)$ between redshifts
$\Delta_z$	Correlation length
$S$	Misfit or objective function
$H$	Hessian
$\mathbf{G}$	Matrix of partial derivatives of the dimensionless distance coordinate
$g$	Kernel of $\mathbf{G}$
$K(z, z')$	Resolving kernel
$\sigma$	<i>A priori</i> uncertainty
$\tilde{\sigma}$	<i>A posteriori</i> uncertainty

## Abbreviations and acronyms

SN	Supernova
FR IIb	Fanaroff-Riley Type IIb radio galaxies
CRS	Compact radio sources
2dFGRS	2dF Galaxy Redshift Survey
CBI	Cosmic Background Imager
ACBAR	Arcminute Cosmology Bolometer Array Receiver
WD	White dwarf
Ch	Chandrasekhar
MCLS	Multicolour Light Curve Shape
BATM	Bayesian Adapted Template Match
CMAGIC	Colour-Magnitude Intercept Calibration
DES	Dark Energy Survey
ESSENCE	Equation of State: SuperNovae trace Cosmic Expansion
SNLS	SuperNova Legacy Survey
pdf	Probability density function
dof	Degree of freedom
MC	Monte Carlo

---

SNAP	SuperNova Acceleration Probe
JDEM	Joint Dark Energy Mission
CSP	Carnegie Supernova Project
SDSS	Sloan Digital Sky Survey
PANS	Probing Acceleration Now with Supernovae
LSST	Large Synoptic Survey Telescope
Pan-	
STARRS	Panoramic Survey Telescope And Rapid Response System
DESTINY	Dark Energy Space Telescope
JEDI	Joint Efficient Dark-energy Investigation
ADEPT	Advanced Dark Energy Physics Telescope
DUNE	Dark UNiverse Explorer
ALPACA	Advanced Liquid-mirror Probe for Astrophysics, Cosmology and Asteroids



---

# List of Figures

---

1	Densitat de matèria i constant cosmològica en un univers pla amb $\Omega_M^0 = 0,3$ i $\Omega_\Lambda^0 = 0,7$ segons el <i>running</i> a l'Escenari 3. . . . .	xviii
2	Regions de confiança per als paràmetres cosmològics utilitzant dos conjunts de dades: R06 i VW07. . . . .	xx
3	Regions de confiança per als paràmetres relacionats amb la forma de l'energia fosca obtinguts amb les dades de la Ref. [56]. . . . .	xxi
4	Reconstrucció de $w(z)$ i $\Omega_\Lambda^0(z)$ a partir de 1000 inversions de les dades de R06 amb <i>priors</i> aleatoris entre $-3 < w(z)^0 < 1$ . . . . .	xxv
5	Com la Figura 4 per les dades de VW07. . . . .	xxvi
6	Regions de confiança per als tres escenaris amb <i>running</i> de la constant cosmològica al pla $(\Omega_M^0, \theta)$ per dades de LSST i SNAP. . . . .	xxix
7	Reconstrucció de $w(z)$ i errors Monte Carlo obtinguts després de 1000 inversions de les dades de LSST <i>deep survey</i> i SNAP. . . . .	xxx
1.1	The four pillars of the standard hot Big Bang model. . . . .	3
1.2	Increment of observed SNe Ia in the recent years and the corresponding increment in the number of papers with the key words <i>Dark Energy</i> or <i>Cosmological Constant</i> . . . . .	10

2.1	First mention to the cosmological constant by Albert Einstein in his paper of 1917 [68]. . . . .	16
2.2	Quantities used in the calculations of the angular and luminosity distances by analogy to an euclidean universe. . . . .	28
2.3	$(\Omega_M^0, \Omega_\Lambda^0)$ plane. The position on the plane determines the geometry and the dynamics of the Universe. . . . .	34
3.1	Evolution of the cosmological constant as an effect of the RGE in three different scenarios. . . . .	50
3.2	Evolution of the density of matter and cosmological constant in a flat universe. . . . .	60
3.3	Evolution of the density of matter and cosmological constant in a closed and in an open universe. . . . .	62
3.4	Deviation $\delta_\Lambda$ and variation rate $(1/\rho_c^0) d\Lambda/dz$ in a flat universe. . . . .	64
3.5	Deviations of the Hubble parameter for different $\nu$ 's with respect to a universe with cosmological constant. . . . .	65
3.6	Redshift evolution of $\Omega_M$ and $\Omega_\Lambda$ . . . . .	67
3.7	Deceleration parameter and transition redshift for a flat universe and an evolving cosmological constant. . . . .	69
4.1	$(p, \rho)$ plane for a component that accelerates the Universe. . . . .	73
4.2	Equation of state for nine different quintessence models. Plot extracted from Weller and Albrecht (2002) [206]. . . . .	77
4.3	Pseudo-equation of state produced by an evolving cosmological constant. . . . .	80
4.4	Evolution of the effective equation of state of a common dark energy component with $p = \tilde{w}\rho$ when the universe is made of a Chaplygin gas. . . . .	81
4.5	Effective equation of state in modified gravity. . . . .	84

4.6	Effective equation of state in DGP (+) models. . . . .	86
4.7	Steps in the determination and explanation of the equation of state from observations of extragalactic sources. . . . .	94
4.8	Degeneracy in luminosity distance for five different dark energy models.	97
5.1	Confidence regions showing BAO constraints on the cosmological pa- rameter plane $(\Omega_M^0, \Omega_\Lambda^0)$ and for a constant equation of state $(w_0, \Omega_M^0)$ .	106
5.2	Classification scheme of supernovae. . . . .	108
5.3	Composite figure with the spectral templates for all types of super- novae and for real objects. . . . .	111
5.4	Schematic light curves for different types of supernovae. . . . .	112
5.5	Spectroscopic evolution of the normal SNe Ia SN1994D. . . . .	113
5.6	Dispersion and composite curve of nearby SNe Ia obtained with the stretch factor method. . . . .	119
5.7	Uncertainty in the magnitude as a consequence of an uncertainty in the redshift determination. . . . .	128
5.8	Hubble diagram and redshift histogram for the 182 SNe Ia from Riess et al. (2006) and the 162 SNe Ia from Wood-Vasey et al. (2007). . . .	130
5.9	Outline of the generation of 1000 data sets via bootstrap resampling from the original set, in this case that of Riess et al. (2004). . . . .	131
6.1	Cosmological parameters obtained with two high redshift supernovae data sets without and with BAO constraints. . . . .	140
6.2	$1\sigma$ , $2\sigma$ and $3\sigma$ confidence regions in the $(\Omega_M^0, (1/\rho_c^0)d\Lambda/dz _{z=0})$ plane for a general evolving cosmological constant in a flat universe. . . . .	142
6.3	Confidence region in the $(\Omega_M^0, \tau)$ space for the evolution in Scenario 1 in a flat universe. . . . .	145

6.4	Confidence regions as in Figure 6.3 but in the $(\Omega_M^0, \eta)$ space, where $\eta$ represents the running in Scenario 2. . . . .	146
6.5	As Figure 6.3 but for the cosmological index of Scenario 3. . . . .	148
6.6	Confidence region in the $(\Omega_M^0, w_0)$ plane for a constant equation of state in a flat universe. . . . .	150
6.7	Confidence region in the $(w_0, w_a)$ plane for an evolving equation of state in a flat universe. Results with and without a prior on $\Omega_M^0$ are shown. . . . .	153
6.8	$1\sigma$ , $2\sigma$ and $3\sigma$ confidence regions for all the dark energy parameters obtained with the data compilation in Ref. [56]. . . . .	155
7.1	Reconstruction of $w(z)$ using 182 SNe from the gold set of Ref. [160] using a non-parametric inverse approach. . . . .	171
7.2	Reconstruction of $w(z)$ (as in Figure 7.1) but with the 162 SNe compiled by the ESSENCE team. . . . .	172
7.3	Mean and $1\sigma$ Monte Carlo errors obtained from 1000 inversions of R06 data with random priors between $-3 < w(z)^0 < 1$ . . . . .	173
7.4	As in Figure 7.3 but for VW07 SNe Ia. . . . .	174
7.5	Reconstruction of $w(z)$ (as in Figure 7.1) but with the 192 SNe from Davis et al. (2007). . . . .	175
7.6	The same as in Figure 7.3, for the compilation in Ref. [56]. . . . .	176
7.7	Evolution of the cosmological constant along redshift obtained from R06. 1000 inversions with priors in the range $-0.2 < \Delta\Omega_\Lambda^0(z) < 0.2$ . . . . .	178
7.8	Evolution of the cosmological constant as in Figure 7.7 but for the VW07 data set. . . . .	179
7.9	Reconstruction of $\Omega_\Lambda^0(z)$ using 1000 sets as in Figure 7.7 and 7.8. The data compilation in D07 is used. . . . .	180

8.1	Uncertainties achieved for different surveys as a function of redshift. . . . .	185
8.2	$1\sigma$ , $2\sigma$ and $3\sigma$ confidence regions in the $(\Omega_M, w_0)$ plane with the addition of different sources of uncertainty related to photometric redshifts in the LSST wide survey. . . . .	191
8.3	Effect of photo- $z$ 's and systematics on $1\sigma$ , $2\sigma$ and $3\sigma$ confidence regions in $(w_0, w_a)$ as obtained with the LSST wide survey. . . . .	193
8.4	Confidence regions for a constant equation of state in the $(\Omega_M, w_0)$ space making use of LSST and SNAP. . . . .	194
8.5	As Figure 8.4 but for an evolving dark energy source parameterized with $(w_0, w_a)$ . . . . .	196
8.6	Reconstruction of the continuous evolution of the dark energy equation of state for two SUGRA models with SNAP data. . . . .	200
8.7	Reconstruction of $w(z)$ and Monte Carlo errors obtained after 1000 inversions of LSST deep survey and SNAP data. . . . .	202
8.8	Confidence regions for three running scenarios in the $(\Omega_M^0, \theta)$ plane for LSST and SNAP data. . . . .	204
8.9	Deviations of the distance modulus $m - M$ for dark energy models with respect to the case of a standard cosmological constant. . . . .	205
8.10	As Figure 8.8 but data simulations use fiducial models other than the cosmological constant without evolution. . . . .	207



---

# List of Tables

---

4.1	Potentials and motivation for their form for some of the quintessence models. . . . .	76
4.2	Different braneworld models as described by the function $L(\rho_\chi)$ . . . . .	87
6.1	$\Delta\chi^2$ as a function of the number of degrees of freedom (dofs) and the desired level of probability when errors are normally distributed. . . . .	136
6.2	Cosmological parameters obtained for a cosmological constant model from R06 and VW07 data. . . . .	141
6.3	Best fits and $1\sigma$ errors for the different models with a running of the cosmological constant presented in this thesis. . . . .	144
6.4	As in Table 6.2 but parameters correspond to a constant dark energy equation of state. A flat universe is assumed. . . . .	151
6.5	Best fit values for the parameters of an evolving equation of state $w(z) = w_0 + w_a z/(1+z)$ retrieved with R06 and VW07 data. . . . .	154
7.1	Priors, results and $1\sigma$ errors for $\Omega_M^0$ , $w_0$ and $w_a$ as obtained from the inverse method in the discrete case and for R06, VW07 and D07. . . . .	177
8.1	Number of SNe Ia per bin for SNFactory, LSST and SNAP surveys. . . . .	186

---

8.2	$1\sigma$ uncertainties in the determination of the cosmological parameters and the dark energy equation of state according to the error in photo- $z$ 's for the LSST wide survey. . . . .	189
8.3	As in Table 8.2 with the addition of systematic uncertainties. . . . .	192
8.4	As in Table 8.3 but for the LSST deep survey. . . . .	195
8.5	Uncertainties in the determination of the cosmological parameters and the dark energy equation of state for three different levels of systematics in the SNAP survey. . . . .	199
8.6	$1\sigma$ uncertainties for the free parameters appearing in the running cosmological constant scenarios obtained with LSST and SNAP. . . . .	203
8.7	As in Table 8.6 but for fiducial models other than the cosmological constant. . . . .	206

---

# Bibliography

---

- [1] ALEPH, DELPHI, L3, OPAL Collab. and the LEP Higgs Working Group, <http://lephiggs.web.cern.ch/LEPHIGGS/www/Welcome.html>.
- [2] ADEPT INFORMATION. [http://www.jhu.edu/news\\_info/news/home06/aug06/adept.html](http://www.jhu.edu/news_info/news/home06/aug06/adept.html).
- [3] ALBRECHT, A., AND SKORDIS, C. Phenomenology of a Realistic Accelerating Universe Using Only Planck-Scale Physics. *Phys. Rev. Lett.* 84 (Mar. 2000), 2076–2079.
- [4] ALBRECHT, A., AND STEINHARDT, P. J. Cosmology for grand unified theories with radiatively induced symmetry breaking. *Phys. Rev. Lett.* 48 (Apr. 1982), 1220–1223.
- [5] ALDERING, G., ADAM, G., ANTILOGUS, P., ASTIER, P., BACON, R., BONGARD, S., BONNAUD, C., COPIN, Y., HARDIN, D., HENAULT, F., HOWELL, D. A., LEMONNIER, J.-P., LEVY, J.-M., LOKEN, S. C., NUGENT, P. E., PAIN, R., PECONTAL, A., PECONTAL, E., PERLMUTTER, S., QUIMBY, R. M., SCHAHMANECHE, K., SMADJA, G., AND WOOD-VASEY, W. M. Overview of the Nearby Supernova Factory. In *Survey and Other Telescope Technologies and Discoveries. Proceedings of the SPIE.* (Dec. 2002), J. A. Tyson and S. Wolff, Eds., vol. 4836, pp. 61–72.
- [6] ALLEN, S. W., RAPETTI, D. A., SCHMIDT, R. W., EBELING, H., MORRIS, G., AND FABIAN, A. C. New constraints on dark energy from Chandra X-ray observations of the largest relaxed galaxy clusters. *ArXiv e-prints 706* (May 2007).
- [7] ALPACA WEB PAGE. <http://www.astro.ubc.ca/LMT/alpaca/>.

- [8] ALPHER, R. A., BETHE, H., AND GAMOW, G. The origin of chemical elements. *Phys. Rev.* *73*, 7 (Apr 1948), 803–804.
- [9] ALTAVILLA, G., FIORENTINO, G., MARCONI, M., MUSELLA, I., CAPPELLARO, E., BARBON, R., BENETTI, S., PASTORELLO, A., RIELLO, M., TURATTO, M., AND ZAMPIERI, L. Cepheid calibration of Type Ia supernovae and the Hubble constant. *MNRAS* *349* (Apr. 2004), 1344–1352.
- [10] AMENDOLA, L. Coupled quintessence. *Phys. Rev. D* *62*, 4 (Jul 2000), 043511.
- [11] APPELQUIST, T., AND CARAZZONE, J. Infrared singularities and massive fields. *Phys. Rev. D* *11* (1975), 2856.
- [12] ARMENDARIZ-PICON, C., MUKHANOV, V., AND STEINHARDT, P. J. Essentials of k-essence. *Phys. Rev. D* *63* (2001), 103510.
- [13] ARXIV DATABASE. <http://arxiv.org/>.
- [14] ASTIER, P., GUY, J., REGNAULT, N., PAIN, R., AUBOURG, E., BALAM, D., BASA, S., CARLBERG, R. G., FABBRO, S., FOUCHEZ, D., HOOK, I. M., HOWELL, D. A., LAFOUX, H., NEILL, J. D., PALANQUE-DELABROUILLE, N., PERRETT, K., PRITCHET, C. J., RICH, J., SULLIVAN, M., TAILLET, R., ALDERING, G., ANTILOGUS, P., ARSENIJEVIC, V., BALLAND, C., BAUMONT, S., BRONDER, J., COURTOIS, H., ELLIS, R. S., FILIOL, M., GONCALVES, A. C., GOOBAR, A., GUIDE, D., HARDIN, D., LUSSET, V., LIDMAN, C., MCMAHON, R., MOUCHET, M., MOURAO, A., PERLMUTTER, S., RIPOCHE, P., TAO, C., WALTON, N., AND SNLS COLLABORATION. SNLS: Measurement of  $\Omega_M$ ,  $\Omega_\Lambda$  and  $w$  from the First Year Data Set. *American Astronomical Society Meeting Abstracts 207* (Dec. 2005).
- [15] BAADE, W., AND ZWICKY, F. On Super-novae. *Proc. of the National Academy of Science* *20* (1934), 254.
- [16] BABIC, A., GUBERINA, B., HORVAT, R., AND STEFANCIC, H. Renormalization-group running of the cosmological constant and its implication for the Higgs boson mass in the standard model. *Phys. Rev. D* *65* (2002), 085002.
- [17] BABIĆ, A., GUBERINA, B., HORVAT, R., AND STEFANIĆ, H. Renormalization-group running cosmologies: A scale-setting procedure. *Phys. Rev. D* *71*, 12 (June 2005), 124041.

- [18] BACKUS, G., AND GILBERT, F. Uniqueness in the inversion of inaccurate gross earth data. *Philos. Trans. R. Soc. London. Ser. A.* 366 (1970), 123.
- [19] BALASTEGUI, A. *A new classification of gamma-ray bursts and its cosmological implications*. PhD thesis, Universitat de Barcelona, April 2006.
- [20] BARREIRO, T., COPELAND, E. J., AND NUNES, N. J. Quintessence arising from exponential potentials. *Phys. Rev. D* 61 (2000), 127301.
- [21] BARRIS, B. J., TONRY, J. L., BLONDIN, S., CHALLIS, P., CHORNOCK, R., CLOCCHIATTI, A., FILIPPENKO, A. V., GARNAVICH, P., HOLLAND, S. T., JHA, S., KIRSHNER, R. P., KRISCIUNAS, K., LEIBUNDGUT, B., LI, W., MATHESON, T., MIKNAITIS, G., RIESS, A. G., SCHMIDT, B. P., SMITH, R. C., SOLLERMAN, J., SPYROMILIO, J., STUBBS, C. W., SUNTZEFF, N. B., AUSSEL, H., CHAMBERS, K. C., CONNELLEY, M. S., DONOVAN, D., HENRY, J. P., KAISER, N., LIU, M. C., MARTÍN, E. L., AND WAINSCOAT, R. J. Twenty-Three High-Redshift Supernovae from the Institute for Astronomy Deep Survey: Doubling the Supernova Sample at  $z > 0.7$ . *ApJ* 602 (Feb. 2004), 571–594.
- [22] BARROW, J., AND TIPLER, F. *The Anthropic Cosmological Principle*. Clarendon, Oxford, U.K., 1986.
- [23] BARROW, J. D., AND COTSAKIS, S. Inflation and the conformal structure of higher-order gravity theories. *Phys. Lett. B* 214 (Dec. 1988), 515–518.
- [24] BENTIVEGNA, E., BONANNO, A., AND REUTER, M. Confronting the IR Fixed Point Cosmology with High Redshift Supernova Data. *JCAP* 1 (Jan. 2004), 1.
- [25] BENTO, M. C., BERTOLAMI, O., REBOUCAS, M. J., AND SILVA, P. T. Generalized chaplygin gas model, supernovae and cosmic topology. *Phys. Rev. D* 73, 4 (Feb. 2006), 043504.
- [26] BENTO, M. C., BERTOLAMI, O., AND SEN, A. A. Generalized Chaplygin gas, accelerated expansion, and dark-energy-matter unification. *Phys. Rev. D* 66, 4 (Aug. 2002), 043507.
- [27] BERNSTEIN, G., AND JAIN, B. Dark Energy Constraints from Weak-Lensing Cross-Correlation Cosmography. *ApJ* 600 (Jan. 2004), 17–25.

- [28] BEZERRA, V. B., ROMERO, C., GREBOT, G., GUIMARAES, M. E. X., AND COLATTO, L. P. Remarks on some vacuum solutions of scalar-tensor cosmological models. *Brazilian Journal of Physics* 34 (June 2004), 526–530.
- [29] BILIĆ, N., TUPPER, G. B., AND VIOLLIER, R. D. Unification of dark matter and dark energy: the inhomogeneous Chaplygin gas. *Phys. Lett. B* 535 (May 2002), 17–21.
- [30] BOJOWALD, M. Quantization ambiguities in isotropic quantum geometry. *Class. Quant. Grav.* 19 (2002), 5113–5230.
- [31] BONANNO, A., AND REUTER, M. Cosmology of the Planck era from a renormalization group for quantum gravity. *Phys. Rev. D* 65 (2002), 043508.
- [32] BOND, J. R., EFSTATHIOU, G., AND TEGMARK, M. Forecasting cosmic parameter errors from microwave background anisotropy experiments. *MNRAS* 291 (1997), L33–L41.
- [33] BOUSSO, R., AND YANG, I.-S. Landscape predictions from cosmological vacuum selection. *Phys. Rev. D* 75, 12 (June 2007), 123520.
- [34] BRANKIN, R., GLADWELL, I., AND SHAMPINE, L. RKSUITE: a Suite of Runge-Kutta Codes for the Initial Value Problem of ODEs. Softreport 92-S1, Department of Mathematics, Southern Methodist University, 1992.
- [35] BRAX, P., AND MARTIN, J. Quintessence and supergravity. *Phys. Lett. B* 468 (1999), 40–45.
- [36] BUCHBINDER, I., ODINTSOV, S., AND SHAPIRO, I. *Effective Action in Quantum Gravity*. IOP Publishing, 1992.
- [37] CABRÉ, A., GAZTAÑAGA, E., MANERA, M., FOSALBA, P., AND CASTANDER, F. Cross-correlation of Wilkinson Microwave Anisotropy Probe third-year data and the Sloan Digital Sky Survey DR4 galaxy survey: new evidence for dark energy. *MNRAS* 372 (Oct. 2006), L23–L27.
- [38] CALDWELL, R. R. A phantom menace? *Phys. Lett. B* 545 (2002), 23–29.
- [39] CALDWELL, R. R., DAVÉ, R., AND STEINHARDT, P. J. Cosmological imprint of an energy component with general equation of state. *Phys. Rev. Lett.* 80 (1998), 081582.

- [40] CALDWELL, R. R., KAMIONKOWSKI, M., AND WEINBERG, N. N. Phantom Energy and Cosmic Doomsday. *Phys. Rev. Lett.* *91* (2003), 071301.
- [41] CANAL, R., MÉNDEZ, J., AND RUIZ-LAPUENTE, P. Identification of the Companion Stars of Type Ia supernovae. *ApJ* *550* (Mar. 2001), L53–L56.
- [42] CARROLL, S. M., DE FELICE, A., DUVVURI, V., EASSON, D. A., TRODDEN, M., AND TURNER, M. S. Cosmology of generalized modified gravity models. *Phys. Rev. D* *71*, 6 (Mar. 2005), 063513.
- [43] CARROLL, S. M., HOFFMAN, M., AND TRODDEN, M. Can the dark energy equation-of-state parameter  $w$  be less than  $-1$ ? *Phys. Rev. D* *68* (2003), 023509.
- [44] CARROLL, S. M., PRESS, W. H., AND TURNER, E. L. The cosmological constant. *ARA&A* *30* (1992), 499–542.
- [45] CHEVALLIER, M., AND POLARSKI, D. Accelerating universes with scaling dark matter. *Int. J. Mod. Phys. D10* (2001), 213–224.
- [46] CLINE, J. M., AND VINET, J. Problems with time-varying extra dimensions or ‘Cardassian expansion’ as alternatives to dark energy. *Phys. Rev. D* *68* (2003), 025015.
- [47] CLOCCHIATTI, A., SCHMIDT, B. P., FILIPPENKO, A. V., CHALLIS, P., COIL, A. L., COVARRUBIAS, R., DIERCKS, A., GARNAVICH, P., GERMANY, L., GILLILAND, R., HOGAN, C., JHA, S., KIRSHNER, R. P., LEIBUNDGUT, B., LEONARD, D., LI, W., MATHESON, T., PHILLIPS, M. M., PRIETO, J. L., REISS, D., REISS, A. G., SCHOMMER, R., SMITH, R. C., SODERBERG, A., SPYROMILIO, J., STUBBS, C., SUNTZEFF, N. B., TONRY, J. L., AND WOUTD, P. Hubble Space Telescope and Ground-based Observations of Type Ia Supernovae at Redshift 0.5: Cosmological Implications. *ApJ* *642* (May 2006), 1–21.
- [48] COORAY, A. R., AND HUTERER, D. Gravitational Lensing as a Probe of Quintessence. *ApJ* *513* (Mar. 1999), L95–L98.
- [49] COPELAND, E. J., LEE, S. J., LIDSEY, J. E., AND MIZUNO, S. Generalised cosmological scaling solutions. *Phys. Rev. D* *71* (2005), 023526.

- [50] COPELAND, E. J., LIDSEY, J. E., AND MIZUNO, S. Correspondence between loop-inspired and braneworld cosmology. *Phys. Rev. D* 73, 4 (Feb. 2006), 043503–+.
- [51] CORASANITI, P. S., BASSETT, B. A., UNGARELLI, C., AND COPELAND, E. J. Model-independent dark energy differentiation with the isw effect. *Phys. Rev. Lett.* 90 (2003), 091303.
- [52] CORRY, L., RENN, J., AND STACHEL, J. Belated Decision in the Hilbert-Einstein Priority Dispute. *Science* 278 (1997), 1270–1273.
- [53] CSP WEB PAGE. <http://csp1.lco.cl/~cspuser1/PUB/CSP.html>.
- [54] DALY, R. A., AND DJORGOVSKI, S. G. A Model-Independent Determination of the Expansion and Acceleration Rates of the Universe as a Function of Redshift and Constraints on Dark Energy. *ApJ* 597 (Nov. 2003), 9–20.
- [55] DALY, R. A., AND DJORGOVSKI, S. G. Direct Determination of the Kinematics of the Universe and Properties of the Dark Energy as Functions of Redshift. *ApJ* 612 (Sept. 2004), 652–659.
- [56] DAVIS, T. M., MORTSELL, E., SOLLERMAN, J., BECKER, A. C., BLONDIN, S., CHALLIS, P., CLOCCHIATTI, A., FILIPPENKO, A. V., FOLEY, R. J., GARNAVICH, P. M., JHA, S., KRISCIUNAS, K., KIRSHNER, R. P., LEIBUNDGUT, B., LI, W., MATHESON, T., MIKNAITIS, G., PIGNATA, G., REST, A., RIESS, A. G., SCHMIDT, B. P., SMITH, R. C., SPYROMILIO, J., STUBBS, C. W., SUNTZEFF, N. B., TONRY, J. L., AND WOOD-VASEY, W. M. Scrutinizing Exotic Cosmological Models Using ESSENCE Supernova Data Combined with Other Cosmological Probes. *ApJ* 666 (Sept. 2007), 716–725.
- [57] DE LA MACORRA, A., AND PICCINELLI, G. General scalar fields as quintessence. *Phys. Rev. D* 61 (2000), 123503.
- [58] DEFFAYET, C., LANDAU, S. J., RAUX, J., ZALDARRIAGA, M., AND ASTIER, P. Supernovae, CMB, and gravitational leakage into extra dimensions. *Phys. Rev. D* 66 (2002), 024019.
- [59] DES WEB PAGE. <https://www.darkenergysurvey.org/>.
- [60] DESTINY WEB PAGE. <http://destiny.asu.edu/>.

- [61] DIAZ-RIVERA, L. M., AND PIMENTEL, L. O. Cosmological models with dynamical Lambda in scalar-tensor theories. *Phys. Rev. D* 60 (1999), 123501.
- [62] DICKE, R. H., PEEBLES, P. J. E., ROLL, P. G., AND WILKINSON, D. T. Cosmic Black-Body Radiation. *ApJ* 142 (July 1965), 414–419.
- [63] DUNE WEB PAGE. <http://www.dune-mission.net/>.
- [64] DVALI, G. R., GABADADZE, G., AND PORRATI, M. 4D gravity on a brane in 5D Minkowski space. *Phys. Lett. B* 485 (2000), 208–214.
- [65] EFSTATHIOU, G. Constraining the equation of state of the Universe from distant Type Ia supernovae and cosmic microwave background anisotropies. *MNRAS* 310 (Dec. 1999), 842–850.
- [66] EINSTEIN, A. Die Feldgleichungen der Gravitation. *Sitzber. Preuss. Akad. Wiss.* (1915), 844. Also in *The Collected Papers of Albert Einstein Vol. 6* (Eds M J Klein et al.) (Princeton, NJ: Princeton Univ. Press, 1995).
- [67] EINSTEIN, A. Erklärung der Perihelbewegung des Merkur aus der allgemeinen Relativitätstheorie. *Sitzungsberichte der Königlich Preußischen Akademie der Wissenschaften (Berlin)* (1915), 831–839.
- [68] EINSTEIN, A. Kosmologische Betrachtungen zur allgemeinen Relativitätstheorie. *Sitzber. Preuss. Akad. Wiss.* (1917), 142. Also in *The Collected Papers of Albert Einstein Vol. 7* (Eds M J Klein et al.) (Princeton, NJ: Princeton Univ. Press, 1995).
- [69] EINSTEIN, A., AND GROSSMANN, M. Entwurf einer verallgemeinerten Relativitätstheorie und einer Theorie der Gravitation. *Zeits. f. Math. und Physik* 62 (1913), 225. Also in *The Collected Papers of Albert Einstein Vol. 5* (Eds M J Klein et al.) (Princeton, NJ: Princeton Univ. Press, 1995).
- [70] EISENSTEIN, D. J., ZEHAVI, I., HOGG, D. W., SCOCCIMARRO, R., BLANTON, M. R., NICHOL, R. C., SCRANTON, R., SEO, H.-J., TEGMARK, M., ZHENG, Z., ANDERSON, S. F., ANNIS, J., BAHCALL, N., BRINKMANN, J., BURLES, S., CASTANDER, F. J., CONNOLLY, A., CSABAI, I., DOI, M., FUKUGITA, M., FRIEMAN, J. A., GLAZEBROOK, K., GUNN, J. E., HENDRY, J. S., HENNESSY, G., IVEZIĆ, Z., KENT, S., KNAPP, G. R., LIN, H., LOH, Y.-S., LUPTON, R. H., MARGON, B., MCKAY, T. A., MEIKSIN,

- A., MUNN, J. A., POPE, A., RICHMOND, M. W., SCHLEGEL, D., SCHNEIDER, D. P., SHIMASAKU, K., STOUGHTON, C., STRAUSS, M. A., SUBBARAO, M., SZALAY, A. S., SZAPUDI, I., TUCKER, D. L., YANNY, B., AND YORK, D. G. Detection of the Baryon Acoustic Peak in the Large-Scale Correlation Function of SDSS Luminous Red Galaxies. *ApJ* 633 (Nov. 2005), 560–574.
- [71] ELIZALDE, E., AND NEVES, R. Modified gravity on the brane and dark energy. *Gen. Rel. Grav.* 38 (2006), 1367–1377.
- [72] ELIZALDE, E., NOJIRI, S., AND ODINTSOV, S. D. Late-time cosmology in a (phantom) scalar-tensor theory: Dark energy and the cosmic speed-up. *Phys. Rev. D* 70, 4 (Aug. 2004), 043539.
- [73] ESPAÑA-BONET, C., AND RUIZ-LAPUENTE, P. Dark Energy as an Inverse Problem. *hep-ph/0503210* (Mar. 2005).
- [74] ESPAÑA-BONET, C., AND RUIZ-LAPUENTE, P. Tracing  $w(z)$  with the latest high redshift supernovae. *Submitted to JCAP* (2007).
- [75] ESPAÑA-BONET, C., RUIZ-LAPUENTE, P., SHAPIRO, I. L., AND SOLÀ, J. Testing the running of the cosmological constant with type Ia supernovae at high  $z$ . *JCAP* 0402 (2004), 006.
- [76] ESSENCE WEB PAGE. <http://www.ctio.noao.edu/wproject/>.
- [77] FABRIS, J. C., SHAPIRO, I. L., AND SOLÀ, J. Density perturbations for a running cosmological constant. *JCAP* 2 (Feb. 2007), 16.
- [78] FERREIRA, P. G., AND JOYCE, M. Cosmology with a primordial scaling field. *Phys. Rev. D* 58, 2 (July 1998), 023503.
- [79] FREEDMAN, W. L., MADORE, B. F., GIBSON, B. K., FERRARESE, L., KELSON, D. D., SAKAI, S., MOULD, J. R., KENNICUTT, R. C., FORD, H. C., GRAHAM, J. A., HUCHRA, J. P., HUGHES, S. M. G., ILLINGWORTH, G. D., MACRI, L. M., AND STETSON, P. B. Final results from the hubble space telescope key project to measure the hubble constant. *ApJ* 553 (2001), 47–72.
- [80] FREESE, K. Generalized cardassian expansion: Models in which the universe is flat, matter dominated, and accelerating. *Nucl. Phys. Proc. Suppl.* 124 (2003), 50–54.

- [81] FREESE, K. Cardassian expansion: Dark energy density from modified friedmann equations. *New Astron. Rev.* *49* (2005), 103–109.
- [82] FREESE, K., AND LEWIS, M. Cardassian Expansion: a Model in which the Universe is Flat, Matter Dominated, and Accelerating. *Phys. Lett. B* *540* (2002), 1–8.
- [83] FRIEMAN, J. A., HILL, C. T., STEBBINS, A., AND WAGA, I. Cosmology with Ultralight Pseudo Nambu-Goldstone Bosons. *Phys. Rev. Lett.* *75* (Sept. 1995), 2077–2080.
- [84] GARCÍA-SENZ, D., BRAVO, E., CABEZÓN, R. M., AND WOOSLEY, S. E. Constraining Deflagration Models of Type Ia Supernovae through Intermediate-Mass Elements. *ApJ* *660* (May 2007), 509–515.
- [85] GARRIGA, J., LINDE, A., AND VILENKIN, A. Dark energy equation of state and anthropic selection. *Phys. Rev. D* *69*, 6 (Mar. 2004), 063521.
- [86] GARRIGA, J., AND VILENKIN, A. Solutions to the cosmological constant problems. *Phys. Rev. D* *64*, 2 (July 2001), 023517.
- [87] GERKE, B. F., AND EFSTATHIOU, G. Probing quintessence: reconstruction and parameter estimation from supernovae. *MNRAS* *335* (Sept. 2002), 33–43.
- [88] GIANNANTONIO, T., CRITTENDEN, R. G., NICHOL, R. C., SCRANTON, R., RICHARDS, G. T., MYERS, A. D., BRUNNER, R. J., GRAY, A. G., CONNOLLY, A. J., AND SCHNEIDER, D. P. High redshift detection of the integrated Sachs-Wolfe effect. *Phys. Rev. D* *74*, 6 (Sept. 2006), 063520.
- [89] GOLIATH, M., AMANULLAH, R., ASTIER, P., GOOBAR, A., AND PAIN, R. Supernovae and the nature of the dark energy. *A&A* *380* (Dec. 2001), 6–18.
- [90] GONDOLO, P., AND FREESE, K. Fluid interpretation of Cardassian expansion. *Phys. Rev. D* *68* (2003), 063509.
- [91] GONZALEZ-DIAZ, P. F. You need not be afraid of phantom energy. *Phys. Rev. D* *68* (2003), 021303.
- [92] GORBAR, E. V., AND SHAPIRO, I. L. Renormalization group and decoupling in curved space. *JHEP* *02* (2003), 021.

- [93] GUBERINA, B., HORVAT, R., AND STEFANCIC, H. Renormalization-group running of the cosmological constant and the fate of the universe. *Phys. Rev. D* 67 (2003), 083001.
- [94] GUNNARSSON, C., DAHLÉN, T., GOOBAR, A., JÖNSSON, J., AND MÖRTSELL, E. Corrections for Gravitational Lensing of Supernovae: Better than Average? *ApJ* 640 (Mar. 2006), 417–427.
- [95] GURVITS, L. I., KELLERMANN, K. I., AND FREY, S. The “angular size - redshift” relation for compact radio structures in quasars and radio galaxies. *A&A* 342 (Feb. 1999), 378–388.
- [96] GUTH, A. H. Inflationary universe: A possible solution to the horizon and flatness problems. *Phys. Rev. D* 23 (Jan. 1981), 347–356.
- [97] GUY, J., ASTIER, P., NOBILI, S., REGNAULT, N., AND PAIN, R. SALT: a spectral adaptive light curve template for type Ia supernovae. *A&A* 443 (Dec. 2005), 781–791.
- [98] HAMUY, M., PHILIPS, M. M., MAZA, J., SUNTZEFF, N. B., DELLA VALLE, M., DANZIGER, J., ANTEZANA, R., WISCHNJWESKY, M., AVILES, R., SCHOMMER, R. A., KIM, Y.-C., WELLS, L. A., RUIZ, M. T., PROSSER, C. F., KRZEMINSKI, W., BAYLIN, C. D., HARTIGAN, P., AND HUGHES, J. SN 1992K: A twin to the subluminous Type Ia SN 1991bg. *AJ* 108 (Dec. 1994), 2226–2232.
- [99] HAMUY, M., PHILLIPS, M. M., SUNTZEFF, N. B., SCHOMMER, R. A., MAZA, J., AND AVILES, R. The Absolute Luminosities of the Calan/Tololo Type Ia Supernovae. *AJ* 112 (Dec. 1996), 2391.
- [100] HAWKING, S. W., AND ELLIS, G. F. R. *The large scale structure of Space Time*. Cambridge University Press, 1973.
- [101] HAWKINS, E., MADDOX, S., COLE, S., LAHAV, O., MADGWICK, D. S., NORBERG, P., PEACOCK, J. A., BALDRY, I. K., BAUGH, C. M., BLAND-HAWTHORN, J., BRIDGES, T., CANNON, R., COLLESS, M., COLLINS, C., COUCH, W., DALTON, G., DE PROPRIIS, R., DRIVER, S. P., EFSTATHIOU, G., ELLIS, R. S., FRENK, C. S., GLAZEBROOK, K., JACKSON, C., JONES, B., LEWIS, I., LUMSDEN, S., PERCIVAL, W., PETERSON, B. A., SUTHERLAND, W., AND TAYLOR, K. The 2dF Galaxy Redshift Survey: correlation

- functions, peculiar velocities and the matter density of the Universe. *MNRAS* *346* (Nov. 2003), 78–96.
- [102] HILBERT, D. Die Grundlagen der Physik. *Nach. Ges. Wiss. Goettingen* (1915), 395.
- [103] HILLEBRANDT, W., AND NIEMEYER, J. C. Type Ia Supernova Explosion Models. *ARA&A* *38* (2000), 191–230.
- [104] HOEKSTRA, H., MELLIER, Y., VAN WAERBEKE, L., SEMBOLONI, E., FU, L., HUDSON, M. J., PARKER, L. C., TERENO, I., AND BENABED, K. First Cosmic Shear Results from the Canada-France-Hawaii Telescope Wide Synoptic Legacy Survey. *ApJ* *647* (Aug. 2006), 116–127.
- [105] HUBBLE, E. A Relation between Distance and Radial Velocity among Extra-Galactic Nebulae. *Proceedings of the National Academy of Science* *15* (Mar. 1929), 168–173.
- [106] HUTERER, D., AND COORAY, A. Uncorrelated estimates of dark energy evolution. *Phys. Rev. D* *71*, 2 (Jan. 2005), 023506.
- [107] HUTERER, D., KIM, A., KRAUSS, L. M., AND BRODERICK, T. Redshift Accuracy Requirements for Future Supernova and Number Count Surveys. *ApJ* *615* (Nov. 2004), 595–602.
- [108] HUTERER, D., AND STARKMAN, G. Parametrization of Dark-Energy Properties: A Principal-Component Approach. *Phys. Rev. Lett.* *90*, 3 (Jan. 2003), 031301.
- [109] HUTERER, D., AND TURNER, M. S. Prospects for probing the dark energy via supernova distance measurements. *Phys. Rev. D* *60*, 8 (Oct. 1999), 081301.
- [110] IBEN, JR., I., AND TUTUKOV, A. V. Supernovae of type I as end products of the evolution of binaries with components of moderate initial mass (M not greater than about 9 solar masses). *ApJS* *54* (Feb. 1984), 335–372.
- [111] ITZYKSON, C., AND ZUBER, J. *Quantum Field Theory*. McGraw-Hill, 1980.
- [112] JAIN, B., AND TAYLOR, A. Cross-Correlation Tomography: Measuring Dark Energy Evolution with Weak Lensing. *Phys. Rev. Lett.* *91*, 14 (Oct. 2003), 141302–+.

- [113] JEDI WEB PAGE. <http://jedi.nhn.ou.edu/>.
- [114] JENA, T., NORMAN, M. L., TYTLER, D., KIRKMAN, D., SUZUKI, N., CHAPMAN, A., MELIS, C., PASCHOS, P., O'SHEA, B., SO, G., LUBIN, D., LIN, W.-C., REIMERS, D., JANKNECHT, E., AND FECHNER, C. A concordance model of the Lyman  $\alpha$  forest at  $z = 1.95$ . *MNRAS* 361 (July 2005), 70–96.
- [115] JHA, S. PhD thesis, Harvard University, 2002.
- [116] JÖNSSON, J., DAHLÉN, T., GOOBAR, A., GUNNARSSON, C., MÖRTSELL, E., AND LEE, K. Lensing Magnification of Supernovae in the GOODS Fields. *ApJ* 639 (Mar. 2006), 991–998.
- [117] KAMENSHCHIK, A. Y., MOSCHELLA, U., AND PASQUIER, V. An alternative to quintessence. *Phys. Lett. B* 511 (2001), 265–268.
- [118] KIM, A. G., LINDER, E. V., MIQUEL, R., AND MOSTEK, N. Effects of systematic uncertainties on the supernova determination of cosmological parameters. *MNRAS* 347 (Jan. 2004), 909–920.
- [119] KNOP, R. A., ALDERING, G., AMANULLAH, R., ASTIER, P., BLANC, G., BURNS, M. S., CONLEY, A., DEUSTUA, S. E., DOI, M., ELLIS, R., FABBRO, S., FOLATELLI, G., FRUCHTER, A. S., GARAVINI, G., GARMOND, S., GARTON, K., GIBBONS, R., GOLDHABER, G., GOOBAR, A., GROOM, D. E., HARDIN, D., HOOK, I., HOWELL, D. A., KIM, A. G., LEE, B. C., LIDMAN, C., MENDEZ, J., NOBILI, S., NUGENT, P. E., PAIN, R., PANAGIA, N., PENNYPACKER, C. R., PERLMUTTER, S., QUIMBY, R., RAUX, J., REGNAULT, N., RUIZ-LAPUENTE, P., SAINTON, G., SCHAEFER, B., SCHAHMANECHE, K., SMITH, E., SPADAFORA, A. L., STANISHEV, V., SULLIVAN, M., WALTON, N. A., WANG, L., WOOD-VASEY, W. M., AND YASUDA, N. New Constraints on  $\Omega_M$ ,  $\Omega_\Lambda$ , and  $w$  from an Independent Set of 11 High-Redshift Supernovae Observed with the Hubble Space Telescope. *ApJ* 598 (Nov. 2003), 102–137.
- [120] KREMER, G. M., AND ALVES, D. S. M. Palatini approach to  $1/r$  gravity and its implications to the late universe. *Phys. Rev. D* 70 (2004), 023503.
- [121] KRISCIUNAS, K., GARNAVICH, P. M., CHALLIS, P., PRIETO, J. L., RIESS, A. G., BARRIS, B., AGUILERA, C., BECKER, A. C., BLONDIN,

- S., CHORNOCK, R., CLOCCHIATTI, A., COVARRUBIAS, R., FILIPPENKO, A. V., FOLEY, R. J., HICKEN, M., JHA, S., KIRSHNER, R. P., LEIBUNDGUT, B., LI, W., MATHESON, T., MICELI, A., MIKNAITIS, G., REST, A., SALVO, M. E., SCHMIDT, B. P., SMITH, R. C., SOLLERMAN, J., SPYROMILIO, J., STUBBS, C. W., SUNTZEFF, N. B., TONRY, J. L., AND WOOD-VASEY, W. M. Hubble Space Telescope Observations of Nine High-Redshift ESSENCE Supernovae<sup>1</sup>. *AJ* 130 (Dec. 2005), 2453–2472.
- [122] LIMA, J. A. S., AND ALCANIZ, J. S. Dark Energy and the Angular Size-Redshift Diagram for Milliarcsecond Radio Sources. *ApJ* 566 (Feb. 2002), 15–18.
- [123] LINDE, A. D. A new inflationary Universe scenario: a possible solution of the horizon, flatness, homogeneity, isotropy and primordial monopole problems. *Phys. Lett. B* 108 (1982), 389–393.
- [124] LINDER, E. V. Probing dark energy with snap.
- [125] LINDER, E. V. Exploring the Expansion History of the Universe. *Phys. Rev. Lett.* 90, 9 (Mar. 2003), 091301.
- [126] LSST WEB PAGE. [http://www.lsst.org/lsst\\_home.shtml](http://www.lsst.org/lsst_home.shtml).
- [127] MAARTENS, R., AND MAJEROTTO, E. Observational constraints on self-accelerating cosmology. *Phys. Rev. D* 74, 2 (July 2006), 023004.
- [128] MALQUARTI, M., COPELAND, E. J., AND LIDDLE, A. R. K-essence and the coincidence problem. *Phys. Rev. D* 68 (2003), 023512.
- [129] MANERA, M., AND MOTA, D. F. Cluster number counts dependence on dark energy inhomogeneities and coupling to dark matter. *MNRAS* 371 (Sept. 2006), 1373–1380.
- [130] MENG, X.-H., AND WANG, P. Palatini formulation of modified gravity with  $\ln R$  terms. *Phys. Lett. B* 584 (2004), 1–7.
- [131] NESSERIS, S., AND PERIVOLAROPOULOS, L. Tension and systematics in the Gold06 SnIa data set. *JCAP* 2 (Feb. 2007), 25.
- [132] NOBBENHUIS, S. *The cosmological constant problem, an inspiration for new physics*. PhD thesis, Institute for Theoretical Physics Utrecht University, June 2006.

- [133] NOJIRI, S., AND ODINTSOV, S. D. Modified gravity with  $\ln R$  terms and cosmic acceleration.
- [134] NUGENT, P., KIM, A., AND PERLMUTTER, S. K-Corrections and Extinction Corrections for Type Ia Supernovae. *PASP* 114 (Aug. 2002), 803–819.
- [135] OLIVE, K. A., STEIGMAN, G., AND WALKER, T. P. Primordial nucleosynthesis: theory and observations. *Phys. Rep.* 333 (2000), 389–407.
- [136] OPPER, R., AND PELINSON, A. Studying the decay of the vacuum energy with the observed density fluctuation spectrum. *Phys. Rev. D* (2004).
- [137] P. NUGENT'S TEMPLATES.  
[http://supernova.lbl.gov/~nugent/nugent\\_templates.html](http://supernova.lbl.gov/~nugent/nugent_templates.html).
- [138] PADMANABHAN, T. Dark Energy and Gravity. *ArXiv e-prints* (May 2007).
- [139] PADOVA-ASIAGO SUPERNOVA CATALOGUE.  
<http://web.pd.astro.it/supern/snean.txt>.
- [140] PAN STARRS WEB PAGE. <http://pan-starrs.ifa.hawaii.edu/public/>.
- [141] PANS WEB PAGE. <http://www-int.stsci.edu/~strolger/>.
- [142] PEEBLES, P. J. E., AND RATRA, B. Cosmology with a time variable cosmological 'constant'. *ApJ* 325 (1988), L17.
- [143] PENZIAS, A. A., AND WILSON, R. W. A Measurement of Excess Antenna Temperature at 4080 Mc/s. *ApJ* 142 (July 1965), 419–421.
- [144] PERCIVAL, W. J., NICHOL, R. C., EISENSTEIN, D. J., WEINBERG, D. H., FUKUGITA, M., POPE, A. C., SCHNEIDER, D. P., SZALAY, A. S., VOGLEY, M. S., ZEHAVI, I., BAHCALL, N. A., BRINKMANN, J., CONNOLLY, A. J., LOVEDAY, J., AND MEIKSIN, A. Measuring the Matter Density Using Baryon Oscillations in the SDSS. *ApJ* 657 (Mar. 2007), 51–55.
- [145] PERLMUTTER, S., ALDERING, G., GOLDHABER, G., KNOP, R. A., NUGENT, P., CASTRO, P. G., DEUSTUA, S., FABBRO, S., GOOBAR, A., GROOM, D. E., HOOK, I. M., KIM, A. G., KIM, M. Y., LEE, J. C., NUNES, N. J., PAIN, R., PENNYPACKER, C. R., QUIMBY, R., LIDMAN, C., ELLIS, R. S., IRWIN, M., MCMAHON, R. G., RUIZ-LAPUENTE, P.,

- WALTON, N., SCHAEFER, B., BOYLE, B. J., FILIPPENKO, A. V., MATHE-  
SON, T., FRUCHTER, A. S., PANAGIA, N., NEWBERG, H. J. M., COUCH,  
W. J., AND THE SUPERNOVA COSMOLOGY PROJECT. Measurements of  
Omega and Lambda from 42 High-Redshift Supernovae. *ApJ* 517 (June 1999),  
565–586.
- [146] PERLMUTTER, S., DEUSTA, S., GABI, S., GOLDHABER, G., GROOM, D.,  
HOOK, I., KIM, A., KIM, M., LEE, J., AND PAIN, R. Scheduled discoveries  
of 7 high-redshift supernovae: first cosmology results and bounds on  $q_0$ . In  
*Thermonuclear Supernovae* (1997), R. C. P. Ruiz-Lapuente and J. Isern, Eds.,  
vol. 486 of *NATO ASI*, Kluwer Academic Publishers, p. 749.
- [147] PERLMUTTER, S., GABI, S., GOLDHABER, G., GOOBAR, A., GROOM,  
D. E., HOOK, I. M., KIM, A. G., KIM, M. Y., LEE, J. C., PAIN, R., PEN-  
NYPACKER, C. R., SMALL, I. A., ELLIS, R. S., MCMAHON, R. G., BOYLE,  
B. J., BUNCLARK, P. S., CARTER, D., IRWIN, M. J., GLAZEBROOK, K.,  
NEWBERG, H. J. M., FILIPPENKO, A. V., MATHESON, T., DOPITA, M.,  
COUCH, W. J., AND THE SUPERNOVA COSMOLOGY PROJECT. Measure-  
ments of the Cosmological Parameters Omega and Lambda from the First  
Seven Supernovae at  $z > 0.35$ . *ApJ* 483 (July 1997), 565.
- [148] PESKIN, M., AND SHRÖDER, D. *An Introduction to Quantum Field Theory*.  
College Press, 1998.
- [149] PHILLIPS, M. M. The absolute magnitudes of Type Ia supernovae. *ApJ* 413  
(Aug. 1993), L105–L108.
- [150] POLARSKI, D. Dark Energy: beyond General Relativity? In *Albert Einstein  
Century International Conference* (Nov. 2006), vol. 861 of *American Institute  
of Physics Conference Series*, pp. 1013–1018.
- [151] PRESS, W., TEUKOLSKY, S., VETTERLING, W., AND FLANNERY, B. *Nu-  
merical Recipes in Fortran*, 2nd ed. Cambridge University Press, 1992.
- [152] PSKOVSKII, I. P. Light curves, color curves, and expansion velocity of type  
I supernovae as functions of the rate of brightness decline. *Soviet Astronomy*  
21 (Dec. 1977), 675–682.
- [153] RANDALL, L., AND SUNDRUM, R. An Alternative to Compactification. *Phys.  
Rev. Lett.* 83 (Dec. 1999), 4690–4693.

- [154] RANDALL, L., AND SUNDRUM, R. Large Mass Hierarchy from a Small Extra Dimension. *Phys. Rev. Lett.* *83* (Oct. 1999), 3370–3373.
- [155] RAPETTI, D., ALLEN, S. W., AND WELLER, J. Constraining dark energy with X-ray galaxy clusters, supernovae and the cosmic microwave background. *MNRAS* *360* (June 2005), 555–564.
- [156] RATRA, B., AND PEEBLES, P. J. E. Cosmological consequences of a rolling homogeneous scalar field. *Phys. Rev. D* *37* (June 1988), 3406–3427.
- [157] RICHARDSON, D., BRANCH, D., CASEBEER, D., MILLARD, J., THOMAS, R. C., AND BARON, E. A Comparative Study of the Absolute Magnitude Distributions of Supernovae. *AJ* *123* (Feb. 2002), 745–752.
- [158] RIESS, A. G., FILIPPENKO, A. V., CHALLIS, P., CLOCCHIATTI, A., DIERCKS, A., GARNAVICH, P. M., GILLILAND, R. L., HOGAN, C. J., JHA, S., KIRSHNER, R. P., LEIBUNDGUT, B., PHILLIPS, M. M., REISS, D., SCHMIDT, B. P., SCHOMMER, R. A., SMITH, R. C., SPYROMILIO, J., STUBBS, C., SUNTZEFF, N. B., AND TONRY, J. Observational Evidence from Supernovae for an Accelerating Universe and a Cosmological Constant. *AJ* *116* (Sept. 1998), 1009–1038.
- [159] RIESS, A. G., PRESS, W. H., AND KIRSHNER, R. P. A Precise Distance Indicator: Type Ia Supernova Multicolor Light-Curve Shapes. *ApJ* *473* (Dec. 1996), 88.
- [160] RIESS, A. G., STROLGER, L.-G., CASERTANO, S., FERGUSON, H. C., MOBASHER, B., GOLD, B., CHALLIS, P. J., FILIPPENKO, A. V., JHA, S., LI, W., TONRY, J., FOLEY, R., KIRSHNER, R. P., DICKINSON, M., MACDONALD, E., EISENSTEIN, D., LIVIO, M., YOUNGER, J., XU, C., DAHLÉN, T., AND STERN, D. New Hubble Space Telescope Discoveries of Type Ia Supernovae at  $z > 1$ : Narrowing Constraints on the Early Behavior of Dark Energy. *ApJ* *659* (Apr. 2007), 98–121.
- [161] RIESS, A. G., STROLGER, L.-G., TONRY, J., CASERTANO, S., FERGUSON, H. C., MOBASHER, B., CHALLIS, P., FILIPPENKO, A. V., JHA, S., LI, W., CHORNOCK, R., KIRSHNER, R. P., LEIBUNDGUT, B., DICKINSON, M., LIVIO, M., GIAVALISCO, M., STEIDEL, C. C., BENÍTEZ, T., AND TSVETANOV, Z. Type Ia Supernova Discoveries at  $z > 1$  from the Hubble

- Space Telescope: Evidence for Past Deceleration and Constraints on Dark Energy Evolution. *ApJ* 607 (June 2004), 665–687.
- [162] RUBANO, C., AND SCUDELLARO, P. On some exponential potentials for a cosmological scalar field as quintessence. *Gen. Rel. Grav.* 34 (2002), 307–328.
- [163] RUBIN, V. C., THONNARD, N., AND FORD, JR., W. K. Extended rotation curves of high-luminosity spiral galaxies. IV - Systematic dynamical properties, SA through SC. *ApJ* 225 (Nov. 1978), L107–L111.
- [164] RUIZ-LAPUENTE, P. Dark energy, gravitation and supernovae. *Class. Quant. Grav.* 24 (Apr. 2007), R91.
- [165] RUIZ-LAPUENTE, P., COMERON, F., MÉNDEZ, J., CANAL, R., SMARTT, S. J., FILIPPENKO, A. V., KURUCZ, R. L., CHORNOCK, R., FOLEY, R. J., STANISHEV, V., AND IBATA, R. The binary progenitor of Tycho Brahe’s 1572 supernova. *Nature* 431 (Oct. 2004), 1069–1072.
- [166] SAHNI, V. Dark matter and dark energy. *Lect. Notes Phys.* 653 (2004), 141–180.
- [167] SAHNI, V., AND STAROBINSKY, A. The Case for a Positive Cosmological  $\Lambda$ -Term. *International Journal of Modern Physics D* 9 (2000), 373–443.
- [168] SAHNI, V., AND STAROBINSKY, A. Reconstructing dark energy. *Int. J. Mod. Phys. D* 15 (2006), 2105–2132.
- [169] SAHNI, V., AND WANG, L. A new cosmological model of quintessence and dark matter. *Phys. Rev. D* 62 (2000), 103517.
- [170] SCHLEGEL, D. J., FINKBEINER, D. P., AND DAVIS, M. Maps of Dust Infrared Emission for Use in Estimation of Reddening and Cosmic Microwave Background Radiation Foregrounds. *ApJ* 500 (June 1998), 525.
- [171] SCHUTZ, B. F. *A First course in general relativity*. Leninogorsk: Izdatel’stvo LPI, 1997.
- [172] SDSS WEB PAGE. <http://www.sdss.org/>.
- [173] SERNA, A., AND ALIM, J. M. Scalar-Tensor Cosmological Models. *Phys. Rev. D* 53 (1996), 3074–3086.

- [174] SHAPIRO, I. L., AND SOLÀ, J. On the scaling behavior of the cosmological constant and the possible existence of new forces and new light degrees of freedom. *Phys. Lett. B* 475 (2000), 236–246.
- [175] SHAPIRO, I. L., AND SOLÀ, J. Scaling behavior of the cosmological constant: Interface between quantum field theory and cosmology. *JHEP* 02 (2002), 006.
- [176] SHAPIRO, I. L., SOLÀ, J., ESPAÑA-BONET, C., AND RUIZ-LAPUENTE, P. Variable cosmological constant as a planck scale effect. *Phys. Lett. B* 574 (2003), 149–155.
- [177] SHTANOV, Y., AND SAHNI, V. Bouncing braneworlds. *Phys. Lett. B* 557 (2003), 1–6.
- [178] SMOOT, G. F., BENNETT, C. L., KOGUT, A., WRIGHT, E. L., AYMÓN, J., BOGGESS, N. W., CHENG, E. S., DE AMICI, G., GULKIS, S., HAUSER, M. G., HINSHAW, G., JACKSON, P. D., JANSSEN, M., KAITA, E., KELSALL, T., KEEGSTRA, P., LINEWEAVER, C., LOEWENSTEIN, K., LUBIN, P., MATHER, J., MEYER, S. S., MOSELEY, S. H., MURDOCK, T., ROKKE, L., SILVERBERG, R. F., TENORIO, L., WEISS, R., AND WILKINSON, D. T. Structure in the COBE differential microwave radiometer first-year maps. *ApJ* 396 (Sept. 1992), L1–L5.
- [179] SNAP WEB PAGE. <http://snap.lbl.gov/>.
- [180] SNFACTORY WEB PAGE. <http://snfactory.lbl.gov/>.
- [181] SNLS WEB PAGE. <http://www.cfht.hawaii.edu/SNLS/>.
- [182] SOLEVI, P., MAININI, R., BONOMETTO, S. A., MACCIÒ, A. V., KLYPIN, A., AND GOTTLÖBER, S. Tracing the nature of dark energy with galaxy distribution. *MNRAS* 366 (Mar. 2006), 1346–1356.
- [183] SPERGEL, D. N., BEAN, R., DORÉ, O., NOLTA, M. R., BENNETT, C. L., DUNKLEY, J., HINSHAW, G., JAROSIK, N., KOMATSU, E., PAGE, L., PEIRIS, H. V., VERDE, L., HALPERN, M., HILL, R. S., KOGUT, A., LIMON, M., MEYER, S. S., ODEGARD, N., TUCKER, G. S., WEILAND, J. L., WOLLACK, E., AND WRIGHT, E. L. Three-Year Wilkinson Microwave Anisotropy Probe (WMAP) Observations: Implications for Cosmology. *ApJS* 170 (June 2007), 377–408.

- [184] SPERGEL, D. N., VERDE, L., PEIRIS, H. V., KOMATSU, E., NOLTA, M. R., BENNETT, C. L., HALPERN, M., HINSHAW, G., JAROSIK, N., KOGUT, A., LIMON, M., MEYER, S. S., PAGE, L., TUCKER, G. S., WEILAND, J. L., WOLLACK, E., AND WRIGHT, E. L. First-Year Wilkinson Microwave Anisotropy Probe (WMAP) Observations: Determination of Cosmological Parameters. *ApJS* 148 (Sept. 2003), 175–194.
- [185] STEIGMAN, G. Primordial nucleosynthesis: Successes and challenges. *International Journal of Modern Physics E* 15 (2006), 1.
- [186] STEINHARDT, P. J., WANG, L., AND ZLATEV, I. Cosmological tracking solutions. *Phys. Rev. D* 59, 12 (June 1999), 123504.
- [187] SULLIVAN, M., ELLIS, R. S., ALDERING, G., AMANULLAH, R., ASTIER, P., BLANC, G., BURNS, M. S., CONLEY, A., DEUSTUA, S. E., DOI, M., FABBRO, S., FOLATELLI, G., FRUCHTER, A. S., GARAVINI, G., GIBBONS, R., GOLDBABER, G., GOOBAR, A., GROOM, D. E., HARDIN, D., HOOK, I., HOWELL, D. A., IRWIN, M., KIM, A. G., KNOP, R. A., LIDMAN, C., MCMAHON, R., MENDEZ, J., NOBILI, S., NUGENT, P. E., PAIN, R., PANAGIA, N., PENNYPACKER, C. R., PERLMUTTER, S., QUIMBY, R., RAUX, J., REGNAULT, N., RUIZ-LAPUENTE, P., SCHAEFER, B., SCHAHMANECHE, K., SPADAFORA, A. L., WALTON, N. A., WANG, L., WOODVASEY, W. M., AND YASUDA, N. The Hubble diagram of type Ia supernovae as a function of host galaxy morphology. *MNRAS* 340 (Apr. 2003), 1057–1075.
- [188] SUSPECT ARCHIVE. <http://bruford.nhn.ou.edu/~suspect/index1.html>.
- [189] TARANTOLA, A. *Inverse Problem Theory*. Elsevier, 1987.
- [190] TARANTOLA, A., AND NERCESSIAN, A. Three-dimensional inversion without blocks. *Geophys. J. R. Astr. Soc.* 76 (1984), 299.
- [191] TARANTOLA, A., AND VALETTE, B. Generalized nonlinear inverse problems solved using the least squares criterion. *Rev. Geophys. & Space Phys.* 20, 2 (1982), 219.
- [192] TARANTOLA, A., AND VALETTE, B. Inverse problems = quest for information. *J. Geophys.* 50 (1982), 159.
- [193] THE 2DF GALAXY REDSHIFT SURVEY WEB PAGE. <http://www.mso.anu.edu.au/2dFGRS/>.

- [194] THE DARK ENERGY SURVEY COLLABORATION. The Dark Energy Survey. *ArXiv Astrophysics e-prints: astro-ph/0510346* (Oct. 2005).
- [195] THE LARGE SYNOPTIC SURVEY TELESCOPE COLLABORATION. Dark energy task force whitepaper. [http://www.lsst.org/Science/docs/LSST\\_DETF\\_Whitepaper.pdf](http://www.lsst.org/Science/docs/LSST_DETF_Whitepaper.pdf).
- [196] TONRY, J. L., SCHMIDT, B. P., BARRIS, B., CANDIA, P., CHALLIS, P., CLOCCHIATTI, A., COIL, A. L., FILIPPENKO, A. V., GARNAVICH, P., HOGAN, C., HOLLAND, S. T., JHA, S., KIRSHNER, R. P., KRISCIUNAS, K., LEIBUNDGUT, B., LI, W., MATHESON, T., PHILLIPS, M. M., RIESS, A. G., SCHOMMER, R., SMITH, R. C., SOLLERMAN, J., SPYROMILIO, J., STUBBS, C. W., AND SUNTZEFF, N. B. Cosmological Results from High- $z$  Supernovae. *ApJ* 594 (Sept. 2003), 1–24.
- [197] TURATTO, M., BENETTI, S., AND PASTORELLO, A. Supernova Classes and Subclasses. *ArXiv e-prints 706* (June 2007).
- [198] UREÑA LOPEZ, L. A., AND MATOS, T. A new cosmological tracker solution for quintessence. *Phys. Rev. D* 62 (2000), 081302.
- [199] VERDE, L., HEAVENS, A. F., PERCIVAL, W. J., MATARRESE, S., BAUGH, C. M., BLAND-HAWTHORN, J., BRIDGES, T., CANNON, R., COLE, S., COLLESS, M., COLLINS, C., COUCH, W., DALTON, G., DE PROPRIIS, R., DRIVER, S. P., EFSTATHIOU, G., ELLIS, R. S., FRENK, C. S., GLAZEBROOK, K., JACKSON, C., LAHAV, O., LEWIS, I., LUMSDEN, S., MADDOX, S., MADGWICK, D., NORBERG, P., PEACOCK, J. A., PETERSON, B. A., SUTHERLAND, W., AND TAYLOR, K. The 2dF Galaxy Redshift Survey: the bias of galaxies and the density of the Universe. *MNRAS* 335 (Sept. 2002), 432–440.
- [200] WALKER, T. P., STEIGMAN, G., KANG, H.-S., SCHRAMM, D. M., AND OLIVE, K. A. Primordial nucleosynthesis redux. *ApJ* 376 (July 1991), 51–69.
- [201] WANG, L., GOLDHABER, G., ALDERING, G., AND PERLMUTTER, S. Multi-color light curves of type ia supernovae on the color-magnitude diagram: a novel step toward more precise distance and extinction estimates. *ApJ* 590 (2003), 944–970.

- [202] WANG, Y., AND MUKHERJEE, P. Model-independent Constraints on Dark Energy Density from Flux-averaging Analysis of Type Ia Supernova Data. *ApJ* 606 (May 2004), 654–663.
- [203] WANG, Y., AND MUKHERJEE, P. Robust Dark Energy Constraints from Supernovae, Galaxy Clustering, and 3 yr Wilkinson Microwave Anisotropy Probe Observations. *ApJ* 650 (Oct. 2006), 1–6.
- [204] WEINBERG, S. *Gravitation and cosmology: principles and applications of the general theory of relativity*. Wiley, 1972.
- [205] WEINBERG, S. Anthropic bound on the cosmological constant. *Phys. Rev. Lett.* 59, 22 (Nov 1987), 2607–2610.
- [206] WELLER, J., AND ALBRECHT, A. Future supernovae observations as a probe of dark energy. *Phys. Rev. D* 65, 10 (May 2002), 103512.
- [207] WETTERICH, C. Cosmology and the fate of dilatation symmetry. *Nucl. Phys. B* 302 (1988), 668.
- [208] WHEELER, J. C., PIRAN, T., AND WEINBERG, S., Eds. *Jerusalem Winter School for Theoretical Physics. Supernovae. Volume 6, Jerusalem, Dec. 28, 1988- Jan. 5, 1989.* (1990).
- [209] WHELAN, J., AND IBEN, I. J. Binaries and Supernovae of Type I. *ApJ* 186 (Dec. 1973), 1007–1014.
- [210] WITTMAN, D. M., TYSON, J. A., KIRKMAN, D., DELL’ANTONIO, I., AND BERNSTEIN, G. Detection of weak gravitational lensing distortions of distant galaxies by cosmic dark matter at large scales. *Nature* 405 (May 2000), 143–148.
- [211] WOOD-VASEY, W. M., MIKNAITIS, G., STUBBS, C. W., JHA, S., RIESS, A. G., GARNAVICH, P. M., KIRSHNER, R. P., AGUILERA, C., BECKER, A. C., BLACKMAN, J. W., BLONDIN, S., CHALLIS, P., CLOCCHIATTI, A., CONLEY, A., COVARRUBIAS, R., DAVIS, T. M., FILIPPENKO, A. V., FOLEY, R. J., GARG, A., HICKEN, M., KRISCIUNAS, K., LEIBUNDGUT, B., LI, W., MATHESON, T., MICELI, A., NARAYAN, G., PIGNATA, G., PRIETO, J. L., REST, A., SALVO, M. E., SCHMIDT, B. P., SMITH, R. C., SOLLERMAN, J., SPYROMILIO, J., TONRY, J. L., SUNTZEFF, N. B., AND ZENTENO, A. Observational Constraints on the Nature of the Dark Energy:

- First Cosmological Results from the ESSENCE Supernova Survey. *ApJ* 666 (Sept. 2007), 694–715.
- [212] ZLATEV, I., WANG, L., AND STEINHARDT, P. J. Quintessence, Cosmic Coincidence, and the Cosmological Constant. *Phys. Rev. Lett.* 82 (Feb. 1999), 896–899.
- [213] ZUNCKEL, C., AND TROTTA, R. Reconstructing the history of dark energy using maximum entropy. *MNRAS* (Aug. 2007), 710.
- [214] ZWICKY, F. On the Masses of Nebulae and of Clusters of Nebulae. *ApJ* 86 (Oct. 1937), 217.



